Étude magnétique des particules en suspension dans l'air (PM) capturées dans des bio-capteurs et des filtres à air dans différents environnements urbains

Arua da Silva Leite

THÈSE

En vue de l'obtention du

DOCTORAT DE L'UNIVERSITÉ DE TOULOUSE

Délivré par : *l'Université Toulouse 3 Paul Sabatier (UT3 Paul Sabatier)*

Présentée et soutenue le *13/05/2022* **par :**

Aruã DA SILVA LEITE

Étude magnétique des particules en suspension dans l'air (PM) capturées dans des bio-capteurs et des filtres à air dans différents environnements urbains

---

JURY

Bruno LARTIGES	Professeur d'Université	Membre du Jury
Edmilson D. FREITAS	Professeur d'Université	Membre du Jury
Helena SANT'OVAIA	Professeur d'Université	Membre du Jury
Christine FRANKE	Enseignant-chercheur	Membre du Jury

École doctorale et spécialité :
SDU2E : Surfaces et interfaces continentales, Hydrologie

Unité de Recherche :
Géosciences Environnement Toulouse (UMR 5563)

Directeur(s) de Thèse :
Melina MACOUIN et *Ricardo I. F. TRINDADE*

Rapporteurs :
France LAGROIX et *Piérre CAMPS*

Étude magnétique des particules en suspension dans l'air (PM) capturées dans des bio-capteurs et des filtres à air dans différents environnements urbains

Acknowledgements

This thesis would not have happened without Melina, who, even before I enrolled in the program, has been helping me in all the ways I can think of till the very last moment. A big and affectionate thank you for bringing me into my favorite city.

I also would like to thank Ricardo for being this constant influence in my life since the early days of my undergraduate geophysics studies, showing me my way, teaching me, and introducing me to countless people who made me a better researcher.

I want to thank my collaborators, Sonia, Jean-François, and Loïc, for all the patience, help, and teachings throughout these three years and a half.

For the friends and colleagues from USPMAG, thank you and miss you. Hopefully, we will meet again soon.

A big shout to all my friends here in Toulouse, without them, I am not sure what would be of me. Much love, thank you, Bia, Romulo, Nati, baby Louise, Bonnie, Paty, Rim, Marina, Hugo, Jessica, Luisa, Estelle, Aleksandra, and Caio, Nico, and Anne-Sophie. You are the best.

Pelas memórias e momentos compartilhados, me ensinaram muito.

Aos meus amigos do interior, Tomás, Lucas, Lucas, Hirgo, Carol, Laura e Ritchie, saudades, vocês são foda.

Quero agradecer especialmente minha família, que sempre me incentivou e me deu coragem e ânimo para continuar. Saudades infinitas, nos vemos em breve Nazareth, Fernando e Daniel. Um grande beijo. Também gostaria de agradecer especialmente meu avô Luiz, sempre presente em minha formação, e um exemplo desde sempre. Muitas saudades, e um grande beijo.

I hope that our future is better than we predict and that we decide to face with courage and sincerity the problems of our time.

Abstract

Airborne particulate matter (PM) is understood nowadays as a major health risk. The finer PM fraction is the most dangerous for human health. Children are among the most vulnerable to PM and air pollution due to their immature respiratory systems and higher respiration rates than adults. Since most of the population spends more time indoors, knowing the different sources of PM in this environment and the contribution of outdoor sources is of great importance. Despite advances in the comprehension of indoor air quality, many gaps still exist regarding PM transfer from outdoors to indoor environments.

Environmental magnetism offers an excellent opportunity for PM investigation. It is sensible to investigate the finer fractions (sub-micrometric) of iron oxides present in PM even when they occur in small concentrations. Magnetic methods are also particularly suited to be used together with bio-sensors, biological samples able to retain pollutants, such as tree leaves and tree bark. Bio-sensors are a great alternative to low-cost sensors, being cost-effective and of low environmental impact. They also offer the opportunity for innovative experimental designs.

Here we combined magnetic methods with bio-sensors to better understand the indoor-outdoor PM problem in different urban contexts. The thesis's main goal was to characterize PM's anthropogenic emissions indoors and outdoors and the relationship between them. The different urban emission sources were characterized in PM2.5 filters, providing information about the magnetic properties of those sources, which were later used in the study of bio-sensors. Bio-sensors were used in citizen science projects to study PM indoors and outdoors in urban environments. In this thesis, innovative magnetic techniques were also used to investigate the ultrafine fraction of magnetic PM regarding grains on the superparamagnetic size range (i.e., below $\sim 30nm$ for magnetite). Scanning electronic microscopy provided complementary morphological information about iron oxides and other PM constituents. The results indicate that different anthropogenic emission sources had a narrow grain size distribution. Traffic emissions dominated the magnetic fraction of PM carried indoors in domestic and school environments. Ultrafine iron oxide spherules of about $50nm$ (and finer) are related to traffic emissions, as detected in the SEM. The indoor environment has a lower concentration of magnetic PM (with mean I/O for SIRM calculated at 0.7 and 0.9 in the schools and 0.5 in the residencies). However, the size fraction is finer than outdoors (in the SSD). The ultrafine fraction (below the SP-SSD boundary) has a mean diameter calculated at $7.7nm$. Other PM sources, besides traffic emissions, are also important indoors, especially in the school environment, as shown by I/O for organic carbon concentrations ranging from 1.1 to 1.9.

Lastly, we investigated the fate of PM emitted in the urban setting. With the hypothesis that PM particles emitted in urban environments are carried away in the water cycle, sediments of the Garonne river were studied. The results show peaks in magnetic susceptibility (reaching values of $2.95 \times 10^6 \mathrm{m}^3/\mathrm{kg}$) and trace metals (such as Cu and Pb reaching concentrations of 139.0 and 73.5ppm) in the downtown region of Toulouse that point to anthropogenic input. The presence of iron oxide spherules with micrometric size (ranging from 10 to 91μm) shows traffic emission sources as the origin of the detected particles.

Overall, this thesis provided new insights on the anthropogenic emission of PM and their indoor-outdoor relationship, which can be used to characterize the air quality of the domestic

and school environment.

Résumé

Les particules en suspension dans l'air (PM) sont aujourd'hui considérées comme un risque majeur pour la santé. Les enfants constituent l'un des groupes les plus vulnérables aux PM et à la pollution atmosphérique. Comme la majorité de la population passe plus de temps à l'intérieur, il est très important de connaître les différentes sources de particules dans cet environnement et la contribution des sources extérieures. Malgré les progrès réalisés dans la compréhension de la qualité de l'air intérieur, de nombreuses lacunes subsistent en ce qui concerne le transfert des particules de l'extérieur vers l'intérieur.

Le magnétisme environnemental offre une grande opportunité pour l'étude des PM, car il est suffisamment sensible pour étudier les fractions les plus fines des oxydes de fer présents dans les PM. Les méthodes magnétiques sont également particulièrement adaptées pour être utilisées avec des bio-capteurs, échantillons naturels capables de retenir les polluants. Les bio-capteurs constituent une excellente alternative aux capteurs à faible coût, car ils sont rentables et ont un faible impact sur l'environnement.

Ici, nous avons combiné des méthodes magnétiques avec des bio-capteurs afin de mieux comprendre le problème des PM intérieur-extérieur dans différents contextes urbains. L'objectif principal de la thèse était de caractériser les émissions anthropiques de PM à l'intérieur et à l'extérieur et la relation entre elles. Les différentes sources d'émissions urbaines ont été caractérisées dans des filtres PM2.5, fournissant des informations sur les propriétés magnétiques de ces sources, qui ont ensuite été utilisées dans l'étude des bio-capteurs. Les bio-capteurs ont été utilisés dans le cadre de projets scientifiques citoyens, afin d'étudier les PM dans les environnements urbains. Dans cette thèse, des techniques magnétiques innovantes ont également été utilisées pour étudier la fraction ultrafine des PM magnétiques. La microscopie électronique à balayage a fourni des informations morphologiques complémentaires sur les oxydes de fer et les autres constituants des PM. Les résultats indiquent tout d'abord que les différentes sources d'émissions anthropiques présentaient une distribution granulométrique étroite. Pour la ville de Toulouse, les émissions dues au trafic routier ont dominé la fraction magnétique des PM qui sont transportées à l'intérieur des habitations. Des sphérules d'oxydes de fer ultrafines d'environ $50nm$ (et plus) liées aux émissions du trafic, ont été détectées au MEB. L'environnement intérieur présente une concentration plus faible de PM magnétiques (avec des I/O moyens pour le SIRM compris entre 0.7 et 0.9 pour les écoles et de 0,5 pour les résidences). La fraction granulométrique est plus fine par rapport à l'extérieur (dans le SSD). La fraction ultrafine pour ce type de grain a un diamètre moyen calculé à $7.7nm$. D'autres sources de particules, outre les émissions du trafic, sont également importantes à l'intérieur, notamment dans l'environnement scolaire, comme le montrent les I/O pour la concentration de carbone organique allant de 1.1 à 1.9.

Avec l'hypothèse que certaines des particules PM émises en milieu urbain sont entraînées dans le cycle de l'eau, les sédiments de la Garonne ont été étudiés. Les résultats montrent des pics de susceptibilité magnétique (atteignant des valeurs de $2.95 \times 10^6 \mathrm{m}^3/\mathrm{kg}$) et de métaux traces (tels que Cu et Pb atteignant des concentrations de 139.0 et 73.5 ppm) dans le centre-ville de Toulouse qui indiquent un apport anthropique. La présence de sphérules d'oxydes de fer de taille micrométrique (allant de 10 à 91μm) montre que les sources d'émission liée au trafic routier sont à l'origine des particules détectées.

En conclusion, cette thèse a fourni de nouvelles informations sur les émissions anthropiques

de particules et sur leur relation intérieur-extérieur, qui peuvent être utilisées pour caractériser la qualité de l'air dans les environnements urbaines.

Contents

List of Figures

List of Tables

Chapter 1

Introduction

1.1 English version

Air pollution is omnipresent in our society and has become a major global problem [WHO, 2021b]. Air pollution is a complex mixture of gasses and particulate matter (PM). PM comprises airborne solid particles and liquid droplets with diverse compositions [Seinfeld and Pandis, 2016]. Sources of air pollution are economical and industrial processes, domestic activities, transportation, and personal habits, among others. The problems posed by air pollution have a complex nature since air pollution is ubiquitous and very specific for every context, from a global to regional to individual scale. Understanding air pollution, its implications, and its consequences are no simple task and require a global vision.

Since the early 1990s, the relationship between anthropogenic PM emissions and health hazards has been thoroughly investigated. Exposure to PM has been directly linked to an increase in mortality, increase in severity of different health conditions, and development of new diseases [Dockery and Pope, 1994, Pope III and Dockery, 2006, Cohen et al., 2017, Burnett et al., 2018, WHO, 2013, Murray et al., 2020]. Children are particularly in danger from PM exposure. Their immature respiratory and neurological systems may be irreversibly affected by PM exposition. Their neuropsychological development may also be impacted [Martins et al., 2020, Kim et al., 2004, Rice and Barone Jr, 2000, WHO, 2021a]. Nowadays, it is understood that the burden of disease associated with PM exposure is on par with other major global health risks such as unhealthy diets and tobacco smoking [Murray et al., 2020]. Moreover, exposure to PM also has economic consequences due to the loss of productivity, health care costs, impact on crops, and damage to buildings and infrastructure, among others [El-Fadel and Massoud, 2000, Nguyen et al., 2017, Bank et al., 2016].

Air quality investigations are generally based on methods characterizing pollutants concentrations, like PM (and their specific size-segregated species like PM10 and PM2.5, referring to particles inferior to 10 and 2.5 μm respectively), nitrogen oxides (NO_2 for instance), ozone (O_3), carbonaceous species (elemental and organic carbon, EC and OC, respectively) among others. For PM, investigations are based on capturing and measuring PM concentrations. Real-time, in situ PM concentration measurements can be achieved using tapered element oscillating microbalance [Patashnick and Rupprecht, 1991, Grover et al., 2005]. Optical measurements are based on counting individual particles [Lombardo et al., 2019]. Both traditional and low-cost PM sensors can be found on optical measurements, usually using

infrared or red lasers [Kuula et al., 2020]. Size selection for PM capture in filters is based on the aerodynamic properties of the PM, and it's selective for 50% of the size distribution, capping at a given maximum size, 2.5 and 10μm for PM2.5 and PM10, for instance, [Chow et al., 1994]. The concentration of PM is estimated from the PM deposition on the air filter using mass measurements. Monitoring air quality stations are capable of high temporal resolution measurements, albeit the costs limit the spatial availability of such stations. Globally, the coverage of monitoring air quality stations for the most common pollutants is inadequate for tracking emissions outside major cities and even absent in some countries [WHO, 2021b].

The spatial availability of air quality data may be increased using mobile or low cost sensors [Gozzi et al., 2016, Castellini et al., 2014, Hasenfratz et al., 2015, Mueller et al., 2016, Elen et al., 2013, Van den Bossche et al., 2016], short term campaigns [Mishra et al., 2012] and air quality modeling [Thunis et al., 2016, Kumar et al., 2011, Lefebvre et al., 2013, Vardoulakis et al., 2003]. Bio-sensors, i.e., biological samples exposed to PM (or other pollutants) emissions, is also an excellent alternative, providing a cost-effective and low environmental impact alternative to other low-cost sensors. The use of bio-sensors is not new in environmental investigations. For instance, exposure to moss (in small mesh bags) has been used for over 40 years to characterize air pollutants [Ares et al., 2012]. Furthermore, bio-sensors may be used in magnetic characterizations to investigate PM emissions [Hofman et al., 2017].

Environmental magnetism methods can be applied to the study of PM since iron oxides are pervasive among the PM constituents [Hunt et al., 1984, Flanders, 1994, Chaparro et al., 2020, Winkler et al., 2021]. In addition, iron oxides in PM have been directly associated with trace metals, such as zinc, cadmium, lead, and chromium, at times being incorporated into the mineral structure during combustion [Moreno et al., 2003, Magiera et al., 2011]. Consequently, their magnetic properties are not only proxies for PM concentration but are of direct interest due to the health-related consequences of human exposure to trace metals. Environmental magnetism methods are cost-effective, easy to implement, and non-destructive. The environmental magnetism methods can be applied for PM investigation in different kinds of samples, from air filters [e.g., Sagnotti et al., 2006, Shi et al., 2014, Leite et al., 2018] used in traditional PM investigation, to settled dust [e.g., Kelepertzis et al., 2019, Kim et al., 2009, Liu et al., 2019a, Bourliva et al., 2016], sediments [e.g., Franke et al., 2009], soils [e.g., Hoffmann et al., 1999] and also to collectors [e.g., Hofman et al., 2017, Sagnotti et al., 2006, Mitchell and Maher, 2009, Chaparro et al., 2020]. These samples allow high flexibility in designing PM monitoring programs in diverse settings, environments, and locations. The magnetic properties of iron oxides provide means to discern the magnetic mineralogy (i.e., soft coercivity carriers and hard coercivity carriers), their size fractions, and estimate their concentrations and relative proportions [e.g., Mitchell and Maher, 2009, Sagnotti et al., 2006, Leite et al., 2021]. Moreover, different magnetic techniques enable the investigation of the finer fractions of iron oxides in the ultrafine size range from PM0.1 (<0.1μm) to nano-sized grains [Sagnotti and Winkler, 2012, Mitchell and Maher, 2009, Leite et al., 2018]. For example, the xARM/SIRM ratio allows the qualitative determination of grain sizes in the single domain range for magnetite [Maher, 1988]. In contrast, the SPCDM protocol gives quantitative concentration for magnetites in grain sizes smaller than $\approx 30nm$ [Leite et al., 2018]. The magnetic susceptibility frequency dependence gives quantitative information on grain size variation for magnetites on the stable single domain-superparamagnetic threshold [Ustra

et al., 2018]. In this way, the magnetic properties of the iron oxides can be used as proxies for the whole of PM, providing complementary information to traditional methods used in PM investigations.

Magnetic properties measured on bio-sensors (vegetable/funghi matter, tree bark, leaves, mosses, among others) may provide additional information and supplementary spatial data to existing air quality monitoring stations, being previously applied to assess local air quality models [Hofman and Samson, 2014, Lazić et al., 2016, De Nicola et al., 2013, Mitchell and Maher, 2009]. The ubiquitous presence of bio-sensors (leaves, tree bark, moss, lichens) in nature provides a cost-effective and easy way to increase the spatial resolution of traditional air quality investigation methods. The environmental impact of using bio-sensors is low, especially compared to low-cost PM sensors. Moreover, bio-sensors allow for innovative experimental designs, increasing the spatial and temporal coverage of surveys and enabling the sampling of indoor and outdoor environments with the same toolkit. Given their nature, they can also be easily incorporated into "citizen science" initiatives.

Awareness of the environment may motivate people to take necessary actions to tackle the environmental problems we face [Pihkala, 2020]. Air pollution, as well as climate change, is a complex problem without simple solutions. It requires not only organized action from governmental institutions but also individual and collective participation of the society as a whole. Environmental education may help deal with those modern challenges, informing the population outside academia and proposing strategies to deal with those challenges. Public awareness of the significant environmental threats of our time (such as climate change) may lead to eco-anxiety development, including depression, general anxiety, and pessimism towards the future, among others [Pihkala, 2020, Russell and Oakley, 2016, Cunsolo Willox et al., 2013].

Citizen science could play a fundamental role in air quality studies. Making the active population players in the construction of scientific knowledge leads to scientific vulgarization, increasing public awareness of the scientific process - of its achievements and limits. In the age of "fake-news" and illiteracy regarding several scientific topics with substantial societal implications, the involvement of non-scientists in the scientific process may provide an essential tool for the dissemination of diverse scientific topics [Irwin, 2018], air quality investigations among them. Besides, citizen science participation allows scientists and environmental educators to inform the public, proposing proactive measures to not only deal with the investigated problem but also mitigate and focus on the eco-anxiety that may arise. Most citizen science studies of PM and air quality involve manufactured low-cost sensors, allowing more excellent spatial resolution on the surveys. But using those low-cost sensors has shortcomings, such as the necessity of some infrastructure (for instance, internet connectivity to data transfer in some cases) and the environmental impact of the sensors' production. Bio-sensors, on the other hand, may provide the ideal low-cost sensor, as they are widely available in nature and have a much lower environmental impact related to their use. Together with citizen science, the use of bio-sensors coupled with environmental magnetism both benefit from and also enhance scientific investigations.

1.1.1 Objectives

This thesis combines traditional air quality monitoring with magnetic investigation in bio-sensors. The main objectives are:

- Assess the use of magnetic methods as proxies to track PM emissions in an urban context, using the magnetic properties on bio-sensors and air filters.
- Track the finer fractions (fine and ultrafine) of iron oxides present in PM, using SEM investigations to complement the information provided by magnetic methods, with morphology, size, and elemental composition of the particles.
- The use of magnetic methods to track different PM emission sources in the urban context, regarding the magnetic mineral content, grain size, magnetic mineralogy, and seasonal influence.
- Investigate the air quality in the school environment, indoor and outdoor spaces, and distance from emission sources through magnetic methods and traditional air quality investigations.
- Investigate the air quality of the domestic environment in a medium-size city through the use of bio-sensors and magnetic investigation methods, the relationship between indoor and outdoor environments, the emission sources, and the general habits of the population.

1.1.2 Thesis presentation

I present in this thesis a series of investigation strategies to characterize airborne particulate matter (PM), which include citizens' participation in some experiments. The scientific investigations are done from the perspective of environmental magnetism, using airborne iron oxides as proxies for the whole of PM, besides direct analysis of PM captured in air filters. The participation of citizens relates to investigating domestic and scholar environments in the city of Toulouse.

In 2018 we started a citizen science project in Toulouse to investigate air quality in the domestic and school environments. Through seminars on scientific vulgarization, we informed the population about the issues related to air pollution and traffic emissions and recruited interested citizens to participate in the project. In the schools, the talks were made with teachers and children. The citizens that participated in the project received a kit for the deployment of bio-sensors, which were exposed for up to a year and later brought back to the laboratory to perform magnetic investigations on them. The citizens were instructed to deploy the bio-sensors, and their role was to deploy and return the sampling kits, besides participating in the vulgarization seminars. After the completion of sampling and measurements, other restitution seminars took place to present and discuss the results with the population.

The first chapter is a state-of-the-art on particulate matter, its effects on health, and the use of magnetic techniques to study them. I start by contextualizing the PM problem with its health concerns and socioeconomic impacts and briefly describing its composition. Then

the last guidelines of the World Health Organization [WHO, 2021b] for PM exposition are presented. The use of environmental magnetism in PM investigation is then addressed, going from its use in the investigation of the magnetic properties of PM air filters, passing through the use of bio-sensors in magnetic investigations, and then the techniques used for the study of the ultrafine fraction of iron oxides. Lastly, some topics on citizen science approaches are presented.

The second chapter introduces a published paper on magnetic properties in PM2.5 air filters from West Africa (Benin and Ivory Coast). The sampling in the region comprises a two-year, weekly campaign in four different sites. Each site has its primary anthropogenic emission source, from two-wheeled vehicles to biomass burning. The magnetic properties of the filters regard their magnetic mineralogy, the grain size distribution of ultrafine fraction (SD magnetite), and concentration. Magnetic properties are related to previously measured PM and carbonaceous species concentrations. Scanning electron microscopy (SEM) characterized the airborne iron oxides for their superficial properties. The variations observed in the magnetic properties at each studied site along the two-year survey are related to the seasonal changes in weather characteristics through time and the specific emission scenarios at each location. The different anthropogenic sources have a narrow grain size range for the iron oxides emissions, below 0.1μm.

The third chapter concerns different study cases in Toulouse, France. It is divided into sections as it introduces more than one study case on air quality and the city's magnetic properties of airborne iron oxides. The chapter starts by introducing the second submitted paper of this thesis, which investigates the air quality in the school environment. Samples consisted of tree bark collected in the courtyards, bio-sensors, and PM1 air filters indoors and outdoors in the classrooms of two schools. The results, including pollutant concentrations (PM1, elemental, and organic carbon concentrations) and magnetic parameters (characterizing the concentration of iron oxides, mineralogy, and grain size), paint a complete picture of the school environment's air quality. SEM investigations provided complementary information on the airborne iron oxides regarding their superficial characteristics, composition, and origin. This work also included interventions of the children and school staff, having a vital citizen science aspect. Continuing on the topic of bio-sensors on PM magnetic investigation, the third paper (in draft form) presents a study on PM in the domestic environment in the city of Toulouse within the scope of the NanoEnvi project. The magnetic investigation of the bio-sensors gave information about the differences in indoor and outdoor settings across the city. Concentration, mineralogy, and grain size were determined for the airborne iron oxides, indicating the primary PM sources in the domestic environment. SEM investigations also further characterized the magnetic fraction of PM captured on the bio-sensors. Still, in this chapter, a complementary section is related to applying a technique to characterize the ultrafine Superparamagnetic (SP) fraction of magnetic particles on the bio-sensors and tree barks for their mean grain size and concentration on the PM.

In the fourth chapter, we present a case study on the Garonne river sediments, collected along a 50 km profile in the surroundings of the city of Toulouse. Magnetic characterization was done to estimate the anthropogenic input on the river, which was complemented by geochemical analysis and SEM investigations. In this way, these results, together with those reported in chapter three, provide a comprehensive picture of the emissions of airborne iron oxides from traffic sources in the city of Toulouse, how they spread to the domestic and school

environments, and lastly, the final destination of part of these anthropogenic particles, being carried away in the waterways.

In the final chapter, the main conclusions of the work are presented, as well as my point of view on the perspectives of the research topic.

1.2 Version française

La pollution atmosphérique est omniprésente dans notre société et est devenue un problème mondial majeur [WHO, 2021b]. La pollution atmosphérique est un mélange complexe de gaz et de matières particulaires (PM). Les PM sont composées de particules solides en suspension dans l'air et de gouttelettes liquides de composition diverse [Seinfeld and Pandis, 2016]. Les sources de pollution atmosphérique sont dues, entre autres, aux processus économiques et industriels, aux activités domestiques, aux transports ainsi qu'aux habitudes personnelles,. Les problèmes posés par la pollution de l'air ont une nature complexe. En effet, la pollution de l'air est non seulement omniprésente mais aussi très spécifique pour chaque contexte, de l'échelle mondiale, régionale et individuelle. Comprendre la pollution de l'air, ses implications et ses conséquences n'est pas une tâche simple et nécessite une vision globale.

Depuis le début des années 1990, la relation entre les émissions anthropiques de particules et les risques sanitaires a fait l'objet d'études approfondies.
L'exposition aux PM a été directement liée à une augmentation de la mortalité, à une augmentation de la gravité de différents états de santé et au développement de nouvelles maladies[Dockery and Pope, 1994, Pope III and Dockery, 2006, Cohen et al., 2017, Burnett et al., 2018, WHO, 2013, Murray et al., 2020]. Les enfants sont particulièrement menacés par l'exposition aux particules. Leurs systèmes respiratoire et neurologique immatures peuvent être affectés de manière irréversible par l'exposition aux PM. Leur développement neuropsychologique peut également être affecté [Martins et al., 2020, Kim et al., 2004, Rice and Barone Jr, 2000, WHO, 2021a]. Aujourd'hui, il est entendu que le poids de la morbidité associée à l'exposition aux PM est équivalent à celui d'autres risques sanitaires mondiaux majeurs tels que les mauvais régimes alimentaires et le tabagisme [Murray et al., 2020]. En outre, l'exposition aux PM a également des conséquences économiques, en raison de la perte de productivité, du coût des soins de santé ainsi que des impacts sur les cultures agricoles, des dommages dans les bâtiments et les infrastructures, entre autres [El-Fadel and Massoud, 2000, Nguyen et al., 2017, Bank et al., 2016].

Les enquêtes sur la qualité de l'air sont généralement basées sur des méthodes caractérisant les concentrations de polluants, comme les PM (et leurs espèces de taille spécifique comme PM10 et PM2.5, se référant aux particules inférieures à 10 et 2.5 μm respectivement), les oxydes d'azote (NO_2 par exemple), l'ozone (O_3), les espèces carbonées (carbone élémentaire, EC et organique, OC) entre autres. Pour les PM, les études sont basées sur la capture et la mesure des concentrations de PM.Les mesures de concentration de PM en temps réel et in situ peuvent être réalisées à l'aide d'une microbalance oscillante à élément conique [Patashnick and Rupprecht, 1991, Grover et al., 2005] ou par mesures optiques,basées sur le comptage des particules individuelles [Lombardo et al., 2019]. Les capteurs de PM à faible coût sont également basés sur des mesures optiques, utilisant généralement des lasers infrarouges ou rouges [Kuula et al., 2020]. La sélection de la taille lors du piègeage des PM sur les filtres est basée sur les propriétés aérodynamiques des PM, et elle est sélective pour 50% de la distribution de la taille, plafonnant à une taille maximale donnée, par exemple 2.5 et 10 μm pour les PM2.5 et PM10[Chow et al., 1994]. La concentration de PM est estimée à partir du dépôt de PM sur un filtre à air, en utilisant des mesures de masse. Les stations de surveillance de la qualité de l'air sont capables d'effectuer des mesures à haute résolution temporelle, bien que les coûts limitent la disponibilité spatiale de ces stations. Au niveau

mondial, la couverture des stations de surveillance de la qualité de l'air pour les polluants les plus courants est très faible en dehors des grandes villes, voire complètement inexistante dans certains pays [WHO, 2021b].

La répartition spatiale de données de qualité de l'air peut être accrue en utilisant des capteurs mobiles ou à faible coût [Gozzi et al., 2016, Castellini et al., 2014, Hasenfratz et al., 2015, Mueller et al., 2016, Elen et al., 2013, Van den Bossche et al., 2016], des campagnes à court terme [Mishra et al., 2012] et la modélisation de la qualité de l'air [Thunis et al., 2016, Kumar et al., 2011, Lefebvre et al., 2013, Vardoulakis et al., 2003]. Les bio-capteurs, c'est-à-dire les échantillons naturels exposés aux émissions de PM (ou d'autres polluants), constituent également une excellente alternative, offrant une alternative rentable et à faible impact environnemental aux autres capteurs à faible coût. L'utilisation de bio-capteurs n'est pas nouvelle dans les études environnementales. Par exemple, l'exposition de mousse végétale dans des petits filets est utilisée depuis plus de 40 ans pour caractériser les polluants atmosphériques [Ares et al., 2012]. En outre, les bio-capteurs peuvent être utilisés dans les caractérisations magnétiques pour étudier les émissions de particules [Hofman et al., 2017].

Les méthodes de magnétisme environnemental peuvent être appliquées à l'étude des PM puisque les oxydes de fer sont omniprésents parmi les constituants des PM ([Hunt et al., 1984, Flanders, 1994, Chaparro et al., 2020, Winkler et al., 2021]. En outre, les oxydes de fer dans les PM ont été directement associés à des métaux traces, tels que le zinc, le cadmium, le plomb et le chrome, pouvant être incorporés dans la structure minérale pendant la combustion [Moreno et al., 2003, Magiera et al., 2011]. Par conséquent, leurs propriétés magnétiques ne sont pas seulement des proxies pour la concentration de PM, mais présentent un intérêt direct, en raison des conséquences sur la santé de l'exposition humaine aux métaux traces. Les méthodes de magnétisme environnemental sont rentables, faciles à mettre en œuvre et non destructives. Les méthodes de magnétisme environnemental peuvent être appliquées à l'étude des particules dans différents types d'échantillons : de filtres atmosphérique [e.g., Sagnotti et al., 2006, Shi et al., 2014, Leite et al., 2018] utilisés dans l'étude traditionnelle des particules, de poussière déposée [e.g., Kelepertzis et al., 2019, Kim et al., 2009, Liu et al., 2019a, Bourliva et al., 2016], de sédiments [e.g., Franke et al., 2009], de sols [e.g., Hoffmann et al., 1999] et également de bio-capteurs [e.g., Hofman et al., 2017, Sagnotti et al., 2006, Mitchell and Maher, 2009, Chaparro et al., 2020]. Ces différents types d'échantillons permettent une grande flexibilité dans la conception de programmes de surveillance des particules dans divers cadres, environnements et lieux. Les propriétés magnétiques des oxydes de fer permettent de discerner la minéralogie magnétique (c'est-à-dire les porteurs de faible et haute coercivité), les fractions de taille, d'estimer leurs concentrations et leurs proportions relatives [voir par exemple Mitchell and Maher, 2009, Sagnotti et al., 2006, Leite et al., 2021]. Par ailleurs, différentes techniques magnétiques permettent d'étudier les fractions les plus fines d'oxydes de fer, sur la gamme de taille ultrafine allant des PM0.1 (>0.1 μm) aux grains de taille nanométrique [Sagnotti and Winkler, 2012, Mitchell and Maher, 2009, Leite et al., 2018]. Par exemple, le rapport xARM/SIRM permet de déterminer qualitativement la taille des grains dans la gamme des "mono-domaine" pour la magnétite [Maher, 1988], tandis que le protocole SPCDM donne une concentration quantitative pour les magnétites dans des tailles de grains inférieures à $\approx 30nm$ [Leite et al., 2018]. La dépendance en fréquence de la susceptibilité magnétique donne des informations quantitatives sur la variation de la taille des grains pour les magnétites dans la gamme mono-domaine-superparamagnétique [Ustra et al.,

2018]. Ainsi, les propriétés magnétiques des oxydes de fer peuvent être utilisées comme des proxies pour l'ensemble des MP, fournissant des informations complémentaires aux méthodes traditionnelles utilisées dans les enquêtes sur les MP.

Les propriétés magnétiques mesurées sur les bio-capteurs (matières végétales/fongiques, écorce d'arbre, feuilles, mousses, entre autres) peuvent fournir des informations supplémentaires et des données spatiales complémentaires aux stations de surveillance de la qualité de l'air existantes [Hofman and Samson, 2014, Lazić et al., 2016, De Nicola et al., 2013, Mitchell and Maher, 2009]. L'omniprésence des bio-capteurs (feuilles, écorces d'arbres, mousses, lichens) dans la nature offre un moyen rentable et facile d'augmenter la résolution spatiale des méthodes traditionnelles d'investigation de la qualité de l'air. L'impact environnemental de l'utilisation des bio-capteurs est faible, notamment par rapport aux capteurs de particules à faible coût. En outre, les bio-capteurs permettent de concevoir des expériences innovantes, en augmentant la couverture spatiale et temporelle des campagnes et en permettant l'échantillonnage des environnements intérieurs et extérieurs avec le même outil. Compte tenu de leur nature, ils peuvent également être facilement intégrés dans des initiatives de "science citoyenne".

La sensibilisation à l'environnement peut donner la motivation nécessaire pour que soient prises les mesures nécessaires pour s'attaquer aux problèmes environnementaux auxquels nous sommes confrontés [Pihkala, 2020]. La pollution atmosphérique, tout comme le changement climatique, est un problème complexe sans solutions simples, qui nécessite non seulement une action organisée de la part des institutions gouvernementales, mais aussi une participation individuelle et collective de la société dans son ensemble. L'éducation à l'environnement peut alors aider à faire face à ces défis modernes, non seulement en informant la population en dehors du milieu universitaire, mais aussi en proposant des stratégies pour relever ces défis. Cette sensibilisation du public aux principales menaces environnementales de notre époque peut conduire au développement de l'éco-anxiété, qui comprend, entres autres, des symptomes dépressifs et d'anxiété générale ainsi qu'un pessimisme envers l'avenir [Pihkala, 2020, Russell and Oakley, 2016, Cunsolo Willox et al., 2013].

La science citoyenne peut jouer un rôle fondamental dans les études sur la qualité de l'air. Faire de la population un acteur actif de la construction du savoir scientifique conduit à une diffusion des connaissances scientifiques, en sensibilisant le public à la démarche scientifique - à ses réalisations mais aussi à ses limites. À l'ère des "fake-news" concernant plusieurs sujets scientifiques ayant d'énormes implications sociétales, la participation de non-scientifiques au processus scientifique peut constituer un outil essentiel pour la diffusion de divers sujets scientifiques [Irwin, 2018], dont les études sur la qualité de l'air. En outre, la participation à la science citoyenne donne l'occasion aux scientifiques et aux éducateurs environnementaux d'informer le public, en proposant des mesures proactives afin non seulement de traiter le problème étudié, mais aussi d'atténuer et d'orienter l'éco-anxiété qui peut survenir. La plupart des études scientifiques citoyennes sur les particules et la qualité de l'air font appel à des capteurs à faible coût, permettant une plus grande résolution spatiale des études. Mais l'utilisation de ces capteurs à faible coût présente des inconvénients, tels qu'une sensibilité moindre des instruments par rapport aux capteurs de qualité de l'air traditionnels, la nécessité d'une certaine infrastructure (par exemple, la connectivité Internet pour le transfert des données dans certains cas) et l'impact environnemental de la production des capteurs eux-mêmes. Les bio-capteurs, en revanche, peuvent constituer le capteur idéal à faible coût,

puisqu'ils offrent la même qualité de données que les échantillons traditionnels en magnétisme environnemental, sont largement disponibles dans la nature et ont un impact environnemental beaucoup plus faible lié à leur utilisation. Avec la science citoyenne, l'utilisation des bio-capteurs couplée au magnétisme environnemental permet à la fois de bénéficier et d'améliorer les études scientifiques.

1.2.1 Objectifs

Cette thèse combine la surveillance traditionnelle de la qualité de l'air avec l'investigation magnétique dans les bio-capteurs. Les principaux objectifs sont les suivants :

- Évaluer l'utilisation des méthodes magnétiques comme proxies pour suivre les émissions de PM dans un contexte urbain, en utilisant les propriétés magnétiques sur les bio-capteurs et les filtres atmosphériques.
- Suivre les fractions plus fines (fines et ultrafines) d'oxydes de fer présentes dans les PM, en utilisant également des méthodes de microscopie pour compléter les informations fournies par les méthodes magnétiques, en déterminant la morphologie, la taille et la composition élémentaire des particules.
- Evaluer le potentiel des méthodes magnétiques pour suivre les différentes sources d'émission de PM dans le contexte urbain, en ce qui concerne le contenu minéral magnétique, la taille des grains, la minéralogie magnétique et l'influence saisonnière.
- Étudier la qualité de l'air dans l'environnement scolaire, en fonction des espaces intérieurs et extérieurs et de la distance par rapport aux sources d'émission, au moyen de méthodes magnétiques et de méthodes traditionnelles sur la qualité de l'air.
- Étudier la qualité de l'air dans l'environnement domestique d'une ville de taille moyenne en utilisant des bio-capteurs et des méthodes magnétique, la relation entre les environnements intérieurs et extérieurs, les sources d'émission et les habitudes générales de la population.

1.2.2 Présentation de la thèse

Je présente dans cette thèse une série de stratégies d'investigation pour caractériser les particules en suspension dans l'air (PM), qui incluent dans certaines expériences la participation des citoyens. Mes recherches sont basées sur l'utilisation du magnétisme environnemental en considérant les oxydes de fer aéroportés comme proxies pour l'ensemble des PM. Elles s'accompagnent aussi d' d'analyses directes des PM capturées dans les filtres atmosphériques. La participation des citoyens concerne l'étude des environnements domestiques et scolaires dans la ville de Toulouse.

En 2018, nous avons commencé un projet de science citoyenne dans la ville de Toulouse, afin d'enquêter sur la qualité de l'air dans les environnements domestiques et scolaires. A travers de séminaires de vulgarisation scientifique, nous avons sensibilisé la population sur les problématiques liées à la pollution de l'air et aux émissions du trafic. Nous avons recruté

des citoyens intéressés pour participer au projet. Dans les écoles, les discussions ont été faites avec les enseignants et les enfants. Les citoyens qui ont participé au projet ont reçu un kit pour le déploiement de bio-capteurs, qui ont été exposés jusqu'à un an et ramenés plus tard au laboratoire afin d'effectuer des études magnétiques. Une fois l'échantillonnage et les mesures terminés, des séminaires de restitution ont eu lieu afin de présenter et de discuter des résultats avec les habitants participants.

Le premier chapitre est un état des lieux sur les particules, leurs effets sur la santé et l'utilisation des techniques magnétiques pour les étudier. Je commence par contextualiser la problématique des particules, leurs problématiques sanitaires et leurs impacts socio-économiques. Je donne une brève description de leur composition. Ensuite, les dernières directives de l'Organisation mondiale de la santé [WHO, 2021b] en matière d'exposition aux PM sont présentées. L'utilisation du magnétisme environnemental sur l'investigation des PM est ensuite abordée, allant de son utilisation sur l'études des propriétés magnétiques des filtres atmosphériques des PM, en passant par l'utilisation des bio-capteurs sur les études magnétiques, puis les techniques utilisées pour l'étude de la fraction ultrafine des oxydes de fer. Enfin, quelques éléments sur les approches de science citoyenne sont présentés.

Le deuxième chapitre présente un article sur les propriétés magnétiques des filtres atmosphérique PM2.5 en Afrique de l'Ouest (Bénin et Côte d'Ivoire). L'échantillonnage dans la région comprend une campagne hebdomadaire de deux ans, dans quatre sites différents. Chaque site a sa propre source d'émission anthropique principale, des véhicules à deux roues à la combustion de la biomasse. Les propriétés magnétiques des filtres concernent leur minéralogie magnétique, la distribution granulométrique de la fraction ultrafine (magnétite SD) et leur concentration. Les propriétés magnétiques sont liées aux concentrations de particules et d'espèces carbonées mesurées précédemment. Les oxydes de fer en suspension dans l'air ont également été caractérisés pour leurs propriétés superficielles par microscopie électronique à balayage (MEB). Les variations observées dans les propriétés magnétiques sur chaque site étudié au cours de l'étude de deux ans sont liées aux changements saisonniers des caractéristiques météorologiques au fil du temps, et aux scénarios d'émission spécifiques à chaque site. Les différentes sources d'émission ne sont pas sélectives quant à la taille des émissions de particules magnétiques, avec une taille de grain étroite inférieure à 0.1μm.

Le troisième chapitre concerne différents cas d'étude dans la ville de Toulouse, en France. Le chapitre commence par présenter le deuxième article de cette thèse, qui est une enquête sur la qualité de l'air dans l'environnement scolaire. Les échantillons étaient constitués d'écorces d'arbres collectées dans les cours, de bio-capteurs et de filtres atmosphériques PM1 à l'intérieur et à l'extérieur des salles de classe de deux écoles primaires différentes. Les résultats, notamment les concentrations de polluants (concentrations de PM1, de carbone élémentaire et organique) et les paramètres magnétiques (caractérisant la concentration d'oxydes de fer, la minéralogie et la taille des grains) dressent un tableau complet de la qualité de l'air de l'environnement scolaire. Les études MEB ont fourni des informations complémentaires sur les oxydes de fer en suspension dans l'air concernant leurs caractéristiques superficielles, leur composition et leur origine. Ce travail a également inclus des interventions des enfants et du personnel de l'école, présentant ainsi un aspect important de science citoyenne. En continuant sur le sujet des bio-capteurs sur l'étude magnétique des PM, la section suivante présente une étude sur les PM dans l'environnement domestique de la ville de Toulouse dans le cadre du projet NanoEnvi. L'étude magnétique réalisée sur les

bio-capteurs a permis d'obtenir des informations sur les différences entre les environnements intérieurs et extérieurs de la ville. La concentration, la minéralogie et la taille des grains ont été déterminées pour les oxydes de fer en suspension dans l'air, mettant en évidence les principales sources de particules dans l'environnement domestique. Les investigations MEB ont également permis de caractériser la fraction magnétique des PM capturées sur les bio-capteurs. La dernière section de ce chapitre est consacrée à l'application d'une technique permettant de caractériser la fraction superparamagnétique (SP) ultrafine des particules magnétiques sur les bio-capteurs et les écorces d'arbres pour leur granulométrie moyenne et leur concentration dans les PM.

Dans le quatrième chapitre, nous présentons une étude de cas sur les sédiments de la Garonne, collectés le long d'un profil de 50 km centré sur la ville de Toulouse. Une caractérisation magnétique a été effectuée afin d'estimer l'apport anthropogique sur le fleuve, qui a été complétée par une analyse géochimique et des caractérisations MEB. De cette façon, ces résultats, ainsi que ceux rapportés dans le chapitre trois, fournissent une image complète des émissions d'oxydes de fer atmosphériques provenant du trafic routier de la ville de Toulouse, de la façon dont elles se répandent dans les environnements domestiques et scolaires, et enfin de la destination finale d'une partie de ces particules anthropiques, étant emportées dans les cours d'eau.

Dans le dernier chapitre, les principales conclusions du travail sont présentées, ainsi que mon point de vue sur les perspectives du sujet de recherche.

Chapter 2

State of Art

2.1 Particulate Matter problematic

2.1.1 Health Hazards

Air pollution and smoke resulting from anthropogenic combustion have been a problem for human societies since at least the 13th century [Ellison and Waller, 1978], with Evelyn's discourse [Evelyn et al., 1961] reinforcing the consequences of combustion emissions in London's furnaces. The problem of air pollutants' origin, distribution, and health hazards started to be addressed in the 19th century (National Society for Clean Air, 1976). In the 20th century, the reports of severe high concentrations of sulfur oxides and particulate matter in the Meuse Valley (Belgium) in 1930 reached a critical point [Firket, 1936], leading to more vigorous efforts to investigate the provenance and dissemination of the pollutants sulfur oxide and particulate matter in the United Kingdom. Between 1937 and 1939, an intensive survey of a typical industrial town [Meetham, 1945] was conducted. The early investigation above concluded that it was needed to control emissions of anthropogenic pollutants, such as particulate matter. The Second World War disrupted such studies and ideas about curbing emissions. It was only after the disastrous London Fog incident in 1952 that severe official concern was shown again to the health hazards of air pollution. It was shown that at least 4000 more people had died in Greater London during the Fog incident compared to normal conditions [Ellison and Waller, 1978]. The disastrous death toll of the London Fog Incident led to the creation of a committee on air pollution. In its final report, the committee stressed the "urgent need for more precise knowledge regarding the effect of polluted air as a cause of disease and death" (see Committee on air Pollution, 1954). In North America, the first recognized smog incident in Los Angeles took place in 1943 with high PM and ozone levels, and several other incidents took place in the summer months (Fig. 2.1) between 1940 and 1950 [Zhang et al., 2015]. The smog in Los Angeles is characterized by its photo-chemical origin, resulting from the exposure to sunlight of nitrogen oxides (NO_x=NO+NO_2) and volatile organic carbons (VOCs), both originating mainly from traffic sources.

Today, air pollution is a global issue that grew with the development of our modern society, still affecting the human population. For instance, Beijing's economy thrived in the past decades, growing its gross domestic public between 2009 and 2013 by 60%, and by 35% its vehicles fleet in the same period [Zhang et al., 2015, Guo et al., 2014]. Since the

Figure 2.1: Photography of Los Angeles Civic Center covered by smog in 1948. Photo: Los Angeles Times; Photographic Archive/UCLA (http://digital2.library.ucla.edu/viewItem.do?ark=21198/zz0002tsmb). Copyright 1948 Los Angeles Times (http://creativecommons.org/licenses/by/4.0/).)

Table 2.1: Comparison between air pollution characteristics in London, Los Angeles, and Beijing. Source: Zhang et al. [2015].

	London	**Los Angeles**	**Beijing**
type of smog	sulfurous	photochemical	photochemical
observed	1800s to 1950s	1940s to present	1990s to present
meteorological conditions	strong inversion layer, low winds, cloudy, cold, winter	sunny, warm, dry, inversion layer, summertime	low winds typically from the south, year-round
pollutants	SO_2, soot and PM	NO_x, VOCs, ozone and PM	NO_x, VOCs, SO_2 and PM
source of pollutants	coal burning, from house heating and power generation	vehicles	vehicles, coal burning, industrial sources

1990s has suffered from deteriorated air quality [Zhang et al., 2015, Guo et al., 2014], where especially during Winter haze events can be severe due to increased emissions from coal combustion (domestic heating) and unfavorable meteorological conditions (Fig. 2.2). Although the government has implemented significant measures since the 1990s to improve air quality in Beijing, for instance, relocating power plants and industrial factories far from the city and replacing coal with cleaner sources of energy (such as natural gas and electricity), reducing primary PM emissions, fine secondary PM has remained elevated, due to the presence of high levels of gaseous precursors from urban transportation and regional industrial facilities. Air pollution in Beijing is similar to that in Los Angeles but different from that in London, as summarized in Table 2.1. Guo et al. [2014] suggested that critical steps for reducing air pollution in Beijing would be regulatory controls for gaseous emissions of VOCs and NO_x from local transportation and SO_2 from regional industrial sources.

Recently, the link between mortality and exposure to PM pollution was thoroughly investigated. The Harvard Six Cities Study provided evidence about mortality increases related to long-term, low-level exposure to PM [Dockery et al., 1993]. After adjusting the data for smoking and other risk factors, the authors found that PM (especially for PM2.5) was positively associated with lung cancer and cardiopulmonary diseases. The findings from Dockery et al. [1993] were confirmed and expanded in a long-term follow-up, using data from 1982 to 1998 of the American Cancer Society (ACS) II cohort [Pope et al., 1995]. This cohort study included around 500,000 adults from metropolitan areas in the US, and Pope et al. [1995] found that an increase of $10\,\mu g\,m^{-3}$ of PM2.5 elevated the mortality risk of all-cause, cardiopulmonary, and lung cancer, respectively by 6, 9 and 14%. Using the data from the same cohort from the ACS II in the Los Angeles region and with a more sophisticated method for estimating the exposure, it was found a higher risk estimate of mortality of 17% for an increase of $10\,\mu g\,m^{-3}$ PM2.5 concentration [Jerrett et al., 2005]. Other cohort studies in Europe align with the North American ones, estimating PM exposure in individual residences

Figure 2.2: Difference between clean and polluted (covered with smog) days on the Campus of the Peking University, Beijing. Source: Zhang et al. [2015].

and showing that traffic emissions are of most significant concern [Hoek et al., 2002, Nafstad et al., 2004, Filleul et al., 2005] found that PM exposure led to an 8.6-month decrease in life expectancy. Worldwide, PM pollution is responsible for almost 3% of death resulting from cardiopulmonary problems, 5% of lung cancer, and 1% from respiratory infections, leading to 0.8 million premature deaths and a 6.8 decrease in years of life [Fang et al., 2013]. Zanobetti et al. [2014] found out that short-term exposure to PM2.5 is strongly associated with an increase of 1.14% (95% CI:0.56) in diabetes hospitalization risk and 0.64%(95% CI:0.42) on all-mortality risk. In London, the same $10\,\mu g\,m^{-3}$ increase resulted in a 0.5% excess in all mortality cases and 1.6% increase in respiratory mortality [Atkinson et al., 2010].

PM2.5 can translocate directly to the circulatory system and consequently differentiate organs [Dockery and Stone, 2007, Shrey et al., 2011]. PM2.5 also leads to oxidative stress and moderate inflammatory response in the respiratory system after several hours or days of exposure [Simkhovich et al., 2008]. Moreover, PM2.5 interacts with the autonomic nervous system through lung receptors [Shrey et al., 2011, Simkhovich et al., 2008]. Those different pathways of PM2.5 in the body worsen or may lead to pneumonia and systemic irritation, atherosclerosis, and changes in the heartbeat capacity [Sarnat et al., 2005]. Exposure to fine PM pollution has strong links with the augmentation of cardiovascular issues such as myocardial infarction, ischemic strokes, vascular dysfunction, cardiac arrhythmias, and hypertension [Bhatnagar, 2006, Du et al., 2015]. In a study in selected clinical outcomes with more than 50 million people in the USA, death was independently associated with PM, and an increase of $20\,\mu g\,m^{-3}$ in PM concentration led to 0.6% more daily cardiopulmonary mortality [Dominici et al., 2003]. In European cities, the same $20\,\mu g\,m^{-3}$ PM concentration increase led to more than 1.5% cardiopulmonary mortality [Analitis et al., 2006]. Jerrett et al. [2005] found that 20-49% increases coronary artery disease due to a $10\,\mu g\,m^{-3}$ PM2.5 concentration increase on long term exposure. Long-term PM exposure can lead to an augmentation of 24% and 76% on cardiovascular problems and mortality, respectively, due to a $10\,\mu g\,m^{-3}$ PM concentration increase in 6 years [Miller et al., 2007].

PM particles larger than 5 um in diameter are deposited in the superior airways, while finer particles are deposited in the edge of the lungs [Berico et al., 1997]. PM size fraction is essential to health outcomes, as particles smaller than 2.5μm (PM2.5) may penetrate deep into the lung's airways and alveoli, resulting in damage [Andrew Churg, 2000, Athanasios Valavanidis, 2008]. Allergies are a common effect of PM exposure [Nagar et al., 2014]. Moreover, other respiratory symptoms and diseases arise from PM exposure, such as respiratory system malfunction, dyspnea, cough, nose congestion, sore throat, phlegm, reduction in lung function, pain and tightness, and occupational asthma [Nkhama et al., 2015, Peng et al., 2009, Bell et al., 2012, Guaita et al., 2011]. Respiratory troubles, worsening of already present respiratory disease, harm to lung tissue, carcinogenesis, premature death, and changes in the body defense system are also results of exposure to PM pollution [Boman et al., 2006, Lebowitz, 1996, Ali et al., 2017]. A 9% increase in hospital admission due to bronchiolitis was reported in a control case study due to a $10\,\mu g\,m^{-3}$ increase in PM2.5 [Karr et al., 2006].

PM pollution is a carcinogen [Hamra et al., 2014, Tomczak et al., 2016]. A positive correlation has been shown between PM exposition and lung cancer development previously [Hales et al., 2012, Raaschou-Nielsen et al., 2011]. The risk of lung cancer development is enhanced by 11% in consequence of an increase in $10\,\mu g\,m^{-3}$ in PM2.5 concentration [Chen

et al., 2015]. Turner et al. [2011] using the follow-up data from 1100 lung cancer deaths in 26 years, found a 15-27% increase in lung cancer mortality with an increase of $10\,\mu g\,m^{-3}$ in PM2.5 concentration. The same $10\,\mu g\,m^{-3}$ increase in PM2.5 concentration was found by Gharibvand et al. [2017] to increase the hazard ratio (HR) of lung cancer to 1.31 (95% CI 0.87-1.97). Using 17 European cohorts, Raaschou-Nielsen et al. [2013] found a positive correlation between PM and lung cancer incidence, with an HR for PM10 of 1.22 (95% CI 1.03-1.45) and an HR for PM2.5 of 1.18. Long-term exposure to PM pollution in Japan correlated with respiratory disease and lung cancer. In 8.7 years follow-up, the HR increased by 1.24 (95% CI 1.2-1.37) with $10\,\mu g\,m^{-3}$ increase in PM2.5 concentration [Katanoda et al., 2011].

2.1.2 Differences in exposure due to socio-economic causes

Socioeconomic status may play an essential role in either the exposition to air pollutants or health hazards from those pollutants [O'Neill et al., 2003]. The health outcome between socioeconomic status and air pollution exposure has three fundamental premises: i) populations with lower socioeconomic status have higher exposition to pollution; ii) populations with lower socioeconomic status may be more susceptible to health effects from air pollution since they already face material deprivation and psycho-social stress; iii) the combination of the two previous premises may lead to an enhancement of the harmful health effects.

Indeed, it has been reported the relation between increased concentrations of air pollution and lower socioeconomic status in Canada [Jerrett et al., 2001]. Other studies in North America have found that low-income and non-white communities are prone to be closer to sources of pollution [PERLIN et al., 1999, Perlin et al., 2001, Morello-Frosch et al., 2002, Green et al., 2004, Finkelstein et al., 2005]. Gunier et al. [2003] found that low-income and non-white children are more likely to live in block groups with high traffic density in California. But this association between lower socioeconomic status and higher exposure to pollutants varies in each specific regional context, as found in other studies, the opposite relationship between the two. For instance, in Mexico City, it was reported that the O_3 (ozone, important air pollutant) concentration was considerably lower in lower-income regions of the city in comparison to the high-income areas in the same town [Castillejos et al., 1995]. The scavenging could explain this by NO_2 (another air pollutant related to traffic emissions), which is higher in dense traffic areas [Godish and Fu, 2019]. In Rome, higher exposure to air pollutants (especially traffic-related) was also found to higher socioeconomic status, were residences of higher socioeconomic class tend to be closer to higher emission areas, especially central ones [Forastiere et al., 2007].

Some factors may explain the higher health susceptibility arising from pollution exposure in lower socioeconomic populations: patterns of environmental exposure to pollutants; healthy individual behaviors and physical exercise; nutrition; psycho-social stress; medical services accessibility and provision on the regional level (e.g., health clinics, supermarkets, waste disposal); physical environment (traffic burden, crowding, and the accessibility to clean water); and the sociological environment [Kawachi and Berkman, 2003]. In Korea, the hospitalizations due to asthma-related reasons in children increased more in lower socioeconomic status populations in comparison to higher ones, due to the same increase in different pollutants (PM10,SO_2,NO_2,O_3, Lee et al. [2006]). In Rome, even though the exposure to air

pollutants is higher in high socio-economic regions of the city, the increase in mortality is linked to lower incomes and socioeconomic status [Forastiere et al., 2007]. The result in Rome points to a higher susceptibility to disease due to a socioeconomic gradient, in a complex accumulation of risk models during the personal life of each individual. In Hamilton, Canada, it was found by Jerrett et al. [2004] higher health consequences due to air pollution exposure in lower-income regions of the city, where the exposure to pollutants is higher.

2.1.3 Economic consequences

The health hazards associated with air pollution and PM exposure will have consequences in morbidity and mortality of the population, and those health consequences result in financial and non-financial welfare losses. Two fundamental principles are used to evaluate the cost related to the health consequences of PM exposure: human capital in mortality effects and cost of illness (COI) in morbidity effects. Human capital places value on premature death, taking into account the net economic productivity of an individual and what would be generated had the individual not died prematurely. Similarly, the COI considers the lost wages and productivity as a consequence of missed days of work or lower productivity due to disease and the cost of treating illness [El-Fadel and Massoud, 2000]. El-Fadel and Massoud [2000], using the city of Beirut as an example, estimated the economic benefits of a PM10 reduction in the concentration of $10\,\mu g\,m^{-3}$ to be between 0.27-12.6MU$ (million American dollars)/year for mortality cases. An economic benefit related to morbidity costs for the same PM10 concentration reduction is 0.14-3.2MU$/year. In Korea, using the same COI method, Nguyen et al. [2017] estimated the economic gains related to curbing PM2.5 and PM10 reduction in the subway system. They used two health endpoints, all lung cancer and cardiovascular disease, to curate $10\,\mu g\,m^{-3}$ in PM2.5 and PM 10 concentrations. They found that the total annual cost savings were 328.2 M KRW (million Korean won), or 124.2 M KRW indirect costs, 186.4 M KRW in premature mortality, and 17.6 M KRW in productivity loss costs, respectively.

In 2013, a study [Bank et al., 2016] estimated global economic impacts of US$143 billion due to lost labor income and US$3.55 trillion in welfare losses due to PM2.5 exposure. In low-income countries, the welfare losses are roughly equal to 1% of the gross domestic product, whereas, in high-income countries (not within the Organisation of Economic Co-operation and Development), it reaches 5% of the gross domestic product. Such substantial economic losses are due to health-related burdens, agricultural impact on crops, damage to infrastructure and buildings, and environmental degradation.

2.1.4 PM origins and composition

PM can be either directly released in the atmosphere (primary) or formed in the atmosphere through gas-to-particle conversions (secondary) [Zhang et al., 2015]. PM primary emissions have anthropogenic and natural origins, and urban direct PM is mainly formed due to anthropogenic processes. In the urban context, primary sources of PM include vehicle emissions (including an exhaust and non-exhaust emissions), industrial fuel combustion, domestic heating, cooking, biomass burning, and paved-road dust re-suspension, among others. Among its constituents, PM has inorganic ions (e.g., ammonium, nitrates, sulfates, and soluble metals), insoluble metals, elemental carbon, organic compounds, biological components, microbial

agents, and water [Kim et al., 2015, Zhang et al., 2015]. PM particle sizes range from a few nanometers to hundreds of micrometers. Its maximum particle size can define it, for instance, PM10 or PM2.5, for particles with aerodynamic size inferior to 10μm and 2.5μm, respectively. The PM fraction with the anthropogenic origin is the most harmful one for human health due to the presence of potentially toxic elements such as As, Cd, Cr, Pb, V, and Zn, besides being found mainly in the finer fraction of PM [Clements et al., 2014], which in itself are more dangerous for health than the coarse ones since they can penetrate more profound in the biological systems [Pope III and Dockery, 2006].

2.1.5 World Health Organization global air quality guidelines

In 2021 the World Health Organization [WHO, 2021b] released a new report on global air quality guidelines (AQG), updating the previous one released in 2006 [WHO, 2006]. Starting in 1987, the WHO has periodically released health-based air guidelines to assist governments and civil society in curbing human exposure to air pollution and its adverse effects. Although there have been remarkable improvements in air quality, global mortality and morbidity due to air pollution exposure have barely declined since the 1990s. The advances in air quality were registered mainly in high-income countries. In contrast, in low to middle-income countries, the air quality has fallen in this time frame, following broad urbanization and economic development. The updated 2021 guideline provides interim targets and recommended air quality levels for the air pollutants: PM2.5, PM10, ozone, nitrogen dioxide, sulfur dioxide, and carbon monoxide. The health benefits of each interim target's consecutive achievement are also provided. Here are the guidelines for PM2.5 and PM10, the subject of this thesis, in Table 2.2.

Table 2.2: Interim targets and air quality guidelines for PM2.5 and PM10 concentrations, for annual and daily exposure. Source:WHO [2021b]. [a]99th percentile (i.e. 3-4 exceeding days per year).

Pollutant	Averaging time	Interim target				AGQ levels
		1	2	3	4	
PM2.5($\mu g\,m^{-3}$)	Annual	35	25	15	10	5
	24-hour[a]	75	50	37.5	25	15
PM10($\mu g\,m^{-3}$)	Annual	70	50	30	20	15
	24-hour[a]	150	100	75	50	45

2.1.6 Air quality in indoor and outdoor environments

Although many epidemiology studies for outdoor air pollution use the concentration outdoors as a stress indicator, the indoor concentration is also of major importance for human exposure estimation, as people spend up to 90% of their time indoors [Klepeis et al., 2001, Schweizer et al., 2007]. Only using outdoor concentrations of PM and other air pollutants may introduce errors in the real exposure and health risks caused by indoor air pollution. Consequently, some authors raised concern about using ambient concentrations as a proxy for personal exposure studies [Avery et al., 2010, Wilson and Brauer, 2006]. Indoor environments may

have important air pollution sources, such as cooking [Sclar and Saikawa, 2019, Sharma and Jain, 2019, Tong et al., 2016], heating [Maher et al., 2021, Sclar and Saikawa, 2019], cleaning habits [both from resuspension and use of cleaning products, Kalimeri et al., 2016, Huang et al., 2015], burning sources [smoking, incense burning, Sclar and Saikawa, 2019, Huang et al., 2015], among others, besides the penetration of outdoor pollutants [Huang et al., 2015]. Some authors investigated the correlation between outdoor and indoor air pollutants. Kalimeri et al. [2016] found in two schools in Greece, the indoor PM levels are derived from outdoor sources (such as traffic) and resuspension from the student's activities. Even though the windows are open between classes, a poor air ventilation rate was detected, but rarely during classes in the cold season. Volatile organic carbons (VOCs) were detected, mostly from indoor sources such as cleaning products, books, furniture, office equipment, occupant's activities, and wall covering, among others. In Beijing, Huang et al. [2015] analyzed 24-h real-time indoor and ambient PM2.5 concentrations in 41 residences for two months. The strong correlation ($r>0.9$, $p<0.0001$) between indoor and outdoor PM2.5 concentrations and the higher outdoor PM2.5 concentrations (with a median I/O concentration ratio of 0.61) points to the main source of indoor PM2.5 concentration outdoor emissions, with minor indoor influences. Using regression analysis, they found that the main factors influencing indoor PM2.5 concentrations are traffic conditions, indoor smoking, indoor cleaning, indoor plants, and the number of occupants. Besides, the large inter-variability of the infiltration factor of outdoor PM2.5 raises concerns of misclassification when using the outdoor PM2.5 mass concentration as a proxy for the indoor one. On office environments, PM2.5 I/O ratios below unity found on several studies [I/O ratios of 0.62, 0.53, 0.86, 0.62, respectively for Kalimeri et al., 2019, Zhu et al., 2015, Niu et al., 2015, Sangiorgi et al., 2013] points to the dominance of outdoor emissions on indoor environments. Conversely, in the school environment, higher PM2.5 I/O concentration ratios (1.44) [Kalimeri et al., 2019] show a different context from the office environment, where particularities such as resuspension and indoor sources such as crafting increase indoor PM2.5 concentrations. Indoor sources may play a fundamental role in indoor air quality and pollutant concentration. Maher et al. [2021] found that the use of solid fuels in open fires (as a heating source, for instance) lead to mass PM2.5 emissions of 60, 30, and 17µg m^{-3} for the use of peat, coal, and wood, respectively. Solid biomass burning may be used for heating and cooking. In rural India, Sharma and Jain [2019] showed that different kitchen (which utilize biomass solid fuels) designs may damper indoor PM concentrations between 15-6%, 14-61% and 20-68% for PM10, PM2.5 and PM1 respectively. In Tibet, Sclar and Saikawa [2019] found high concentrations of indoor PM2.5 in sedentary homes and nomad tents due to the burning of yak dung, among other habits. In measurements of up to 4h, the average PM2.5 concentrations inside nomad tents and sedentary homes were respectively 2286 and 509µg m^{-3}. In Hong Kong, Tong et al. [2016] found in elderly households that are cooking and incense burning are the main sources of indoor PM2.5, with 50.3% of the investigated households having PM concentrations higher than the WHO indoor air quality standard for PM2.5 concentration. Proper kitchen ventilation during cooking positively impacts indoor air pollutants concentration. The cited examples show different contexts for sources and emissions of indoor pollutants, and each specific context plays a role in the indoor air quality and pollutants concentration. The question of indoor air pollution and sources and its relationship with outdoor air pollution is rather complex. Each case will have particularities that should be investigated to properly characterize exposure to air pollutants

(such as PM, VOC, etc.) within a particular case scenario.

2.2 Environmental magnetism

2.2.1 Environmental magnetism in PM investigation

Environmental magnetism has been used in PM investigations for some decades now. Early works analyzed directly magnetic particulate sampled on PM filters. Using magnetic susceptibility, anhysteretic remanent magnetization (ARM) and isothermal remanent magnetization (IRM) acquisitions Hunt et al. [1984] investigated power station fly ashes and motor vehicle emissions, finding higher concentrations of hard coercivity carriers in power station fly ash in the superparamagnetic-stable single domain boundary with a distinct viscosity.

As the use of magnetic methods in the investigation of anthropogenic emissions grew, innovative analysis techniques were proposed. With the coercivity distribution of ARM demagnetization curves of the ARM and using a linear combination of appropriate functions, Spassov et al. [2004] found different magnetic sources for the total magnetization. They found two main components, characterized by low coercivity and a higher coercivity, linked to less polluted and large urban sites, respectively. Chemical analysis and quantitative source attribution to the PM were carried out on the same sites. The higher coercivity fraction's absolute and relative magnetic contributions correlate very well with exhaust emissions' absolute and relative mass contributions.

Concentrations of air pollutants were correlated with magnetic parameters linked to the concentration of iron oxides, showing that the magnetic fraction may as well be used as a proxy for the whole of PM. Sagnotti et al. [2006] found strong empirical correlations between PM10 and magnetic susceptibility on filters from the Latium region. An experimental procedure to estimate the percentage of non-magnetic PM10 transported long distances is also presented. The magnetic mineralogy in PM10 is dominated by low-coercivity magnetite-like particles, with a varied granulometry source dependent. The anthropogenic magnetic fraction present in PM10 was dominated by fine superparamagnetic (SP) mixed with large multidomain (MD) grains. The SP fraction was found to be linked to exhaust emissions, and the MD fraction was linked to the abrasion of metallic parts. Using PM2.5 and PM10 filters, Saragnese et al. [2011] also found a close correlation between the magnetic moment calculated in their work with total nitrogen oxides, suggesting that the majoritarian iron oxides present in PM originate in combustion processes. Saragnese et al. [2011] also proposed low-temperature measurements to estimate different magnetic granulometry fractions. The magnetic protocol included the acquisition of SIRM at room temperature and 77K. It was also performed stepwise IRM acquisition in both room and 77K temperatures to characterize magnetic mineralogy. Magnetite-like low coercivity carriers dominated the magnetic mineralogy with a minor contribution of high coercivity carriers, hypothesized to be the result of the oxidation of the smallest magnetite grains. Magnetic granulometry is in the SP-SD range, with the prevalence of SP particles observed in the magnetic measurements and the SEM investigation. SEM investigation identified a spherical shape for the Fe-rich particles, with the presence of other metals in the spherules identified by the energy dispersive X-ray elemental analysis.

Magnetic properties of PM can also point out differences related to traffic emissions and other emissions in PM. For instance, Winkler et al. [2021], analyzing PM10 air filters from Rome during the covid lockdown of 2020 and after the relaxing of measures found a difference between the correlation of magnetic susceptibility during and PM10 concentration during and after lockdown. Magnetic susceptibility reflected the changes in the traffic regime, whereas PM10 remained at similar levels.

Information about the provenance of the magnetic grains (for instance, from magnetic mineralogy), grain size fractions and variations (from domain states, low-temperature measurements), and concentrations are reached through the use of magnetic methods in PM investigation and air quality studies, complementing traditional investigations (based on the direct analysis of PM and other air pollutants).

2.2.2 Bio-sensors in environmental magnetism investigations

Besides using PM selective air filters, magnetic methods have been widely used on bio-sensors, i.e., biological samples exposed to air capable of retaining PM and airborne iron oxides on their surface [Hofman et al., 2017]. The bio-sensors provide time-integrated and location-specific information on air quality. Sensors in magnetic investigations comprise vegetable/Funghi matter (mosses and lichens, plant leaves, bark, and wood) and animal matter (insects, crustaceans, mammal tissue, including human tissue). Samples from human provenance can trace the impact of airborne pollution on human health, for instance, being detected in the frontal cortex of human brains [Maher et al., 2016] and brainstems [Calderón-Garcidueñas et al., 2020]. Bio-sensors from vegetable/Funghi provenance provide a cheap, environmentally friendly alternative to other air pollution sensors, besides being ubiquitously present [Hofman et al., 2017]. Vegetable/Funghi collectors may be collected in situ (for instance, collecting tree leaf, as in Fusaro et al. [2021]) or moved into another sampling site (for example, introducing previously collected mosses, as in Chaparro et al. [2020]). Using diverse vegetable bio-sensors (lichens, mosses, poplar leaves, dandelions, and needles) Jordanova et al. [2010] investigated clean and polluted sites with an industrial profile. When comparing the different collectors, they found that lichens and mosses were the ones with the highest capacity for trapping the magnetic fraction of PM, with mean SIRM values on clean and polluted sites of $396.32 \times 10^{-6}\,\mathrm{A\,m^2\,kg^{-1}}$ and $996.62 \times 10^{-6}\,\mathrm{A\,m^2\,kg^{-1}}$. In contrast, poplar and dandelions have means of $16.67 \times 10^{-6}\,\mathrm{A\,m^2\,kg^{-1}}$ and $173.17 \times 10^{-6}\,\mathrm{A\,m^2\,kg^{-1}}$ on the same sites.

In formal investigations, mosses and lichens have been used for over 40 years as environmental biomonitors through bulk-chemical (ICP-MS, for instance) and particle-based characterizations (SEM-EDX). Different species have different capacities to retain airborne pollution particles. Due to their high accumulation capacity and surface-to-volume ratio, they are suitable for magnetic investigation of airborne pollution (Fig. 2.3). Chaparro [2021], using three different species of pollution tolerant lichens, could detect the magnetic enhancement of the bio-sensors, and posterior decontamination in situ, due to rainfall. Using lichens *Evernia prunastri* exposed to traffic sources in Milan, Winkler et al. [2020] found strong correlations between magnetic susceptibility and trace elements concentration of Fe, Cr, Cu, and Sb. SEM and EDX microanalysis confirmed the anthropogenic, non-exhaust origin of the analyzed particles due to their composition, morphology, and grain size.

Figure 2.3: Moss bag as a PM bio-sensor in place. Source: Winkler et al. [2020].

Plant leaves have a large surface area, making them suitable for magnetic investigations. Indeed, numerous studies have used magnetic properties on plant leaves as monitors of air pollution [Hofman et al., 2017]. Like lichens and mosses, different species of plant leaves have different capacities for accumulating particulate material due to differences and specificities in their morphology, phenology, and specific leaf characteristics (area density, wax layer, micro surface roughness, presence of trichomes), among others. Measured SIRM on leaves have a large variation, from 0.002 to $27.50 \times 10^{-3}\,\mathrm{A\,m^2\,kg^{-1}}$ (mass normalized) or 4.17×10^{-10} to 777×10^{-6}A (area normalized, Hofman et al. [2017]). Leaf magnetic particle concentration is related to exposure time [Lehndorff et al., 2006, Hofman and Samson, 2014], source distance [Matzka and Maher, 1999, Moreno et al., 2003, Szönyi et al., 2008], source strength [Kardel et al., 2012] and leaf sampling height [Mitchell et al., 2010, Hofman and Samson, 2014]. To investigate functional damage on plant leaves by PM, Fusaro et al. [2021] used a series of joint magnetic properties, trace elemental composition, and morpho-functional traits measurements. Magnetic properties found on the leaves refer to the traffic on-exhaust origins of airborne iron oxides. The magnetic susceptibility had a tight positive correlation with trace metals found on the leaves' surface. PM affected functional traits related to the first photochemical process reactions, suggesting a shading effect on leaves.

Tree bark and trunk wood (Fig. 2.4) are generally exposed to atmospheric pollution for longer time frames than tree leaves (year-round or even longer). However, the exact duration of exposure may not be simple to infer. Mass normalized magnetic parameters in tree bark are generally lower than in leaves due to its higher mass to area ratio. But its normalized surface parameters are comparable to or even higher than leaves due to the longer exposition time frames. Using tree branches of the *Platanus x acefolia Willd*, Wuyts et al. [2018] found SIRM values ranging from 18 to 650×10^{-6}A (area normalized), with a median calculated at 106×10^{-6}A. Median SIRM values were up to 135% higher on busy roads than in quieter environments such as city parks or quiet street canyons. The samples on busy roads had the presence of Fe-rich particles and trace metals such as Cr, Cu, Zn, and Mn on the surface. Values of SIRM varied within the branches, increasing with each year of exposure. Within the crown, SIRM branch values generally decreased with crown height. Using in situ measurements, Chaparro [2021] investigated magnetic properties of PM collected on street tree barks in Buenos Aires, showing that the magnetic fraction of PM has mostly traffic origins, dominated by magnetic carriers of low coercivity with ultrafine size range (sub-micron). The iron oxides trapped on the tree barks possessed toxic trace elements such as Ba, Cr, Cu, Mo, Ni, Pb, Sb, Sn, V, Zn, Al, Si, Ca, Ti, and Ce.

2.2.3 Magnetic ultrafine concentration quantification

The ultrafine fraction of the iron oxides is ubiquitously present in rocks, sediments, and airborne particles. They may be formed in particular natural and anthropogenic processes. In the scope of this thesis, we consider the anthropogenic airborne fraction, firstly as proxies of fine and ultrafine PM, but also because the airborne iron oxides (especially the ultrafine ones) may themselves pose health hazards, as previously discussed.

The ultrafine fraction of the magnetic minerals may be defined as the one spanning the Superparamagnetic (SP) and Stable Single Domain (SSD) range [Wang et al., 2010]. The SSD range is characterized by its time-stable magnetic remanence (on a geological time-

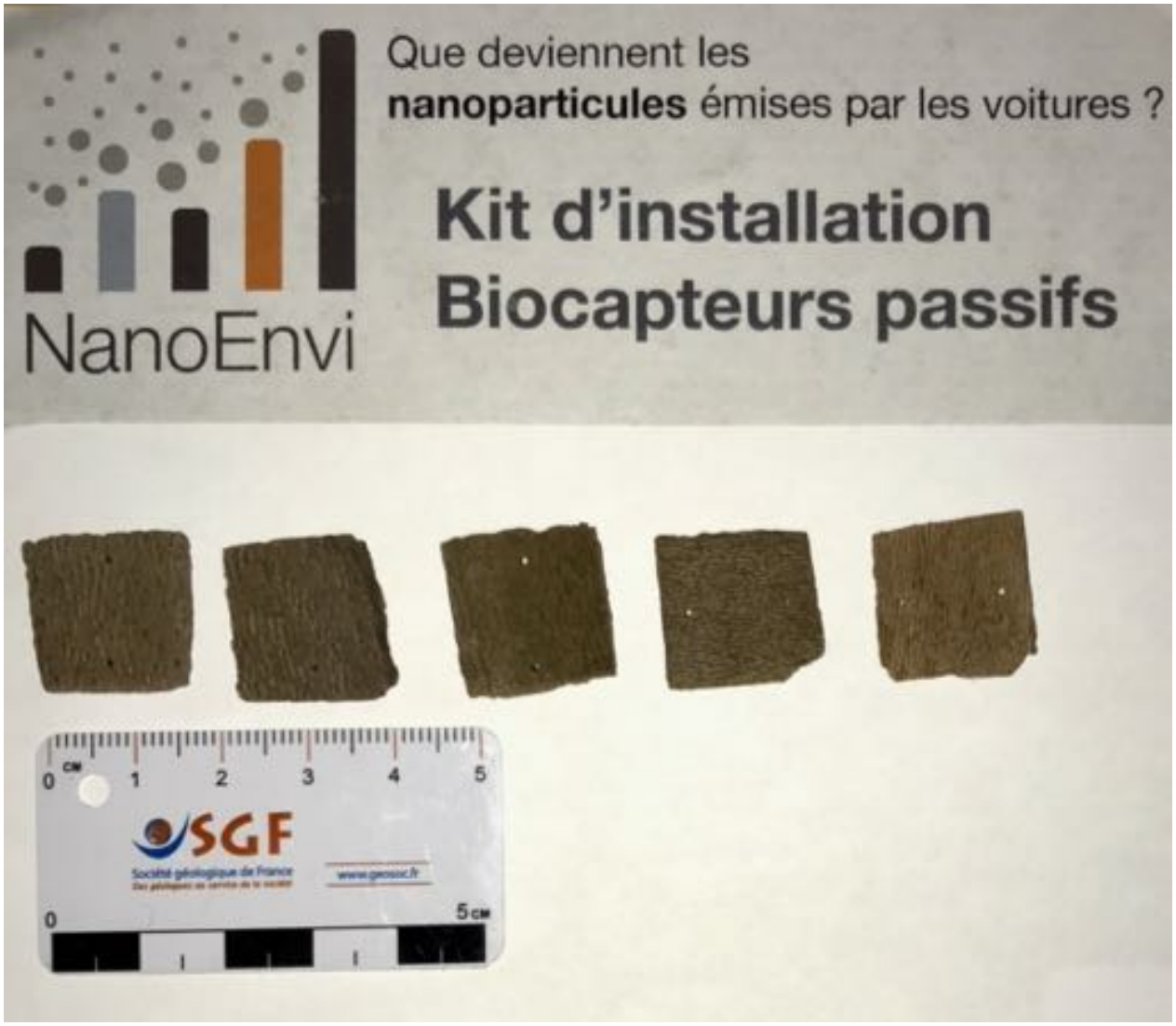

Figure 2.4: Tree bark is used as bio-sensors in the frame of the Nanoenvi project. The five wood pieces (linked by a nylon thread) would be hung and exposed indoors or outdoors in domestic environments. Photo by the author.

scale), which arises from the internal magnetic moment in the mineral, organizing itself in one domain (hence the name). The SP fraction is contained in the SSD range. Still, due to its small grain size, the magnetic energy is comparable to the thermal one on the mineral grain, which leads the magnetic moments towards disorganization, resulting in an unstable magnetization over the observation time. The time scale in which the SP fraction relaxes its remanence is in the order of seconds or less. The transition between the SP behavior and the SSD stability has a characteristic viscous time remanence, in the order of seconds to tens of seconds. Due to the exponential characteristic of the relaxation time, small variations in grain size result in large variations in the relaxation time. We can then separate the SP fraction into the one with nearly instantaneous relaxation time and the one with viscous decay in the order of seconds (SP and VSP, for Superparamagnetic and Viscous superparamagnetic). Regarding its size, for an equidimensional magnetite mineral at 20°C, the SP behavior is observed for diameters inferior to 0.025-0.03 $\mu g\,m^{-3}$, and the SSD threshold is observed just until 0.05-0.06 $\mu g\,m^{-3}$ [Dunlop and Özdemir, 2001].

The SP content is generally identified through the frequency effect on the magnetic susceptibility [Dearing et al., 1996], from measurements achieved in at least two frequencies (470 and 4700Hz, for Bartington Instruments Ltd). When the SP fraction is absent, the variation of the magnetic susceptibility with frequency is negligible, so the frequency effect is zero (the difference of measurement between both frequencies). In the time domain, the relaxation of the remanence may be used to estimate the concentration of the SP content after turning off the induction field. This kind of measurement requires an adequate time window and resolution to characterize the decaying magnetization properly. Worm [1998] proposed a IRM time decay acquisition to characterize the ultrafine fraction, introducing a viscous decay coefficient $S_d = \frac{(IRM_{15s}) - IRM_{2000s}}{log\frac{2000s}{15s}}$, where IRM_{15s} and IRM_{2000s} where the IRM after respectively 15s and 2000s from the induction. This time frame was used due to instrument limitation, and from the relaxation time from the SP fraction is evident that it is not adequate to characterize it. Machac et al. [2007] improved on the protocol proposed by Worm [1998], introducing a set of time intervals and field intensities. A close association was found between the time and frequency domain percentage parameters. This experiment's time frame of 60s was used, which is still too large for SP decay rates. Wang et al. [2010] proposed a new protocol, using a J-meter coercivity spectrometer [Jasonov et al., 1998], which allowed for remanence measurements just after turning off the induction field. They propose a relative contribution of the SP fractions to the total remanence $J_v\% = 100 \times \frac{(Jr_{0s} - Jr_{100s})}{Jr_{0s}}$, where Jr_{0s} is the remanence just after turning off the induction field and Jr_{100s} the final remanence after 100s. The $J_v\%$ parameter, expressed as it is, is a semi-quantitative concentration parameter. By fitting the Langevin function in the magnetization curve, Leite et al. [2018] proposed a new method of estimating the concentration of ultrafine magnetic carriers with a priori information of the mineral family. Using different levels of magnetic induction in a VSM and posterior magnetization relaxation after the external field is turned off, it is possible to separate the remanence of the SSD fraction present in a given sample and then use the different levels to feed an inverse problem based on the Néel model of superparamagnetism [Néel, 1955], obtaining the individual magnetic moment for a carrier and its saturation magnetization, and from its constitutive relationship a numeric concentration of individual carriers of fast magnetization decay. Using the individual magnetic moment can also calculate a mean volume for the

carriers in a sample. The method, Superparamagnetic Concentration and Dipole Moment [SPCDM Leite et al., 2018] presented excellent results when applied in synthetic nanoscaled ($\sim 8nm$) magnetite samples with a known concentration. This method has much in common with previous methods that used Langevin fitting to calculate the individual magnetic moments and their volumes, such as Berkov et al. [2000] and Woodward et al. [2007]. Still, it is innovative in how it expands it to calculate numeric concentrations of ultrafine magnetic carriers, which was done in relative and semi-quantitative ways in previous works.

2.3 Citizen science participation

The term "citizen science" is used to describe scientific investigations done in contributory, collaborative, and co-created with amateur or citizen scientists [Bonney et al., 2009]. The participation of citizen scientists is embroiled in the history of science, as before the 19th century, almost all research was conducted by amateurs, or people not who were not paid as scientists [Vetter, 2011]. Citizen science projects bring clear benefits for scientists, such as access to more extensive databases that wouldn't be possible otherwise [De Craemer et al., 2020], data points in hardly accessible locations) and helping with the processing of comprehensive databases [Fritz et al., 2013]. Moreover, citizen science research projects may have an essential role in the vulgarization and sensibilization of necessary scientific inquiries, allowing populations from different backgrounds and cultures to use science to tackle community-driven questions [Bonney et al., 2014]. Citizen science projects also bring to the general public scientific literacy and nurture their curiosity in science [Miller-Rushing et al., 2012].

Citizen science investigations have been widely used on air quality monitoring [Varaden et al., 2021, Hsu et al., 2017, Mahajan et al., 2020, 2021, West et al., 2020]. Using low-cost sensors allows for massive deployment between citizens, given information at the neighborhood and city scales [Perelló et al., 2021]. Air quality studies may benefit from the citizen science approach since the awareness brought to the population may be an important tool in addressing the intangibility of the air pollution problem, which is virtually invisible [Varaden et al., 2021].

Chapter 3

PM2.5 magnetic properties in relation to combustion sources in Southern West Africa

3.1 Contextualization

This chapter presents the magnetic investigation of PM2.5 from different urban sources in West Africa. This investigation took place in the cities of Abidjan (Ivory Coast) and Cotonou (Benin), where PM emissions are a source of concern. The weather in this region is characterized by the African Monsoon, with distinct dry and wet seasons. Four sites with different PM emission contexts linked to other urban sources (two-wheeled gasoline vehicles, four-wheeled diesel vehicles, waste burning, and biomass burning) were subject to the investigation using PM2.5 air filters. The data regarding PM2.5, EC, and OC concentrations and optical depth were published by Djossou et al. [2018]. The sampling done comprehends a two-year campaign with weekly PM2.5 air filters. It was published as a scientific article in the Journal Atmosphere (MDPI) in 2021 as A. d. S. Leite, J.-F. Léon, M. Macouin, S. Rousse, R. I. F. d. Trindade, A. Proietti, L. Drigo, P. Y. J. Antonio, A. B. Akpo, V. Yoboué, et al. Pm2. 5 magnetic properties about urban combustion sources in southwest Africa. Atmosphere, 12(4):496, 2021. doi: 10.3390/atmos12040496.

3.2 PM2.5 Magnetic Properties in Relation to Urban Combustion Sources in southern West Africa

A. da Silva Leite [1]****, J.-F. Léon*** [2]***, M. Macouin***[1]***, S. Rousse*** [1]***, R. I. F. da Trindade***[3]***, A. Proietti***[4]***, L. Drigo***[1]***, P. Y. J. Antonio***[3]***, A. B. Akpo***[5]***, V. Yoboué***[6] ***and C. Liousse***[2]

[1] *Géosciences Environnement Toulouse, Université de Toulouse, CNES, CNRS, IRD, UPS, (Toulouse) France; melina.macouin@get.omp.eu, sonia.rousse@get.omp.eu, loic.drigo@get.omp.eu*

[2] *Laboratoire d'Aérologie, Université Paul Sabatier-Toulouse 3, CNRS, Toulouse, France; jean-francois.leon@aero.obs-mip.fr, cathy.leal-liousse@aero.obs-mip.fr*

[3] *Universidade de São Paulo, Instituto de Astronomia, Geofísica e Ciências Atmosféricas, São Paulo, Brasil; ricardo.trindade@iag.usp.br, paulantonio0931@gmail.com*

[4] *Centre De Microcaractérisation Raimond Castaing, Toulouse, France; arnaud.proietti@ums-castaing.fr*

[5] *Laboratoire de Physique du Rayonnement, Université d'Abomey Calavi, BP 526, Cotonou, Bénin; akpoarist@yahoo.fr*

[6] *Laboratoire de Physique de l'atmosphère, Université Félix-Houphouët-Boigny, Abidjan, Côte d'Ivoire; yobouevero1@gmail.com*

**Correspondence: arualeite@gmail.com; Tel.: +33-06 34 38 78 55*

Abstract: The physicochemical characteristics of particulate matter (PM) in African cities remain poorly known due to the scarcity of observation networks. Magnetic parameters of PM are robust proxies for the emissions of Fe-bearing particles. This study reports the first magnetic investigation of PM2.5 (PM with aerodynamic size below 2.5μm) in Africa performed on weekly PM2.5 filters collected in Abidjan (Ivory Coast) and Cotonou (Benin) between 2015 and 2017. The magnetic mineralogy is dominated by magnetite-like low coercivity minerals. Mass normalized SIRM are $1.65 \times 10^{-2}\,\mathrm{A\,m^2\,kg^{-1}}$ and $2.28 \times 10^{-2}\,\mathrm{A\,m^2\,kg^{-1}}$ for Abidjan and Cotonou respectively. Hard coercivity material (S-ratio=0.96 and MDF=33 mT) is observed during the dry, dusty season. Wood burning emits fewer iron oxides by PM2.5 mass when compared to traffic sources. PM2.5 magnetic granulometry has a narrow range regardless of the site or season. The excellent correlation between the site-averaged element carbon concentrations and SIRM suggests that PM2.5 magnetic parameters are linked to primary particulate emission from combustion sources.

Keywords: Environmental magnetism; Air pollution; PM composition

3.3 Introduction

Ambient Particulate Matter (PM) is a complex mixture of solid and liquid particles in suspension in the air [Seinfeld and Pandis, 2016]. The adverse health effect of PM has been established in epidemiological studies over recent decades [Pope III and Dockery, 2006, Dockery and Pope, 1994, Cohen et al., 2017, Burnett et al., 2018]. In terms of hazardousness,

the finer fractions of PM are the ones most nocive to human health [Pope III and Dockery, 2006, Martins et al., 2020]. A common definition for the finer fraction of PM is particles with aerodynamic size inferior to 2.5 μm, known as PM2.5 [Pope III and Dockery, 2006]. PM2.5 was the fifth-ranking mortality risk factor in 2015 leading to 4.2 million deaths worldwide [Cohen et al., 2017]. Regional decreases in PM2.5 concentrations have been observed over the last decade in China [Yin et al., 2020] or in the USA, except in wildfire-prone areas [McClure and Jaffe, 2018]. Conversely, low and middle-income countries experience an increase in the emission of atmospheric pollutants, including PM2.5 due to population and economic growth [Anenberg et al., 2019]. The population of sub-Saharan Africa (SSA) is projected to double by 2050 [United Nations and Social Affairs, 2019] associated with growing urbanization [United Nations and Social Affairs, 2014] and rapid increase in energy consumption, making SSA a major hot spot of anthropogenic emissions in the near future. Liousse et al. [2014] has estimated that Africa will contribute to half of the global emission of particulate organic carbon in 2030. Carbonaceous particles (elemental and organic carbon) are emitted by combustion due to transportation, the use of biofuels or agricultural waste for domestic cooking, and open-air waste burning [Keita et al., 2018]. Open biomass burning originating from agricultural practices and savanna burning also contributes to the urban PM2.5 burden in SSA [Junker and Liousse, 2008, Menut et al., 2018]. SSA is largely impacted by mineral dust transported by the northeasterly Harmattan wind during the dry winter period [Afeti and Resch, 2000]. Dust is a major contributor to PM all year long [Adon et al., 2020]. It is responsible for sharp increases in PM during outbreaks reaching the Gulf of Guinea [Djossou et al., 2018, Léon et al., 2021].

Most of the urban areas in SSA lack an air quality network, leaving large, densely populated areas without PM observations. Our ability to fully understand and quantify the impact of PM levels in SSA cities is currently limited by the scarcity of monitoring data. The Dynamic Aerosol–Cloud–Chemistry Interaction in West Africa (DACCIWA) research program investigated the possible role of local air pollution in climate change in West Africa, providing an unprecedented set of observations on the PM concentrations and chemical composition in the South West African cities of Abidjan (Ivory Coast) and Cotonou (Benin) [Knippertz et al., 2015a]. PM2.5 mass and carbonaceous fraction were measured on a weekly basis at both cities between 2015 and 2017 [Djossou et al., 2018]. The measurements were targeted towards the characterization of urban aerosols from specific combustion sources [Adon et al., 2020] and the assessment of personal exposure of nearby populations [Xu et al., 2019].

As an alternative to standard PM sampling, environmental magnetism has been proven to be a robust, quantitative technique for identifying ambient concentrations of anthropogenic PM [Dekkers et al., 2004, Hofman et al., 2017]. Iron oxides contained in PM offer the possibility to investigate PM concentrations through their magnetic properties. Magnetic susceptibility, which relates to iron oxides concentration, may have a linear relationship with PM concentration [Sagnotti et al., 2006, Castañeda-Miranda et al., 2014]. Several studies conducted in European cities established that the magnetic fraction present in urban PM is mostly composed of ferrimagnetic soft coercive magnetite-like grains [Muxworthy et al., 2001, Sagnotti et al., 2006, Mitchell and Maher, 2009, McIntosh et al., 2007, Spassov et al., 2004, Saragnese et al., 2011, Revuelta et al., 2014, Jordanova et al., 2014, Mantovani et al., 2018]. These iron oxides present in PM have a natural and anthropogenic origin. Early works in environmental magnetism demonstrated the potential of magnetic methods to successfully

differentiate these sources [Hunt et al., 1984, Chester et al., 1984, Hunt, 1986]. These methods enable to identify the magnetic minerals [Shu et al., 2001, Spassov et al., 2004, Saragnese et al., 2011], the magnetic domain state which relates to grain size of the iron oxides [Shu et al., 2001, Saragnese et al., 2011], and concentration of magnetic carriers [Sagnotti et al., 2006, Castañeda-Miranda et al., 2014]. Iron oxides are often associated with nitrogen oxides [Saragnese et al., 2011, Jordanova et al., 2014] as well as heavy metals [Shu et al., 2001, Revuelta et al., 2014, Jordanova et al., 2014] known to be among the most harmful constituents of particulate matter [Di Gilio et al., 2017]. Iron oxides have also been found among soot [Shi et al., 2015]. The magnetic fraction of traffic emission particles is generated by the combustion of fossil fuels and vehicle wear, especially by brake disk abrasion [Hoffmann et al., 1999, Hunt et al., 1984, Sagnotti et al., 2006, Sagnotti and Winkler, 2012, Saragnese et al., 2011, Revuelta et al., 2014].

The natural origin of iron oxides in this region is due to aeolian dust sourced from lateritic desert zone soils.

The iron oxides carried by the Harmattan wind include a mix of low coercivity (magnetite-like) and antiferromagnetic high coercivity minerals (hematite, goethite) [Maher, 2011]. The magnetic methods may be able to distinguish the origins of iron oxides from natural to anthropogenic and thus allow the investigation of the seasonal and source influences in the PM from those distinct origins.

The objective of this study is to assess the potential of magnetic methods to track sources and emissions variations from different urban activities in West Africa in the context of geogenic iron oxides inputs from continental winds. We study PM2.5 filter samples collected through the DACCIWA research program in Africa between 2015 and 2017 to characterize the iron oxides in terms of concentration, grain size distribution, and magnetic mineralogy. The data previously published in Djossou et al. [2018] for the filters enable the comparison between the presence of magnetic particles and quantitative indicators of combustion like the carbonaceous fraction and also PM2.5 concentration.

3.4 Methods

3.4.1 Sampling sites

PM2.5 filters were sampled in Abidjan (Ivory Coast) and in Cotonou (Benin), between February 2015 and March 2017. These two cities are the main economic centers of their respective countries. The urban areas of Abidjan and Cotonou have a population of 5.2 and 2.5 million, respectively. They are both located on the northern shore of the Gulf of Guinea (Figure 3.1).

They benefit from a sub-equatorial climate with two dry and two wet seasons. The long wet season stretches from April to July (Figure 3.2) and is dominated by Southwestern prevailing winds carrying humidity to the continent, and it is also known as the West African Monsoon [Knippertz et al., 2015b]. The long wet season is followed by a short dry period from August to September, associated with the lowest temperatures and highest winds. The short wet period lasts for 2 months from October to November and is characterized by a Southwestern wind from the Gulf of Guinea with a meridional component being higher in Cotonou than in Abidjan due to its eastern position [Lélé et al., 2015]. The long dry

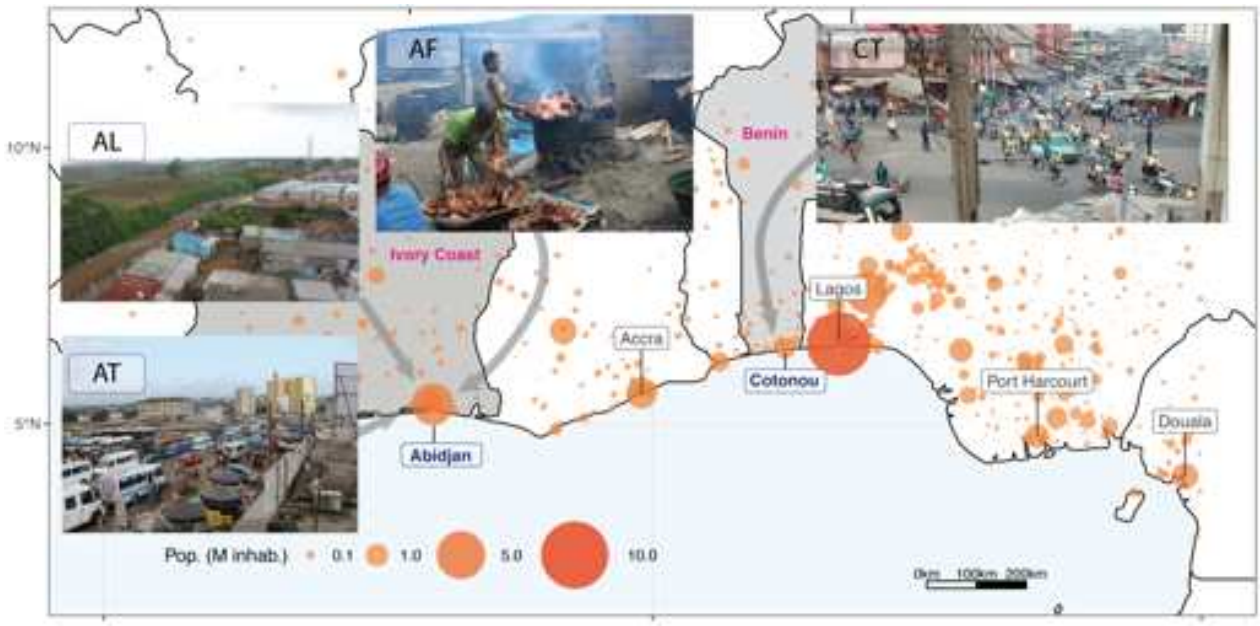

Figure 3.1: Localization of Abidjan and Cotonou in West Africa. Insets show the sampling sites (AT: Abidjan traffic, AL: Abidjan Landfill, AF: Abidjan fireplace and CT: Cotonou traffic).

season stretches from the end of November to March, when the region is influenced by dry Northeasterly winds from the Sahel, also known as the Harmattan, that bring mineral dust from arid areas [Adetunji et al., 1979]. The drop in the meridional wind component (V) in the weekly time series (Figure 3.2) indicates the Harmattan period, although the V component is still largely influenced by the coastal sea breeze [Bajamgnigni Gbambie and Steyn, 2013]. The Harmattan is usually associated with an air temperature drop and dusty conditions. December and January are the most affected by the Harmattan regime, in particular during the 2015-2016 winter. During this period pollutants emitted by savanna and agricultural waste burning are also advected to the coast by continental outflow [Marais et al., 2014]. Air temperature variations in both cities are very similar, following closely the same trends (Figure 3.2). The air temperatures reach a maximum (30° C) in April and a minimum (25° C) in July or August.

To characterize different emissions sources, four sites were sampled: two traffic sites (Cotonou site CT and Abidjan site, AT) and in addition in Abidjan a waste burning site (AL) and domestic fires site (AF). The combustion sources investigated were targeted to transportation, food smoking and waste burning [Djossou et al., 2018]. PM emissions in the African urban centers are derived from or are due to transportation but also from heavily polluting combustion sources, like charcoal making, food smoking and barbecue or open-air waste burning [Keita et al., 2018, Dominutti et al., 2019].

The traffic site in Cotonou (CT) is located in the Dantokpa area, one of the biggest markets in Africa. The transport sector in Cotonou is dominated by two-wheel vehicles with gasoline as the main fuel source. The sampler instrument is located on a 4 meters high

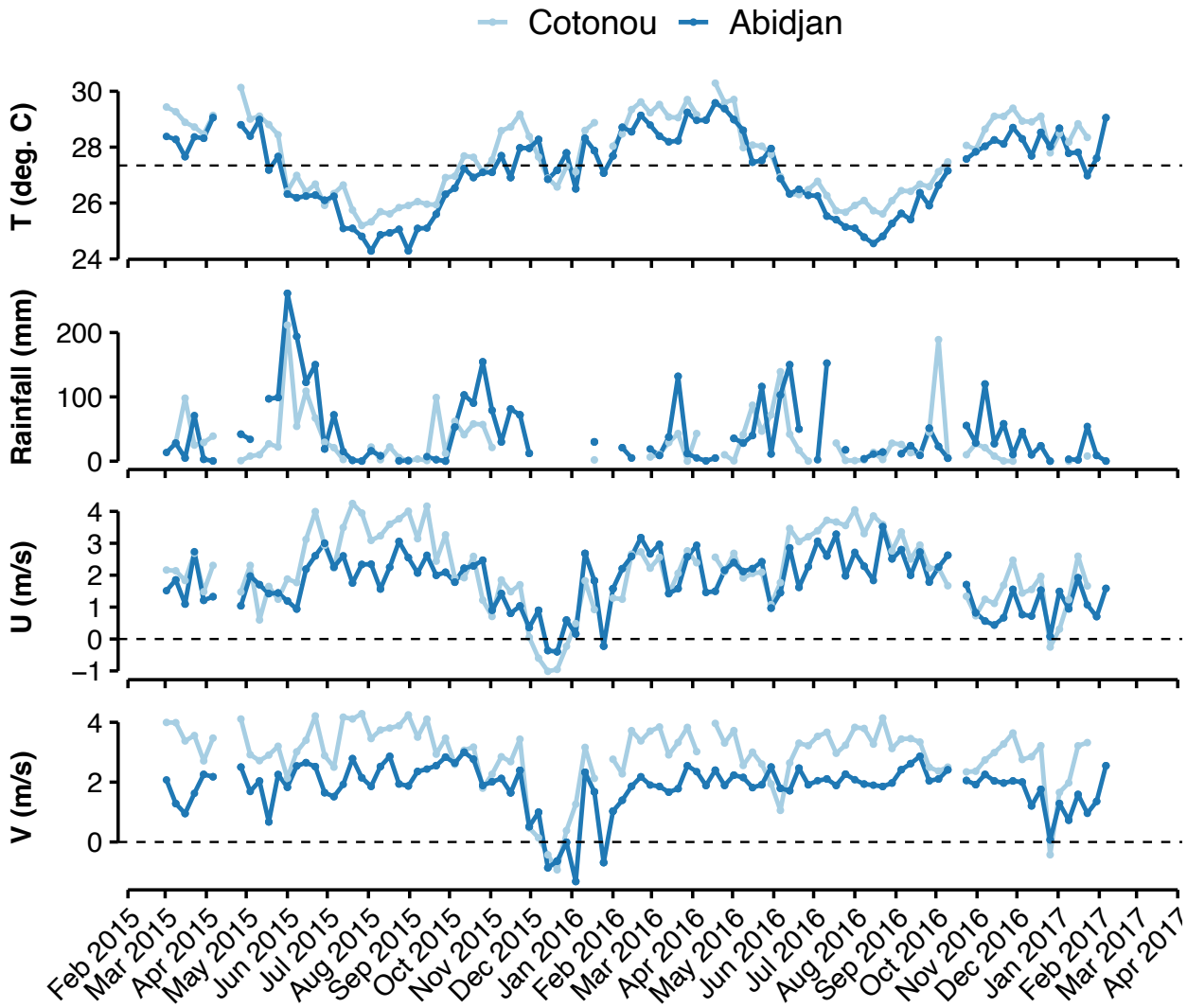

Figure 3.2: Weekly mean temperature, cumulative rainfall, mean zonal U(U>0 indicates wind from the West) and meridional V(V>0 indicates wind from the South) winds recorded in Abidjan (Felix Houphouet Boigny airport) and Cotonou (Cadjehoun airport) from February 2015 to March 2017.

balcony, above a major cross-road (Figure 3.1). The traffic site in Abidjan (AT) is located in the Adjamé sector. The traffic in Abidjan is dominated by cars and small buses using diesel fuel. The sampler is located on the roof of a commercial building. The domestic fireplace site (AF) is located in the market courtyard of Yopougon-Lubafrique. There is heavy use of fireplaces to smoke meat and fish or roast peanuts, and the main fuel source is hevea wood, in a total of 25 fireplaces (Figure 3.1). The instrumentation in this case is located on a 3-meter height tower. The waste burning site (AL) is located near the public landfill of Abidjan, in the village of Akeoudo. The landfill of Abidjan was closed in 2019 and until then was collecting all the waste produced in the district of Abidjan for the last 50 years. The dump has received about 1M t of waste a year in the last years [Adjiri et al., 2015]. The dump is connected to the city by unpaved roads (Figure 3.1). The workers at the landfill burn waste for recycling mainly in the dry season. Also, during this season spontaneous ignition of the waste can also occur. The sampling instrument is located in a three-store building at roughly 12 m above ground and at a distance of about 500 m from the place where the trashes are burnt.

3.4.2 Sampling

The sampling was done with a mini Partisol PM2.5 inlet using an airflow of 5Lmin^{-1} [Djossou et al., 2018]. Samples were taken weekly (some weeks were not sampled due to technical issues), by pumping ambient air for 15 min every hour. A total of 440 samples were retrieved from February 2015 to March 2017. For each sample, two 47 mm diameter filters (PTFE and quartz filters) were collected, thanks to two sampling lines running in parallel and equipped with NILU filter holders [Djossou et al., 2018]. After the exposure, the filters were stored individually in Petri dishes covered by aluminum foil. The quartz filters were used for carbonaceous aerosols analysis using a DRI thermo/optical carbon analyser [Chow et al., 1993, 1994, 2004, 2006] and following the IMPROVE protocol [Chiappini et al., 2014b]. PTFE filters were used for gravimetric measurements using a microbalance Sartorius MC21S. The total volume of air sampled each week is measured using a Gallus-type G4 gas meter. The PM2.5 concentration and carbon species data are reported in Djossou et al. [2018]. The 440 PTFE filters were cut in half with a ceramic scissor, with one half being used in this study. Observations are normalized by the corresponding surface. The filters were folded and put inside gel caps to facilitate their handling. The gel caps were placed inside paleomagnetic sample plastic boxes for the measurements. Due to technical issues, only 356 were successfully analyzed. The AT and AF sites have missing magnetic data on the first half (from March 2015 to November 2015) and the second half (from March 2016 to April 2017) of their time series respectively.

3.4.3 Magnetic methods

The magnetic investigation of the 356 quartz filters was done in the Laboratory of Paleomagnetism and Rock magnetism of the University of Sao Paulo (USPMAG), Brazil. The measurement protocol started using an alternating field demagnetization (AF), followed by anhysteretic remanent magnetization acquisition (ARM) and isothermal remanent magnetization acquisition (IRM). The AF demagnetization, ARM acquisition, and measurement and

IRM measurements were performed with a 755-1.65 DC SQUID magnetometer (2G enterprises), with a precision of 10^{-9} emu, located in a magnetically shielded room with an ambient field inferior to 500 nT. The IRM inductions were imparted on a pulse magnetizer (Magnetic Measurements Ltd.). All measurements are an average of three repeated measures of the magnetic moment. All samples were demagnetized along three axis in an AF peak field of 300 mT. After that, 94 samples were subject to progressive stepwise acquisition of the ARM under 30 µT bias field up to 300mT and AF demagnetization from 300mT (demagnetization curve of the ARM following Egli [2004]). The remaining samples (262) were given a one-step ARM in a bias field of 30 µT with superimposed AF of 100mT. The susceptibility of the ARM (xARM) is calculated by dividing the magnetic moment in $\mathrm{A\,m^2}$ by the bias field in A/m. IRMs were imparted by inducing fields of 1T (in this case considered as the saturation isothermal remanent magnetization, SIRM) and a backfield of 300mT ($\mathrm{IRM_{-300mT}}$). The SIRM parameter gives a qualitative concentration of the soft coercive magnetic carriers [Evans and Heller, 2003]. The mean destructive field (MDF) is determined from the intersection of the acquisition and demagnetization of the ARM curves, where half of the magnetization is lost. It gives information about the coercivity of the magnetic mineral, which is how hard it is for a mineral to lose its magnetization under demagnetization conditions [Dankers, 1981]. Low coercivity minerals could be ferrimagnetic magnetite-like, and high coercivity minerals could be hematite and goethite. The S ratio (defined by $\mathrm{IRM_{-300mT}/SIRM}$) is used to evaluate the proportion of high and low coercivity magnetic minerals in the sample [King and Channell, 1991]. Volume normalized SIRM ($\mathrm{SIRM_V}$) gives the concentration of iron oxides in air volume, in $\mathrm{A\,m^{-1}}$. Mass normalized SIRM ($\mathrm{SIRM_M}$) provides the magnetic content in PM2.5, expressed in $\mathrm{A\,m^2\,kg^{-1}}$. The same normalization was applied in the ARM values, with $\mathrm{ARM_V}$ and $\mathrm{ARM_M}$ for volume and mass normalizations respectively. The ratio between xARM/SIRM is a useful tool for discerning the size of ferrimagnetic magnetite-like minerals, and when plotted against the MDF of the ARM it will distinguish between fine and coarse grain sizes [Maher, 1988].

3.4.4 Scanning Electronic Microscopy

Morphology and size of the iron oxides in representative samples (4 filters) were characterized through Scanning Electronic Microscopy (SEM), using a JEOL JSM 7100F. For characterization of composition, EDS was performed with an Oxford Instrument Detector ($\mathrm{X_{MAX}}$=80mm^2). All micro-characterizations were done at the Centre De Microcaractérisation Raimond Castaing (Toulouse, France). The samples (quartz filters) were pretreated with a carbon coating and using conductive silver adhesives.

3.5 Results

3.5.1 Magnetic mineralogy

ARM acquisition curves display saturation varying from 1.88×10^{-5} to $2.15 \times 10^{-4}\,\mathrm{A\,m^2}$, at 80 mT. Mean MDF's range from 33 mT to 35 mT.

S-ratio varies from 0.90 to 1.00 at the AF site, between 0.67 to 1.00 at the AL site, between 0.65 and 1.00 at the AT site, and between 0.87 and 1.00 at the CT site. Mean values

Table 3.1: Summary of calculated means and standard deviations for the magnetic parameters, concentrations of elemental carbon and PM2.5, and organic and elemental carbon ratio (OC/EC). SIRM is presented as both mass and volume normalized ($SIRM_M$ and $SIRM_V$, respectively) and MDF is the Mean Destructive Field. Stars indicate values from Djossou et al. [2018].

Whole period	AT	CT	AL	AF
$SIRM_V$ (10^{-10} A m^{-1})	6.32 (± 3.09)	4.90 (± 1.91)	4.88 (± 1.98)	6.83 (± 4.24)
$SIRM_M$ (10^{-2} A m^2 kg^{-1})	2.23 (± 1.18)	2.28 (± 1.31)	2.21 (± 1.31)	0.53 (± 0.38)
S-ratio	0.97 (± 0.05)	0.97 (± 0.03)	0.96 (± 0.04)	0.96 (± 0.02)
MDF (mT)	33.55 (± 4.46)	33.76 (± 2.76)	35.08 (± 2.95)	33.55 (± 2.58)
xARM/SIRM (10^{-4} m A^{-1})	7.32 (±2.78)	6.57 (±1.82)	6.93 (±4.22)	7.24 (±2.38)
EC (µg m^{-3})⋆	7.64 (± 4.02)	2.15 (± 1.26)	4.22 (± 2.60)	13.01 (± 6.77)
PM2.5 (µg m^{-3})⋆	37.01 (± 29.70)	30.64 (± 32.01)	28.44 (± 19.79)	153.55 (± 73.29)
OC/EC ⋆	1.93 (± 1.07)	3.72 (± 1.37)	2.54 (± 1.49)	6.00 (±2.66)
Harmattan period				
$SIRM_V$ (10^{-10} A m^{-1})	7.57(±4.38)	6.13(±2.19)	5.94(±1.97)	5.50(±1.74)
$SIRM_M$ (10^{-2} A m^2 kg^{-1})	1.37(±0.66)	1.72(±1.25)	1.24(±0.58)	0.70(±0.39)
S-ratio	0.97(±0.02)	0.95(±0.04)	0.97 (±0.02)	0.97(±0.01)
EC (µg m^{-3})⋆	10.45(±4.69)	3.51(±1.54)	6.84 (±4.04)	10.56(±5.59)
Monsoon season				
$SIRM_V$ (10^{-10} A m^{-1})	6.76 (±2.86)	4.14 (±1.23)	4.16 (±2.01)	9.81 (±5.81)
$SIRM_M$ (10^{-2} A m^2 kg^{-1})	3.25 (±1.50)	2.98 (±1.54)	2.41 (±1.53)	0.46 (±0.32)
S-ratio	0.98 (±0.01)	0.97 (±0.01)	0.96 (±0.02)	0.95 (±0.03)
EC (µg m^{-3})⋆	4.99 (±1.12)	1.52 (±0.74)	3.61 (±0.93)	21.08 (±8.06)

for S-ratio are above 0.96 for all sites (Table 3.1), pointing out to dominance of low coercivity minerals for all sites and a mainly small component of high coercivity minerals like goethite and hematite.

3.5.2 Particulate matter magnetic properties

Volume normalized SIRM ($SIRM_V$) values range between 4.87×10^{-12} A m^{-1} and 2.62×10^{-9} A m^{-1} (Figure 3.4) with site means between (Table 3.1) 6.83×10^{-10} A m^{-1} (AF site) and 4.90×10^{-10} A m^{-1} (CT site).

Mass normalized SIRM ($SIRM_M$) values evolve between 2.87×10^{-5} A m^2 kg^{-1} to 7.55×10^{-2} A m^2 kg^{-1}. Site means display similar values of 2.23×10^{-2} A m^2 kg^{-1}, 2.28×10^{-2} A m^2 kg^{-1} and 2.21×10^{-2} A m^2 kg^{-1} for the AT, CT and AL sites respectively, whereas the AF site presents the lowest value (0.53×10^{-2} A m^2 kg^{-1}).

The weekly xARM/SIRM ratio ranges from 8.06×10^{-5} to 7.02×10^{-3} m A^{-1}. Mean ratios are between 6.57×10^{-4} and 7.32×10^{-4} m A^{-1} for CT and AT sites, respectively. Weekly values of $SIRM_V$ display moderate but significant correlations with PM2.5 concentration (Figure 3.3**a**), with Pearson correlation coefficients R values of 0.42, 0.44, 0.37 and 0.28 for the AT site, CT site, AL site and AF site respectively. Considering all the sites, the correlation coefficient is R=0.40 ($p < 0.01$). The average $SIRM_V$ for each site is strongly correlated to the average EC concentrations (R=0.94) (Figure 3.3**b**) while the R coefficient

is 0.77 for the correlation with the PM2.5 concentration means.

3.5.3 Time series of concentration (volume normalized) parameters

Both traffic (AT and CT) and AL sites present similar variations (Figure 3.4) in the concentration of PM2.5 and EC, having well-marked peaks during the Harmattan periods in both years. The magnetic parameters (ARM_V and $SIRM_V$) also follow similar patterns in those sites, albeit with a stronger variability, especially in the AL site.

The domestic fire site (AF) presents the opposite behavior compared to the other sites, displaying an increase in the concentrations of PM2.5 and EC in the first months of sampling. The AF site shows a large increase in the concentrations of EC and PM2.5 peaking in July of 2015, which can be also observed in the magnetic parameters. The mid-seasons bring a decrease in the concentrations of EC and PM2.5 till the beginning of the Harmattan period in December. The magnetic parameters follow the trends of the PM2.5 and EC concentrations, with greater variability (Figure 3.4).

For the AL and CT sites (Figure 3.4), the time series starts in February 2015, at the end of the Harmattan wind period. The concentrations of PM2.5 and EC stagnate at low values till the end of the Monsoon season. In the mid-seasons, from August of 2015 to November, there is an increasing trend in the PM2.5 and EC concentrations at the AL and CT sites. This is also observed in the magnetic parameters at the CT site. The transition from the small wet period in November to the Harmattan period in December of 2015 in the AT, AL, and CT sites (the AF site has no data after January of 2016) is marked by a large increase in the concentrations of EC and PM2.5, with concentrations multiplied by two to three times fold. Magnetic parameters show similar increases, especially at the traffic sites (AT and CT). As the Harmattan period progresses, the concentrations of EC and PM2.5 decrease till March of 2016, when they stay stable at the three sites (AT, CT, and AL). The magnetic parameters display those same trends, especially at CT and AT sites. All parameters remain stable till the beginning of the Harmattan period, once again increasing the concentrations of EC and PM2.5 and magnetic parameters at the three sites (AL, CT and AT) (Figure 3.4).

We can observe a large influence of the wind on the PM2.5 concentration and the magnetics parameters, except for the AF site. The alternation of the Monsoon and Harmattan regimes is well reflected by the meridional wind component (V) variation. The anti-correlation between PM2.5 and the meridional component of the wind reaches R=-0.75 for the AT site. An increase in the V component reflects the influence of clean marine air carried by the Monsoon flow towards the sites. Conversely, low V component indicates a Northeasterly Harmattan wind carrying continental aerosols to the sites and thus increasing the PM2.5 concentrations.

The AF site is not affected by such a feature, however, the rainfall may have an impact on emissions during wood combustion [Djossou et al., 2018, Keita et al., 2018].

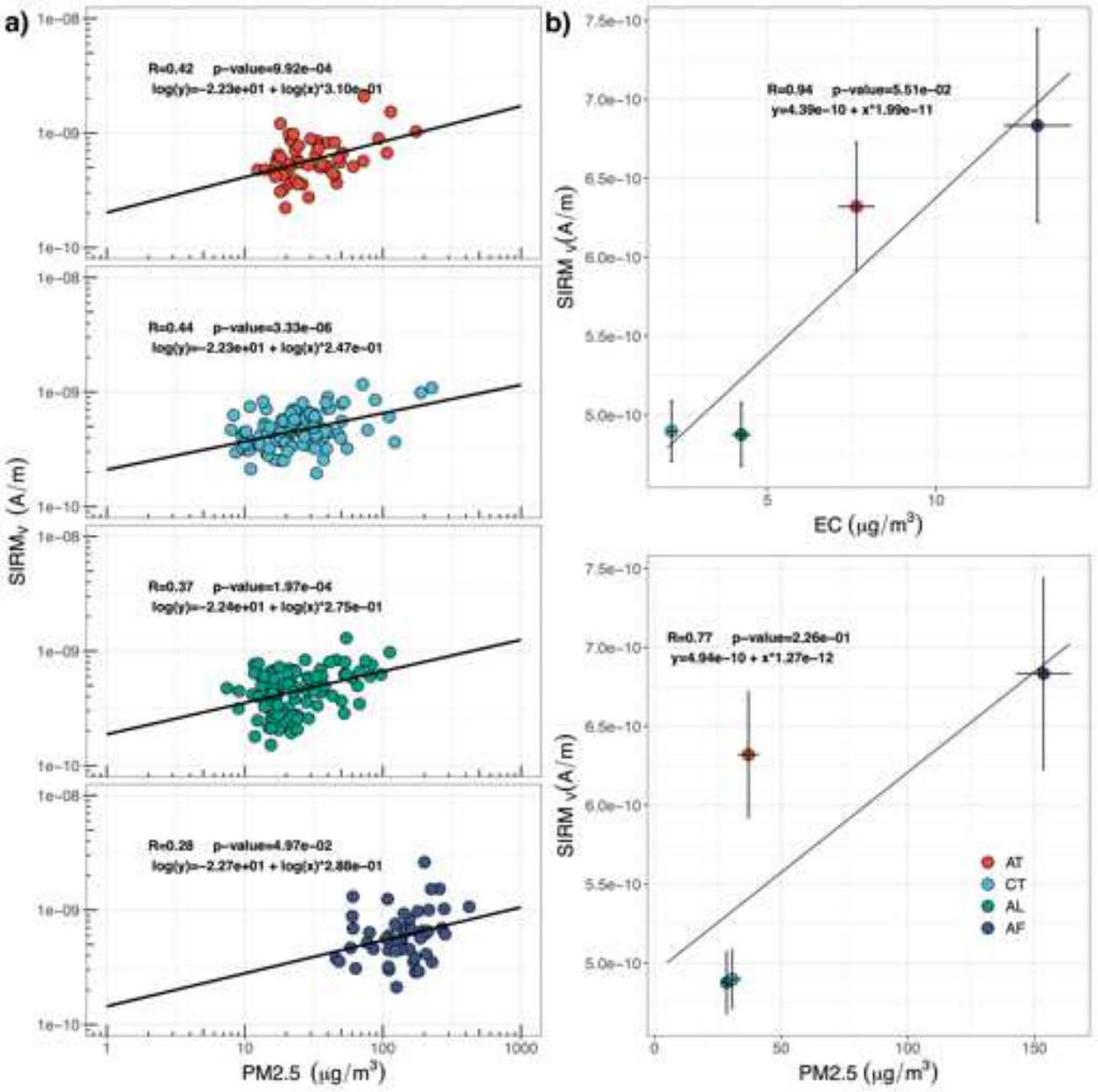

Figure 3.3: (**a**)Weekly values of $SIRM_V$ versus PM2.5 concentration for each site. (**b**) Correlation between $SIRM_V$ means and EC and PM2.5 concentrations means for the whole data series in each site. Error bars are the standard errors.

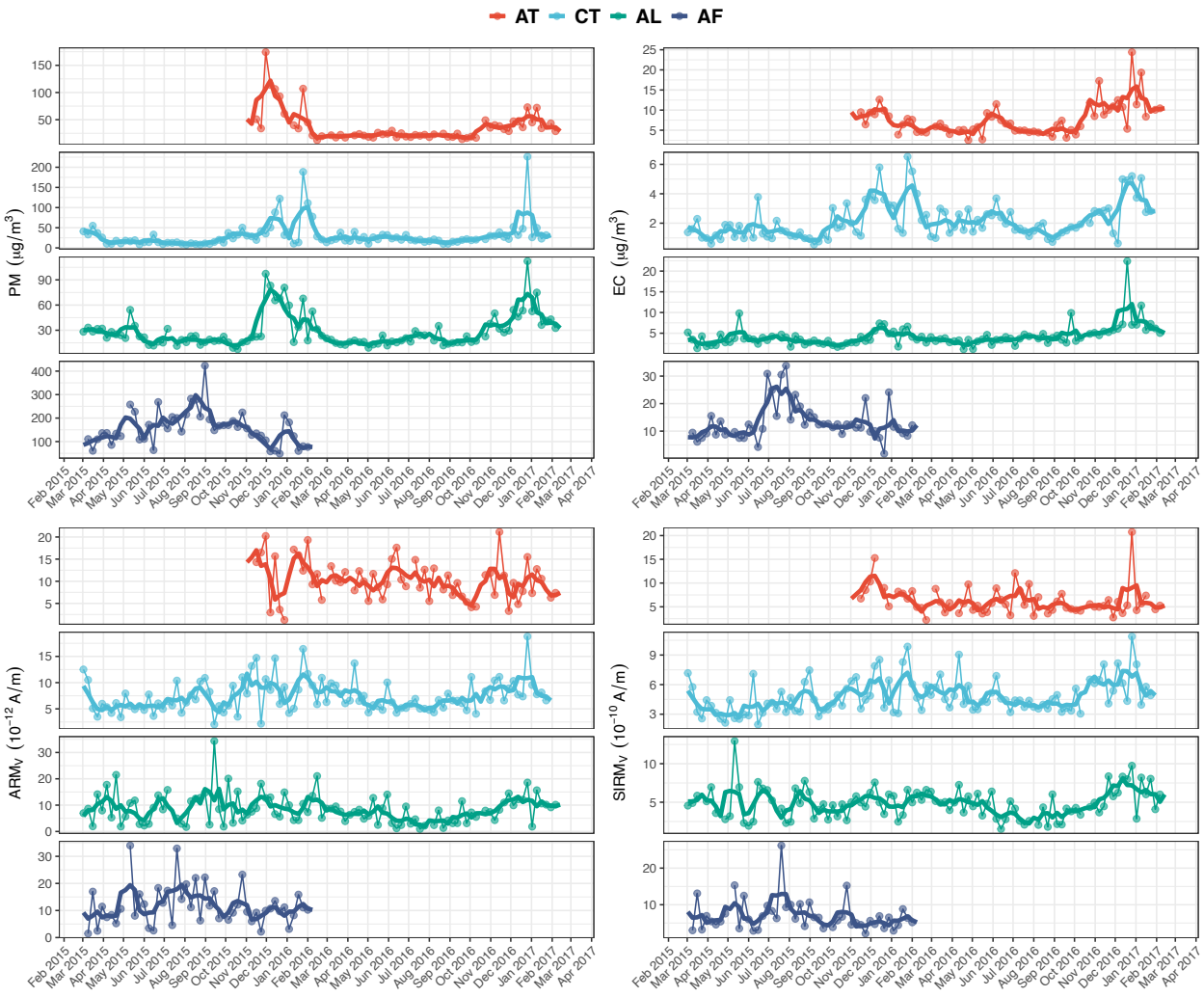

Figure 3.4: Concentration parameters PM2.5, EC, ARM_V and $SIRM_V$. The lines are the monthly running means and points the individual weekly measurements.

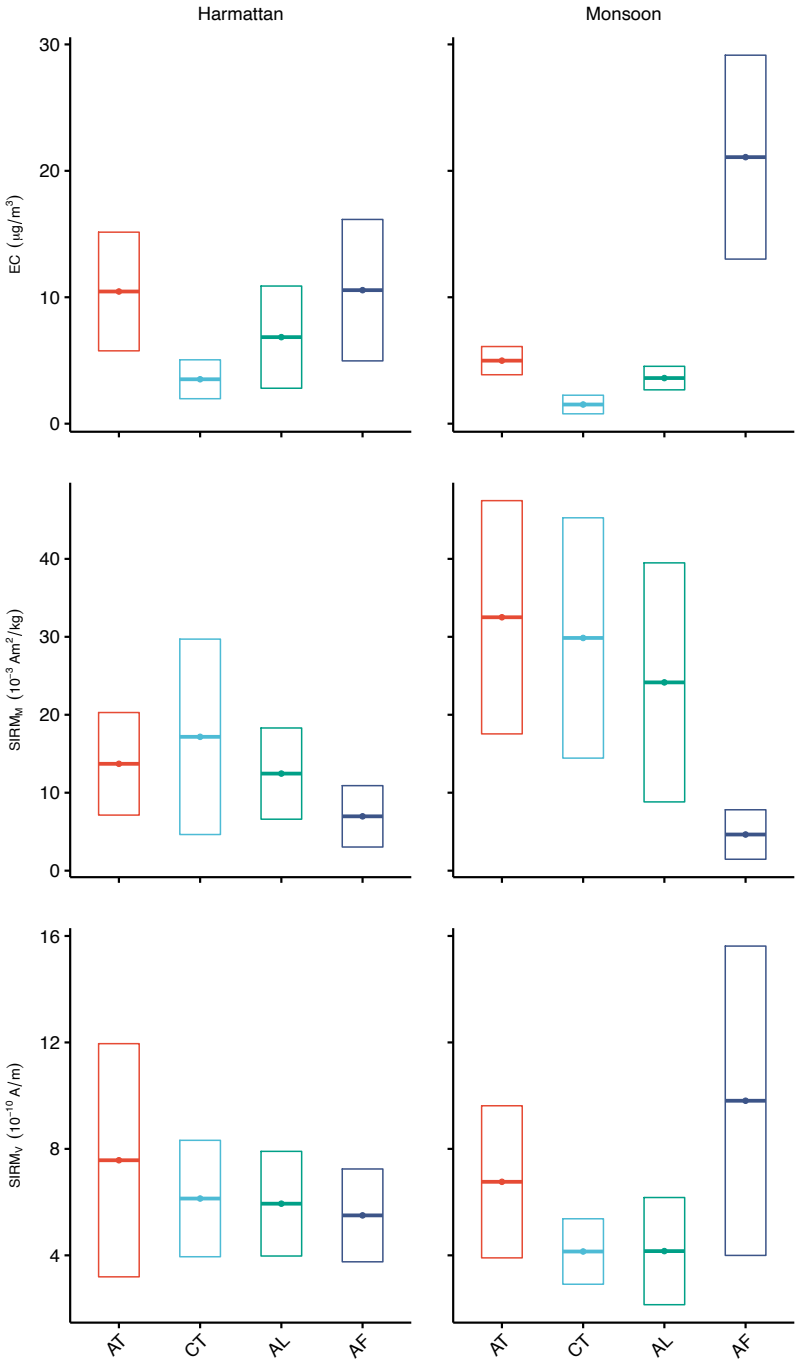

Figure 3.5: EC concentrations and magnetic content in air volume and PM ($SIRM_V$ and $SIRM_M$, respectively) for the two characteristic weather events: the Harmattan period (dry season) and the monsoon season. Means (horizontal lines in the center of the square) and standard deviations (size of the square) are reported.

3.5.4 Seasonal influence of Harmattan wind and West African monsoon

To investigate the influence of the meteorological conditions (Figure 3.2), we selected the most characteristic periods, meaning the lowest values for pluviometry and Southwestern winds for the period influenced by the Harmattan wind (three first weeks on December 2015 and the two last weeks in January 2016), and the highest pluviometry and Southwestern wind for the monsoon period (June and July, of 2015 for AL, AF and CT sites and 2016 for AT site).

Seasonal $SIRM_V$ means (Figure 3.5) display higher values at the AT site in comparison to the CT site, in both seasons, with means ranging from $7.57 \times 10^{-10}\,A\,m^{-1}$ to $6.76 \times 10^{-10}\,A\,m^{-1}$ in the AT site and ranging from $6.13 \times 10^{-10}\,A\,m^{-1}$ to $4.14 \times 10^{10}\,A\,m^{-1}$ in the CT site during the Harmattan and Monsoon seasons respectively. The value of $SIRM_V$ at the AL site is higher during the dry period ($5.94 \times 10^{-10}\,A\,m^{-1}$) compared to the wet one ($4.16 \times 10^{-10}\,A\,m^{-1}$). The AF site has a lower mean value during the Harmattan season ($5.50 \times 10^{-10}\,A\,m^{-1}$) in comparison to the Monsoon season ($9.81 \times 10^{-10}\,A\,m^{-1}$).

The $SIRM_M$ means calculated for the traffic sites (AT, CT) and the AL site during both seasons display similar behaviors in being higher during the Monsoon than during the Harmattan period. Seasonal means during the Harmattan and Monsoon seasons are 1.37×10^{-2} and $3.25 \times 10^{-2}\,A\,m^2\,kg^{-1}$ in the AT site, 1.72×10^{-2} and $2.98 \times 10^{-2}\,A\,m^2\,kg^{-1}$ in the CT site, 1.24×10^{-2} and $2.41 \times 10^{-2}\,A\,m^2\,kg^{-1}$ in the AL site, respectively. Conversely, the AF site has a smaller mean during the wet period ($0.46 \times 10^{-2}\,A\,m^2\,kg^{-1}$) than during the Harmattan period ($0.70 \times 10^{-2}\,A\,m^2\,kg^{-1}$).

S-ratio means (Table 3.1) of the four sites during the Harmattan period vary between 0.95 and 0.97. During the Monsoon, the S-ratio means range from 0.98 to 0.95 with the highest values at the AT site and the lowest at the AF site.

The Harmattan wind affects more the traffic sites and AL site, depicted by a mineral input from dust characterized by high coercivity minerals (hematite, goethite). The Harmattan wind also facilitates resuspension due to its drier characteristic, resulting in an increase in EC concentration in those sites. The AF site, on the other hand, is affected by the humidity of the Monsoon season, with enhanced values in EC concentration and volume normalized magnetic parameters ($SIRM_V$ and ARM_V).

3.5.5 Grain size parameters

As the magnetic mineralogy is dominated by low coercivity minerals, assessment of grain size may be achieved with the ratio between xARM and $SIRM_M$. In Figure 3.6, the xARM/SIRM ratio is plotted against the MDF. The samples presented in this study range in xARM/SIRM from $1.0 \times 10^{-4}\,m\,A^{-1}$ to $1.7 \times 10^{-3}\,m\,A^{-1}$. They are well-grouped without any distinctions regarding the site. Four samples from the AT site are located below the xARM/SIRM of $5.0 \times 10^{-4}\,m\,A^{-1}$, and one sample from the AL site is located above $1.5 \times 10^{-3}\,m\,A^{-1}$. These five samples lying outside the main group were all collected in December in both years.

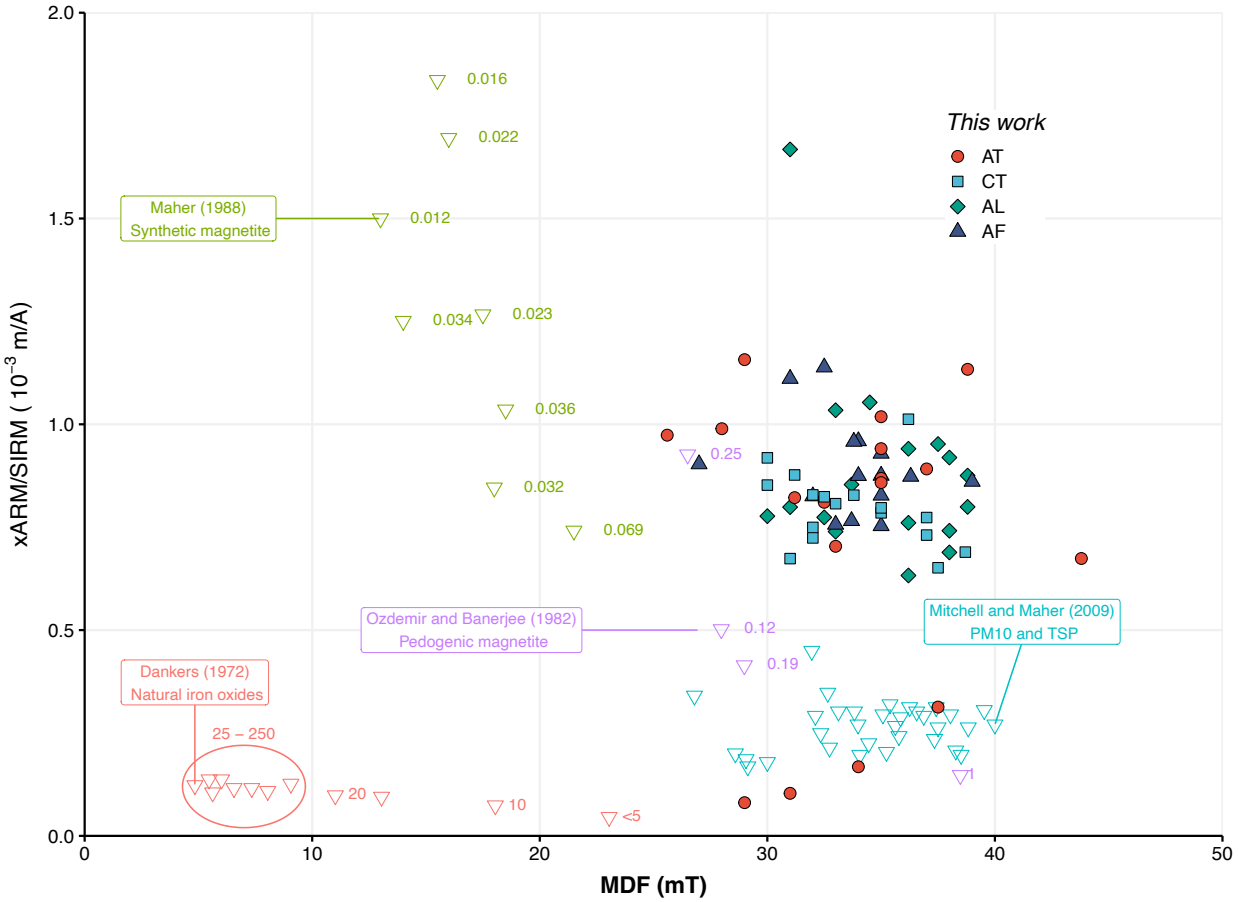

Figure 3.6: xARM/SIRM versus MDF for selected samples in the four sites (circle-AT, square-CT, diamond-AL, triangle-AF, all filled) and data from Dankers [1978], Özden Özdemir and Banerjee [1982], Maher [1988] and Mitchell and Maher [2009] (open inverse triangles in salmon, purple, green and blue respectively). Iron oxides reported in Dankers [1978], Özden Özdemir and Banerjee [1982] and Maher [1988] are all composed of synthetic magnetite or ferrimagnetic magnetite-like iron oxides, with known grain sizes (represented by the numbers above the symbols, in μm). Data from Mitchell and Maher [2009] are measurements performed in PM10 filters and leaves (total suspended particles, TSP).

3.5.6 Scanning Electronic Microscopy

SEM observations indicate that the PM2.5 particles captured in the filters are a mix of carbon-rich chains, fluffy soot aggregates (Figure 3.7), iron oxides with different shapes (spherical fly ashes and irregular shapes, Figure 3.7), and aggregates containing different proportions of elements (including Al, Ca, S, PB, Si, K, Figure 3.7). The spherical fly ashes (iron oxide spherules) were found in all sites with the exception of the CT site. The AT site shows carbon fluffy aggregates trapped in the filter matrix (Figure 3.7**a**), with five sub-micron spherical fly ashes (with sizes ranging from 50 to 500nm), composed of iron oxides (Figure 3.7**c**). Some of them are agglomerations of smaller spherules. Figure 3.7**b** illustrates such agglomeration displaying six spherules with sizes ranging from 50 to 300nm, entrapped among the carbon chains. EDS spectra (see an example in Figure 3.7**c**) indicate that spherule compositions are dominated by iron and oxygen, with traces of C and Si. Si, present in all samples, may correspond to the matrix of the filter (Quartz).

The observations of the other sites (CT, AL, AF) are presented in Figure 3.7**d**, Figure 3.7**e** and Figure 3.7**f** and respective EDS spectra are presented in Figure 3.7**g**, Figure 3.7**h** and Figure 3.7**i**. We detected iron oxides in all sites. In the CT and AL sites, we observe bright irregular shaped particles at the center of the figures (Figures 3.7**d** and 3.7**e**, respectively). In Figure 3.7d, some carbon aggregates, with a bright particle at its center, points out to a heterogeneous composition. The bright particle has an irregular shape, with dimensions of 0.96μm and 0.79μm, composed mainly of Fe and O and traces of S, Ca, Al, Na and Si (Figure 3.7**g**). Figure 3.7**e** has almost no visible carbon aggregates and chains. The central bright particle is composed of Fe and O with traces of Pb, Zr, Cl, K, Al, Na, C and Si (Figure 3.7**h**) with a size of 1.33μm in width. The filter from the AF site, (Figure 3.7**f**) is much more charged in carbon particles than the others, several carbon fluffy aggregates can be observed on one quartz fiber. The bright spherule is composed of Fe and O, with traces of C and Si (Figure 3.7**i**). It has a diameter of 0.75μm.

The iron oxide spherules (or fly ash particles) found at the AT and AF sites (Figures 3.7**a** and 3.7**f**) have sub-micron size. They present mainly a Fe-rich composition with C, related to the carbon species released by the different combustion processes in those sites. Those elements point clearly to anthropogenic origin for those particles. The irregular iron oxides found at CT and AL sites (Figures 3.7**d** and 3.7**e**) are generally bigger than the spherules.

3.6 Discussion

The magnetic properties of the coarse PM fraction (PM10 and TSP) are largely influenced by non-exhaust vehicular emissions [Sagnotti et al., 2006, 2009, Sagnotti and Winkler, 2012] that contain Fe-bearing particles and other transition metals. However, the finer fraction (PM2.5) and the influence of combustion emission on its magnetic properties have been less investigated. Iron oxides in urban PM2.5 consist of mixed Fe phases with variable morphologies, particle sizes, and aggregates [Mitchell and Maher, 2009, Shi et al., 2014]. Recently, Fe-bearing particles were found in association with carbonaceous material [Shi et al., 2015] and a wide variety of trace elements [Pattammattel et al., 2021]. Here, for the first time in West Africa, iron oxides are reported in anthropogenic emissions of particulate material in air through the use of environmental magnetism methods.

All sites present iron oxides, among soot and/or aggregates containing crustal elements (Al, Ca, K, Zr), sea salt (Na, Cl) and elements from anthropogenic activities (S, Pb) [Liu et al., 2019a] detected via magnetic and microscopic methods (Figure 3.7). The detected fly-ash spherules are a marker of anthropogenic combustion emissions, in the sub-micron size range (Figure 3.7).

The iron oxides detected in West Africa PM2.5 are a mix of ultrafine magnetite-like grains and high coercivity minerals (hematite, goethite). The presence of both ferrimagnetic magnetite-like grains and hard coercivity minerals is detected in all sites and seasons, with a greater influence of the hard coercivity minerals in the dry period.

The presence of soft coercivity magnetic carriers is illustrated by the fact that ARM saturation was achieved at 80 mT [Mitchell and Maher, 2009]. The dominance of magnetite-like minerals on the magnetic fraction seems to be the hallmark of urban PM emissions [Gonet and Maher, 2019, Gonet et al., 2021b, Liati et al., 2015, Bardelli et al., 2011]. Indeed, this was reported in numerous cities (e.g. Mitchell and Maher [2009] in Lancaster, UK, Muxworthy et al. [2001] in Munich, Germany, Mantovani et al. [2018] in Parma, Italy, Saragnese et al. [2011] in Torino, Italy, Jordanova et al. [2014] in Bulgaria, Castañeda-Miranda et al. [2014] in Quéretaro, Mexico, Chaparro et al. [2020] in Mar del Plata, Argentina and Shu et al. [2001] in Shanghai, China). When reported, S-ratios are generally close to 1. Revuelta et al. [2014] calculated S-Ratio of 0.99 on PM2.5 filters in Barcelona. Sagnotti et al. [2006] obtained for the Latium region (Italy) a mean S-ratio=1.00 for PM10 filters. Wang et al. [2017] calculated for Nanjing a mean S-ratio=0.97. The S-ratios reported here are mainly slightly lower, indicating the presence of high coercivity minerals. S-ratio means range between 0.97 (traffic sites AT, CT) and 0.96 (AL and AF sites), and MDF means are close to 33 mT in AT, CT, and AF sites and 35 mT in AL site. Those values highlight the influence of the high coercivity minerals such as hematite and goethite in all sites. S-ratio values lower than 0.97 and MDF values above 30 mT have been shown by Frank and Nowaczyk [2008] to be due to a mix of hematite and magnetite.

Seasonal variance plays an important role on the air quality, as weather characteristics, such as wind and rain, will change the carrying of continental pollutants and dust through long distances, and facilitate resuspension of local PM [Djossou et al., 2018, Yahi et al., 2013]. High coercivity minerals (goethite/hematite) could be expected in African cities due to intense laden-wind carrying minerals from lateritic soils [Schroth et al., 2009, Formenti et al., 2014]. The wind blows dust from arid areas in the SSA region. It has a magnetic com-

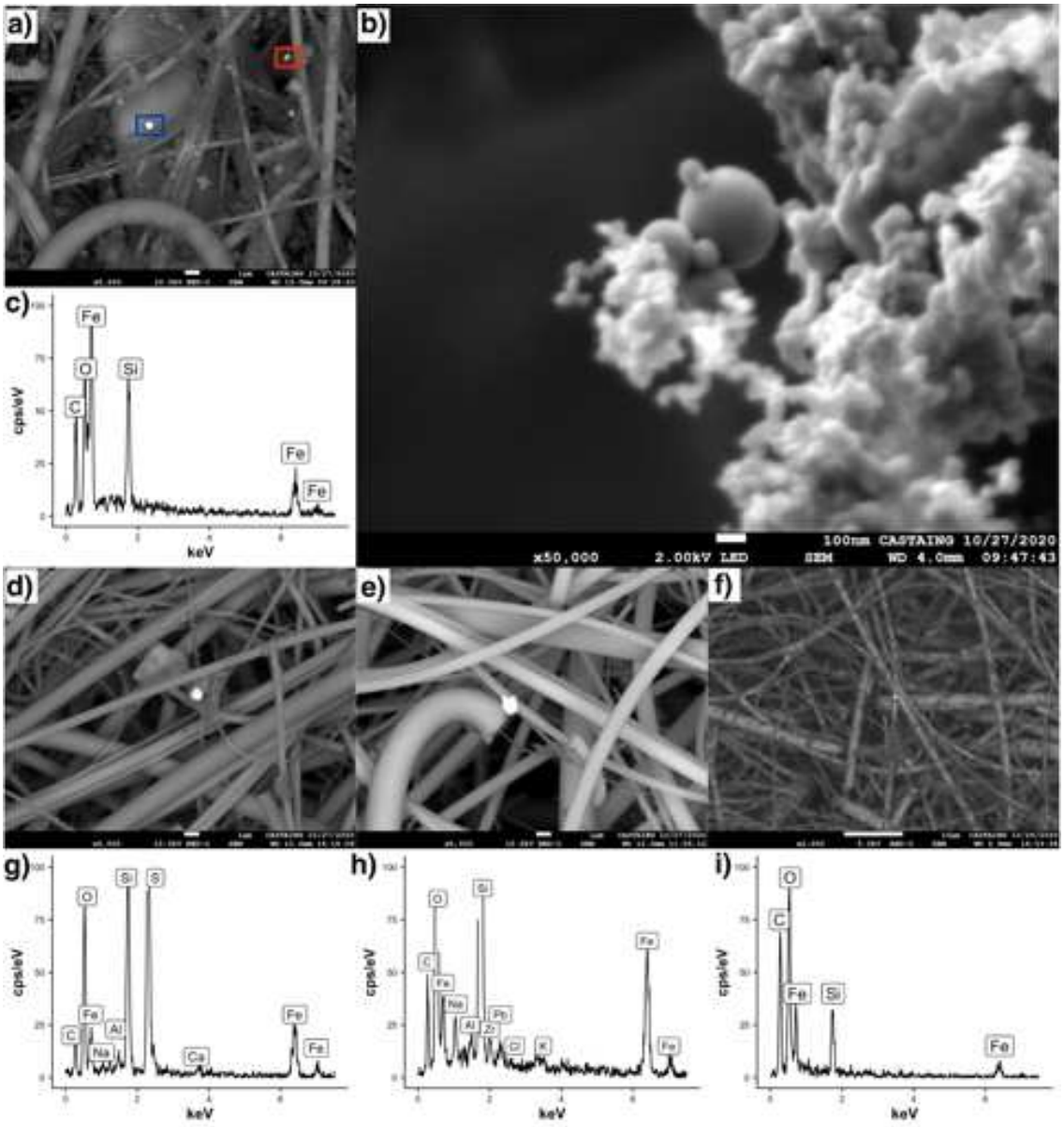

Figure 3.7: SEM images for the four sites: (**a**) Abidjan traffic (AT) site showing five iron oxide agglomerations and individual spherules, with sizes ranging from 50 to 500 nm.(**b**) A detail from (a) of one of the agglomerations (marked in red in figure a), displaying six spherules with sizes ranging from 50 to 300 nm.(**c**) EDS spectrum of the central spherule marked in blue in figure (a), showing a composition of Fe, O, Si and C. (**d**) Cotonou traffic site (CT), showing a particle agglomeration with a central particle composed of Fe and S with low traces of Ca, Al, Na, O. The aggregate surrounding this particle has a composition of C, Ca and Al, and a maximum dimension of 3.22μm. (**e**) Abidjan landfill site (AL) with a bright irregular shaped particle at the center, composed of Fe and O, and traces of Pb, Zr, Cl, K, Al, Na with dimension of 1.33μm. (**f**) Abidjan domestic fire site (AF), with a central spherule of 0.75μm in diameter, composed of Fe and O.(**g**) EDS spectrum for the central particle (marked in blue) from the CT site. (**h**) EDS spectrum from the central particle (marked in blue) from the AL site. (**i**) EDS spectrum from the spherule (marked in blue) from the AF site. All spectra have the presence of Si, related to the matrix of the filter.

position of low (magnetite-like) and high coercivity carriers, such as hematite and goethite [Lyons et al., 2010, Maher, 2011]. The Harmattan period, characterized by dry weather and northeasterly winds, displays a change in the magnetic mineral composition of the PM2.5 at both traffic sites and at the AL site. This is further substantiated by a lower S-ratio during this period in comparison to the Monsoon season indicating a higher contribution of high coercivity minerals (hematite, goethite). Evidently, during the Monsoon, the resuspension and carrying of wind-blown dust are diminished, enhancing the influence of the main source of PM (traffic emissions for AT, CT, and AL and wood burning for AF) in those sites. Moreover, at the AL site, the burning of trash is done mainly during the dry season, increasing the output of emissions during this period [Djossou et al., 2018]. The traffic sites (AT, CT) and AL site also exhibit peaks of concentration of PM2.5, EC, and magnetic content in the air ($SIRM_V$) during this period, due to resuspension and long-distance carrying of pollutants [Djossou et al., 2018, Yahi et al., 2013]. Conversely, the Monsoon season has a diminished influence from non-local sources.

In Abidjan and Cotonou, mean values for the concentration of iron oxides in PM2.5 ($SIRM_M$) -meaning SIRM normalized by PM2.5 mass- equals to $1.65 \times 10^{-2}\,A\,m^2\,kg^{-1}$ and $2.28 \times 10^{-2}\,A\,m^2\,kg^{-1}$ respectively, close to the few magnetic results reported for PM2.5 collected in filters. $SIRM_M$ values reported from Barcelona [Revuelta et al., 2014] and Beijing [Shi et al., 2014] range from $2.53 \times 10^{-2}\,A\,m^2\,kg^{-1}$ to $4.56 \times 10^{-3}\,A\,m^2\,kg^{-1}$ respectively. In both cities, the presence of iron oxides in PM has mainly anthropogenic origins due to traffic and urban emissions (at least in the absence of a strong crustal PM source with North African origin for Barcelona). Conversely, in Nanjing, Wang et al. [2017] report (for PM2.5 samples taken twice a day) higher $SIRM_M$ values of $4.98 \times 10^{-1}\,A\,m^2\,kg^{-1}$ (winter) and $5.42 \times 10^{-1}\,A\,m^2\,kg^{-1}$ (summer). Such high values compared to our own and other studies are probably due to the highly industrialized context.

Magnetic content in the air ($SIRM_V$) corresponds to the concentration of iron oxides in air volume (SIRM normalized by air volume pumped in a filter). $SIRM_V$ values on PM2.5 are rarely reported in the bibliography. Shi et al. [2014] found in Beijing a value for $SIRM_V$ of $4.31 \times 10^{-10}\,A\,m^{-1}$, in the same order of magnitude to the values found in Abidjan and Cotonou. Magnetic content marked by $SIRM_V$ and ARM_V are significantly higher in the AF site compared to traffic sites (Table 4.1). The high values of magnetic content (volume normalized) and high EC mean concentration in comparison with the traffic sites indicate a higher volume of emissions at the AF site.

$SIRM_V$ and ARM_V time series are moderately correlated with PM2.5 mass concentrations. Revuelta et al. [2014] found a high correlation between the SIRM (normalized by filter area) and total PM with R=0.89. Mitchell and Maher [2009] reported a strong correlation between SIRM (normalized by filter area) of PM10 filters and their PM10 concentrations (R=0.88). Mantovani et al. [2018] obtained correlations with R=0.34 between the area normalized SIRM for the PM10 filters and concentration of PM10 from a nearby weather station and R=0.50 between the area normalized SIRM in PM10 filters in comparison to PM2.5 concentration from the same nearby weather station. The time series of the concentration parameters (EC and PM2.5) presented in this work displays some similar trends to the time series of the magnetic parameters in the air ($SIRM_V$ and ARM_V), although the magnetic parameters have greater variability, with periods where they do not follow the concentration parameters. Nonetheless, the site-average PM2.5 is reasonably correlated to the $SIRM_V$ when excluding

the wood-burning site (AF). Wood burning for smoking food leads to the largest concentrations of PM2.5. The combustion process is known to produce ashes with a distinct magnetic signal dominated by low coercivity magnetite-like minerals (e.g., McClean and Kean [1993] in wood and Jordanova et al. [2006] in cigarette ashes). The AF site displays a generally higher PM emission than other sites with PM2.5 and EC concentrations one order of magnitude higher than the other sites. However, the PM2.5 magnetic content ($SIRM_M$) is much lower in the AF site in comparison to the others. This implies that wood-burning emits fewer iron oxides than traffic per unit of PM2.5 emitted during combustion.

The site-wise correlation between means $SIRM_V$ and EC concentration is better than between means $SIRM_V$ and PM2.5 concentration. This indicates that the iron oxides in PM2.5 detected by this method are mostly related to combustion sources, EC concentration being an indicator of primary emission by combustion.

Our sampling allows us to discern two types of sources: traffic (sites AL, CT, and AT) and wood combustion (site AF). The AL site, although subject to waste burning emissions, presents a behavior closer to those of the traffic sites when considering the investigated parameters (magnetic properties and EC/OC ratio from Djossou et al. [2018]). This could be explained by the location of the observation base, far from the source, favoring a greater impact of the traffic on the nearby road. Nonetheless, differences in PM sources are not reflected by the magnetic grain size parameters. The xARM/SIRM versus MDF plot displays a narrow distribution for the calculated parameters in all sites, regardless of the sources or the seasons (Figure 3.6). Outliers in our sample group consist of four samples from the AT site lying close to the PM10 and TSP in Mitchell and Maher [2009], and one sample from the AL site plotting above our main group. Those outliers were all sampled in the month of December (both 2015 and 2016), during the dry period when the Harmattan wind is at its peak, blowing dust from arid areas and facilitating the resuspension of particles. Clearly, the Harmattan period brings other sources of iron oxides into the sites, carried in dust and from resuspension, making the source of anthropogenic emissions less clear. The main group of our PM2.5 filters in the Figure 3.6 correspond to sizes below 0.1μm synthetic magnetite in terms of xARM/SIRM [Maher, 1988] agreeing to the nanometric size of the fly-ash spherules observed under microscope (Figure 3.7). However, larger irregular-shaped iron oxides and fly ash spherules were also observed (0.3μm-1.3μm).

The two investigated traffic sites (AT and CT) show very similar levels of PM2.5 mass concentrations and magnetic parameters. Despite their close location to emission sources, the sampled air is largely affected by large-scale transport as reflected by the high correlation with winds and the similarities in the time series while the sites are located 1000 km apart. The traffic from AT site is mostly dominated by diesel vehicles, resulting in an EC concentration that can reach four times fold the EC concentration recorded in CT (Table 4.1), where traffic is dominated by two-stroke gasoline vehicles. The OC/EC ratio reflects this difference, reaching a factor of two between those two traffic sites [Djossou et al., 2018]. The OC/EC ratio is not reflected by the magnetic grain size of the PM2.5 fraction. The two sites display similar $SIRM_M$ but distinctive $SIRM_V$. This indicates higher emissions of iron oxides in Abidjan per air volume agreeing with a higher EC concentration.

The smoking place site (AF) is less affected by regional scale transport. The increase in EC and PM2.5 concentrations during the Monsoon period is associated with an increase in the $SIRM_V$ data. This expresses an increase in the release of magnetic particles in the same

proportion as EC concentrations. However, the proportion of magnetic particles ($SIRM_M$) and mineralogy (S-ratio) are changing from one season to the other. Wood type and humidity can affect the combustion temperature [Ghafghazi et al., 2011] and efficiency resulting in the emission of more organic material as was observed on the AF site. Nevertheless, further investigation of the release of Fe-bearing particles by traditional smoking activities under varying conditions is required.

3.7 Conclusion

In this work, we presented the magnetic investigation of the PM2.5 captured by air filters, previously sampled in a two-year campaign on the western SSA.

- Iron oxide spherules (fly-ash), among other particle shapes and compositions, have been detected on PM2.5 pumped-air filters in Abidjan and Cotonou cities. This particular shape is evidence of anthropogenic origin for the iron oxides that originate from the combustion sources (traffic and wood-burning) in the vicinity of the sampling locations. The granulometry of the iron oxides in all sites has a narrow distribution, showing that the different sources of emissions are not selective for size in the PM2.5.

- The magnetic mineralogy is composed of a mix of low (magnetite-like) and high coercivity minerals (hematite, goethite). The influence of the high coercivity minerals is stronger in the dry season in the traffic sites. The waste burning site has a stronger influence from dust since the observation is considerably further from the source of emission.

- Weekly $SIRM_V$ and ARM_V measured over a 2-years period follow the same seasonal pattern as the PM2.5 and EC (elemental carbon) mass concentrations although the correlation between the time series remains moderate. Both mass and volume SIRM for African cities are in a similar range as previously published values for Europe or Asia.

- Although the samples were acquired in the vicinity of major combustion sources, the alternance of the northeasterly Harmattan wind and the southwesterly Monsoon flow has a significant impact on the magnetic properties. The Harmattan period shows a higher contribution of high coercivity material and an increase in PM2.5 concentrations indicating a supply of aeolian mineral dust. During the Monsoon, the local source has an enhanced effect on the PM2.5 composition.

- $SIRM_M$ for wood-burning activities are lower than for traffic due to the large emission of organic carbon during biomass combustion.

- We found a robust correlation between elemental carbon mass concentrations and $SIRM_V$ and ARM_V both for the traffic sites and for the domestic fire site.

Chapter 4

Urban environments air quality investigation through passive & active sensors

4.1 Contextualization

This chapter presents a series of studies on air quality and PM investigation in Toulouse, France. It is based on air quality investigations in urban environments, using passive (i.e., bio-sensors) and active (i.e., air filters) sampling. At the end of this chapter, I also present an investigation of the ultrafine fraction (strictly SP, "fast-decay" type) of the airborne iron oxides with the use of the SPCDM (Superparamagnetic Concentration and Dipole Moment). The SPCDM is an experimental technique with the use of an inversion procedure.

Comprehending air quality in domestic and school environments is necessary to understand the exposition in the urban setting, as people spend most of their time indoors. In 2018, with the NanoEnvi project in Toulouse, we investigated the air quality in both domestic and scholar environments in Toulouse.

The school investigation begot the second paper of this thesis, which is under the peer-review process. It was submitted to Geohealth. Here, traditional PM1 sampling (for PM1, EC, and OC concentrations) is coupled with magnetic measurements (both in bio-sensors and air filters), providing a comprehensive study of the air quality, indoors and outdoors, in two schools in the city of Toulouse. SEM measurements complemented the information on the PM's ultrafine fraction (below 1μm). Lastly, this investigation was also conducted with citizen science participation, which brought some new insights from the citizen perspective on air quality investigation.

The third paper of this thesis comprehends the magnetic investigation on bio-sensors exposed indoors and outdoors in residencies throughout Toulouse. It is in draft form. In the scope of the NanoEnvi project, citizens were recruited in vulgarization seminars performed in Toulouse. Those citizens participated in the sampling, installing the bio-sensors in their homes, indoors and outdoors. A total of 59 semi-structured sociological interviews were performed with the participants. After retrieval of the samples and acquisition of the first results, restitution seminars were given to the participants to discuss the first results and

the context of the project. The magnetic properties measured on tree bark pieces showed important outdoor influences for the magnetic fraction.

Lastly, the SPCDM section presents the theoretical aspects of the method, including a summary of the Neel model for superparamagnetism on which it is based, the development of the inverse procedure, and the creation of the database. Then I present a brief study case with data measured on the bio-sensors exposed in the domestic environment and from courtyard tree bark from the schools from the second and third papers of this thesis.

4.2 Barking up the right tree: Using tree bark to track airborne particles in school environment and link science to society

A. da Silva Leite [1]***, S. Rousse*** [1]***,J-F. Léon*** [2]***, R. I. F. da Trindade***[3]***,S. Haoues-Jouve***[4]***, C. Carvallo***[5]***, M. Dias-Alves*** [2]***, A. Proietti***[6]***, E. Nardin***[1]***, M. Macouin***[1]

[1] *Géosciences Environnement Toulouse, Université de Toulouse, CNES, CNRS, IRD, UPS, (Toulouse) France;*

[2] *Laboratoire d'Aérologie, Université Paul Sabatier-Toulouse 3, CNRS, Toulouse, France;*

[3] *Universidade de São Paulo, Instituto de Astronomia, Geofísica e Ciências Atmosféricas, São Paulo, Brasil;*

[4] *Laboratoire Interdisciplinaire Solidarités Sociétés Territoires, CNRS, Université Toulouse 2, EHESS, ENSFEA, Université Toulouse 2, France;*

[5] *Sorbonne Université, UMR 7590, Institut de Minéralogie, de Physique des Matériaux et de Cosmochimie, F-75005 Paris, France;*

[6] *Centre de Microcaractérisation Raimond Castaing, Université Toulouse 3, UAR3623, 3 rue Caroline Aigle 31400 Toulouse, France;*

Keypoints:

- Magnetic methods and carbon analyses evidence high concentrations of indoor and outdoor PM1 due to traffic sources.
- Proximity of traffic source and absence of ventilation favorize accumulation of PM indoor, threatening children's health and learning skills.
- Passive monitoring using vegetal media facilitates teacher and pupil involvement and prevents eco-anxiety.

Abstract Children's exposure to air pollution affects both their health and learning skills. Fine and ultrafine particulate matter (PM2.5, PM1), notably issued from urban centers' traffic sources, are the most potentially harmful health hazards. However, their monitoring and society's awareness of their dangers needs to be consolidated. In this study, raising teacher and pupil involvement for air quality improvement in their school environment is reached through developing a passive monitoring technique (bio-sensors made of tree bark). The experiment was implemented in two urban elementary schools close to the main traffic road in Toulouse (South of France). Magnetic properties, carbonaceous fraction measurements, and SEM-EDX investigations were realized both on passive bio-sensors and filters issued from active sampling. We find that traffic is the main PM1 source for both outdoors and indoors at schools. Higher levels of outdoor PM in the school's environments are reached compared to the urban background, especially in the cold period. The school's proximity to the main traffic source and lack of ventilation are the main causes of observed PM1 accumulation in classrooms. The co-working experiment with educational teams and pupils shows that the use of bio-sensors is a driver for children's empowerment to air pollution and therefore represents a potential key tool for the teachers though limiting eco-anxiety. As PM accumulation

is observed in many scholar environments across Europe, the proposed methodology is a step toward a better assessment of PM's impact on pupils' health and learning skills.

Plain Language Summary Children's exposure to air pollution affects both their health and learning skills. Monitoring airborne particles in school environments from a knowledge co-production perspective seems essential to address school air pollution. Here we use tree bark and filter samples to monitor school air quality. Teachers and pupils are involved in the implementation process. The experiment was set up in two schools in Toulouse (France), close to the busy ring road. Traffic is the main source of air pollution inside and outside classrooms. Quantities of airborne particles are higher during cold periods. The proximity of the highway and poor ventilation in the schools are the leading cause of airborne particles accumulation inside classrooms. Collaboration with school staff and students shows that using trees has been a driving force for children to embrace the project and understand the context of air pollution, limiting anxiety related to this topic.

4.2.1 Introduction

Children are particularly vulnerable to air pollution exposure [Szabados et al., 2021, Khreis et al., 2017, Ferguson and Solo-Gabriele, 2016, Kelly and Fussell, 2015], one of the most important environmental causes of premature death in Europe [Agency, 2021]. They have higher air intake compared to adults, leading to higher absorption of pollutants through respiration, besides having immature respiratory and neurological systems [Martins et al., 2020, Kim et al., 2004, Rice and Barone Jr, 2000]. Health consequences in infants from the exposure to pollutants and particulate matter (PM) may include respiratory diseases, impairments in their cardiovascular system, and worsening of their neuropsychological development [and references therein WHO, 2021a]. In terms of health hazards, the fine and ultrafine fractions are the most harmful ones [Pope III and Dockery, 2006, Martins et al., 2020] as they may penetrate deeper into the respiratory system. The translocation from the lungs to the bloodstream is more likely to happen in poorly soluble ultrafine particles, thereby enhancing the deleterious effects of associated hazardous substances [Pope III and Dockery, 2006]. Ensuring good air quality for children's environments also provides optimal conditions for learning [Höfner and Schütze, 2021, Vornanen-Winqvist et al., 2020, Annesi-Maesano et al., 2013, Mendell and Heath, 2005], in addition to preserving their health. However, PM2.5 concentrations (i.e. particle sizes smaller than 2.5μm) inside classrooms could be higher than outdoors, at least in European schools [Kalimeri et al., 2019]. Children spend a lot of their school time indoors, making their indoors exposure to PM as important as the outdoors one. In France, students between 4 and 14 years old spend on average 3.8h of their daily time in schools [Zmirou et al., 2002]. For a non-negligible part of the children, it is common that this time represents 10h on a weekday (as it includes childcare in schools). It is therefore important to assess the level of fine and ultrafine particles (PM2.5 and PM1) in the air inside and outside classrooms, as well as identify practices that can improve air quality. Children's exposure depends on local outdoor air quality, indoor sources, and the ventilation system [Dimitroulopoulou, 2012]. Children's lungs can notably be irreversibly impacted by local traffic exposure, regardless of regional air quality [WJ et al., 2007]. For example, manual ventilation of the classroom by opening the windows can also induce inconveniences (temperature, wind, and ambient noise outside), which can affect the pupils

learning conditions and academic performance [Mumovic et al., 2009]. Raising awareness about contaminants, sensors, and the role of ventilation is not enough to create leverage towards a more active approach [Tham, 2016]. Direct contextualization has been shown to be important [West et al., 2020] in environmental education. Environment education also needs to account for the risk of eco-anxiety raise [Pihkala, 2020]. In the light of these facts, in this study, the approach chosen to study air pollution was to use vegetation media as bio-sensors or bioindicators [Nakazato et al., 2018, Parviainen et al., 2020, Chaparro et al., 2020]. Environmental magnetism methods can be applied to natural media. They have been used to monitor anthropogenic PM trapped on vegetation such as leaves, lichens and bark [Sagnotti et al., 2009, Muñoz et al., 2017, Limo et al., 2018, Urbat et al., 2004, Zhang et al., 2008, Moreno et al., 2003, Chaparro et al., 2020, Vezzola et al., 2017, Dawaï et al., 2021]. Such methods rely on tracking magnetic minerals, e.g., iron oxides like magnetite, hematite, and maghemite [Winkler et al., 2021, Leite et al., 2018, Marié et al., 2018]. For traffic-related sources, these magnetic minerals can originate from internal fuel combustion of vehicles, disk brakes abrasion, and pavement erosion. This study was carried out in two primary schools in Toulouse using environmental magnetism, carbonaceous fraction measurements, and SEM-EDX investigation. Our aim is to explore how the use of environmental magnetism using bio collectors (tree bark) in addition to conventional techniques helps in transformative ways to tackle air pollution in schools by assessing the indoor/outdoor transfer of particles from traffic and by co-working with teachers and children.

4.2.2 Materials and methods

Location, meteorological & pollutants conditions

The city of Toulouse and its surroundings stands on quaternary alluvial terraces incised by the Garonne river. The terrace substratum is made of molasse consisting of fluvial deposits made of clay, marls lacustrine/palustrine limestones, and channelized sandstones and conglomerates derived from the North Pyrenean foreland basin [and references therein Christophoul et al., 2014].

Toulouse is the fourth biggest city in France, with a metropolitan population of approximately 1,331,000 inhabitants. The ring road constitutes one of the main traffic roads of Toulouse with a total of 35 km, linking important state highways to the city traffic. It has three lanes in each way, with a mean flow of ca. 120,000 vehicles per day (in 2019) on its southern part (consulted on January of 2022, `https://www.aua-toulouse.org/wp-content/uploads/2022/02/AUAT_chiffres_transports_2022.pdf`).

The two schools, separated by 1.3 km, are located south of downtown Toulouse, on the east bank of the Garonne river. School 1 and School 2 are located approximately 150 meters and 300 meters north and northwest of the Toulouse ring road, respectively. Both schools' courtyards are planted with Platanus trees (Figure 4.1). In School 1, the total number of pupils is around 360, divided into 15 classes with an average of 24 pupils per class. This school has two courtyards, separated by a school building. The West and the East courtyards have an area of 1400 and 3800 m^2, respectively. School 2 counts 140 pupils for eight classes, with classrooms of 12 to 26 students. It has one courtyard with an area of 4400 m^2. School buildings from School 2 and the bordering West courtyard of School 1 were built in

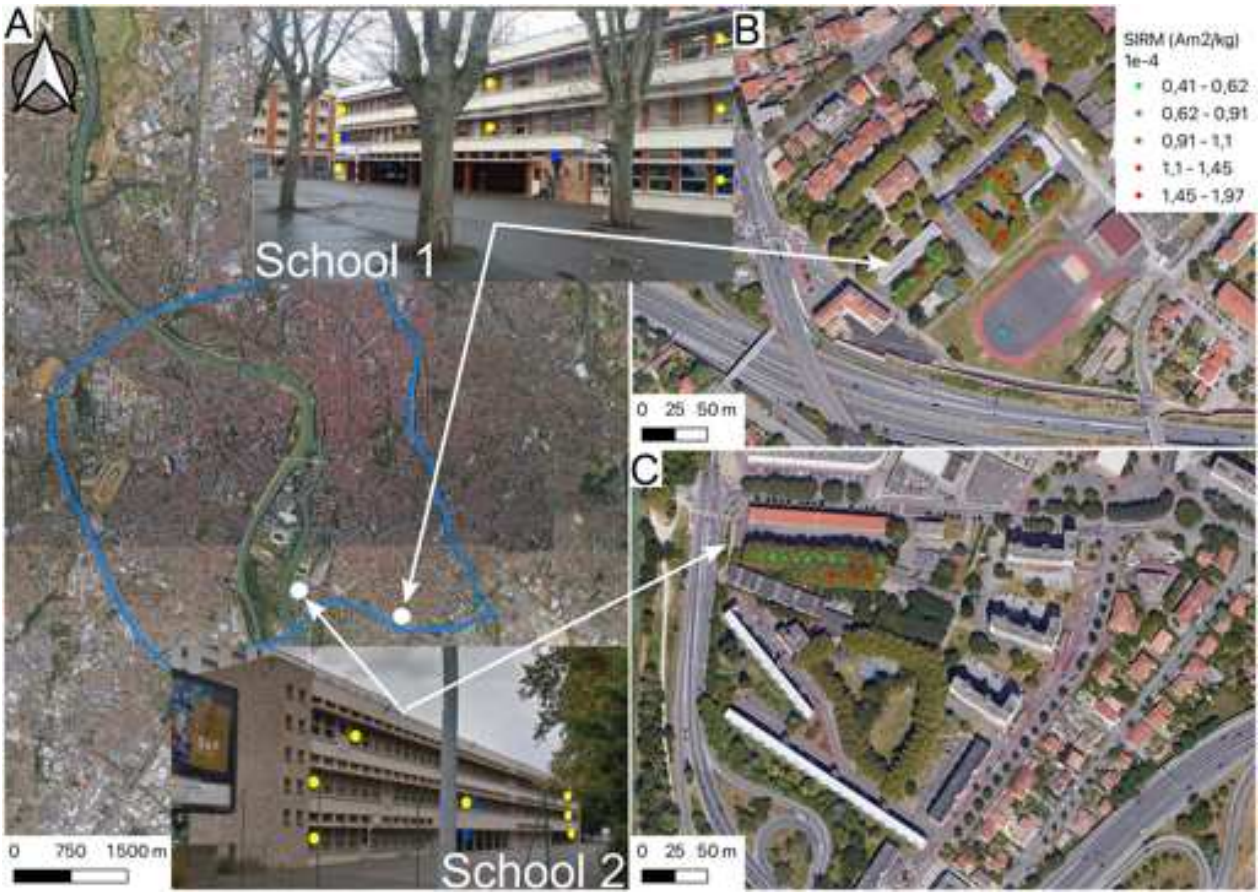

Figure 4.1: A) Satellite view of Toulouse (modified from Google Earth) with school locations and photographs of instrumented school buildings (insets). The ring road is highlighted in blue. The position of bio-sensors (yellow) and PM1 air filter location (blue) are marked with dots on the pictures. B-C) Zoom on Schools 1 and 2 locations. SIRM values obtained on tree barks from the sampled courtyard trees are displayed. The same color scale for schools 1 and 2.

the 1950s in the same architectural style and materials. They have classrooms of around 58 m^2. Buildings from the East courtyard of School 1 are historical buildings from the 1930s. This study sampled courtyards and selected classrooms with bio-sensors, tree bark, and air filters. In School 1, the bio-sensors and air filters were placed only in the school building bordering the West courtyard. Concerning meteorological conditions, Toulouse has a continental climate and is located in a ventilation corridor sometimes affected by either SE wind from the Mediterranean sea or NW winds from the Atlantic ocean. Winters are cold and cloudy with degraded air quality due to low ventilation and increased emissions from traffic and domestic heating (`https://www.atmo-occitanie.org`). During spring and early summer, air quality improves due to increased ventilation and rainfall. Experiments were launched between the end of 2018 and the first half of 2019. Meteorological parameters from Blagnac Airport and air quality stations from ATMO OCCITANIE in Toulouse (Supplementary - Figs. B.1 and B.2) show the differences between the sampled periods for NO_2, PM10 and PM2.5 concentrations, daily rainfall, and wind speed.

Methodology

Both active and passive sampling methods were deployed. The active sampling consisted of deploying Cyclone air filtration pumps with a cutoff size of PM1. Two different sets of samples were used for the passive sampling. The first set was composed of trees collected from the Platanus trees planted in the school courtyards. The second one consists of 15 couples of bio-sensors made of non-contaminated Platanus tree bark squares developed in the framework of the NanoEnvi project (`https://nanoenvi.omp.eu`). Using both Platanus tree bark and bio-sensors derived from the co-working experiment with educational teams and pupils

Low volume (2 $L.min^{-1}$) Cyclone (BGI by Mesa Labs) with a cutoff size of 1μm in diameter (PM 1) and air filtration pumps (SKC Air Touch) were used for the active sampling. Two sampling lines were run in parallel, the first equipped with a Whatman quartz filter and the second with a Teflon (Polytetrafluoroethylene or PTFE filter). The lines were continuously active over one or two weeks, in January/February (period 1) and April/June (period 2) of 2019, with six filtration lines each season. In each school, they were deployed in one classroom hosting between 20 and 25 children (indoor, at around 2 m high) and outdoor in the courtyard (at the height of approximately 2.5 m; Fig. 4.1). PM1 mass deposits were measured with the gravimetric method, with a high precision scale (SARTORIUS MC21S). The filters were kept in the weighing room for 24h at an ambient relative humidity of 30±15 % before the mass measurement. Atmospheric concentrations are estimated by dividing the mass deposit by the sampled volume. Concentrations of the carbonaceous fractions were achieved through optical-thermal analyses (IMPROVE protocol allowing the separation of the carbonaceous components, Chiappini et al. [2014a], Ouafo-Leumbe et al. [2018]) with an DRI model 2001 thermal/optical carbon analyser [Atmoslytic Inc., Calabasas, CA, Chow et al., 1993, 1994, 2004, 2006]. The DRI analyzer has a detection limit of 0.4, 0.1, and 0.3 $\mu gC\ cm^{-2}$ for Total Carbon (TC), Elemental Carbon (EC), and Organic Carbon (OC) estimated through the instrument blank. Our measurements have an estimated accuracy of 5% for TC and 10% for EC and OC.

Courtyard tree barks were collected for magnetic measurements on each available tree in

November and December of 2018 for School 2 and School 1, respectively. The trees are solely from the species *Platanus × acerifolia*, whose bark has an annual growth cycle. A total of 48 trees were sampled (32 in School 1 and 16 in School 2). In School 1, 7 trees were sampled in the West courtyard and 25 in the East courtyard. In School 2, the trees sampled form two parallel lines. School 1 courtyard trees have different arrangements in each courtyard. The West one displays a single line parallel to the building, and the East one presents trees on a square disposition around the courtyard, with two columns in the middle (Fig. 4.1). Around 30 g of tree bark per tree were collected between1 and 2 m above the ground. A small amount of each bark sample was pulverized into a fine homogeneous powder and then put in two different gel caps sizes, with a mass of 0.1 g to 0.8 g.

The bio-sensors consist of garlands composed of 5/6 4 cm^2 squares of *Platanus x acerifolia* species bark pieces that are suspended from a nylon thread. The tree bark used to build the bio-sensors was collected in areas far from traffic perturbations and had their Saturation Isothermal Remanent Magnetization (SIRM) previously measured under 1T fields to assess their almost null level of magnetic content. Bio-sensors were exposed between December 2018 and July 2019 (7 months) in a total of 7 rooms in School 2 and 8 rooms in School 1 (Figure 4.1). For each classroom, two bio-sensors were placed, indoors and outdoors, at heights of approximately 2 m to prevent children from touching them. After collection, they were ground into a fine, homogeneous powder. The powders were put into gelcaps, with masses ranging from 0.8 to 0.1g in each gelcap.

Most of the measurements were realized in the magnetic platform at GET (University of Toulouse). Complementary analyses were performed at the paleomagnetic Laboratory at the USP (São Paulo, Brazil). SIRM was acquired on filters and courtyard tree bark using JR-6 and JR-5 spinning magnetometers, with 2.4 μA/m sensitivity. On the JR-6, the high sensibility mode was used, and each measurement was repeated five times. A pulse magnetizer (Magnetic Measurements Ltd.) induced the SIRM with a saturating magnetic field of 1T. The SIRM gives a qualitative concentration of the magnetic carriers [Evans and Heller, 2003]. PTFE filters were chosen to carry out the magnetic investigation since in a pilot conducted in blank filters, the PTFE filters had, on average, 20% the SIRM of quartz filters after 1T field induction. Filters were normalized by pumped air volume in the filters ($SIRM_V$). Courtyard tree bark was mass normalized by sample mass ($SIRM_M$).

Hysteresis cycles and back-field remanence curves were measured with a Vibrating Sample Magnetometer (μ-VSM) 3900 from Princeton Measurements Corporation at the IPGP-IMPMC Mineral Magnetism Analytical Facility (Paris, France). The μ-VSM has a sensitivity of 0.5 x 10^{-6} emu. Hysteresis parameters for tree barks and bio-sensors were then calculated, namely the saturation magnetization (M_S) and coercive force (H_C). The remanent saturation magnetization (M_{RS}) and coercive remanent force (H_{CR}) were obtained from the backfield remanence curve. The ratio between the hysteresis parameters (M_{RS}/M_S and H_{CR}/H_C) when plotted against each other creates the so-called Day Plot [Dunlop, 2002].

Bio-sensors magnetic measurement protocol consisted of alternated field (AF) demagnetization with 100mT peak field, followed by one step anhysteretic remanent magnetization (ARM) acquisition and then isothermal remanent magnetization (IRM) acquisition. The measurements were done in a 755-1.65 DC SQUID magnetometer (2G enterprises), with a sensitivity of 10^{-9}emu, located in a magnetically shielded room with an ambient field inferior to 500nT. The ARM acquisition was performed with a superimposed AF field of 100mT

under a bias field of 30μT. When divided by the bias field, the ARM magnetization gives the susceptibility of the ARM, xARM [Evans and Heller, 2003]. The IRM inductions were imparted on a pulse magnetizer (Magnetic Measurements Ltd.). All measurements were done three times and then averaged. The samples were induced in the pulse magnetizer at room temperature to acquire IRM, with field values of 1T for the SIRM and 300mT for the backfield IRM (IRM_{-300mT}).

The S-ratio gives the relative contribution of high and low coercivity magnetic minerals to the magnetization. The S-ratio is given by IRM_{-300mT}/SIRM, as at 300mT, only soft coercivity magnetic carriers (magnetite, for instance) will align their magnetic moments with the applied magnetic field. At 1T, all magnetic minerals (soft and hard coercivity carriers) will align their moments with this field [King and Channell, 1991]. The xARM/SIRM ratio is widely used as a proxy for grain size variation on magnetite-like magnetic minerals [Maher, 1988] because of its ability to distinguish between coarse and fine grain sizes.

Surface characteristics of the carbonaceous aerosols and the iron oxides were obtained from representative samples of PM1 filters and bio-sensors through Scanning Electronic Microscopy (SEM) observations using a Field-emission gun FEG SEM JEOL JSM 7100F at the Microcaracterization Center Raimond Castaing (`https://centrecarcastaing.cnrs.fr`). Composition characterization was obtained through energy dispersive X-ray spectrometer (EDS) measurements using an Oxford Instrument Detector (X_{MAX}=80mm_2 and Ultim Max=100mm^2). The samples were fixed using silver paint and coated with carbon.

Involvement of pupils and teachers in the experiments in schools and social assessment

The rollout of the experiment to the schools was conducted in several phases. After contacting the city councilor responsible for the elementary school, the first step was to establish a relationship with the school principals via the parent association (School 1) and the local community association (School 2). The second step consisted of the visit of researchers to the school. This intervention, aiming at presenting the project to pupils and teachers, was carried out for classes of children 9 to 12 years old (6 classes for School 1 and 5 classes for School 2). The intervention was designed as follows: a first part (20 min) of presentation on the air quality, airborne particles, and the project, a second part composed of experimentation workshops and scientific manipulations and an artistic approach, and concluded in the third part by a general discussion. The workshops were designed to provide an understanding of the project process by discovering the magnetic phenomena (different games and experiments with magnets and ferrofluids), the measurements by the students on a Bartington MS2 field magnetic susceptibility meter of bark samples localized on a map and by extracting magnetic particles from mud. The installation of the active pumps was the subject of a short lecture and discussion in the selected school class of each school during a third intervention. The final step involves the reporting of the results. This was only done in the two classes that hosted the pumps, as the COVID health crisis blocked possible external interventions during this time.

Teachers from the two classes that hosted the pumps were interviewed in a semi-structured manner to assess their awareness of air quality, the ventilation habits they implemented in the classrooms, and the impact of the experiments on the children and teachers.

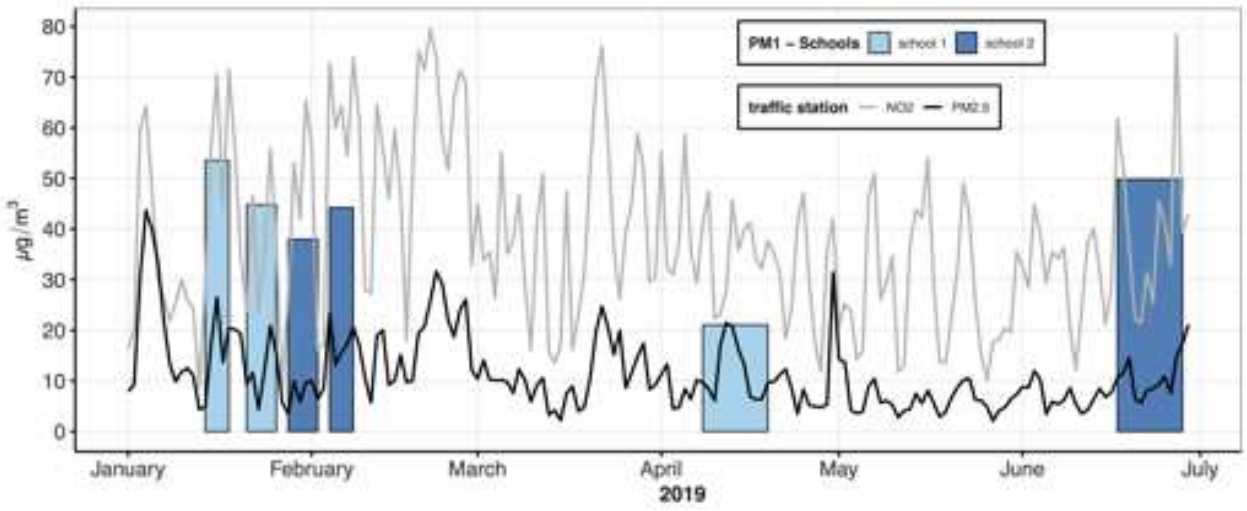

Figure 4.2: Daily (black line) PM2.5 and (grey line) NO_2 concentrations measured at a traffic station in Toulouse (route *d'Albi*) and (vertical bars) weekly PM1 measured at the schools between January and July 2019.

4.2.3 Results

Air filters

Outdoor PM1 concentration from period 1 ranges from 41.1 to 49.2 µg m^{-3} , while outdoors PM1 concentration from period 2 ranges from 21.1 to 49.8 µg m^{-3} (Table 4.1). Indoors, concentration values reveal higher levels during period 1 (varying from 35.7 to 40.7 µg m^{-3} for School 1 and 2 respectively) than during period 2 (ranging from 24.2 to 29.3 µg m^{-3} for School 2 and 1 respectively). During the first half of the year 2019, the ambient daily mean concentrations of NO_2 and PM2.5 recorded by AtmoOccitanie at the traffic station (route d'Albi - about 8 km to the North of the schools) range between 8.0 and 80.0 µg m^{-3} and 2.0 and 44.0 µg m^{-3}, respectively (Figure 4.2). This rather large daily variability reflects the proximity of traffic emissions. The school filters display higher PM1 concentrations in comparison to the PM2.5 measurements. The average PM2.5 concentration during the sampling periods of the filters (see Table 1) is on average, three times lower than the PM1 filter concentration. This shows an overall higher concentration of PM in these school environments compared to the urban background of Toulouse.

Figure 4.2 presents the measured PM1 concentration on the school filters alongside the daily measured PM2.5 and NO_2 concentration at official air quality stations (ATMO OCCITANIE). The station is located in Toulouse (route *Albi*) and represents the traffic background of the city. Generally, the school filters display higher PM1 concentrations during period 1 compared to the PM2.5 measurements from the air quality stations. During period 2, the concentration of PM1 on the school filters is comparable to the highest PM2.5 concentration values from the air quality stations. This shows an overall higher concentration of PM in these school environments compared to the urban background of Toulouse. The NO_2 concentration patterns follow the PM1 concentration patterns measured in both schools.

The elemental carbon (EC) indoors concentrations reach a maximum value ($0.8\,\mu g\,m^{-3}$) in School 1 during period 2, and in this school, the values are almost stable throughout the experiments. The minimum concentration is reached in School 2 during period 1 ($0.4\,\mu g\,m^{-3}$). In School 1, the values are almost stable throughout the experiments. In school 2, the value nearly doubles from period 1 to 2. Outdoor EC concentrations are higher than indoor and higher during period 1, reaching a maximum in School 1 ($1.6\,\mu g\,m^{-3}$). The minimum value is recorded for the outdoor environment in School 2 during period 2 ($0.8\,\mu g\,m^{-3}$).

The values of organic carbon (OC) concentration in the filters are higher indoors (Table 4.1), with a maximum value in School 1 of $5.5\,\mu g\,m^{-3}$ during period 2, and a minimum value in School 2 of $2.8\,\mu g\,m^{-3}$ in the same period. The outdoor values are maximum in School 1 during period 1 ($4.4\,\mu g\,m^{-3}$) and minimum in School 2 during period 2 ($2.6\,\mu g\,m^{-3}$).

The OC/EC ratio can be used to infer the source of the carbonaceous aerosols and also the formation of secondary organic carbon [SOC, Xu et al., 2015]. The values observed in the schools are higher indoors than outdoors (Tables 4.1). The indoor values slightly vary between the periods in School 1, with a maximum of 6.9 during period 2. In School 2, the OC/EC ratio decreases from 12.2 to 4.0 from periods 1 to 2. The outdoor ratio values have less variation, having a maximum in period 2 of 3.2 in both schools and a minimum at School 2 of 2.1 for period 1.

Table 4.1: Elemental (EC) and organic carbon (OC), PM1 concentrations, and $SIRM_V$ measured at School #1 and #2 on PTFE filters during the 4 field experiments in 2019. The ratio between indoor and outdoor concentration (I/O) is indicated for each parameter and sampling period.

School #1		EC ($\mu g\,m^{-3}$)	OC ($\mu g\,m^{-3}$)	OC/EC -	PM1 ($\mu g\,m^{-3}$)	$SIRM_V$ ($10^{-10} A\,m^2$)
14 -26 Jan.	indoor	0.7	4.7	6.7	40.7	2.87
	outdoor	1.6	4.4	2.7	49.2	3.21
	I/O (no unit)	0.4	1.1	-	0.8	0.9
08 -18 Apr.	indoor	0.8	5.5	6.9	29.2	0.97
	outdoor	0.9	2.9	3.2	21.1	0.49
	I/O (no unit)	0.9	1.9	-	1.4	1.9
School #2						
28 Jan. -9 Feb.	indoor	0.4	4.9	12.2	35.7	1.08
	outdoor	1.4	3.1	2.1	41.1	1.98
	I/O (no unit)	0.3	1.6	-	0.9	0.5
17 -27 Jun.	indoor	0.7	2.8	4.0	24.3	0.42
	outdoor	0.8	2.6	3.2	49.8	1.94
	I/O (no unit)	0.9	1.1	-	0.5	0.2

$SIRM_V$ measurements were carried out on the Teflon filters. It allows direct comparison between the concentration of iron oxides captured by the filters and PM1 concentration measured on the Quartz filters. $SIRM_V$ values in School 1 have maximum and minimum measured values of 3.21×10^{-10} and $0.49 \times 10^{-10}\,A\,m^{-1}$ in the outdoor environment in periods 1 and 2 respectively. School 2 maximum and minimum values are reported outdoors during period

1 and indoors during period 2, with measured values of 1.98×10^{-10} and $0.42 \times 10^{-10}\,\mathrm{A\,m^{-1}}$ respectively.

Courtyard tree bark and bio-sensors

$\mathrm{SIRM_M}$ values for the courtyard tree bark's samples vary between $17.68 \times 10^{-5}\,\mathrm{A\,m^2\,kg^{-1}}$ and $3.63 \times 10^{-5}\,\mathrm{A\,m^2\,kg^{-1}}$ (Figure 4.1). Mean $\mathrm{SIRM_M}$ values are close in all courtyards, ranging from $6.40(\pm3.50)\times10^{-5}\,\mathrm{A\,m^2\,kg^{-1}}$ (on School 1 West courtyard) to $10.62(\pm3.26)\times10^{-5}\,\mathrm{A\,m^2\,kg^{-1}}$ (on School 1 East courtyard). School 2 tree bark $\mathrm{SIRM_M}$ values have a mean of $8.61(\pm3.71)\times10^{-5}\,\mathrm{A\,m^2\,kg^{-1}}$. In School 1, a difference in the distribution of $\mathrm{SIRM_M}$ values is noticeable between both courtyards, with higher values in the Eastern courtyard.

Bio-sensors were placed inside and outside the classrooms on different building floors. $\mathrm{SIRM_M}$ values for both indoor and outdoor bio-sensors of School 1 are higher than those obtained from School 2 (Table 4.2). In School 1, indoor bio-sensors have mean $\mathrm{SIRM_M}$ values of $1.35(\pm0.46)\times 10^{-5}\,\mathrm{A\,m^2\,kg^{-1}}$ whereas mean values for outdoor samples are $1.88(\pm0.49)\times10^{-5}\,\mathrm{A\,m^2\,kg^{-1}}$. $\mathrm{SIRM_M}$ mean values for School 2 bio-sensors are $0.95(\pm0.23)\times10^{-5}\,\mathrm{A\,m^2\,kg^{-1}}$ (indoor) and $1.08(\pm0.43)\times10^{-5}\,\mathrm{A\,m^2\,kg^{-1}}$ (outdoor). The mean of $\mathrm{SIRM_M}$ value for bio-sensor displays a similar trend than $\mathrm{SIRM_V}$ and EC concentrations measured in the air filters, with higher values outdoors, in School 1.

Table 4.2: $\mathrm{SIRM_M}$, S-ratio and xARM/SIRM means and standard deviation measured on bio-sensor at School #1 and #2. N is the number of samples, and I/O is the ratio between indoor and outdoor $\mathrm{SIRM_M}$.

School #1		$\mathrm{SIRM_M}$ ($10^{-5}\mathrm{A\,m^2\,kg^{-1}}$)	S-ratio	xARM/SIRM (10^{-4}m/A)	N
Garland bio-sensors	Indoor	1.35 ±0.46	0.95 ±0.01	9.14 ±3.04	8
12/13/18-07/04/19	Outdoor	1.88 ±0.49	0.97 ±0.02	4.83 ±2.76	8
	I/O (no unit)	0.7			
Courtyard tree bark	West	6.40±3.50	0.89±0.07		7
	East	10.62±3.26	0.92±0.04		25
School #2					
Garland bio-sensors	Indoor	0.95 ±0.21	93.1 ±4.7	5.69 ±3.27	7
12/2018-06/28/19	Outdoor	1.08 ±0.43	88.5 ±4.8	5.31 ±3.88	6
	I/O (no unit)	0.9			
Courtyard tree bark		8.61±3.71	0.87±0.05		18

The S-ratios calculated for the courtyards' barks display similar values for the three yards with $0.92(\pm0.04)$, $0.89(\pm0.07)$, and $0.87(\pm0.05)$ for School 1 East and West ones and School 2 one, respectively. Results of the bio-sensors (Table 4.2) show greater variability in School 2 when compared to School 1. The mean S-Ratio calculated for bio-sensors of School 1 are $0.95(\pm0.01)$ and 0.97 (±0.02) in indoor and outdoor environments, respectively. School 2 presents lower mean S-ratio values than the bio-sensors from School 1, with indoor and outdoor values at $0.93(\pm0.05)$ and $0.89(\pm0.05)$, respectively, indicating a higher content of high coercivity minerals than for School 1 samples.

Hysteresis parameters from both tree bark from the schoolyards' trunks and bark used as bio-sensors displayed an extensive range of parameters compared, for example, to data obtained in Roma (Italy) on leaves [Szönyi et al., 2007] and on PM10 filters [Sagnotti et al., 2006]. They extend to values obtained by Sagnotti et al. [2009] and Sagnotti and Winkler [2012]from exhaust residues from gasoline and diesel motors and brake wear dust collected directly in situ. This could result from different sources of particles, meaning different magnetic mineralogy such as high coercivity minerals like hematite(of geological origin, for example) or metallic iron (linked to abrasion of combustion cylinder, pads, and disk brakes), which influences SIRM and coercivity values [Gorka-Kostrubiec et al., 2019, Gorka-Kostrubiec and Szczepaniak-Wnuk, 2017] and therefore impact the S-Ratio and/or grain sizes parameters.

The highest xARM/SIRM values are found at the indoor environment of School 1 (Fig. 4.4, Table 4.2), with mean at $9.14(\pm3.04)\times10^{-4}$m/A, whereas the outdoor ones have a mean of $4.83(\pm2.76)\times10^{-4}$m/A. School 2 has close calculated mean values in the indoor and outdoor environments, with values of $5.69(\pm3.27)\times10^{-4}$m/A and $5.31(\pm3.88)\times10^{-4}$m/A, respectively. School 2 mean values are also close to the outdoor value of School 1.

The ratio of the indoor to the outdoor parameters (hereinafter called I/O; Table 4.2) is a simple and straightforward way to quantify the indoor-outdoor concentration relationship of a given compound, being used widely in air quality studies [Kalimeri et al., 2019, , and references therein]. I/O for EC shows similar variation in both schools, increasing from period 1 to 2, with values of 0.4 to 0.8, and 0.3 to 0.9 for School 1 and 2, respectively (Table 4.2). Similarly, I/O for PM1 shows an increasing trend toward summer from 0.8 to 1.4 and 0.9 to 1.3 in schools 1 and 2, respectively. I/O for SIRMV goes from 0.9 to 2.0 from periods 1 to 2, showing more than a two-fold increase, whereas, in School 2, there is a decrease from 0.5 to 0.2. The I/O for SIRMM on both school bio-sensors have close values.

SEM

SEM results on the filters show the dense quartz matrix of the filters, encrusted with agglomerations of carbon "fluffy" soot aggregates, iron oxides aggregates, and spherules. Figure 4.5A and 4.5B show backscattered electron images (BSE) from School 1 outdoor and indoor filters respectively (collected in period 2). For the outdoor filter (Figure 4.5A), one can notice an agglomeration containing iron (particle number 1), aluminum, and sulfur, with a dimension of 2.1μm and an elongated shape. Some carbon-rich agglomerates are also visible, for instance, particle 2, 1μm in size, mainly composed of carbon with some Na. Particle 3 is an 82 nm diameter spherule composed mainly of iron and oxygen. A secondary electron image (SE) with greater magnification (x40000) (Figure 4.5A(a)) enables us to investigate further the topography of the iron oxide spherule (particule 3). It highlights the spherule and soot aggregate cementation to the quartz fiber.

The SEM image of the indoor filter (Figure 4.5B) shows an agglomeration of iron oxide spherules attached within a carbon "fluffy" soot aggregate (dimension of 1 μm) on the quartz fiber. There are at least 6 spherules trapped (agglomerate1), with sizes of 40, 57, 99, 123, 128 and 157 nm. SEM secondary electron image (Figure 4.5B(b)) displays in greater detail the spherule agglomeration cemented on the quartz filter fiber with soot aggregates. Figure 4.5C displays typical particles from an outdoor bio-sensor in School 1. Particles are arranged in irregularly shaped agglomerates. Particle 1 is an iron oxide with a dimension of 1.3 μm.

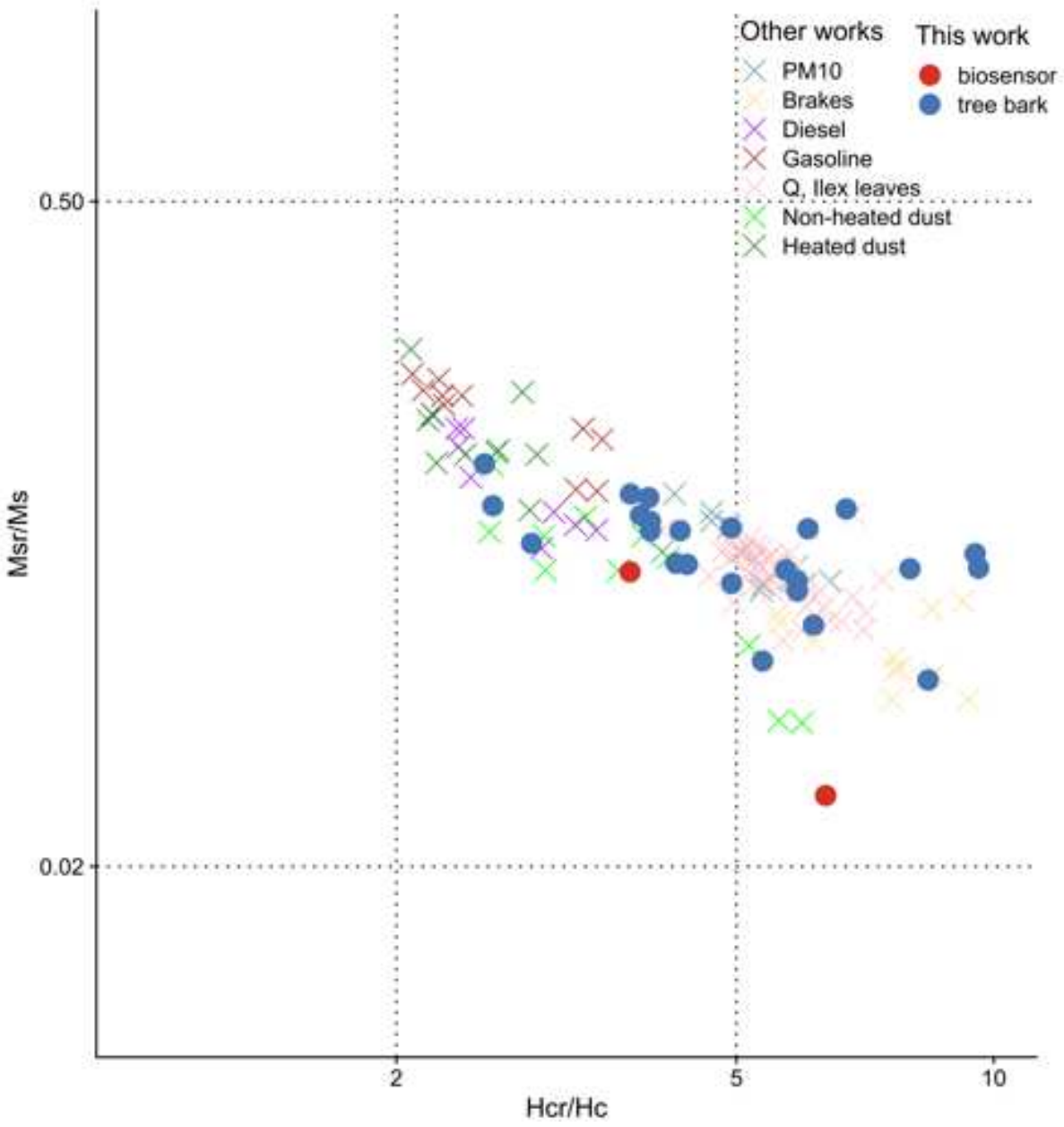

Figure 4.3: : Day plot of the tree bark (circles) and previously published data (crosses). Data from Q. ilex leaves are from Szönyi et al. [2007], data for PM10 filters from Sagnotti et al. [2006], data for gasoline, brakes and diesel from Sagnotti et al. [2009] and Sagnotti and Winkler [2012], and data from dust (heated and non-heated) are from Gorka-Kostrubiec et al. [2019].

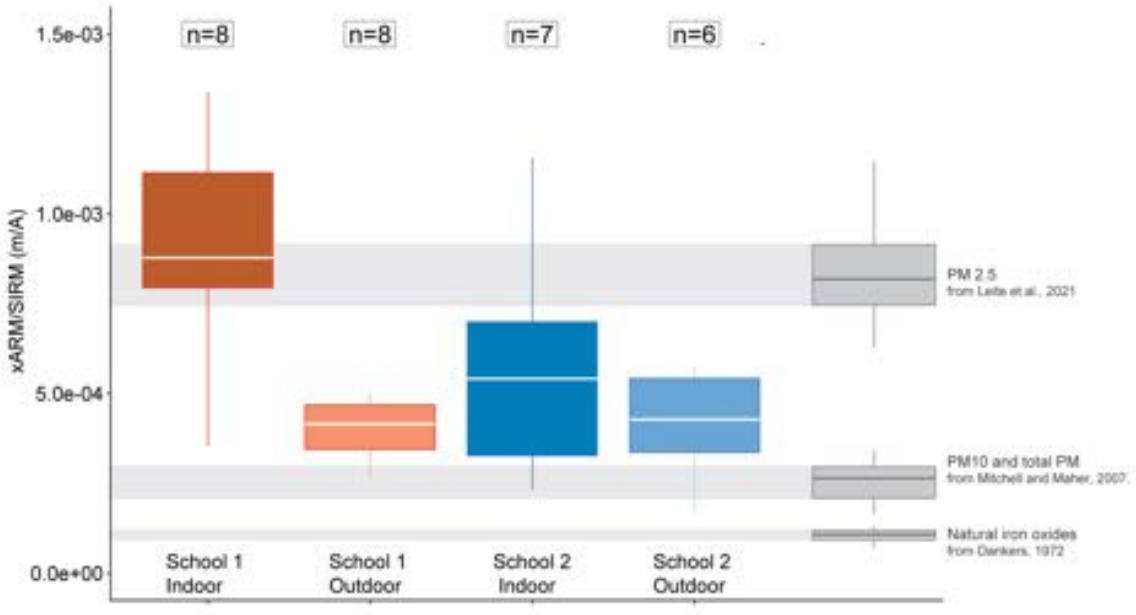

Figure 4.4: Box plot for calculated xARM/SIRM ratio in both school bio-sensors (indoor and outdoor) and bibliographical values [Dankers, 1978, Mitchell and Maher, 2009, Leite et al., 2021, for natural iron oxides, PM10 and total PM and PM2.5 respectively]. Data points in black dots, outliers in red dots, the median is the horizontal line inside the box, the interquartile range by the box size, and maximum and minimum values are the vertical whiskers.

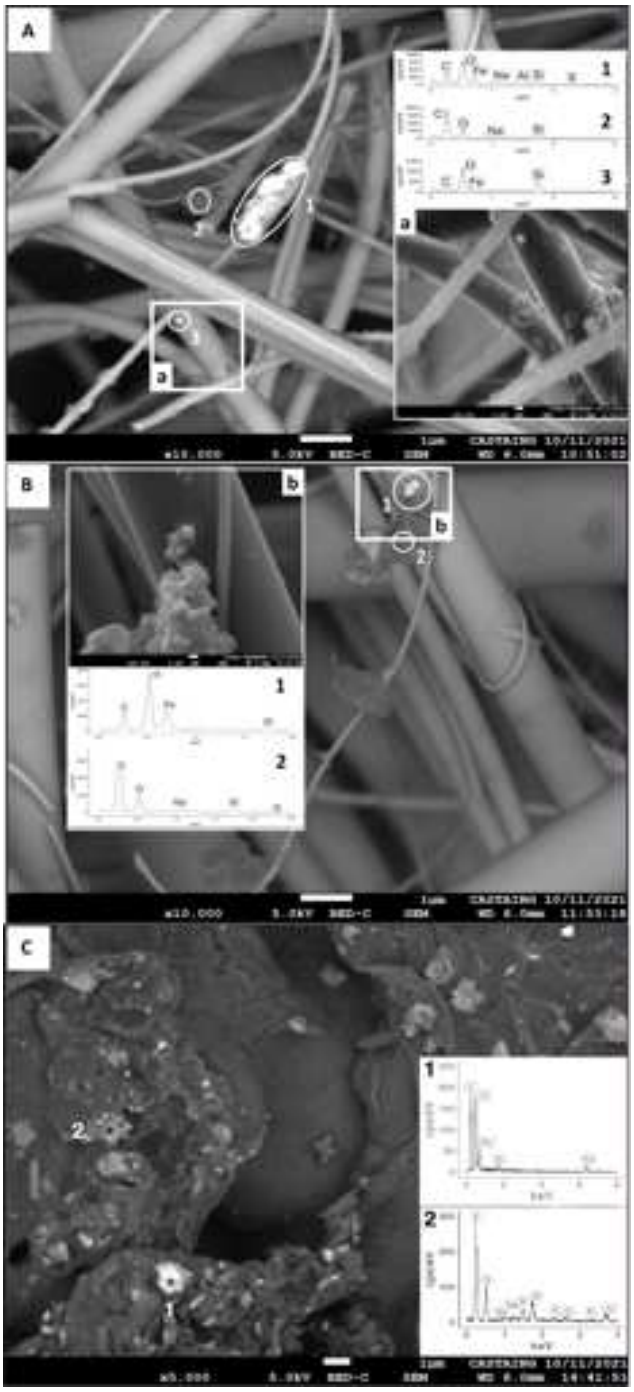

Figure 4.5: A: Backscattered electron SEM image (BSE) of School 1 outdoor filter iron from period 2 with spectra of oxide spherule, iron oxide agglomerations, and soot aggregates; a) Blow-up in Secondary electron image (SE) of iron oxide spherule (particule 3). B: Backscattered electron SEM image (BSE) of School 1 indoor filter from period 2 showing agglomeration of at least six iron oxides spherules (1) and carbon-rich aggregates (2); b) Secondary electron image (SE) of agglomeration of iron oxide spherules (1); C: Backscattered electron SEM image (BSE) from outdoor bio-sensors exposed in School 1 showing several agglomerated-like particles with irregular shapes including iron oxides.

Spectrum from the particle #2 has a classical lithic composition (containing Mg, Al, Si, K and Na, Al and Si, respectively) and size of 1.3 μm.

Teacher's interviews

Two teachers were interviewed. One of the teachers reported that there are no official guidelines regarding air pollution except for avoiding outdoor sports during pollution peaks. Nevertheless, poor air quality in the school environment linked to traffic emission is assumed by both teachers due to the visible proximity to the main traffic road for School 1 and an important access road to the city for School 2. For the latter, occasional trash burning nearby the school is also mentioned. One of the teachers has a scientific background and says that his classrooms are receptive to environmental topics. This teacher was involved in the intervention design by asking the researchers to come and explain the needs of the children. From the teacher's point of view and observations, the fact that the researchers came to show the sensors made from bark, which is an inexpensive setup, was vital in the appropriation of the project by the children. For this teacher, even if children didn't understand all the scientific background behind it, this is not problematic. Both teachers revealed the importance that children were able to meet the researchers on more than one occasion and to touch and use the experimental material in their classrooms. Both teachers reported the problem of noise when the windows are open. Noises arise from children's activities in the schoolyard, helicopters, and traffic, notably the honking of car and vehicle noises that reflect anger and stress. Besides the noise and difficulty of opening windows due to their dilapidated state, one of the teachers also reported some reluctance to vent to prevent traffic pollution from entering the classroom. The classroom is ventilated by the windows in the morning during cleaning before the arrival of children and sometimes during the day. Managing troubles in concentration and ventilating with an appropriate frequency is difficult for the teacher. The opening of windows during the day is induced by human sweat smelling and heating during the spring months. Inconvenience due to the noise generated by the cyclone pump inside the classroom was reported by the pupils to their teachers after a few days of the experiment running. The teacher also reported relief at the end of the experiment with the active system despite the great motivation of pupils and teachers. Therefore, noise related to common active systems may prevent teachers' involvement in monitoring air quality in their classrooms. Developing passive vegetal-oriented captors systems might be a way to develop their collaboration.

4.2.4 Discussion

Outdoor School Environment

The data indicate that the main source of the PM1 captured in both schools by the air filters is traffic emissions. Traffic emissions are generated by internal engine combustion and abrasion both from the vehicle's parts (disk brakes, for instance) and asphalt. Outdoors, Viana et al. [2007] reports OC/EC ratio values characteristic of traffic emissions in urban settings during Winter and Summer for Belgium (4.4 and 3.5 respectively), Netherlands (4.7 and 2.8, respectively) and Spain (5.6 and 4.6, respectively). In Athens, OC/EC ratios of 4.7 and 2.9 [Paraskevopoulou et al., 2014, Remoundaki et al., 2013, respectively] were found on

traffic-related urban sites. Reported OC/EC ratios from outdoor samples in this study have a similar range compared with previous OC/EC ratios in European cities, pointing out traffic emission (specifically internal diesel combustion) as the main source of the captured PM1 in this study.

This traffic-sourced origin is further reinforced by the similarity of the measured trends obtained from the daily variations in NO_2 and PM2.5 concentrations (Figure 4.2). NO_2 is a secondary pollutant formed mainly from nitric oxide (NO), the predominant species in vehicle exhaust [Henderson et al., 2007]. The covariation between PM2.5 and NO_2 indicates that vehicle exhaust is the main source of PM2.5 in the city of Toulouse. The presence of iron-rich fly ash spherules among soot carbon chains (Figure 4.5A, B) on the PM1 filters is also an indicator of internal combustion engine emissions found both indoors and outdoors [Leite et al., 2021, Shi et al., 2015]. The presence of magnetite in PM is often linked to combustion and traffic sources, in line with the shapes detected for some iron oxides on the PM 1 filters (Figure 4.5A,B) by the SEM microscopy [spherules- Leite et al., 2021, Gonet et al., 2021a, Gonet and Maher, 2019, Liati et al., 2015, Sagnotti and Winkler, 2012, Castañeda-Miranda et al., 2014, Winkler et al., 2021, Bardelli et al., 2011]. The magnetic mineralogy of airborne iron oxides captured on tree bark and bio-sensors is composed of low coercivity carriers (magnetite-like) and high coercivity magnetic grains (e.g. hematite, goethite) as suggested by the S-ratio values between 0.89 and 0.97 [outdoors of Schools 2 and 1 respectively Frank and Nowaczyk, 2008, Bloemendal et al., 1992]. Some of the magnetic grains present in PM may have a geological origin, for instance, being carried by wind over long distances ([Formenti et al., 2014]. Nevertheless, the magnetization (SIRM and ARM) is mostly dominated by the magnetite-like component.

Since traffic is the primary source of PM in these school environments, the variability in $SIRM_M$s between courtyards, interpreted as a variation of PM accumulation, could be caused by the impact of building configurations/architectural features (Figure 4.1). School 1 (West) and School 2 courtyards have similar configurations and similar $SIRM_M$ values. Both present a tree line parallel to the main 3-floors school building making a corridor shape with the adjacent building that may increase venting. Conversely, School 1 (East) courtyard presents a u-shape configuration with the open side facing a sports ground and the ring road. The higher $SIRM_M$ values observed in this courtyard could result from either the highest influence of the ring road [due to its proximity and open setting, Hofman and Samson, 2014] and/or from the enclaved configuration limiting the venting.

Measured PM1 values in the schoolyards revealed a higher content in PM in both school environments than the background PM concentration from Toulouse monitored by official stations and especially during Period 1. This shows the influence of traffic emission sources in the studied schools due to their proximity to important major highways and access streets. Moreover, the two schools from Toulouse present comparatively high concentrations of PM1 compared to PM1 and PM2.5 data from European schools located in big urban centers (Figure 4.6). Outdoors, concentrations recorded in Toulouse are comparable to Western European cities such as Milan, Munich, and Barcelona, all of which have larger populations (1.4 M, 1.5 M, and 1.6 M, respectively) than Toulouse (0.5M). Each school has a particular context in a given city, explaining the large scatter in the recorded values (Figure 4.6).

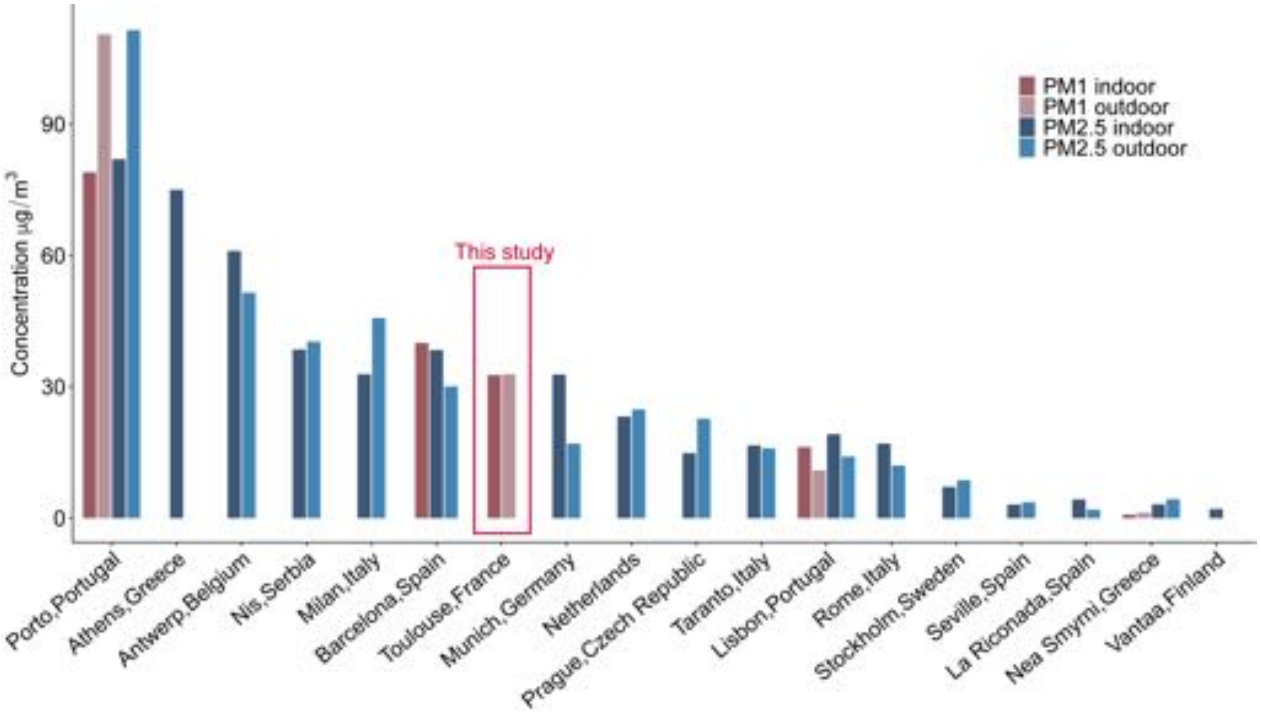

Figure 4.6: PM1 and PM2.5 mean concentrations in primary schools across Europe, in indoor and outdoor environments. See supplementary material for studies references.

School's indoor environments

As there are no indoor combustion sources, EC is a marker of outdoor air penetration. The I/O for EC increases between the first and the second period, indicating a higher influence of outdoor air in the classrooms with the changing seasons and temperature due to more frequent windows opening, as reported by the teachers. The mean I/O for EC for both sampled season periods equals 0.6 in both schools, similar to the one obtained from total magnetic PM measured on bio-sensors (0.6 and 0.9, respectively, for Schools 1 and 2). The magnetic fraction of PM found indoors also points to external sources, hence traffic sources, in agreement with previous studies that found that magnetic particles on household dust are derived from traffic and industrial activities [Kelepertzis et al., 2019, Jelenska et al., 2017, Gorka-Kostrubiec and Szczepaniak-Wnuk, 2017]. Other known potential sources of magnetic PM indoors are cooking, combustion processes, smoking [Jordanova et al., 2006] and laser printing —[ink composed of nanoparticles Pirela et al., 2015], all of which are absent in the studied schools.

High indoor values of OC concentration (Table 4.1), reflected on I/O for OC (Tables 4.1,4.2), points to indoor sources, such as organic emissions from children and staff, cotton fibers from clothes, wood furniture, crafting in school's activities (with the use of glue), among others [Fromme et al., 2006, Kalimeri et al., 2019, Rivas et al., 2014, Branis and Safranek, 2011, Weschler and Shields, 1999]. OC could also be generated indoors by reactions between oxidants from outdoors and gas-phase compounds emitted indoors, forming secondary organic

aerosols (SOA) [Hodas et al., 2016, Weschler, 2011, Weschler and Shields, 1999, Long et al., 2000, Wainman et al., 2000, Waring and Siegel, 2013, 2010, Waring, 2014, Waring et al., 2011]. Considering the high indoor OC concentration values reported in this study, especially during period 1 in School 2 and period 2 in School 1 (Table 4.1), the importance of proper ventilation on the school's environment becomes evident, given the potential toxicity of OC and SOC.

Proper ventilation is known to be an important issue in the school environment. In addition to the emission of particles, the accumulation of fine PM indoors (PM2.5, PM1) can occur in classrooms. Indeed, magnetic grain size distribution measured in School 1 displays a clear difference between indoor and outdoor environments, with a finer magnetic granulometry indoors close to the xARM/SIRM ratio of PM2.5 filters obtained by Leite et al. [2021]. Conversely, School 2 samples present a similar magnetic grain size distribution indoor and outdoor typical of the entire PM range [Mitchell and Maher, 2009]. School 1 outdoor environment also falls in this latter range. Although both schools have the same architecture, the teacher's interview revealed that all windows of School 2 were changed following the AZF industrial accident of 2001 allowing the windows to be fully open and classrooms properly ventilated, while School 1 has old tilt windows that can never be fully opened, which could have led to the differentiation in the size range.

Indoor PM partly results from the penetration of PM from outdoor ambient air via openings (doors and windows) and building cracks [infiltration/exfiltration, Hodas et al., 2016]. They can also be transported into the classroom by children and teachers [Chen and Zhao, 2011] via hair, clothes, and bags. Here, high PM concentrations inside classrooms are related to poor venting. Indeed, the window ventilation is one of the most important actions to promote good air quality in schools [Chithra and Nagendra, 2014, 2012, Almeida et al., 2011, Blondeau et al., 2005, Rovelli et al., 2014] without automatic venting systems such as here, in Toulouse. The measurements of high CO_2 concentrations in School 1, required by law, also highlight a lack of ventilation, especially in the instrumented classroom. A CO_2 concentration of 3200 ppm is reported in 2018 for this specific classroom (Report of the 12/06/32018) and over the ten classrooms investigated, seven are above 1000 ppm. This is due to the aging of the openings and lack of renovation. At the school in concern, only five were still functioning over the ten existing windows, and the teacher could effectively open only three. The teachers' interviews also indicated that the classroom is ventilated (opening the windows) in the morning during cleaning before the arrival of children and sometimes during the day. As also stated by Mumovic et al. [2009], managing troubles in concentration and the required ventilation is not easy for the teacher. One of the teachers reported that there are no official guidelines regarding air pollution except for avoiding outdoor sports during pollution peaks and that they are unaware of the official CO_2 monitoring in their classrooms. The opening of windows during class time is described as subjecting children to noise, draughts, and changes in temperature that have the effect of dispersing the group's attention.

High indoor concentration values of fine PM appear to be the hallmark of the school environment. Indeed, significant PM concentrations are recorded indoors, especially in School 1 for period 1, as highlighted by high I/O for PM1 (Table 4.2) and SIRM values. High concentrations of fine PM (PM2.5) have also been previously reported indoors in the school environment throughout Europe. A mean I/O ratio of 1.44 has been reported for 122 European schools [Kalimeri et al., 2019]. Similar high values were obtained, among others, from

27 schools in Belgium with I/O ratios varying from 1 to 2.7 [Stranger et al., 2008] in 20 schools in Portugal with a mean IO ratio of 1.45 [Madureira et al., 2012] or from 39 Spanish schools with IO ratios varying from 1.2 to 1.5 [Rivas et al., 2014].

Vegetal passive collectors to monitor airborne particles and student-teacher involvement

The recorded concentrations in schools from Toulouse are higher than the air quality guidelines [WHO, 2021b] both outside and inside the classrooms. As one of the teachers explicitly stated, teachers and students suspected poor air quality because of the direct view and noise of the large entrance road next to the yard.

Both the informal exchanges between the teachers and researchers and the official interview led to a co-design of the process and to the co-production of knowledge. Teachers were involved in the intervention design by asking the researchers to come more than once into the classrooms and explain the needs of the children. From the teacher's point of view and observations, the fact that the sensor was made with almost nothing (verbatim *"trois fois rien"*) and from trees similar to those present in the yard was the predominant factor of endorsement by the children. The fact that children were able to meet the researchers several times and touch and experiment with concrete materials in their classrooms is the most important. Eco-anxiety as defined by Pihkala [2020] could impact all participants [Russell and Oakley, 2016], the children, teachers, and researchers. Both scientific activities around magnetic phenomena and the use of natural media help the discussion on air quality and its possible impact to be less anxiogenic for all actors.

The capacity of bark to accumulate airborne particles was already demonstrated for Neem trees by Dawaï et al. [2021] in Cameroon and for various street trees by Chaparro et al. [2020] in Buenos Aires (Argentina) and Milan (Italy) by Vezzola et al. [2017]. Here we demonstrated that bark also efficiently accumulates PM in indoor environments, as reflected by SIRM values and SEM images.

For the monitoring of air quality in the school environment and the evaluation of children's exposure, the collaboration between the school (teachers, management, and students) and the researchers makes it possible to better adapt the measurement points via the feeling, acceptance, and perceptions. Such an approach enables solutions or assessments to emerge. This empowers students and teachers to know their environment and to move towards solutions ranging from conscious acceptance to advocacy, legitimized by collaboration for practical measures. In this case, the co-building of solutions was initiated when preliminary results became available. Notably, they are concerned about the default in ventilation of the classrooms. However, the dialogue was abruptly interrupted by the sanitary crisis of 2020.

4.2.5 Conclusion

A combination of magnetic and chemical methods highlights high ultrafine and fine PM concentrations of airborne particles both inside and outside the classrooms of two elementary schools in the city of Toulouse. Since the main source for PM is identified as traffic, both the proximity to the ring road and a lack of ventilation explain the measured values.

Higher outdoor PM1 concentrations in both schools compared to the official traffic stations from downtown Toulouse point toward the fact that the local environment (i.e. distance to a source), here consisting of the proximity to the ring road and a major access road, is of crucial importance for the potential exposures of pupils. In addition, the microenvironments constrained by the architectural and vegetation configuration also have impacts on local PM concentrations. Collaboration between teachers, students, and scientists benefits the knowledge production about the influence of traffic sources in schools, school microenvironments, and environmental education. The use of vegetation as support for particle trapping, in addition to active sampling on filters, benefits both scientific studies by allowing the use of multiple sensors/stations and environmental education by promoting school children's participation while reducing the anxiety associated with this type of environmental assessment. A comparison of PM accumulation in Toulouse and European schools shows a global tendency for higher PM concentrations in classrooms despite discrepancies in outdoor air quality. Epidemiological surveys inside school environments are urgently required to understand potential health and learning skills impacts on children of PM accumulation inside classrooms and would benefit from passive bio-sensors monitoring.

4.2.6 Acknowledgments

The authors sincerely thank the pedagogical teams and children of Jules Julien and Leo Lagrange schools of Toulouse. The authors acknowledge the support of the city of Toulouse. The authors thank the communication team of the CNRS-délégation Occitanie Ouest for their help along this project. This study was funded by the French National Research Agency ANR-grant number ANR-19- CE04-0008 through the BREATHE project and has received financial support from the CNRS through the MITI interdisciplinary programs - Osez l'interdisciplinarité-NanoEnvi. A.L. was supported by a scholarship from the French Government and Ministry of Education. This work has been (partially) performed at USP-Mag lab at Instituto de Astronomia, Geofisica e Ciencias Atmosféricas (IAG) at Universidade de São Paulo (USP) funded by CAPES/FAPESP/CNPQ. The authors have no conflicts of interest to declare.

4.3 Citizen science initiative for extensive mapping of indoor and outdoor particulate matter concentration in Toulouse (France) combining bio-sensors and environmental magnetism

Abstract: Air pollution studies are often concerned about the outdoor concentration of particulate matter. Yet, investigating indoor environments is key to understanding the health risks of air pollution, as people spend more time in it. This study presents an air quality investigation combining indoor and outdoor in the urban domestic environment through bio-sensors and magnetic methods. To obtain a broad coverage of residences, we involved the population in a Citizen Science program, where inhabitants were invited to participate in the sampling by placing passive bio-sensors in their homes. Higher concentrations of magnetic grains were detected outdoors than indoors. Low coercivity carriers dominated the magnetic mineralogy, as seen by IRM unmixing curves finding mean coercivities of 21.3 and 32.4mT indoor and outdoor, respectively. The magnetic properties and the detected spherical morphologies of the particles point to the internal combustion origin of the magnetic particles. Traffic emissions are one of the primary air pollutants sources in urban environments, affecting both outdoor and indoor environments. In Toulouse, the central regions of the city with higher population density and heavier traffic of vehicles were found to have more concentration of outdoor iron oxides.

4.3.1 Introduction

Air pollution is one of the biggest health concerns in urban settings, with its burden comparable to other major health threats such as tobacco smoking and poor diets [Murray et al., 2020]. In the urban lifestyle, it is customary to spend most of our time indoors [Klepeis et al., 2001, Schweizer et al., 2007]. Indoor sources of air pollution may lead to worse air quality, which has to be estimated to fully comprehend the threats posed by air pollution [Tofful et al., 2021, Semple et al., 2015, Jones et al., 2000]. Besides, personal exposure to pollutants may vary widely in a given city due to distance to sources, geographic features, and time spent in any given environment [Kalimeri et al., 2017, Monn et al., 1997]. Particulate matter (PM) is one of the primary air pollutants, and it is composed, among others, of inorganic ions (e.g., ammonium, nitrates, sulfates, and soluble metals), insoluble metals, elemental carbon, organic compounds, biological components, microbial agents and water [Kim et al., 2015, Zhang et al., 2015]. It has both anthropogenic and natural sources and is associated with several health consequences. Moreover, finer fractions of PM may be more harmful due to its capacity to penetrate deeper into biological systems [Pope III and Dockery, 2006, Martins et al., 2020]. The presence of iron oxides among the PM constituents allows the use of environmental magnetism methods for its investigation. The magnetic methods have advantages compared to traditional PM investigations, such as cost and a solid capacity to investigate size ranges on the iron oxides. Besides that, magnetic methods allow for inventive samples, such as biological sensors (bio-sensors, for instance, vegetable matter, funghi matter, animal matter, Hofman et al. [2017]), which in turn allows for novel experimental

designs. When paired with citizen science investigations, the advantages of the use of bio-sensors are enhanced. The indoor concentration of PM is directly linked to the outdoor one, but this relationship is not straightforward [Kalimeri et al., 2019, Avery et al., 2010, Wilson and Brauer, 2006]. Infiltration of outdoor pollutants in indoor environments is controlled by building characteristics, ventilation, occupancy characteristics, etc. Besides the outdoor source of PM, indoor sources have also been shown to be critical in understanding PM's indoor concentration. Indeed personal habits influence the indoor domestic concentration of PM and other air pollutants. Personal habits are much linked to the context of a given population. Solid biomass burning may be an important source of indoor PM in countries such as India, Tibet, and Senegal, where it is used for heating and cooking [Sharma and Jain, 2019, de la Sota et al., 2018, Sclar and Saikawa, 2019]. In Hong Kong, cooking and incense burning are sources of indoor PM [Tong et al., 2016]. In Europe, a study in six countries found that the main factors impacting indoor air quality are gas stove usage, smoking, and outdoor weather characteristics (temperature, wind speed) which may relate to indoor ventilation and heating [Lai et al., 2006]. Smoking may lead to a ten times increase in indoor PM2.5 concentration when compared to non-smoking households, as detected in residences in Scotland [Semple et al., 2015]. Even cleaning habits may increase indoor PM concentration, such as using vacuum cleaners that favor resuspension and emit PM through their motors [Vicente et al., 2020]. In the last years, the use of citizen science in air quality investigations has been growing, showing promising results regarding the impact and vulgarization of the scientific work on society [Varaden et al., 2021, Hsu et al., 2017, Mahajan et al., 2021, 2020, West et al., 2020]. Citizen science enables a more excellent spatial resolution at the city scale [Perelló et al., 2021]. Despite its apparent advantages, using low-cost PM sensors has its challenges. Compared to traditional research-grade PM sensors, low-cost ones have varying linear correlations on the measured PM concentration that can vary in different environments [Oluwadairo et al., 2022, Northcross et al., 2013]. Using bio-sensors on environmental magnetism protocols and citizen science participation in air quality investigations presents an innovative approach, as it retains the cost-effective and ease-of-use advantages of the low-cost air sensors. Besides, bio-sensors are inherently environmentally friendly. In that sense, the joint approach between citizen science and magnetic investigations on bio-sensors improves the qualities of each other while taking on their drawbacks. In this study, we present the investigation of airborne iron oxides in Toulouse, France. The context of PM emissions is mostly from traffic since other vital sources of PM are absent in this city. The main goal of this study is to investigate differences between indoor and outdoor domestic environments throughout the city regarding the concentration of the magnetic fraction of the PM, its origins, and grain size distribution. We developed an innovative approach with citizen science participation and bio-sensor investigation by magnetic means.

4.3.2 Methodology

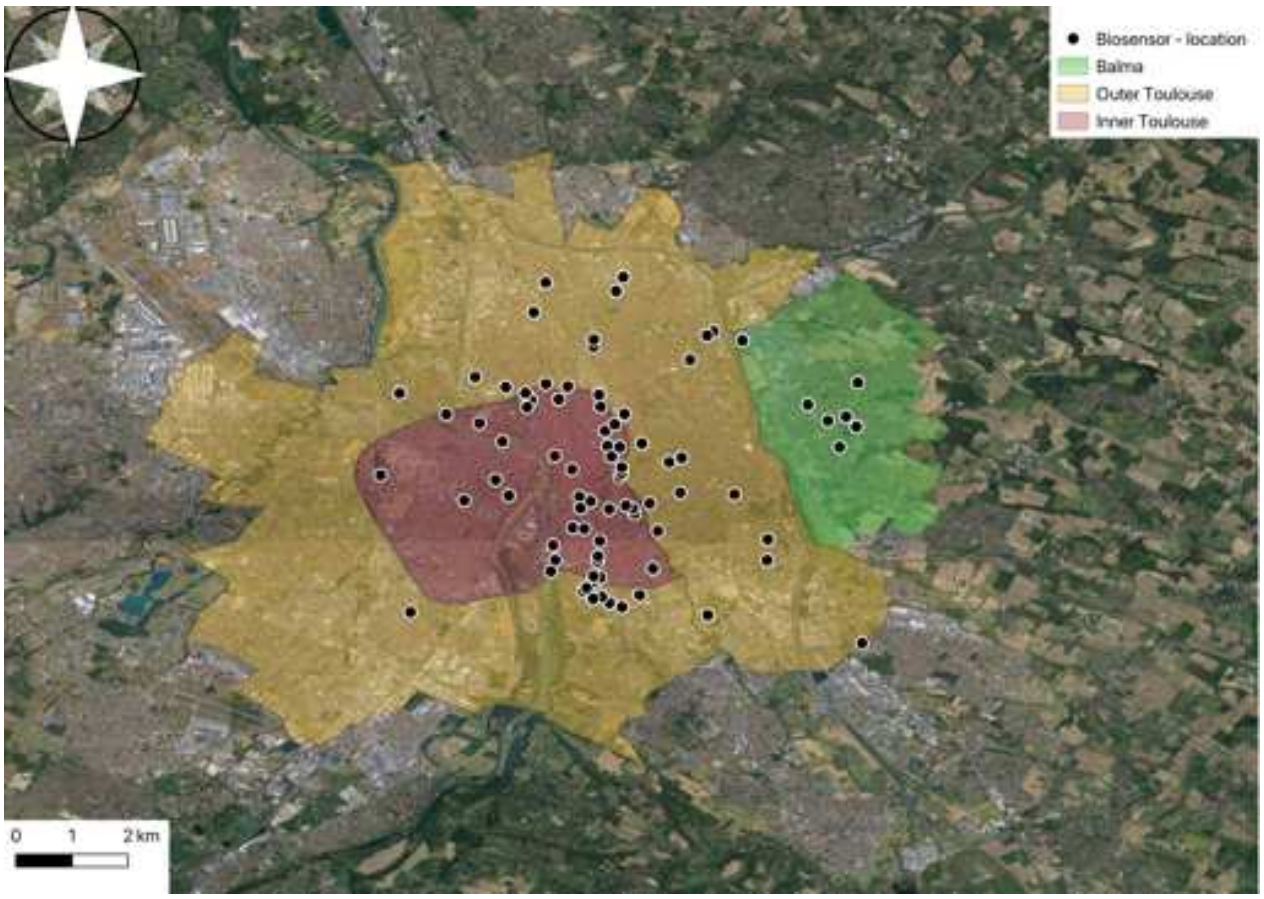

Figure 4.7: Toulouse city divided into inner (red) and outer (yellow) city, defined by main traffic roads in the city. Also the town of Balma (in green). Black dots show the bio-sensors kits location.

Toulouse (1º26'4"E 43º36'15"N) is located in the South-West of France, 80km North of the Pyrenees chain, 140km to the West of the Mediterranean Sea and 220km East of the Atlantic Ocean. It is the fourth-largest French city in terms of population, with 479 553 inhabitants in 2017 [Métropole, 2021]. The Garonne river crosses the city (including the downtown area) from South to North. This paper separates Toulouse into two main areas, Inner and Outer Toulouse. The limits between Inner and Outer Toulouse are delimited in the South and East by the ring road (A620), an interstate highway with a total extension of 35km and three lanes each way, with a mean flow of vehicles in the order of 120,000 vehicles per day (in 2019) on its Southern part of the A620 highway (consulted on January of 2022, `https://www.aua-toulouse.org/wp-content/uploads/2022/02/AUAT_chiffres_transports_2022.pdf`). The North and West Inner and Outer Toulouse are separated by municipal avenues that board the Canal du Midi just until the Port de l'Embouchure (Fig. 4.7). Inner Toulouse has a diameter of approximately 7km, with a population of 189 317 inhabitants in 2018 (with a population density equal to 0.009 inhabitant/m^2). Outer

Toulouse extends for about 20km in diameter, with a population of 286,120 in 2018 (population density of 0.003 inhabitant/m^2). The town of Balma is part of the Toulouse metropole, with a population of 16,520 and an area of 1660 hectares, with the lowest population density of 0.001inhabitant/m^2 (Fig. 4.7).

During events of scientific vulgarization on PM emissions, we recruited citizens interested in participating in the investigation. The citizens were given a kit containing two bio-sensors (guirlandes composed of 5 to 6 pieces of bark) and instructions on its manipulation and installation. After one year, the samples were returned to the laboratory for analysis. The kits were deployed to the city's population in the Autumn of 2018, on the scope of the NanoEnvi project (`https://nanoenvi.omp.eu`) developed at the GET-OMP. These kits consisted of a pair of bio-sensors, latex gloves for their manipulation, instructions for the installation, and ziplock bags. The participants received instructions to expose one of the bio-sensors indoors and the other outdoors in either horizontal or vertical orientation. A return kit was provided at the end of the experiment containing an envelope to return the kits to selected drop-off locations or by mail. Over 150 bio-sensor sampling kits were distributed to the population, with the retrieval of 90 tackles. After the results were available, restitution seminars were given to the participants, in which results were explained and discussed between researchers and citizens. Bio-sensors were assembled in the laboratory. They consist of a garland of 5 to 6 pieces of tree bark, cut in a square format (about 4cm^2, Fig 4.8). A nylon thread joins the pieces by passing through 2 small holes per piece of bark. Tree bark was collected in isolated areas from emission sources. They were sterilized in an autoclave at 115°C to avoid spreading diseases specific to plane trees. The bio-sensors were exposed for an average of 6 months, after which they were returned by mail to the laboratory.

Magnetic susceptibility was acquired and measured in a KLY-5 (Agico) at the GET laboratory. Bio-sensors were measured inside their plastic collecting bag to avoid contamination due to the manipulation. The high sensitivity mode of the equipment was used. Three repetitions of measurements were performed. Then, samples were gently pulverized in agathe mortar with liquid nitrogen. They were placed inside gel caps in powder form, with an average mass per sample of 0.6 grams.

All remanence measurements were done at USPMAG, Brazil. The laboratory has a μ-metal shielded room with an ambient field no greater than 500nT. Remanence measurements were done in a 755-1.65 DC SQUID magnetometer (2G enterprises), with a sensitivity of 10^{-9}emu and an automatic sample handler. All measurements consisted of an average of three automatic measurements done by the SQUID magnetometer. The samples were at first demagnetized using alternating magnetic fields (AF) with a peak field of 100mT. Afterward, samples were magnetized in a bias field of 30μT with a superimposed AF of 100mT to acquire one-step anhysteretic remanent magnetization (ARM). When the ARM value is divided by the bias field's value gives the ARM's susceptibility (xARM). Then, samples were imparted in a 1T inducing field, using a pulse magnetizer (Magnetic Measurements Ltd.), and here considered as the saturation of the isothermal remanent magnetization (SIRM). Backfields of 300mT were imparted following the saturation step. All samples were measured in this step.

Hysteresis cycles and DC remanence demagnetization (DCD) curves were measured in a Vibrational Sample Magnetometer (VSM) 3900 at the CORE laboratory, Brazil. A total of 80 samples were measured in this step. The VSM 3900 has a sensitivity of 0.5x10^{-6}emu.

Figure 4.8: Bio-sensors used on the NanoEnvi project, consisting of tree bark pieces to be hUng with a nylon cord. Source: `https://nanoenvi.omp.eu`.

Hysteresis parameters were determined, namely the parameters saturation magnetization (M_S) and coercive force (H_C). The remanent saturation magnetization (M_{RS}) and coercive remanent force (H_{CR}) were obtained from the DCD curve. The ratio between the hysteresis parameters (M_{RS}/M_S and H_{CR}/H_C) when plotted against each other, creates the so-called Day Plot [Dunlop, 2002] to discern the grain size of the magnetic minerals. Given the weak signal, twenty-three samples provided satisfactory hysteresis curves and parameters after stacking four cycles. The DC remanence remagnetization curves were used with the unmixing protocol proposed by Maxbauer et al. [2016], by modeling the IRM acquisition curve as a cumulative log-Gaussian function in terms of the mean coercivity of an individual grain population (Bh), the component saturation magnetic remanence (Mr) and the dispersion parameter (DP). A total of 25 samples (16 outdoor, nine indoor) were successfully analyzed this way. Selected (4 in total) samples were observed with a JEOL7800 scanning electronic microscope (SEM) for investigation of surface characteristics of captured iron oxides on the bio-sensor. Composition investigation of the micron and submicron particles was achieved with energy dispersive X-ray spectrometer (EDS) measurements using an Oxford Instrument Detector (X_{MAX}=80mm_2). Samples were pretreated by sticking silver conductive adhesives and carbon coating.

4.3.3 Results

Magnetic results

Magnetic susceptibility measurements indicated a magnetic susceptibility dominated by the diamagnetic matrix of the tree bark, having negative values, being discarded from further analysis.

SIRM measured on the bio-sensors (Fig. 4.9 , Table 4.3) have higher values outdoors than indoors, with a mean at $2.28(\pm1.51)\times10^{-5}\,\mathrm{A\,m^2\,kg^{-1}}$, varying from $0.43\times10^{-5}\,\mathrm{A\,m^2\,kg^{-1}}$ to $6.02\times10^{-5}\,\mathrm{A\,m^2\,kg^{-1}}$. Indoor bio-sensors have a mean SIRM of $0.79(\pm0.57)\times10^{-5}\,\mathrm{A\,m^2\,kg^{-1}}$, varying from $4.32\times10^{-8}\,\mathrm{A\,m^2\,kg^{-1}}$ to $3.76\times10^{-5}\,\mathrm{A\,m^2\,kg^{-1}}$. One indoor bio-sensor was discarded in this step, having saturation two orders of magnitude higher than the mean. Besides being generally lower, indoor SIRM values have narrower distribution (Fig. 4.9), while the outdoor samples have a distribution skewed to higher values. Indoor/outdoor ratios of the SIRM (SIRM I/O) are majoritarian below one, with only nine samples with higher values of SIRM indoors than outdoors, and a mean value of the SIRM IO at 0.52(±0.52) (Table 4.3).

ARM values range from $0.30\times10^{-7}\,\mathrm{A\,m^2\,kg^{-1}}$ to $7.03\times10^{-7}\,\mathrm{A\,m^2\,kg^{-1}}$, being close indoors and outdoors. The outdoor bio-sensors have a slightly higher mean (Table 4.3) of $2.03(\pm1.30)\times10^{-7}\,\mathrm{A\,m^2\,kg^{-1}}$ while indoor bio-sensors have a mean ARM of $1.69(\pm1.13)\times10^{-7}\,\mathrm{A\,m^2\,kg^{-1}}$. Figure 4.10 shows the bio-sensor SIRM individual values throughout the city, in both indoor (Fig. 4.10a) and outdoor (Fig. 4.10b) environments. The figure also displays the population density of each neighborhood divided by quartile ranks. SIRM values in both environments are generally higher in more densely populated neighborhoods.

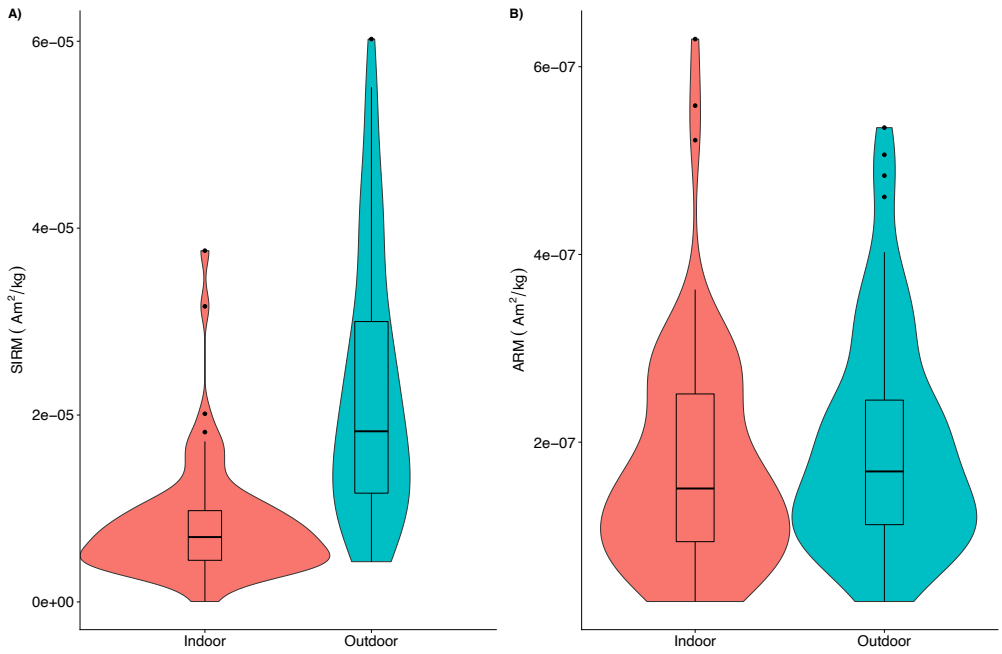

Figure 4.9: Violin and box plot of SIRM (A) and ARM (B) measurements values on bio-sensors placed indoors (orange) and outdoors (blue). Quantiles are marked as horizontal lines (0.25, 0.5 and 0.75 from bottom to top) and the numeric means are marked on the asterisk.

Table 4.3: Average, standard deviation and number of samples for the measured and calculated magnetic parameters SIRM, I/O SIRM, ARM, S-ratio, xARM/SIRM and Bh for the bio-sensors.

Variable	Site	Average	Std	n
SIRM (10^{-5} A m^2 kg^{-1})	Indoor	0.79	0.57	90
	Outdoor	2.28	1.51	88
SIRM IO		0.52	0.52	
ARM (10^{-7} A m^2 kg^{-1})	Indoor	1.69	1.13	86
	Outdoor	2.03	1.30	84
S-ratio (%)	Indoor	90	6	73
	Outdoor	91	6	69
xARM/SIRM (10^{-3}m/A)	Indoor	1.10	0.99	84
	Outdoor	0.55	0.70	85
Bh (mT)	Indoor	21.3	7.7	9
	Outdoor	32.4	6.8	16

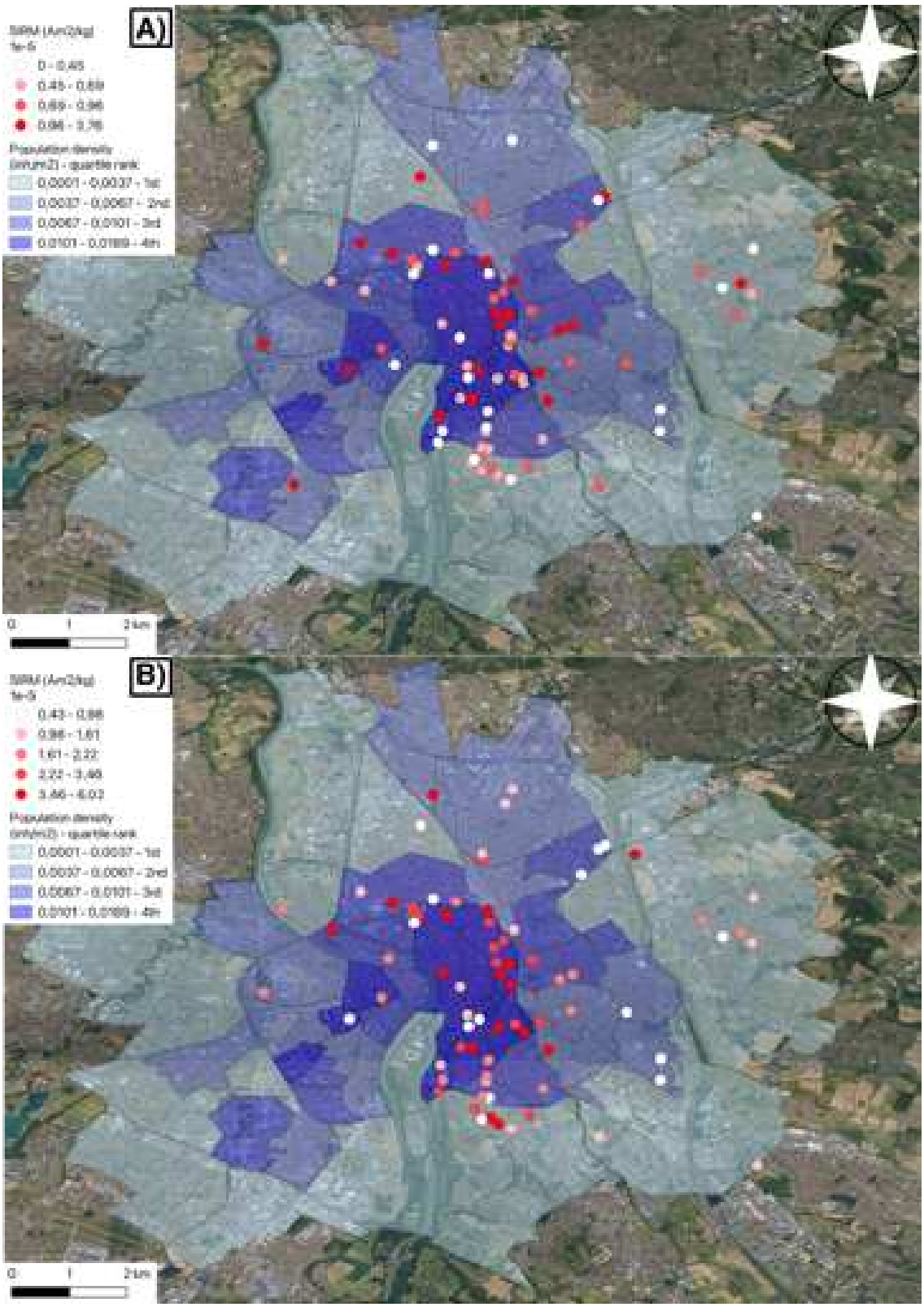

Figure 4.10: SIRM individual values for each bio-sensor, indoors (above) and outdoors (below). Population density and respective quartile rank for each city neighborhood in shades of blue.

To analyze the influence of the geographical location of the samples regarding the measured SIRM, we separated Toulouse as the Inner and Outer city, with the ring road as the limit for these two regions (Fig.4.7), besides using Balma as a separate area. Indoors, SIRM means are stable, ranging from $0.66(\pm 0.28)\times 10^{-5}\,\mathrm{A\,m^2\,kg^{-1}}$ to $2.68(\pm 12.35)\times 10^{-5}\,\mathrm{A\,m^2\,kg^{-1}}$ in Balma and in Inner Toulouse respectively (Fig.4.11a, Table 4.4). Outdoors, values on the Inner Toulouse have a tendency towards higher values, reaching a mean of $2.56(\pm 1.51)\times 10^{-5}\,\mathrm{A\,m^2\,kg^{-1}}$. We sectorized the population density (calculated with the area and population of each neighborhood) of the city of Toulouse by its quartiles (Figs. 4.10,4.11b) to analyze the SIRM value distribution further. Again we notice that indoor SIRM values remain stable in all quartile ranges (Table 4.5), whereas outdoor deals have a clear tendency of higher importance in more densely populated neighborhoods, reaching a mean value of $2.84(\pm 1.42)\times 10^{-5}\,\mathrm{A\,m^2\,kg^{-1}}$ on the 4th quartile of population density.

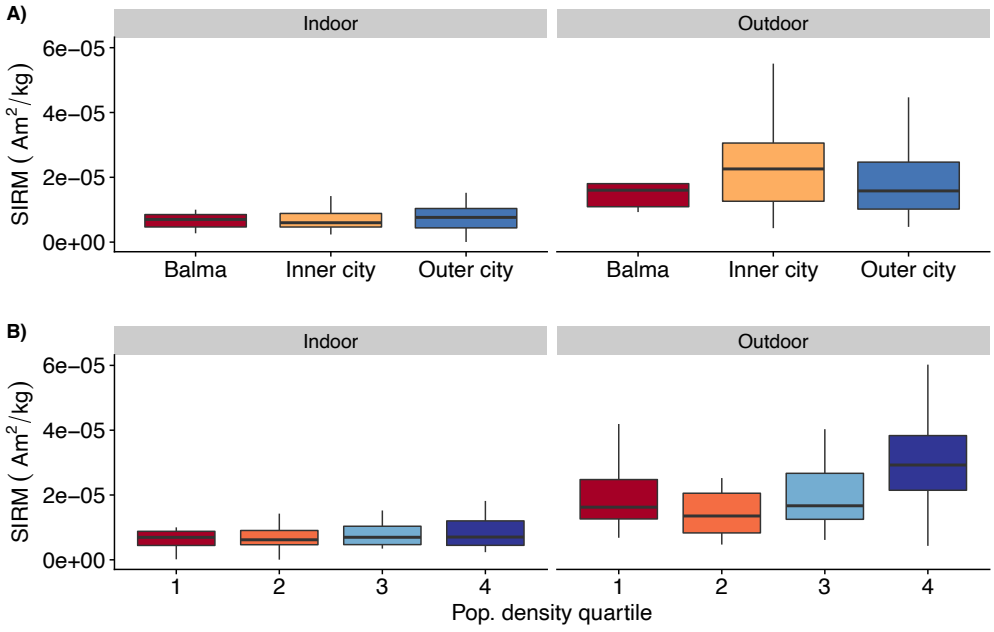

Figure 4.11: Box plot for SIRM values in indoor and outdoor bio-sensors, separated in city regions (A) and population density quartiles (B) Median is the horizontal line inside the box, the interquartile range by the size of the box, maximum and minimum values are the vertical whiskers.

Table 4.4: SIRM averages ($\times 10^{-5}$ A m^2 kg^{-1}), standard deviation, and number of samples by sector as defined in Fig. 4.7.

Site	Sector	Average	SD	n
Indoor	Balma	0.66	0.28	6
	Inner city	2.68	12.35	43
	Outer city	0.83	0.58	36
Outdoor	Balma	1.76	0.99	6
	Inner city	2.56	1.51	37
	Outer city	1.95	1.23	34

Table 4.5: SIRM averages ($\times 10^{-5}$ A m^2 kg^{-1}), standard deviations, and number of samples for each quartile of population density divided for indoor and outdoor environments, as defined in Figure 4.10.

Site	Quartile	Average	SD	n
Indoor	1	0.70	0.40	21
	2	0.81	0.67	21
	3	0.74	0.34	21
	4	0.97	0.79	21
Outdoor	1	1.99	1.06	20
	2	1.86	1.48	19
	3	2.23	1.43	19
	4	2.84	1.42	19

The xARM/SIRM ratio is a parameter that is inversely proportional to magnetic grain size [Maher, 1988]. Bio-sensors have higher values and dispersion indoors than outdoors, with respective means of $1.10(\pm 0.99)\times 10^{-3}$m/A and$0.55(\pm 0.70)\times 10^{-3}$m/A (Table 4.3, Fig. 4.12). Indoors, values range from 1.86×10^{-4}m/A to 5.03×10^{-3}m/A while outdoors the ratio ranges between 2.91×10^{-3}m/A to 5.83x10^{-3}m/A.

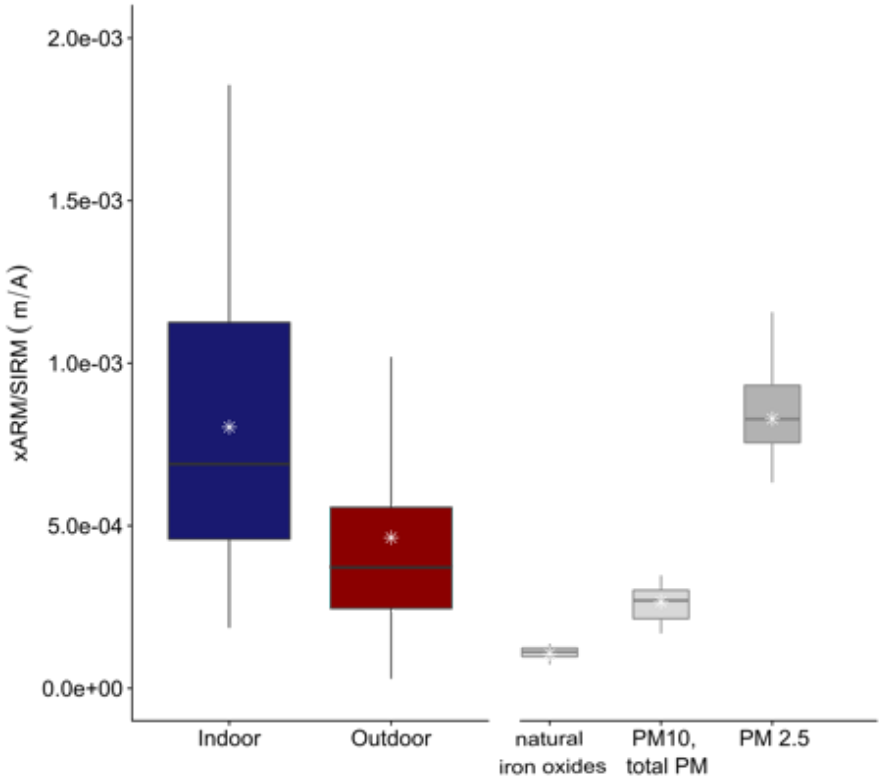

Figure 4.12: Boxplot for the ratio values xARM/SIRM on the bio-sensors, indoors and outdoors. Bibliographic data for natural iron oxides, PM10 and total PM and PM 2.5 from Dankers [1978], Mitchell and Maher [2009] and Leite et al. [2021] respectively.

Hysteresis parameters (M_S, M_{RS}, H_C and H_{CR}) allows for the computation of M_{RS}/M_S and H_{CR}/H_C that are represented in the classical Day Plot [Day et al., 1977] (Fig. 4.13). All samples lie in the PSD area. Indoor samples (Fig. 4.13) display higher M_{RS}/M_S and lower H_{CR}/H_C than the outdoor ones. This indicates a finer magnetic granulometry indoors. Samples have a gradient of SIRM (represented by the color scale) that increases as M_{RS}/M_S decreases, and H_{CR}/H_C increases towards the MD region of the Day Plot.

IRM acquisition curves were acquired in a total of 30 samples. Using the MaxUnmix analysis (Fig. 4.14, Maxbauer et al. [2016]) we were able to fit the IRM curves in 25 samples. Due to the low magnetic signal in our samples resulting in high noise on the curves, we choose only to fit one component in all samples. This way, we retrieve information regarding only a mean coercivity characterizing the samples, not their different components. Indeed, it is not clear if a high coercivity component is present. Low to moderate coercivities were found both indoors and outdoors. Indoor values have smaller Bh's (Table 4.3), ranging from 9.3 to 33.1mT, with mean of 21.3 ($\pm$7.7)mT. Outdoors, Bh values range from 21.1 to 47.5mT, with a mean value of 32.4($\pm$6.8)mT.

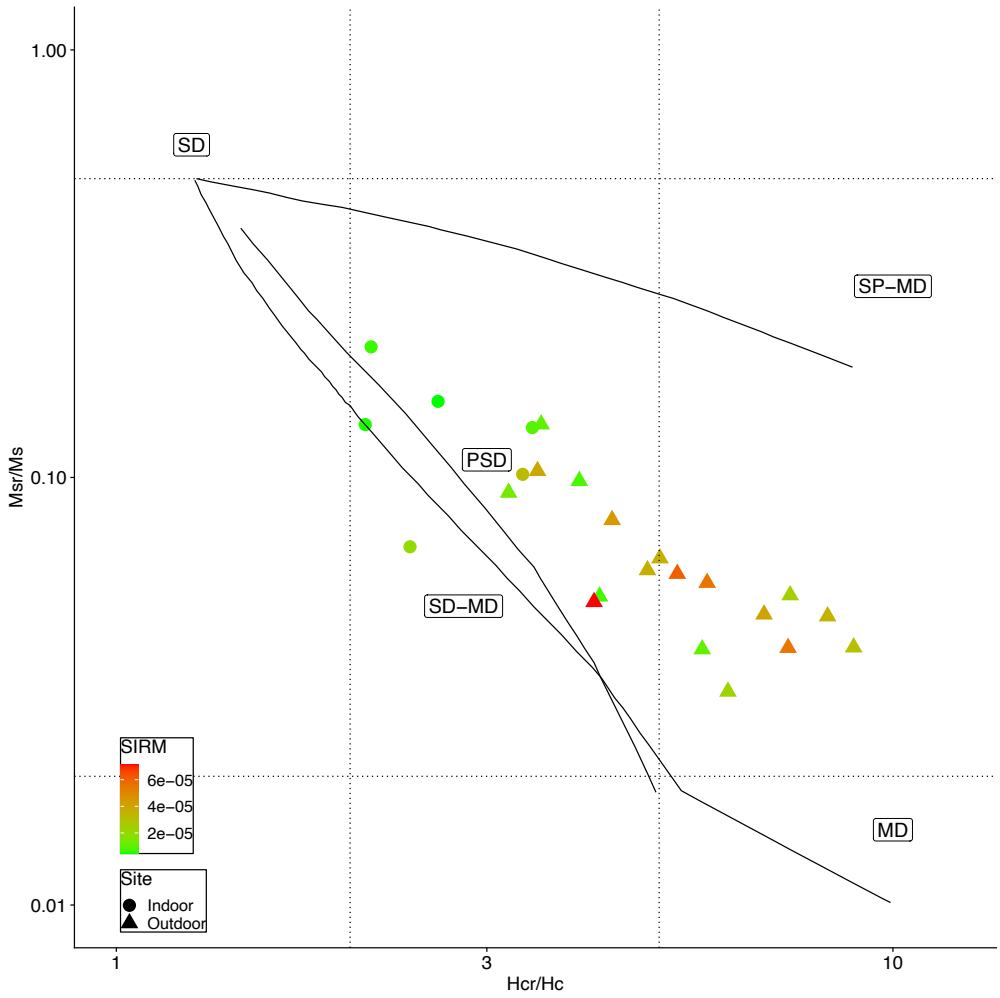

Figure 4.13: Hysteresis parameters and SIRM values measured on bio-sensors plotted on a Dayplot [Dunlop, 2002, Day et al., 1977]. Mixing lines from Dunlop [2002]

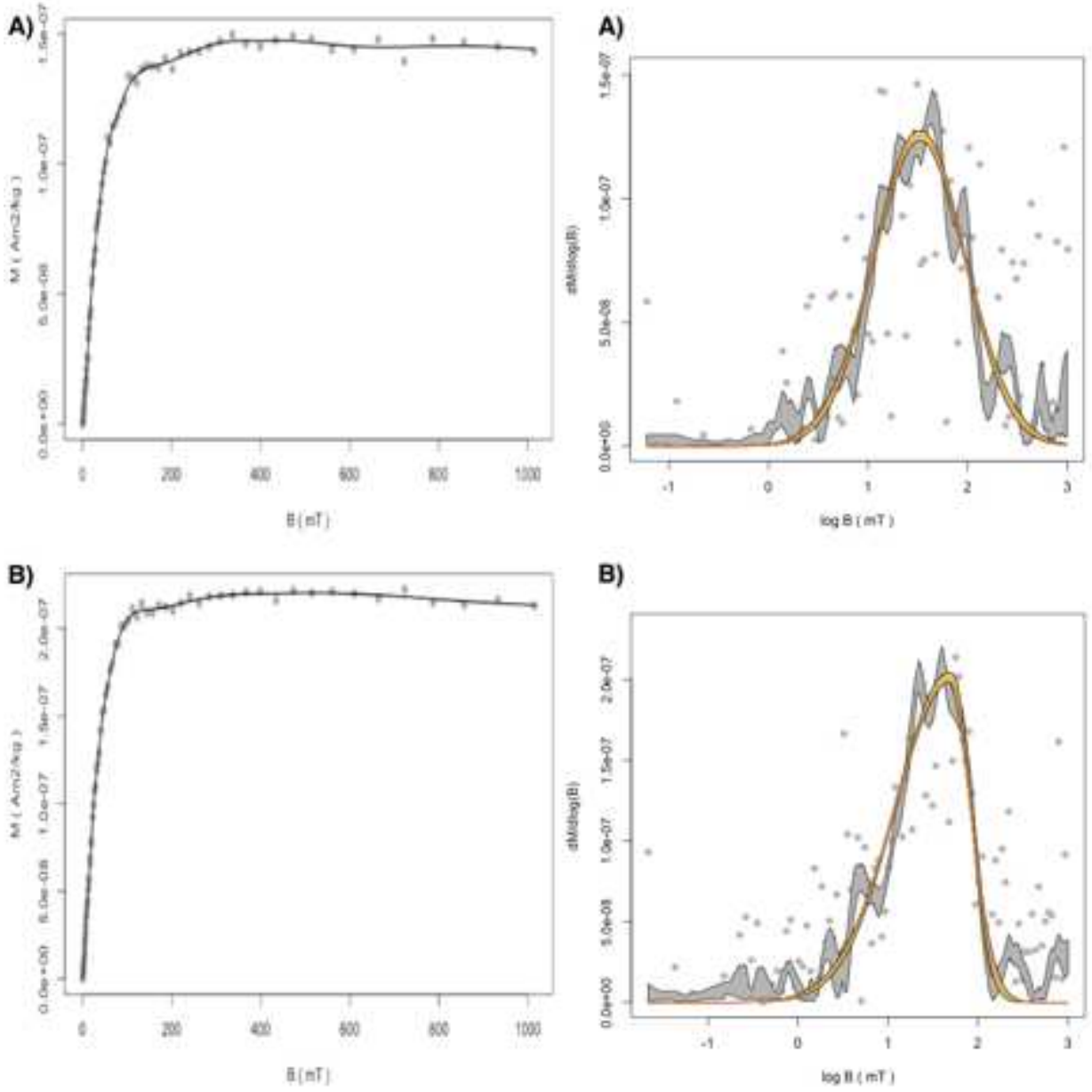

Figure 4.14: Unmixing of the IRM acquisition curves [Maxbauer et al., 2016] on an outdoor and indoor sample (A and B, respectively). On the left the black line and dots are the experimental data, with a smooth factor of 0.4. On the right, the derivative of the magnetization in function of the (log) of the B field (mT), used on the unmixing. Points and gray curve are the experimental data, fitted components represented by the yellow line. Outdoor sample has a Bh=32.6mT and Dp=1.0 and indoor sample has a Bh=24.5mT and Dp=1.0.

Scanning electron microscopy

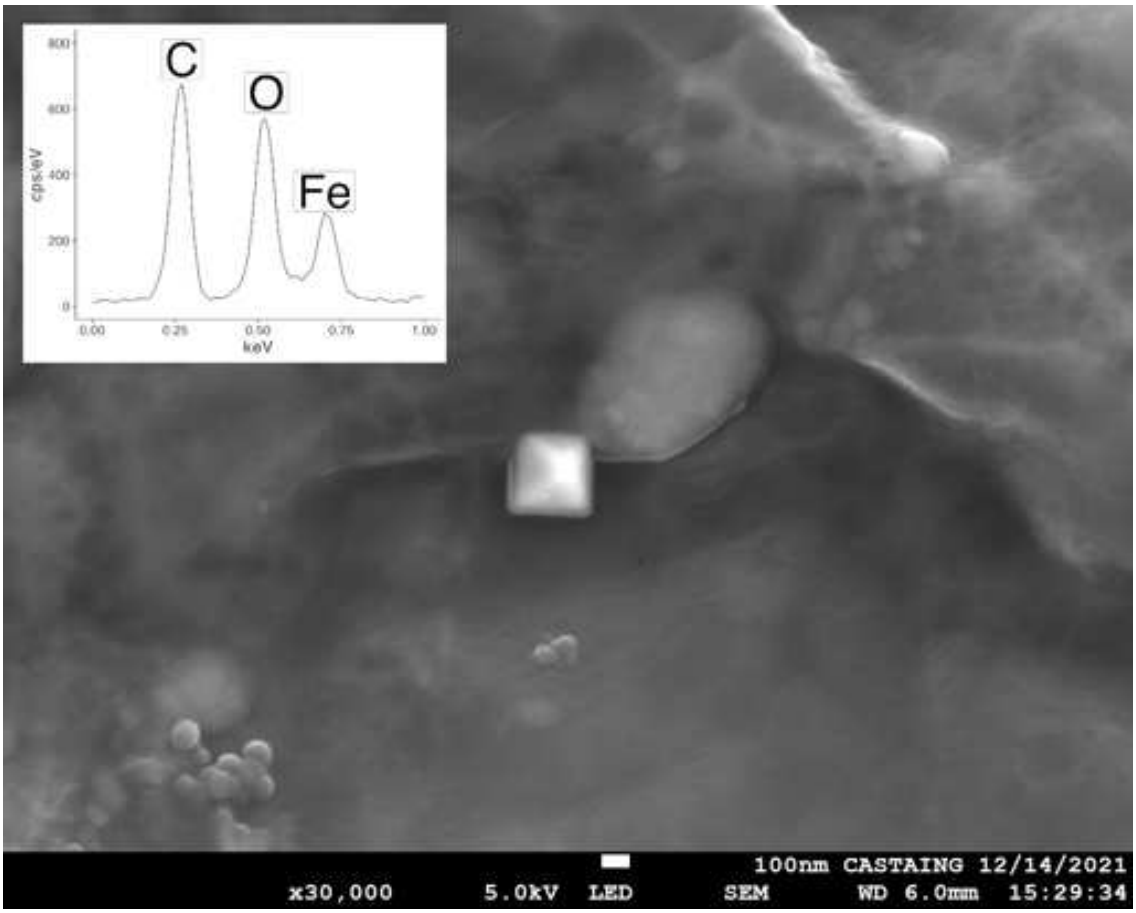

Figure 4.15: Secondary eletronic image of a nanometric iron oxide with octahedral shape (with vertices lengths at 265 and 241 nm) found in an outdoor bio-sensor.

SEM investigation revealed superficial features, composition, and sizes of iron oxides and other particles trapped on the bio-sensors. We identified spheric, octahedral, accumulations, and irregular shapes for the iron oxides, ranging from nanometric to micrometric sizes. Aggregations with carbon composition and silicates were also identified with micrometric size. Figure 4.15 shows an octahedral-shaped iron oxide with 241 and 265 nm nanometric dimensions for its sides. The particle presents a remarkable regular shape. Figure 4.16 shows a glass microsphere [Migaszewski et al., 2022] with nanometric size (diameter of 188nm), and composed of Fe, Zr and Si. Figure 4.17 shows an iron oxide spherule with micrometric size of 8.1μm. It presents indications of a cracked interior that looks empty from the SEM backscatter picture. Its surface is also not completely homogeneous. Figure 4.18 shows 4 agglomerations of iron oxides without clear shape, with micro and sub-micro metric dimensions of 1.3μm; 1.8μm; 0.5μm, 0.7μm. The presence of submicron metric iron oxide (with a diameter of 0.14μm) inside carbon chain-like particles highlights the source as being traffic-related in internal engine combustion [Leite et al., 2021, Shi et al., 2015]. The soot chain has dimensions of 1.5 and 1.6μm

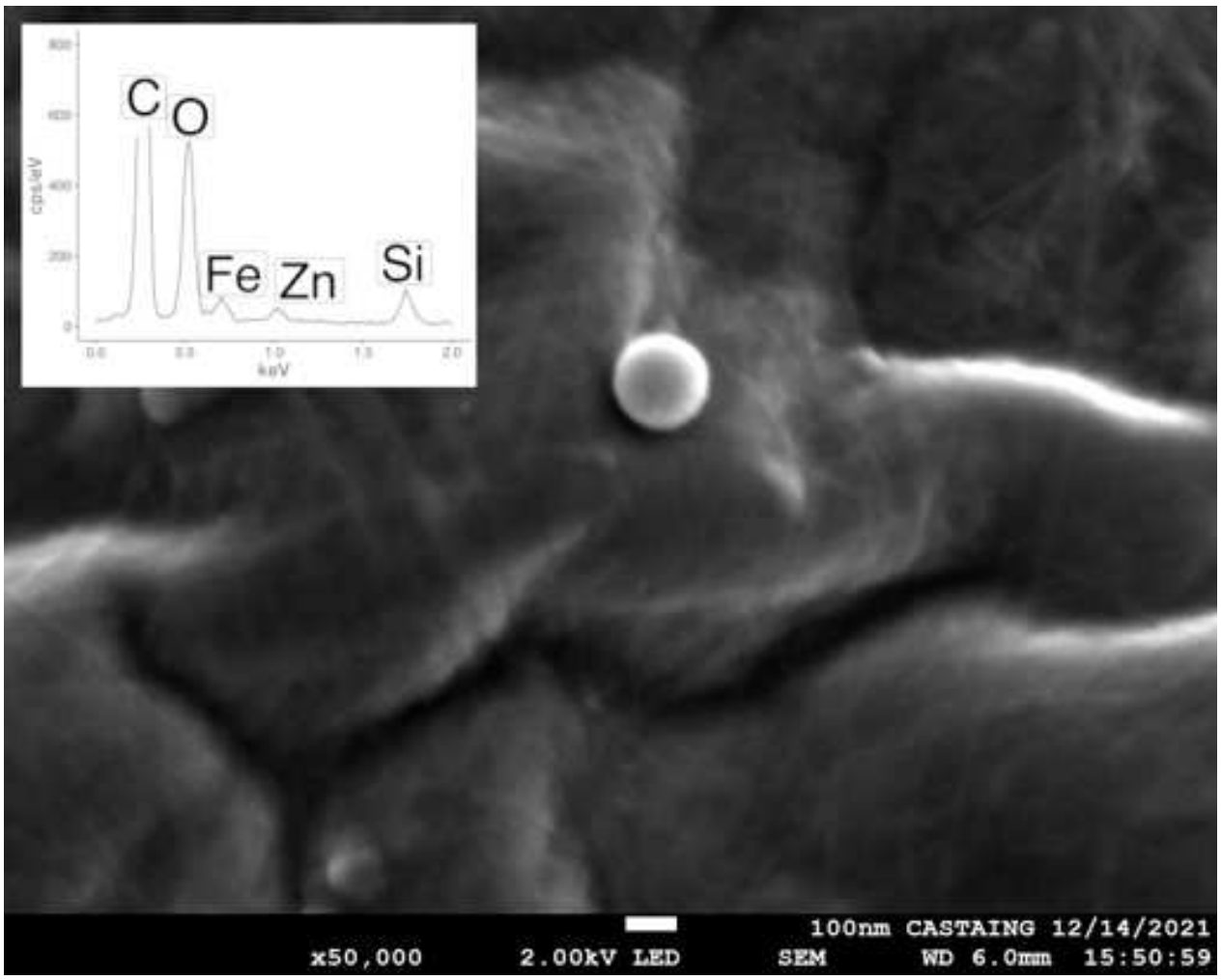

Figure 4.16: Secondary eletronic image of a nanometric spherule with 188nm of diameter. Its composition shows the presence of Zn, Fe and Si.

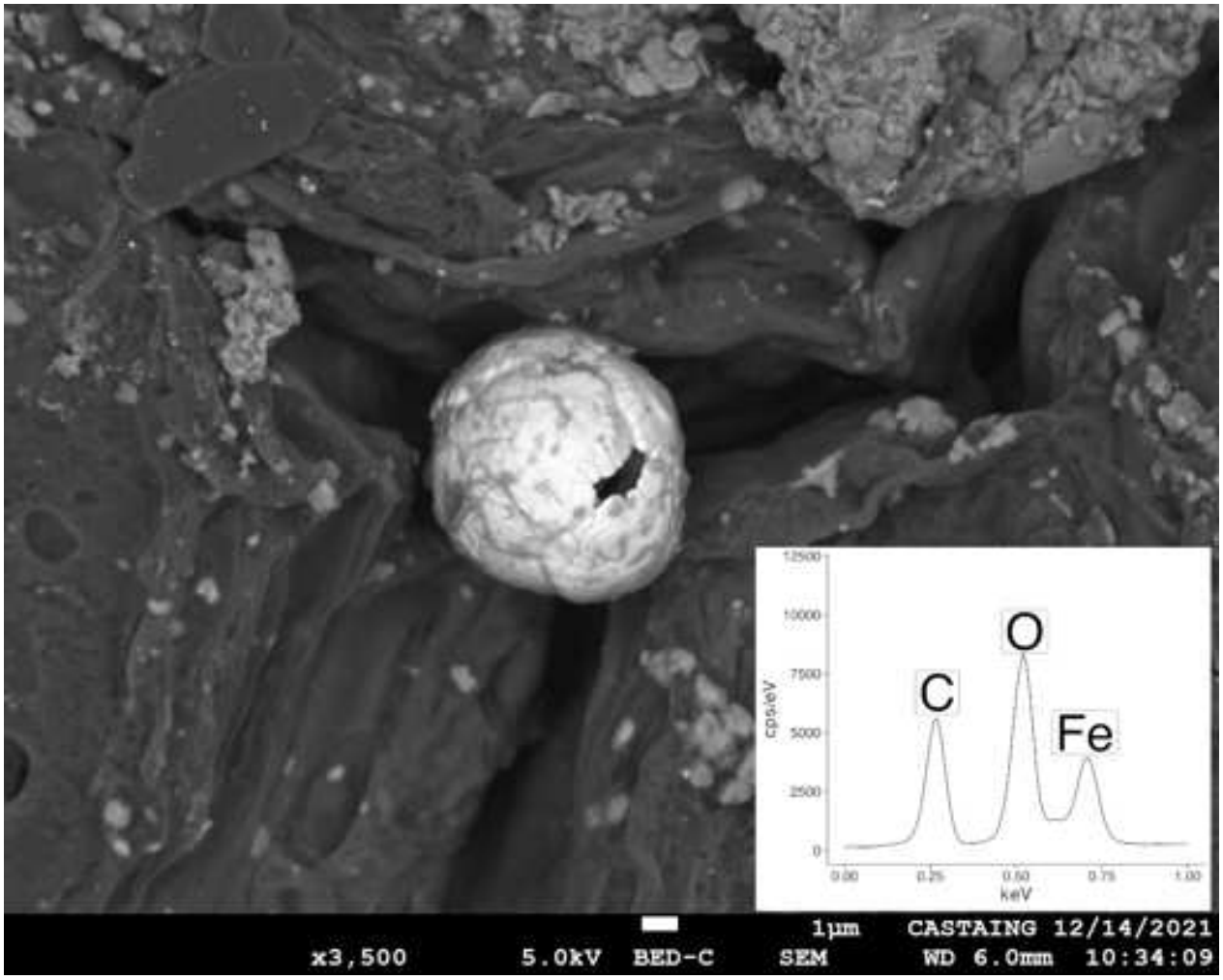

Figure 4.17: Back scatter image of a iron oxide spherule with rough surface, with evident stress marks and a crack revealing a possibly empty interior. The spherule is micrometric with diameter of 8.14μm

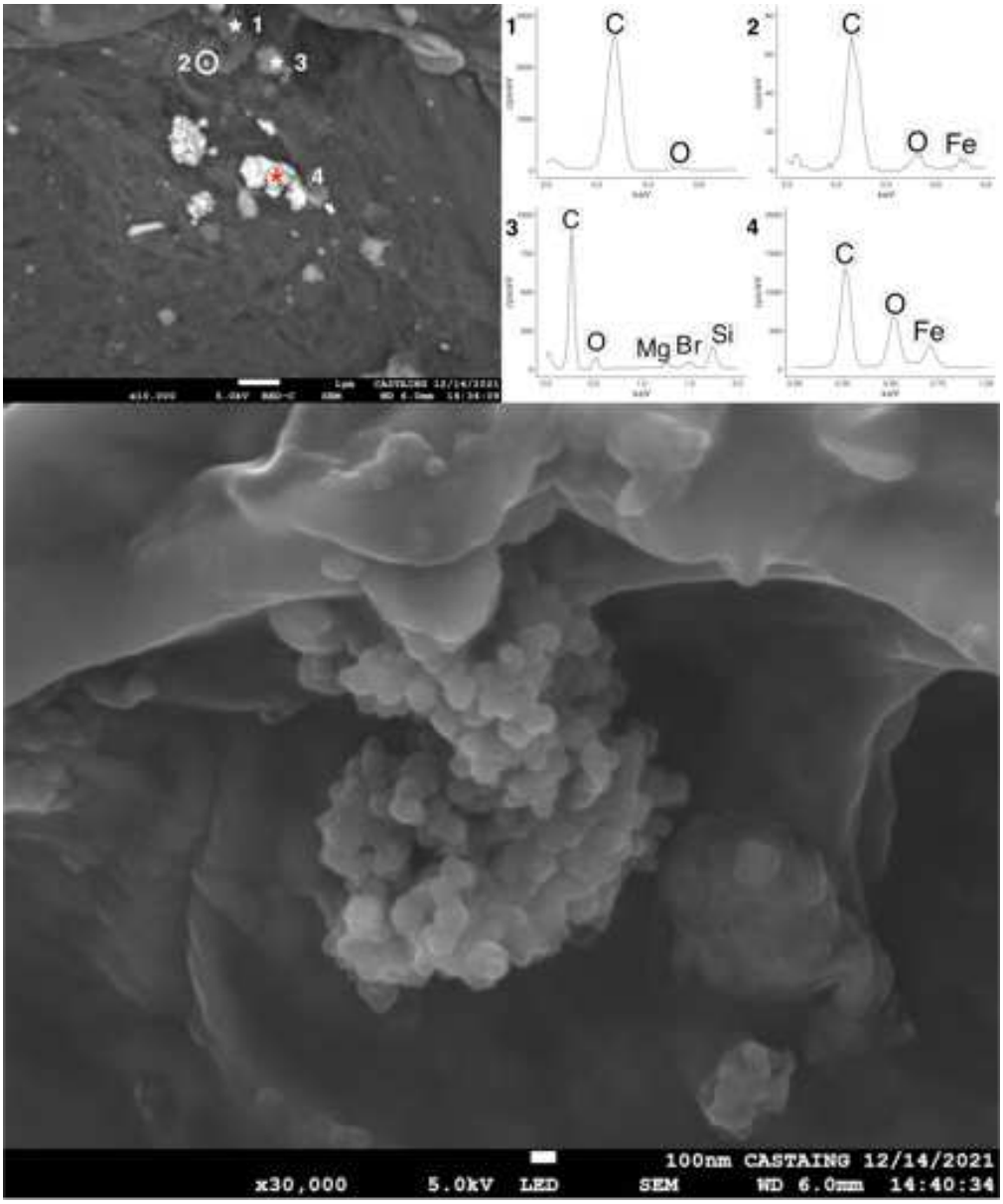

Figure 4.18: A) Different agglomerates are trapped on the outdoor bio-sensor. At the top of the image, we notice a chain-like carbon structure (particle 1) resembling soot chains, with dimensions of 1.6 and 1.5 μm. We notice a small iron oxide (particle 2) below the left without a clear shape, with a submicron metric size of 0.14μm. Still close to the soot chain, to the right, we notice another agglomerate without a clear shape and micrometric size of 1.0μm and composed of Br, Mg, and Si (particle 3). Below, in the center of the image, we can count four bright iron oxides agglomerates (particle 4, for instance, the other have similar spectra) without clear shape, and micro and submicron sizes of 1.3 and 0.9μm; 1.8 and 0.8μm; 0.5 and 0.3μm, 0.7 and 0.5μm. B) Secondary image with greater magnification of the soot chain-like agglomeration, resembling other soot particles captured in air filters.

4.3.4 Discussion

Source of airborne iron oxides

The main source of the airborne iron oxides trapped on the bio-sensors is traffic emissions, both indoors and outdoors, as shown by the dominance of magnetite-like iron oxides in the magnetic fraction, besides the detection of morphologies associated with traffic emissions. IRM curves reached saturation majoritarian (95%) below 300mT, indicating ferrimagnetic magnetite-like minerals [Chaparro et al., 2013a]. Similarly, low-moderate coercivities found on the unmixing of the IRM, ranging from 9.3 to 47.5mT (Table 4.3, Fig. 4.14) points to magnetite-like carriers (magnetite and oxidized magnetite, maghemite, Kruiver and Passier [2001], Dawaï et al. [2021], Maxbauer et al. [2016]). High DP indicates either a large dispersion in grain sizes or arises from the fact that we analyzed the samples with only one component due to the high noise in the data. The presence of magnetite-like minerals in PM is a marker of traffic emissions as reported in previous studies [e.g., Leite et al., 2021, Dawaï et al., 2021, Winkler et al., 2020, Chaparro et al., 2013a, Winkler et al., 2021, Chaparro et al., 2020]. The low-moderate coercivities found in the unmixing of the IRM cannot discard the presence of higher coercivity carriers. The presence of iron oxides among the carbon chains of soot (Fig. 4.18) and iron or glass spherules (Figs. 4.16, 4.17) are a marker of internal combustion of motor vehicles, emphasizing the presence of particles from road traffic [Leite et al., 2021, Dawaï et al., 2021, Shi et al., 2015, Chaparro et al., 2013a, Marié et al., 2018]. Higher indoor SIRM values detected in low densely populated regions (Balma, for instance, Fig. 4.10) may indicate indoor sources of PM, as traffic is expected to be lower in sparsely populated neighborhoods. Besides the penetration of outdoor generated particles in indoor environments, personal habits have been linked to the emission of magnetic particles. For instance, combustion sources such as smoking and biomass burning (for heating) have been shown to produce magnetic particles [Maher et al., 2021, Jordanova et al., 2006]. Smoking may be an important source of indoor pollutants, with PM2.5 concentrations being reported ten times higher in smokers' households compared to non-smokers' households [Semple et al., 2015]. The use of printers may result in magnetic PM, as the ink used contains nanometric iron oxides [Pirela et al., 2015]. Cleaning may be a source of indoor magnetic grains by facilitating resuspension, as this activity has been reported in resuspension of PM2.5 [Tofful et al., 2021].

Magnetic concentrations in indoor and outdoor environments

The outdoor environment has a higher concentration of iron oxides, as expressed by the I/O for SIRM (Table 4.3). SIRM values measured on outdoor bio-sensors have a more extensive distribution with a tendency towards high values, in contrast to indoor SIRM values, which have a narrower distribution. Higher outdoor concentrations (in comparison to indoor environments) of airborne iron oxides have been reported before, with Rachwał et al. [2018] finding higher magnetic susceptibility on bio-sensors (spider web) exposed outdoors. Similarly, Rutkowski et al. [2020] also analyzed spider webs in domestic settings, finding higher magnetic susceptibility values in the outdoor environment. PM2.5 concentration values have been reported to be higher outdoors also in office environments, with an average PM2.5 concentration IO ratio of 0.62±0.24 based on values measured in 140 office rooms in Europe

[Kalimeri et al., 2019]. Conversely, in the domestic environment, higher concentrations of PM were reported in Portugal, Sweden, and the U.K. [Custódio et al., 2014, Monn et al., 1997, Jones et al., 2000]. Only when personal habits were not a source of indoor PM the I/O for PM was below unity [Monn et al., 1997]. Our magnetic data, pointing to higher concentrations of airborne iron oxides outdoors (through the SIRM values, Table 4.3 and Fig. 4.9), in opposition to the reported PM works on households, can be explained by the source of magnetic minerals in our case being majoritarily traffic-related, and dominant about indoor sources of airborne magnetic grains. Besides, outdoor environments may be more affected by resuspension than indoor ones, from wind to traffic flow, which could significantly increase exposure to traffic emitted particles [Abu-Allaban et al., 2003]. Values reported in this work (with means of 0.79×10^{-5} and $2.28 \times 10^{-5}\,\mathrm{A\,m^2\,kg^{-1}}$ for indoor and outdoor means, respectively) are in line with values reported in Italy by Vezzola et al. [2017] with SIRM means of $1.5(\pm1.8)\mathrm{x}10^{-5}$ and $0.21(\pm0.16)10^{-6}\,\mathrm{A\,m^2\,kg^{-1}}$ in Milan with 42 trees and Santa Caterina with 20 trees respectively. Vezzola et al. [2017] used 18 different species in Milan (including *Prunus padus, Sophora japonica* and *Cedrus atlantica*) and *Picea abies* in Santa Caterina. On Argentina, [Chaparro et al., 2020] using tree bark (*F. excelsior, F. pensylvanica, C. australis, Acer negundo, A. pseudoplatanus, Catalpa speciosa, Prunus cerasifera, Albizia julibrissin, Cedrus deodora, Tilia moltkei* and *Populus nigra*) measured SIRM values from traffic origins considerably higher than Toulouse, with a mean of $9.3(\pm4.3)10^{-3}\,\mathrm{A\,m^2\,kg^{-1}}$ for bark collected in 54 trees. This parameter reflects each city's specific and local context, possibly influenced by the different tree species used in each study.

Magnetic granulometry in Indoor-outdoor environments

Our data set presents a clear distinction on the magnetic grain size distribution between indoor and outdoor environments, with finer grains indoors (Fig. 4.12, 4.13). The indoor environment presents a larger distribution of values of the xARM/SIRM ratio. In contrast, outdoors the values of the ratio are concentrated in low values (meaning coarser grains, Fig. 4.12). Indoor values are comparable to those reported in Leite et al. [2021] for iron oxides collected in PM2.5 filters with traffic and combustion sources. Outdoor values have an average comparable to values reported for PM 10 and total PM size range with traffic origins [Mitchell and Maher, 2009]. This indicates some sort of filter for the indoor environment, where majoritarily the finer grains are transported indoors. Indoor and outdoor samples have a clear distinction in the DayPlot (Fig. 4.13, with the indoor ones presenting a lower H_{CR}/H_C and higher M_{RS}/M_S in comparison to the outdoor ones, in agreement with a finer granulometry in indoor samples.

Urban concentration of magnetic PM regarding geographic localization

The tendency of high outdoor SIRM values and low indoor SIRM values is observed all over the city, regardless of the area (Inner Toulouse, Outer Toulouse, or Balma) and population density in a given neighborhood (Figs. 4.10, 4.11). Moreover, the concentration of iron oxides (given by parameter SIRM) indoors is close in all residencies, indicating a homogeneous lower concentration, regardless of localization in the city. The primary source of airborne iron oxides indoors is from outdoor origins, from building penetration and ventilation, and possibly

carried inside by the inhabitants (in clothes, for instance). In the outdoor environment, higher SIRM values were measured in samples located in densely populated neighborhoods, which are majoritarialy in the Inner part of the city (Fig. 4.10). The more densely populated neighborhoods and central areas have enhanced traffic sources, which could explain the higher outdoor SIRM values in those regions and reinforce the source of the magnetic fraction of PM in Toulouse being traffic related.

Citizen science participation

The interventions during the NanoEnvi project (both during recruiting and restitution to the citizens) stirred interest in the urban air quality topic by the participants. The citizens expressed concern about the issue, which could lead to the development of eco-anxiety [Pihkala, 2020]. The restitution interventions were vital for the researchers to approach the citizens. Besides discussing some scientific results during the restitution seminars, researchers were able to help deal with negative feelings by offering coping strategies and possible actions. Tackling eco-anxiety and promoting proactive changes for the population may help deal with some of the challenges of the air pollution issue [Russell and Oakley, 2016].

4.3.5 Conclusion

We presented a participatory citizen science project to investigate air quality in indoor and outdoor domestic environments in an urban setting. Using bio-sensors distributed to the population of Toulouse and environmental magnetism methods, the importance of traffic emissions becomes evident as the primary source of the magnetic fraction of PM. Magnetite-like grains dominate the magnetic mineralogy, as shown by the low-moderate coercivities found on the unmixing of the IRM (with indoor and outdoor means of 24 and 32mT respectively) besides IRM curves achieving saturation majoritarily below 300mT. Low coercivity carriers (magnetite-like) are linked to traffic emissions, and the iron oxide spherules detected by SEM microscopy point to traffic emissions as the primary source of the magnetic fraction of the PM. Outdoor environments have higher concentrations than indoors, reflected in the I/O for SIRM of 0.5. Although traffic emissions are dominant in the emission of air pollutants, indoor sources may explain some of the higher SIRM values detected indoors, such as smoking, biomass burning, and cooking. Higher SIRM values outdoors were seen in central, more densely populated neighborhoods, indicating higher concentrations of airborne iron oxides related to increased traffic in these regions.

4.4 Superparamagnetic concentration & dipole moment

4.4.1 Theoretical aspects

This section discusses the theory behind the SPCDM method [Leite et al., 2018]. It starts with the superparamagnetic magnetization model of Néel [Dunlop and Özdemir, 2001] and quantitative data analysis based on this model, the formulation of the direct and inverse problems for the characterization of grain-size and total magnetization of the SP fraction, and, finally, the experimental procedure developed according to this formulation.

Neel's model for SP magnetism

The superparamagnetic (SP) fraction is defined by a blocking volume below which the ferromagnetic mineral grains don't sustain stable remanent magnetization at room temperature. Below this blocking volume, the individual magnetic moment of the particles is disturbed by thermal fluctuations, resulting in a zero net magnetization. When exposed to an external magnetic field, the individual magnetic moments of an SP grain assembly orient themselves according to the inducing field, resulting in a non-zero magnetization in the lattice. Such magnetization, however, does not hold in the absence of an external inducing field. In this situation, the reorientation process of the magnetic moments is expressed by an exponential decay of the magnetization with time, with a characteristic decay time or relaxation time (τ). This decay is defined as [Evans and Heller, 2003]:

$$M(t) = M_i e^{\frac{-t}{\tau}} \tag{4.1}$$

M_0 being the initial magnetization at instant t = 0 and M(t) the magnetization at instant t after the removal of the external field. The relaxation time is described by the Néel-Arhennius equation [Néel, 1955]

$$\tau = \tau_0 e^{\frac{-E_1}{E_2}} \tag{4.2}$$

With τ_0 being a time factor, E_M being the barrier magnetic potential energy, and E_T being its thermal energy. The time τ_0 ranges from 10^{-12} to 10^{-8}s [Dormann et al., 1996, Worm, 1998] and corresponds to the time average between two random, successive thermal excitations [Berndt et al., 2015]. The barrier magnetic potential energy E_M is associated with the rotation of the magnetic moment of the grains and is equal to KV with K being the anisotropy coefficient of the magnetic grain and v its volume. The thermal energy E_T is expressed by K_bT , with $K_b = 1.38 \times 10^{-23}[JK^{-1}]$ the Boltzmann constant and $T[K]$ the temperature. The magnetization decay thus represents a competition between an alignment tendency due to the E_M term (magnetostatic energy) and a disorganization tendency associated with the E_T term (thermal energy). In constant temperature experiments, the relaxation time depends on the ratio v/K, where v is the volume of the grain and K is its magnetic anisotropy coefficient, both parameters that depend on the mineral. Figure 4.19 illustrates how small differences in grain size (assuming a spherical volume) result in a wide distribution of relaxation time values. For equidimensional magnetite ($M_S = 480[kAm^{-1}]$, $K = 2.31 \times 10^4[Jm^{-3}]$) at room temperature the relaxation time ranges from 1.98×10^{-8}s for a 10nm diameter grain, through approximately 24 s for a 20 nm grain, to 9.4×10^{11} years for a 28nm grain. Experimentally

it turns out that the blocking volume for magnetite is between 25 and 30nm [Dunlop and Özdemir, 2001] and 17nm for hematite [Jiang et al., 2014].

For an acquisition window of 100 s (Figure 4.19 b), as is usually employed in SP fraction studies [Wang et al., 2010, Worm, 1999], it can be seen that a very narrow fraction of magnetic grains (close to the SP-SD boundary) can be captured. Smaller particles exhibit much faster, almost instantaneous decay. The viscous SP decay can thus be related to a "coarser" mineralogy (near the SP-SD boundary, Figure 4.19b). The "instantaneous" SP decay, on the other hand, can be related to an ultra-fine fraction (Figure 4.19b). One realizes then that techniques that seek to model viscous decay apply to a narrow fraction of grain sizes close to the SP-SD stability transition.

For a pure assembly of ultrafine grains, the transient magnetization cancels out within microseconds, hence the need to introduce the term "instantaneous SP decay" as indicative of SP behavior for particles with a volume less than the blocking volume.

The SP magnetization under external field $H_0[Am^{-1}]$ can be written as [Dunlop and Özdemir, 2001]

$$M(H_0, T) = M_S \tanh \alpha \tag{4.3}$$

sendo

$$\alpha \equiv \frac{\mu_0 V M_S H_0}{K_b T}. \tag{4.4}$$

where

$$\alpha \equiv \frac{\mu_0 V M_S H_0}{K_b T}. \tag{4.5}$$

and L(α) is the Langevin function

$$L(\alpha) \equiv \coth \alpha - \frac{1}{\alpha}. \tag{4.6}$$

In Equation 4.4, M_S is the saturation magnetization ($480kAm^{-1}$ for magnetite), $\mu_0 = 4\pi \times 10^{-7}$ the magnetic permeability of vacuum, V the volume of the grain, and Kb is the Boltzmann constant. The magnetic moment product, $\mu = VM_S$ [Am^2], expresses the dipole moment associated with the magnetic grain in the SP regime.

The saturation magnetization is such that $M_S = n\mu$[Am^{-1}] , where n[m^{-3}] is the concentration of the magnetic grains in the sample. For a sample with density ρ [kgm-3], the magnetic carriers' mass concentration is obtained by n/ρ. The concentration n can be considered as the concentration of SP carriers and not necessarily the concentration of particulate material in aggregates. Considering $VM_S = \mu$ and$\mu_0 H_0 = B$ we can rewrite the α term in Equation 1.4 as

$$\alpha = \frac{\mu B}{K_b T}, \tag{4.7}$$

making the expression of the magnetization SP, according to the Neel model, equal to

$$M(B, T) = M_S L(\frac{\mu B}{K_b T}). \tag{4.8}$$

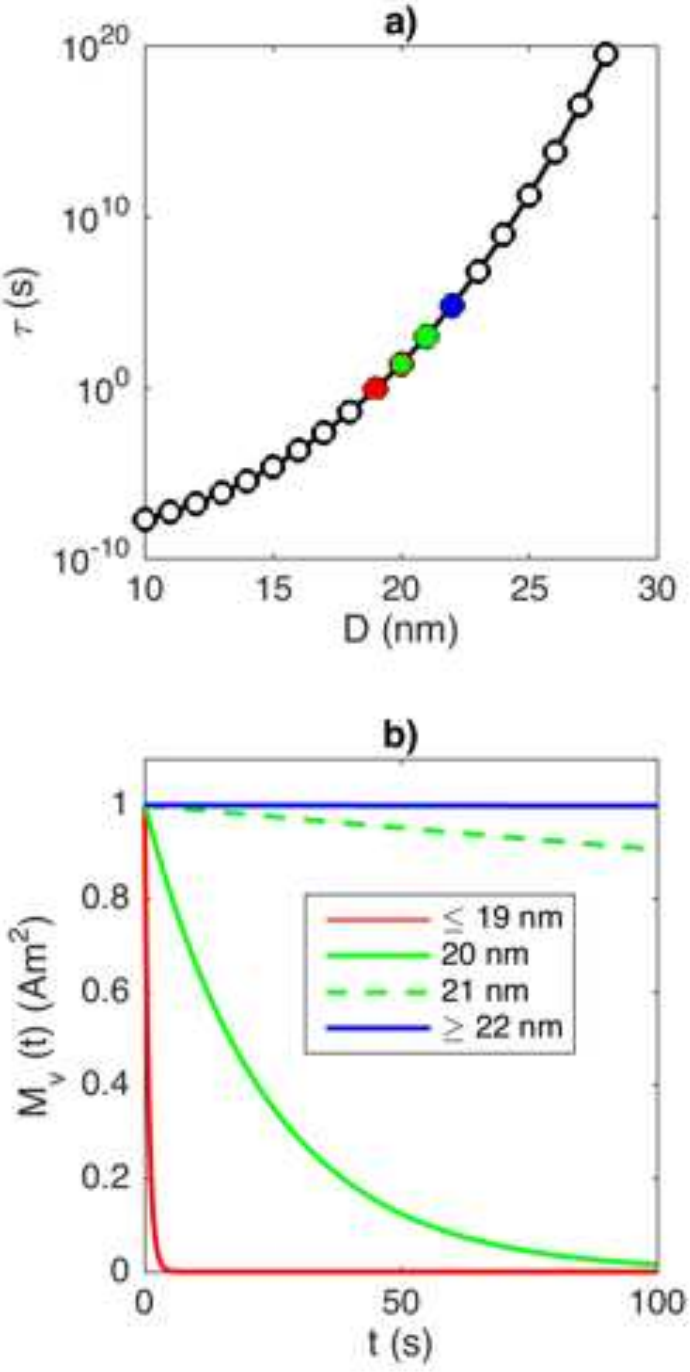

Figure 4.19: Variation of τ with particle size for magnetite-type minerals. The SP fraction can be separated into an upper boundary (blue) where the blocking volume produces stable magnetization, the fraction just below the stability boundary (green) showing viscous magnetic behavior, and the lower fraction (red) with rapid magnetic relaxation. b) Decay of magnetization (Mv) for magnetite-type minerals, considering spherical grains with different diameters. Source: Leite et al. [2018].

According to Equation 4.7, Neel's model relates known parameters (B, T, Kb) associated with the measurement process and unknown parameters (M_S,μ) that describe the SP magnetization and that are characteristic of the magnetic carrier. The methodology presented in section 1.2 combines experimental and analytical procedures to determine the two unknown parameters of the model. The experimental procedure involves creating a unified database to formulate an inverse problem, under which the procedure for quantitative data analysis is developed. In determining M_S and mu, the magnetic grain concentration is determined from the constitutive relationship $n = M_S/\mu$.

Inverse and direct problem

Let us consider a set of magnetization measurements $M_i = M(H_i)$, for samples subjected to external fields $H_i, i = 1 : N$ at constant temperature T (room temperature). By Neel's model for SP magnetization, the magnetization M_i, when the sample is subjected to the field $B_i = \mu_0 H_i$, is such that

$$M(B_i) = M_S L(\frac{\mu B_i}{K_b T}) \tag{4.9}$$

The determination of the unknown model parameters, M_S and μ, can be formulated in terms of minimizing a functional $Q(\bar{p})$ such that

$$Q(\bar{p}) = \sum_{i=1}^{N} [M_i - M(B_i, \bar{p})]^2. \tag{4.10}$$

As per standard terminology for formulating inverse problems [Aster et al., 2011], the unknown model parameters are grouped into a vector $\bar{p}$, in this case such that $\bar{p} = [M_s \ \mu]^T$. The superscript T denotes the operation of transposition. The depreciation of the functional $Q(\bar{p})$ as defined in Equation 4.10 prescribes a fit to the database according to the least-squares criterion. The coordinate pair $\bar{p}$, with particular values of $\bar{M_S}$ and $\bar{\mu}$ that minimize $Q(\bar{p})$ constitute a solution to the inverse problem, in the sense that they allow the fit to the data at the threshold of experimental errors. Formally, a solution $\bar{p}$ is such that $Q(\bar{p}) < \varepsilon$, where ε is the estimate of the mean error of the data.

As defined in Equation 4.9, the inverse problem associated with determining the M_S and μ parameters from magnetization data $M_i, i = 1 : N$ configures a nonlinear (and nonlinearizable) problem that, as such, must be solved by applying iterative methods [Aster et al., 2011].

Since it is a relatively simple inverse problem, due to the reduced number of unknown parameters (two, in this case), the SPCDM inversion can make use of the mapping of the functional $Q(\bar{p})$ (Figs. 4.22b, 4.23b), generically called "object function mapping". This mapping consists of, from a database $M_i, i = 1 : N$, computing the value of the functional $Q(\bar{p})$ for regularly distributed values in a window in parameter space, such that $p(1) = M_S$ varies in the interval$M_{S,min} \leq p(1) \leq M_{S,max}$ and $p(2) = \mu$ in the interval $\mu_{min} \leq p(2) \leq \mu_{max}$. In the object function mapping, the solution of the inverse problem is visually identified as the minimum point of $Q(\bar{p})$. The ambiguity associated with the parameter estimate (minimum point) is determined by the intervals projected on the $p(1)$ and $p(2)$ axes such that $Q(\bar{p}) < \varepsilon$. Determining the minimum point of the functional $Q(\bar{p})$ can also be implemented in

the form of optimization algorithms that generically solve problems of determining maxima and/or minima of multivariate functions.

Experimental procedure for SPCDM analysis

The experimental procedure for SPCDM analysis requires building a database to isolate the SP response (Fig. 4.20a). The SPCDM method involves measuring the magnetization of the sample when it is exposed to external fields $H_i i = 1 : N$ and, after completion of the SP decay, the measurement of the remaining magnetization (Fig. 4.20a). For carriers in the ultrafine fraction, the SP relaxation time is on the order of 10^{-6}s, meaning that measurements 0.5-1.0 s after the external field is switched off are practically free of SP decay unless the ambient magnetic field induces the effect. The subtraction of the magnetizations measured when under the action of the H_i field and after its removal isolates the SP effect since the ambient field is present in both situations, thus being canceled in the subtraction. The residual magnetization after SP decay is of the IRM (isothermal remanent magnetization) type. The difference $M_0 - M_q$ isolates (Fig. 4.20b) the SP response allows its analysis by the Neel model.

The SP magnetization will appear superimposed to stable magnetization for magnetic grains containing a mixture of SP-SD pr SP-MD domains. Figure 4.21 (modified from [Leite et al., 2018]) illustrates the difference between pure SP and mixed SP-SD/SP-MD mineral fractions. Fig. 4.21a and 4.21b shows pure SP behavior, recorded on synthetic samples calibrator 2853 YIG sphere (from a MicroMag VSM 3900) and pure nano magnetites with diameter around 8nm. Figures 4.21c, 4.21d, 4.21e, 4.21f show mixed behavior, with IRM acquisition between the stepwise induction fields. Figures 4.21 c, d, e, and f are sediments from Jaragua Cave (Brazil), a PM air filter collected in a tunnel in São Paulo (Brazil), and indoor and outdoor bio-sensors used previously (Sections), respectively. Due to the low signal, it is possible to notice considerable noise on the curves from the bio-sensors.

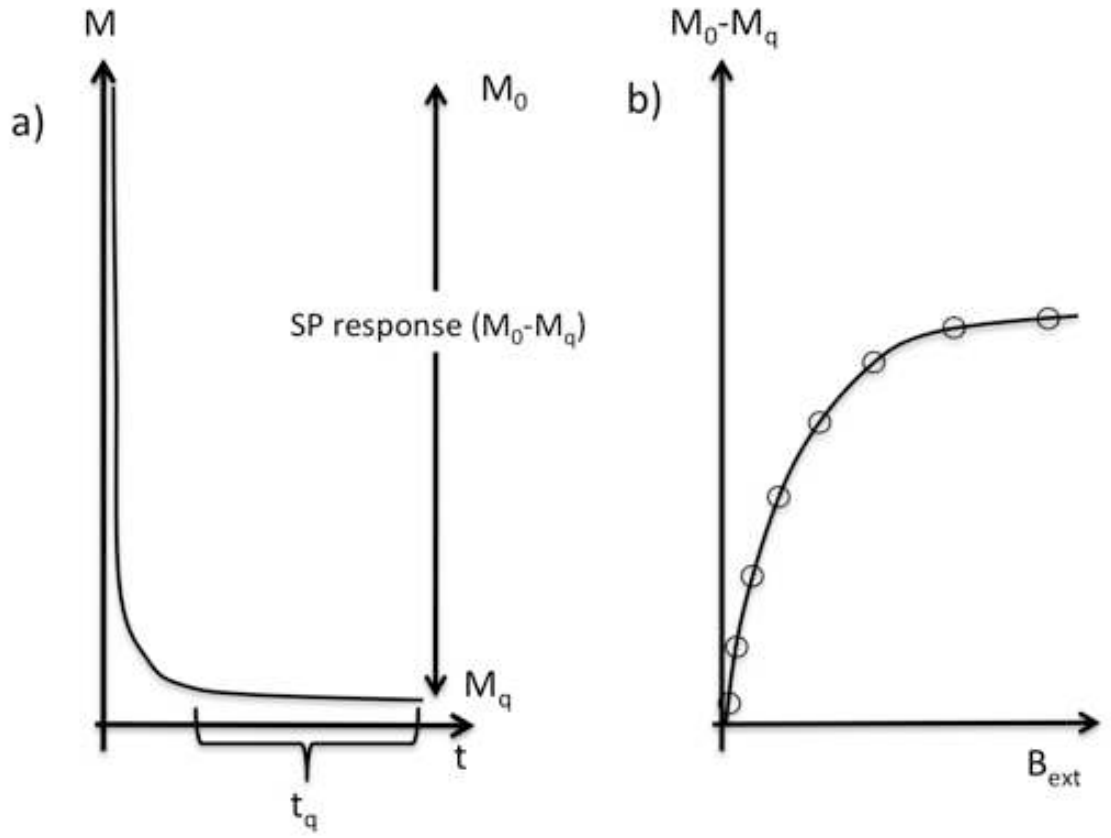

Figure 4.20: Schematic representation of the database construction to isolate the SP effect. (a) The decay of the magnetization from M_0, under B_extt field, and interval t_q with M_q magnetization. The subtraction M_0 - M_q isolates the SP response. (b) By repeating this procedure for several B_extt fields we obtain a database suitable for interpretation according to Neel's model for superparamagnetism.

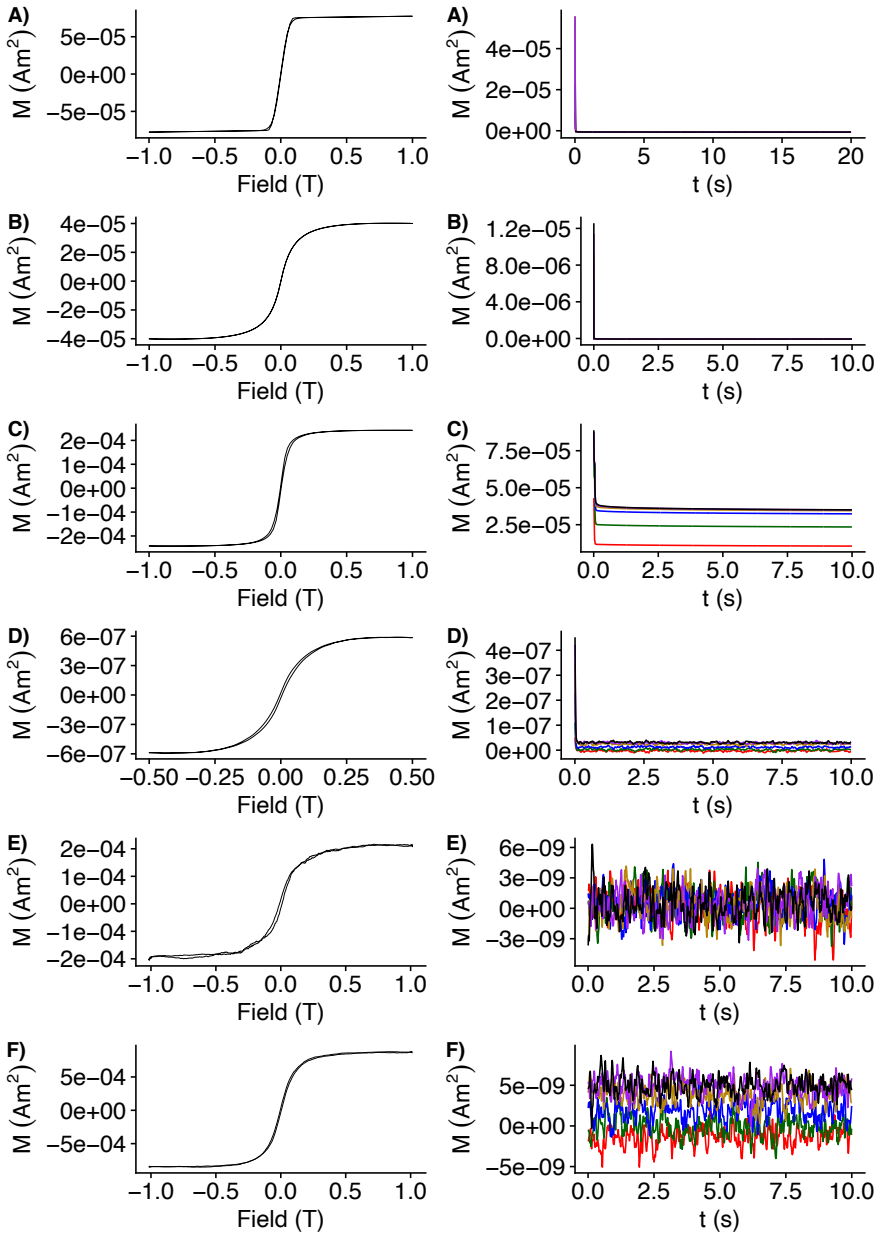

Figure 4.21: Hysteresis curves (on the left) and magnetization decay curves (right) after stepwise IRM inductions. a)calibrator 2853 YIG sphere with pure SP behavior; b) nanoparticles of synthetic magnetite with 8nm of diameter, with pure SP behavior; c) sediments from Jaragua Cave, Brazil, with mixed magnetic behavior; d) air particulate matter collected in janio Quadros tunnel, São Paulo, Brazil, with mixed magnetic behavior; e) bio-sensor exposed indoors in Toulouse, France, with mixed magnetic behavior; f) bio-sensor exposed in Toulouse, outdoors, with mixed magnetic behavior. a-d are from Leite et al. [2018].

Table 4.6: Results from the SPCDM inversion for the domestic bio-sensors group of samples. Means and standard deviations (in parenthesis) are given for parameters diameter, μ, n and %SP. Number of samples given by N.

bio-sensors					
Site	Diameter (m) 10^{-9}	μ [10^{-19}]	n [10^{11}]	%SP (%)	N
Indoor	7.88 (1.79)	1.42 (1.05)	2.79 (3.02)	82.22 (10.30)	23
Outdoor	7.72 (1.31)	1.26 (0.78)	6.72 (5.77)	87.03 (8.32)	33

Parameter %SP

To estimate the share of SP magnetization exhibited in an external saturation field relative to the total saturation magnetization in a sample, a %SP parameter is proposed such that

$$\%SP = (\frac{M_{SP}}{M_{S,1T}}) \times 100 \tag{4.11}$$

$M_{S,1T}$ being the total saturation magnetization of the sample measured during the hysteresis cycle (and thus representing the total saturation magnetization of all particle size fractions present in the sample) and $M_{SP,1T}$ is the saturation magnetization of the SP fraction, calculated from Equation 4.8, using the parameters μ and M_S obtained in the data inversion, with a saturation field $B_{ext} = 1T$. Thus, the %SP parameter represents the fraction corresponding to the SP magnetization, providing a quantitative estimate of the SP magnetization expressed in a sample while applying an external saturation field.

4.4.2 Results

SPCDM acquisition was performed on bio-sensor samples (Figs. 4.22, 4.23) that had a signal strong enough to be characterized through hysteresis cycles. A total of 56 samples were measured, of which 33 were exposed outdoors and 23 indoors. Generally, dia/paramagnetic correction was necessary; only one sample skipped this step.

Table 4.6 presents means, medians, standard deviations, and several samples for each environment for the dipole moment of the grain (μ) and calculated parameters diameter, n and %SP. μ mean values are statistically equivalent in both environments, at 1.42×10^{-19} A m^{2}indoors, while outdoors, this parameter has a mean of 1.26×10^{-19} A m^2. Both environments have statistically equivalent calculated diameters, close to 8nm. Regarding the concentration, absolute n have higher values outdoors, with a mean equal to 6.72x10^{11}, and mean %SP, relative to the fraction of magnetization due to SP grains regarding the whole spectrum reaching 87.03%. I/O for n is calculated at 0.42.

Table 4.4.2 presents results from the courtyard tree bark from School 1 (Courtyard 1 East and West, Fig. 4.24) and School 2 (Courtyard 2). Calculated diameters are quite close, reaching 7.7nm in the School 2 courtyard. Magnetic dipole μ are also close in both school's courtyards, ranging from 1.01×10^{-19} A m^2 in West School 1 courtyard, to 1.21×10^{-19} A m^2, in both School 1 East Courtyard and School 2 Courtyard. Absolute concentration n is similar in both schools. In School 1 n means reach 11.89x10^{11} and 10.44x10^{11} in the East and West courtyards, respectively, and in School 2 n mens reach 6.42x10^{11}. The percentage %SP of the magnetization from the ultrafine fraction is similar in both schools.

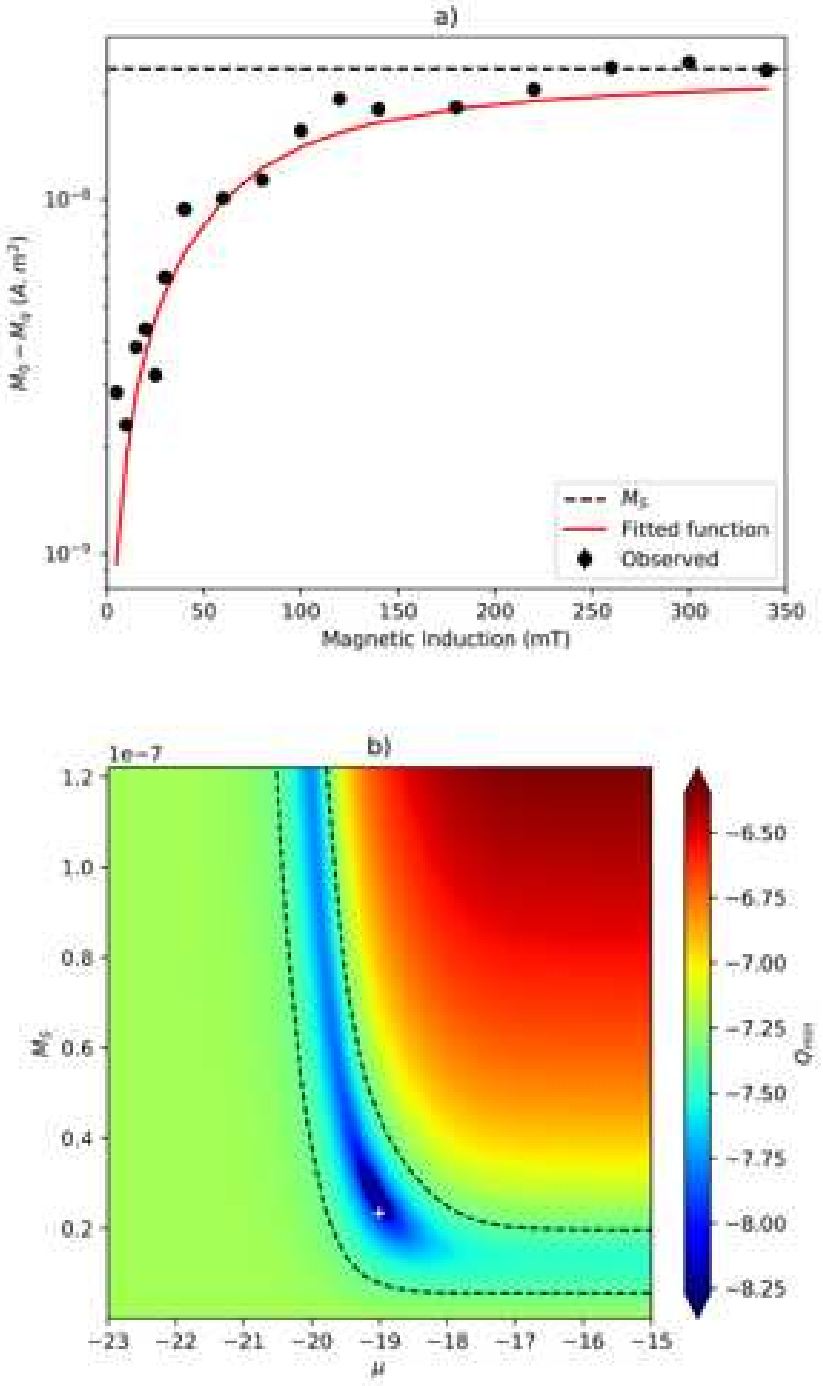

Figure 4.22: Example of the inversion SPCDM procedure (a) and map of the objective function (b) showing the found solution by the white cross, for the indoor bio-sensor shown in Fig.4.21e.

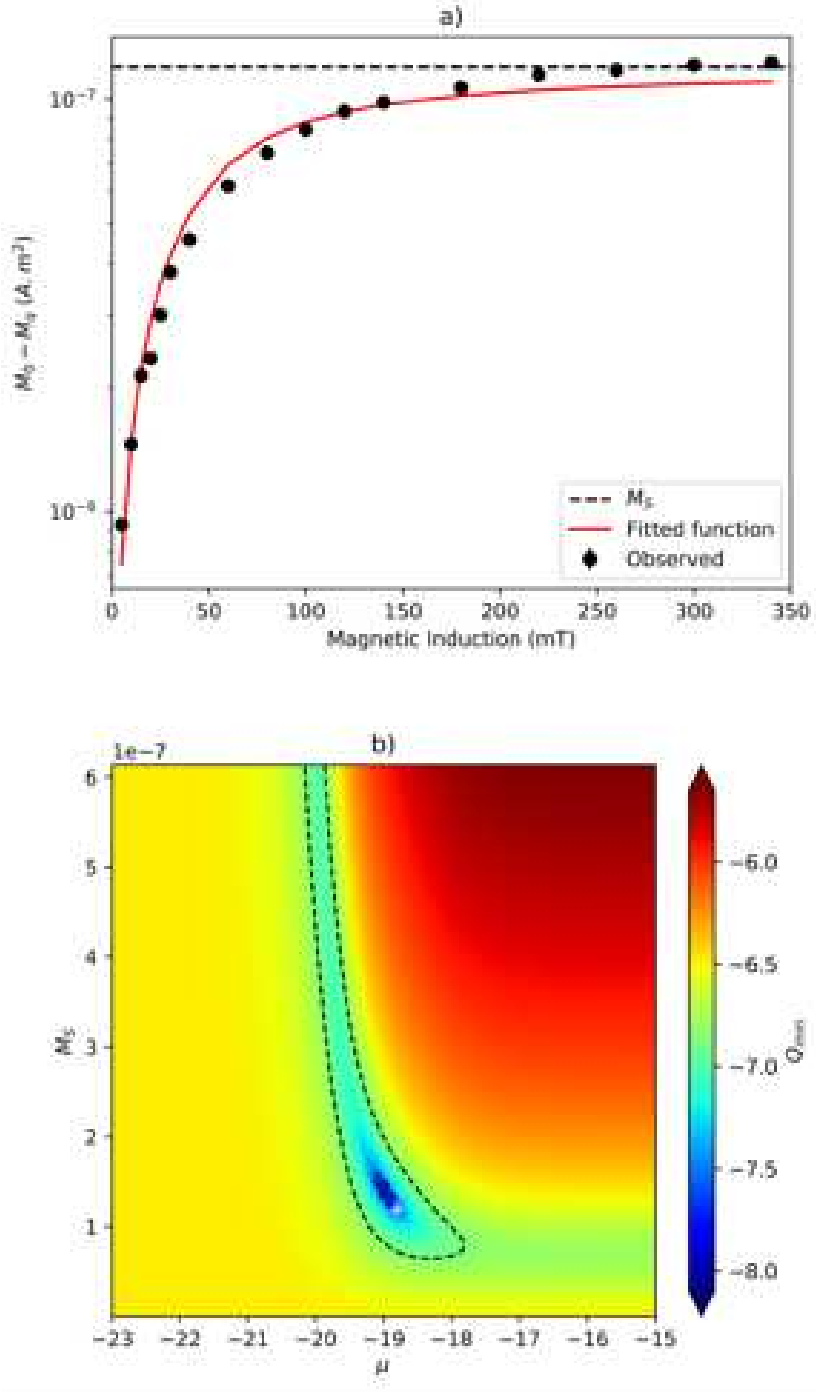

Figure 4.23: Example of the inversion SPCDM procedure (a) and map of the objective function (b) showing the found solution by the white cross, for the outdoor bio-sensor shown in Fig.4.21f.

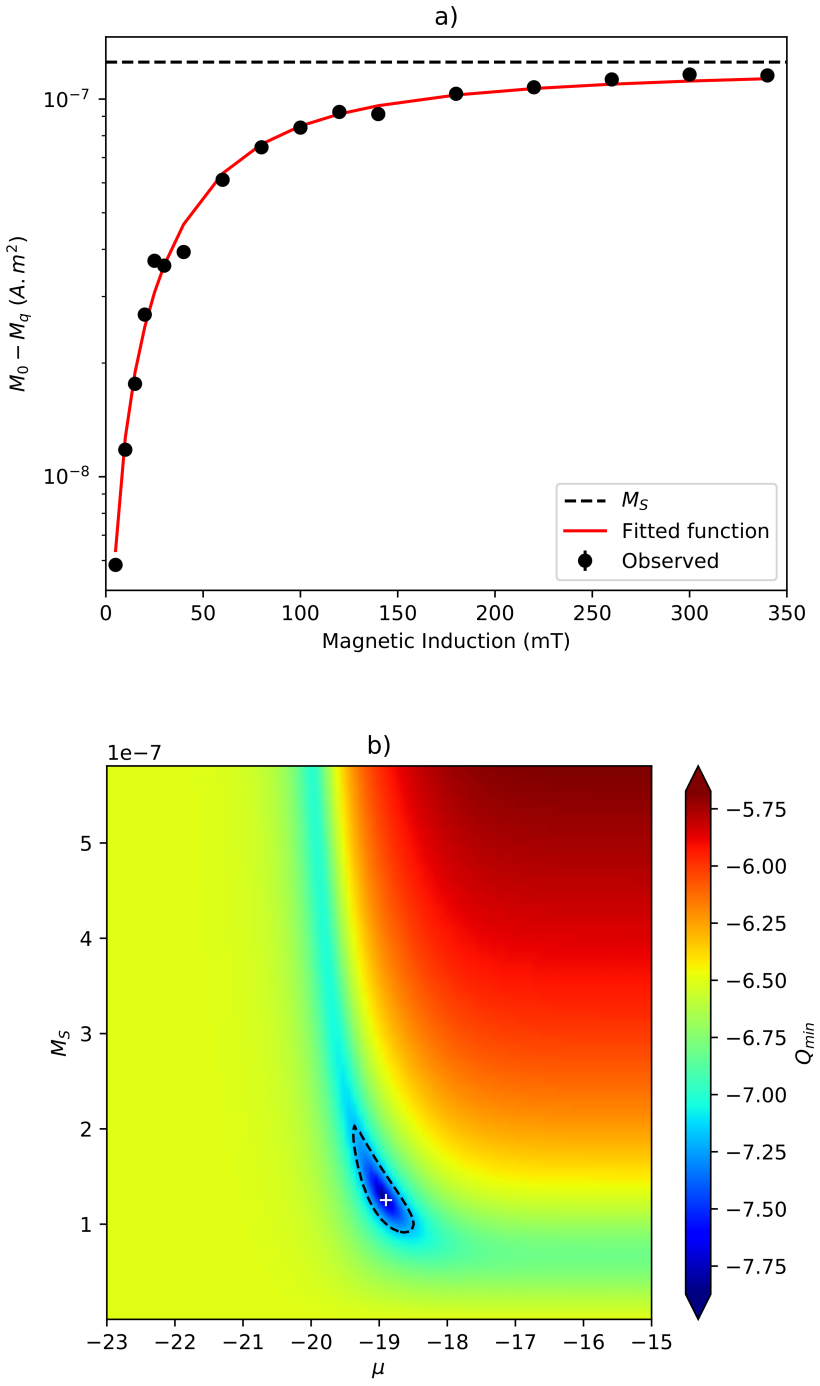

Figure 4.24: Example of the inversion SPCDM procedure (a) and map of the objective function (b) showing the found solution by the white cross, for the the courtyard tree bark from School 1.

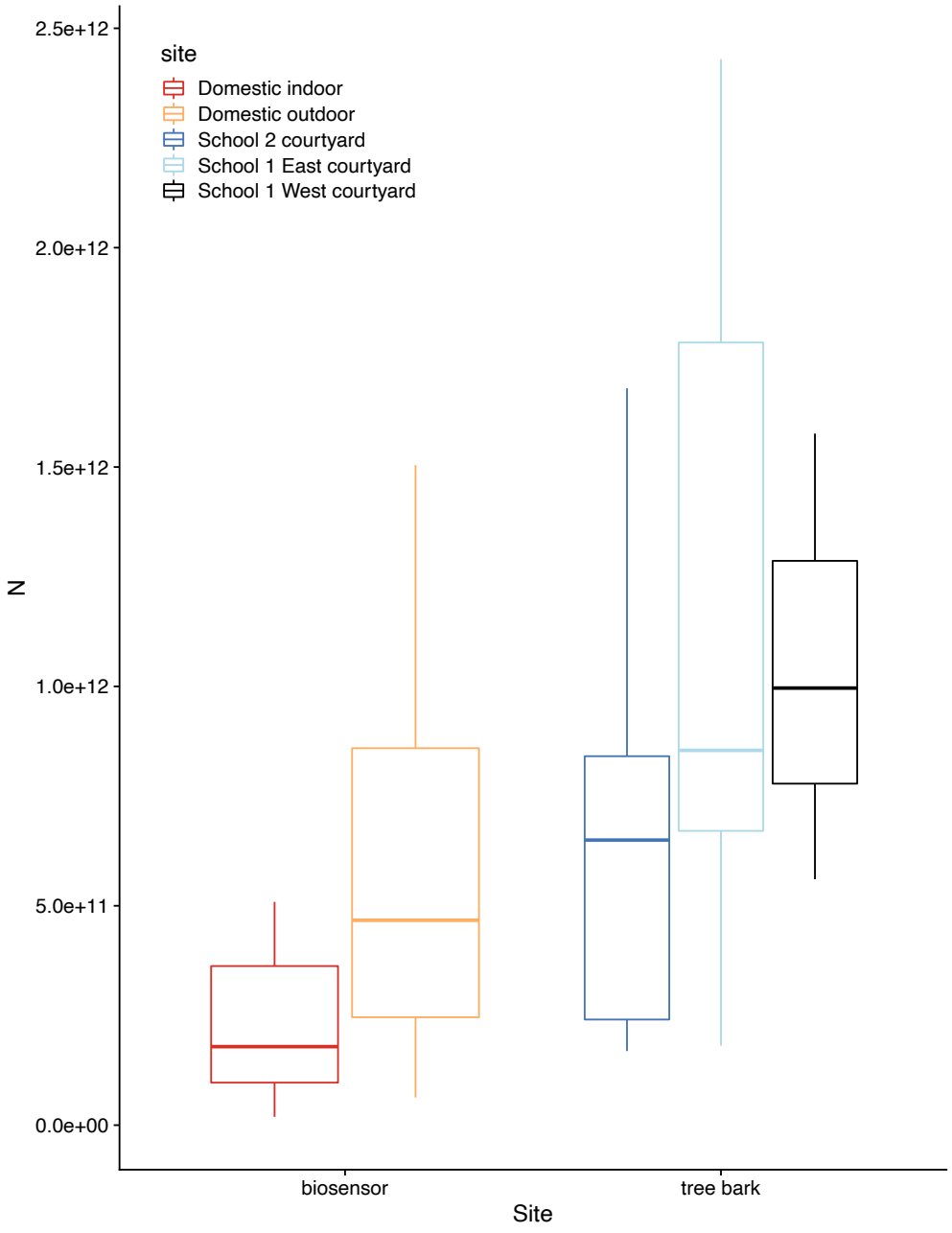

Figure 4.25: Boxplots for the N concentration parameter on bio-sensors exposed on domestic environments (indoors and outdoors) and school courtyard tree bark. Median is the horizontal line inside the box, the interquartile range by the size of the box, maximum and minimum values are the vertical whiskers.

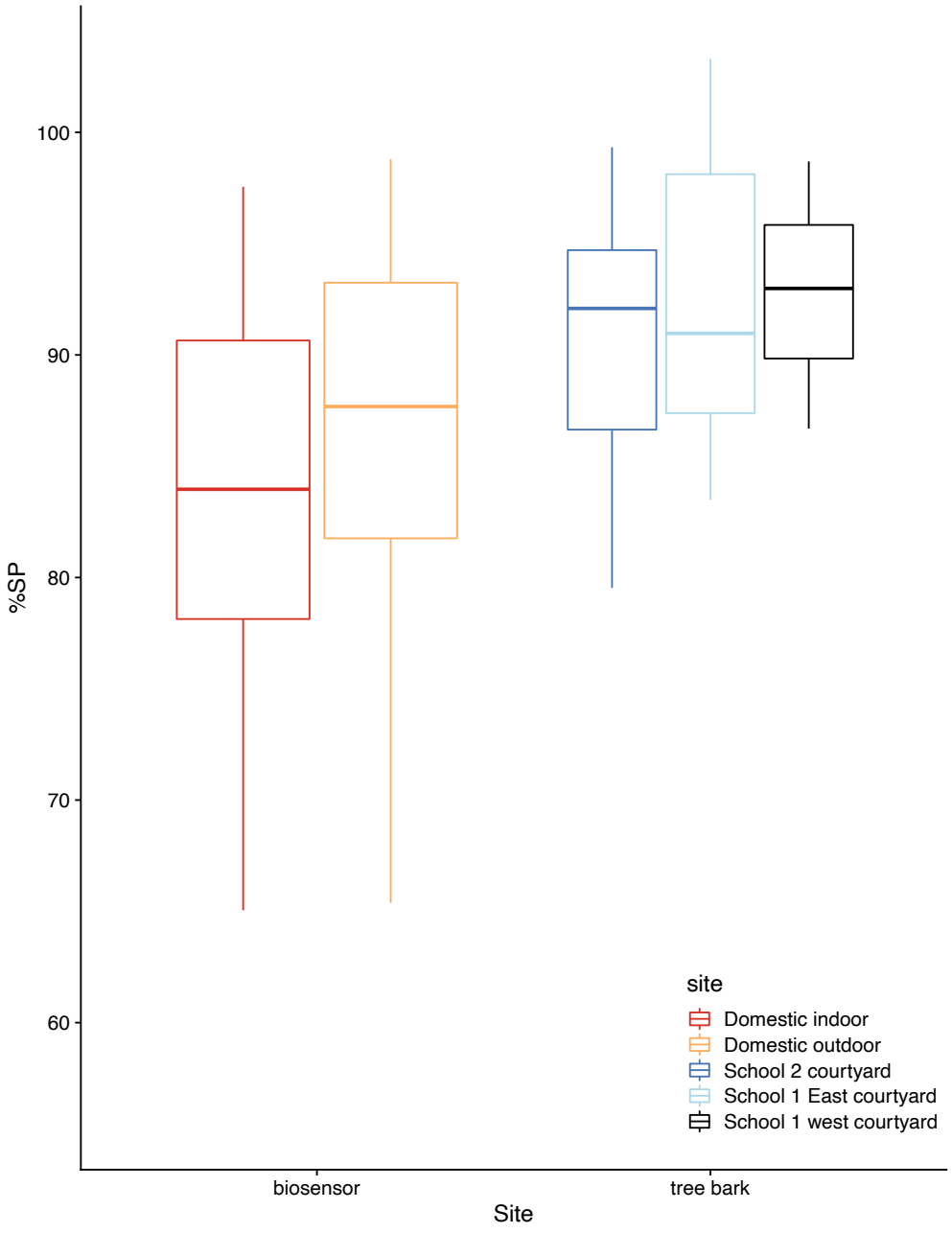

Figure 4.26: Boxplots for the %SP parameter on bio-sensors exposed on domestic environments (indoors and outdoors) and school courtyard tree bark. Median is the horizontal line inside the box, the interquartile range by the size of the box, maximum and minimum values are the vertical whiskers.

Table 4.7: Results from the SPCDM inversion for the school's courtyard tree bark group of samples. Means and standard deviations (in parenthesis) are given for parameters diameter, μ, n, and %SP. Number of samples given by N.

Courtyard tree bark					
Site	Diameter (m) 10^{-9}	μ [10^{-19}]	n [10^{11}]	%SP (%)	N
School 2	7.77 (0.79)	1.21 (0.38)	6.42 (4.46)	90.26 (6.30)	13
School1 East	7.77 (0.75)	1.21 (0.37)	11.89 (7.32)	92.65 (6.88)	11
School 1 West	7.35 (0.60)	1.01 (0.24)	10.44 (5.09)	92.79 (6.00)	3

4.4.3 Discussion

Overall, both domestic environments (indoor and outdoor) and the school's courtyards present similar characteristics of the ultrafine magnetic grains ("fast-decay" type). Diameters are close to 8nm in all environments. Such fine granulometry on airborne iron oxides has been reported before on PM filters from São Paulo city [Leite et al., 2018]. Ronkko et al. [2014] relates particles emitted in traffic emissions around 7nm to metals in motor oil lubricants. The SPCDM results on synthetic nanosize (with the average size of 8nm) magnetites used by control and the magnetic fraction on PM presented by Leite et al. [2018] gives much resemblance with the characterization of the ultrafine fraction ("fast-decay" type) of the iron oxides trapped on the bio-sensors and school courtyards. High standard deviations in both the absolute n and %SP shows that all environments have statistically equivalent concentrations of ultrafine "fast-decay" magnetic carriers (Figs. 4.25 and 4.26). The homogeneity in the different environments regarding the concentration of the ultrafine fraction ("fast-decay" type) might be related to re-suspension, as such fine particles have important influence from Brownian motion force [Chang and Hu, 2008]. Coarser particles sediments faster, due to gravity and impaction [Nazaroff, 2004]. Traffic-related emissions release ultrafine particles. Using a dual scanning mobility particle sizer (SMPS) over a size range of 3-500nm, Li et al. [2018] found one mode on particle number-size distribution around 16nm, measured on traffic tunnels in Pittsburgh, U.S.A. In the same study, data from a thermodemoder (TD) coupled with the SMPS shows that the median diameter of the particle number-size distribution shifted to 7nm. The shift in the median diameter is due to volatile evaporation, possibly indicating a mix of volatile and non-volatile phases in the particles [Li et al., 2018]. The SPCDM method applied in this section and inLeite et al. [2018] found a mean particle diameter for the magnetic SP "fast-decay" fraction of PM, calculated around 8nm. These ultrafine iron oxides emitted in PM could be related to the non-volatile phase of the particles detected by Li et al. [2018]. The mix of volatile and nonvolatile PM phases has been detected in air quality magnetic investigations, with iron oxides spherules emitted in traffic emissions among soot [Leite et al., 2021, Shi et al., 2015], and also in the PM1 filters exposed in the School environment in Toulouse (Section 4.2, Fig. 4.5). Such fine particles are hazardous health-wise due to their capability to penetrate deeper into the human body and more nocive composition [heavy metals Pope III and Dockery, 2006, Martins et al., 2020].

4.4.4 Conclusion

This section presents a study case of the biocollecors previously used in the school and domestic environment. The methodology used (SPCDM, Leite et al. [2018] aims to characterize the ultrafine fraction ("fast-decay" type) of the iron oxides in terms of concentration and grain size. A uniform concentration was found in all environments. The size found for the iron oxides (just below 8nm) was reported before, in the work of Leite et al. [2018] but also in works analyzing traffic emissions with other techniques [Ronkko et al., 2014, Li et al., 2018].

Chapter 5

Going down the river: the fate of urban airborne particles

5.1 Introduction

PM is an important air pollutant, comprising anthropogenic and natural sources. The health consequences of PM exposure have been investigated for the last decades, and nowadays, it is understood as one of the primary sources of disease, on par with tobacco smoking and unhealthy diets [Murray et al., 2020].

After its emission, PM may linger in the atmosphere, transported by wind to other locations. It may also sediment due to gravity into the ground as dust or adhere to vegetation or urban structures due to impaction. Eventually, the PM may be washed by rain, for instance, being removed from plant surfaces [Zhou et al., 2021]. PM's final destination may be linked to the water cycle, eventually being carried on water bodies such as rivers; as with rain, PM can be taken by the washout effect [Guo et al., 2016].

Magnetic concentrations have been shown to significantly correlate with anthropogenic antimony-rich iron oxides in river sediments from the Seine river in Paris [Franke et al., 2009]. On the Ponnaiyar river (India), magnetic methods coupled with geochemical analysis showed a dominance of soft coercive (magnetite-like) carriers associated with heavy metals concentration in the most polluted areas [Chaparro et al., 2013b]. Magnetic methods are then a suitable tool for investigating anthropogenic input on river sediments, especially when coupled with other techniques such as geochemistry analysis and SEM investigations.

The effects of PM exposure on human health is a well-investigated topic, but PM infiltration and the impact of PM in natural environments, such as water bodies, remains poorly known [Zuhara and Isaifan, 2018]. Understanding the final destination of PM can help track anthropogenic emissions from urban centers. To investigate this transfer from anthropogenic emissions into the river, this chapter presents an investigation done in the sediments of the Garonne river in the region of Toulouse. The Garonne passes through downtown Toulouse, from South to North. Samples were taken along a 50km profile in two campaigns in 2018 and 2019. They were subject to magnetic investigation, geochemistry analysis, and SEM microscopy to characterize the anthropogenic PM among the river sediments.

Figure 5.1: Garonne river at downtown Toulouse. Pont Saint Pierre and Dome de la Grave in the background. Photo by the author.

5.2 Urban & Geological setting

Toulouse city has 783,353 inhabitants in 45,820ha. The territory of Toulouse is 42.8% in area from natural parks, forests, and agricultural regions (`https://www.toulouse-metropole.fr/collectivite/en-chiffres`). Toulouse city was built along the Garonne river margins (Figs. 5.1, 5.2), with the river crossing the city from South to North. Toulouse city has a ring road countorning the central neighborhoods of the city, composed of the A620 highway in the South and East and on the North and West by municipal avenues that board the Canal du Midi just until the Port de l'Embouchure (Section 4.3). The South part of the ring road includes 35km from highway A620, with three lanes each way and a mean traffic flow of vehicles in the order of 120,000 per day (in 2019, Report Toulouse Metropole). Runoff water from the city of Toulouse into the Garonne river has been shown to contain xenobiotic pollutants [polychlorinated biphenyls, linear alkylbenzene sulphonates, diethyl hexyl phthalate, and hydrocarbons, Sablayrolles et al., 2011] and trace metals [Pb and Cu, Garneau et al., 2017].

Before entering Toulouse, the Garonne river environment comprises agricultural and economic (companies warehouses) areas, along with preserved sites (Fig. 5.3). Muret is a small town before Toulouse on the Garonne, with 24,797 inhabitants in 2019 and an area of 5,700ha. After Toulouse city, the Garonne river is surrounded by agricultural areas. Around 20km from Toulouse, Grenade is another small town with 8,884 inhabitants in 2019 and around 37,000ha of area. The Garonne river originates in the Pyrenees Mountains at the Franco-Spanish border, stretching for a total of 647km in length ([David et al., 2016] before flowing into the Atlantic Ocean. It is one of the most important rivers in France with a mean river discharge of 617, m^3s^{-1}. A complex rain-snow regime [Pardé, 1928] characterizes the Garonne due to the influence of oceanic, Mediterranean, and mountain climates. The Garonne river may be divided into upper, middle, and downstream segments. Pyrenean tributaries feed Upper Garonne; steep slopes and an unstable confined channel mark this region. The confluence with the Ariège river in Portet-sur-Garonne (5km before Toulouse) marks the transition from the upper to the middle Garonne. The middle section of the river (subject to this study, in the region of the city of Toulouse) is characterized by a widening valley and unstable channel increase.

Before the urban region of Toulouse, the input of particles into the Garonne river was mostly from geological origins. At the source of the Garonne river, the Pyrenees mountain chain is composed of a central axial zone (with primary terrain formed by granites, gneiss, and shale formations) and an internal metamorphic zone (granites, migmatites, and gneiss). Secondary Eocene coverage (limestones, marls, and shales) form the first Pyrenees foothills [Probst and Bazerbachi, 1986]. The molasse foreland basin is formed by tertiary terrain (soft rocks, generally carbonates) with Oligocene and Miocene ages.

5.3 Material & Methods

192 sediment samples were taken along the Garonne River from Muret to Grenade, passing through Toulouse. In addition, the Ariège River was sampled just before its junction with the Garonne river (5km from Toulouse). Two campaigns were done, the first in November 2018 and the second in May 2019. Thirty-two and 62 sites were sampled in 2018 and 2019, respectively. For each site, at least two samples were taken when possible. A first one, named A, was taken from the river within 2 meters of the edge (Figs. 5.4a, 5.4b,5.4c) and a second one was taken at the river bank. During the sampling seasons, the river had 0.35m (63 m^3s^{-1}) and 0.41m (220 m^3s^{-1}) of river height (`https://www.hydro.eaufrance.fr/stationhydro/O200008001/series`) in the years of 2018 and 2019 respectively.

Magnetic phase and susceptibility measurements were performed in a KLY-5 Kappabridge, with a sensitivity of $2x10^{-8}$SI for a magnetic field of 400 A/m on wet (2018 and 2019 campaign) and dry samples (2019 campaign). Wet measurements were performed on the day of collection. Frequency-dependant measurement is made possible by measuring the out-of-phase magnetic susceptibility at the same time as in-phase magnetic susceptibility measurement, enabling the calculation of their phase. The X_{on} parameters is calculated by $X_{on} = \frac{200}{\pi} tan\delta_{LF}$, where δ_{LF} is the phase angle measured at low frequency [Hrouda et al., 2013]. Samples were oven-dried at 35°C for five days. Samples were ground in an agate mortar in a fine and homogeneous powder for trace elements analysis, other magnetic measurements (hysteresis

Figure 5.2: Garonne river in Toulouse, from above. Three bridges are noticeable, Pont Saint Michel, Pont Neuf and Pont Saint Pierre, from the right to the left. Photo by the author.

Figure 5.3: Garonne river just before Toulouse, in Saubens (around 11km before Toulouse). Photo by the author.

Figure 5.4: Sampling on the Garonne river. On (a), close to the Pont de l'A621 sur la Garonne. On (b) close to Grenade. On (c), close to the Parc du Confluent. Photos by the author.

curves), and scanning electronic microscopy.

Eight sites (in a total of 15 samples) were selected to be subject to a magnetic extraction to analyze and image individual magnetic particles. The magnetic extraction consists of separating the magnetic phase from the sediments through attraction to a magnet and the decantation in a fluid. This was achieved by mixing 1 gram of the powdered sample with 20mL of Ethanol 99.9% in a small beaker. The mixture was stirred for about 20 seconds while a neodymium magnet was attached to the cup's outer wall. During the decantation of the sediments, the iron oxides were trapped by the magnetic field. After one minute, the separated iron oxides were retrieved with a plastic pipette. The contents of the pipette were placed in a small plastic tube with a magnet in the bottom so the magnetic minerals would decant faster than the remaining sediments in the mix. This process was repeated from 5 to 7 times until it was not possible anymore to notice the presence of magnetic minerals in the beaker. The contents in the tube were oven-dried for a day at 35°C.

Twenty-eight samples (14 sites) from the 2018 campaign were used in the geochemical analysis. Major and trace element data were obtained at the Service d'Analyse des Roches et Minéraux (SARM, CNRS, Nancy). Major element compositions were measured using an emission spectrometer ICP-OES (ICap 6500 Thermo Fischer) and trace elements by ICP-MS (Thermo Elemental X7) following the method detailed in Carignan et al. [2001]. Typical analytical precisions were ca. 2% for major elements and 5-8% for trace elements. The enrichment factor (EF) is a way of calculating the relative enrichment for a given element about the concentration of the crustal composition [Loubet et al., 2003], and it is given by $EF = (C_{i,tot})/(CAL_{tot})/(C_{i,cc})/(CAl_{cc})$ where $C_{i,tot}$,CAL_{tot},$C_{i,cc}$ and CAl_{cc} are, respectively, the concentrations of the element in question measured on the sample, the Al concentration measured on the sample, the element in question on the crustal composition and the Al concentration on the crust.

Images from scanning electron microscopy (SEM) from 8 sites (totalizing 15 samples) from the 2019 campaign. Backscatter (BSE) and secondary electron (SE) images were acquired with a Jeol JSM6360LV SEM, with an accelerating voltage of 20kV. Correlation coefficients were calculated on 28 samples using R and the packages corrplot and corrr. The method used was Pearson.

5.4 Results

5.4.1 Magnetic results

Samples from the 2018 campaign display magnetic susceptibility values between 3.38x10^{-8} and 4.19×10^{-8} m^3/kg for samples collected inside the river and on the margin the magnetic susceptibility of the samples ranges from 4.89×10^{-8} to 3.54×$10^{-8}$$m^3$/kg. In 2018 mean values (standard deviations in parenthesis) for magnetic susceptibility were 1.05(±0.72)×10^{-7} and 9.90(±5.14)×$10^{-8}$$m^3$/kg for samples A and B respectively. The following year, magnetic susceptibility values ranged from1.53×10^{-8} to 3.51×$10^{-6}$$m^3$/kg for sediments collected inside the river and 4.51×10^{-8} to 4.36×$10^{-6}$$m^3$/kg for the ones from the river margin (Fig. 5.5). In 2019 mean values for susceptibility were 3.14(±5.34)×10^{-7} and 3.07(±5.75)×$10^{-7}$$m^3$/kg for samples A and B respectively. In 2018, the magnetic susceptibility profile was stable from

Muret to Toulouse (Fig. 5.6, increasing to a peak of $4.19\times10^{-7}m^3/kg$ after entering the inner part of Toulouse and decreasing again to values close to the mean. The campaign of 2019 increases to a peak after Muret city center where the magnetic susceptibility reaches a value of $2.66\times10^{-7}m^3/kg$, decreasing to values close to the mean before Toulouse and then increasing again after Toulouse city center (Fig. 5.7), reaching a maximum value of $3.51\times10^{-6}m^3/kg$. After passing through Toulouse, magnetic susceptibility values again fall to values close to the mean. Samples collected in the river and on the Garonne margin have equivalent values in both years (Fig. 5.5).

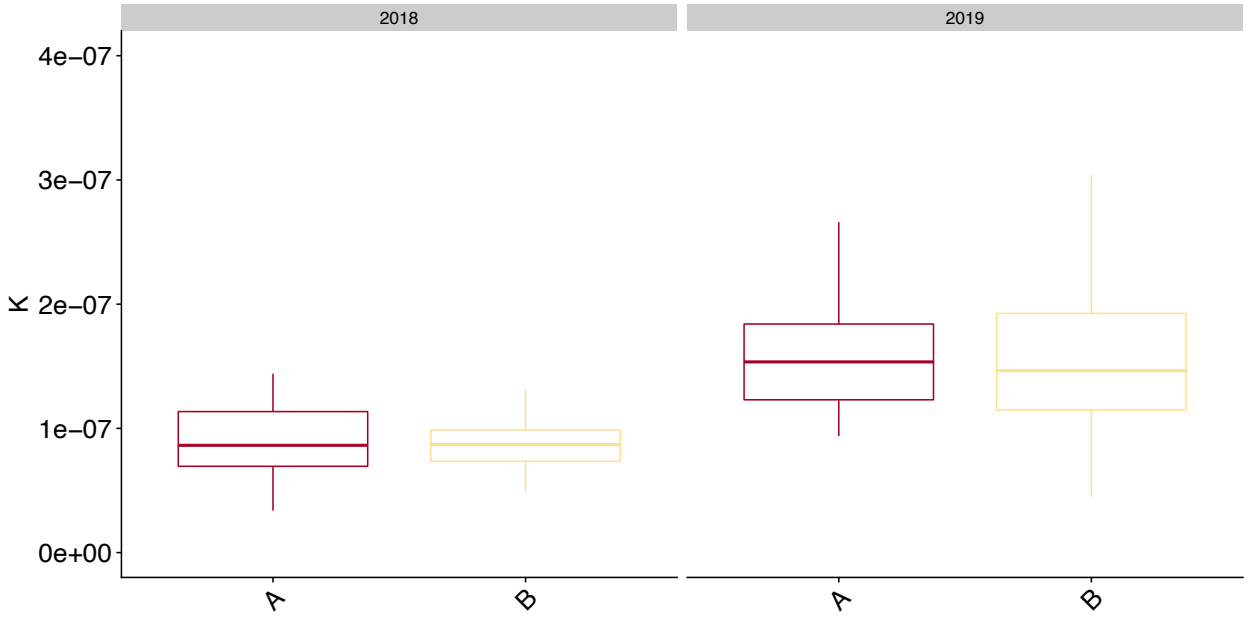

Figure 5.5: Boxplot for magnetic susceptibility values in both campaigns (2018 and 2019). A and B refers to samples collected in the river and in the river margin, respectively.

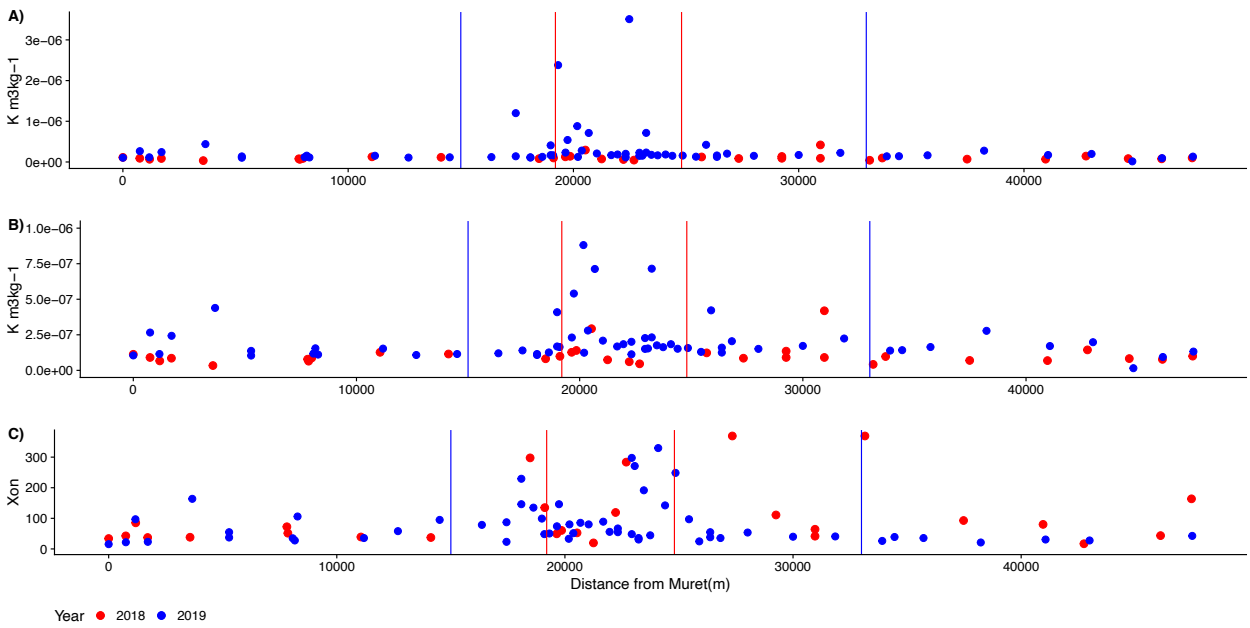

Figure 5.6: a) Magnetic susceptibility (K) profile (50km), from Muret to Grenade, passing through Toulouse. Toulouse is delimited by the vertical lines, with the city limits in blue (at distances of 15 and 33km of Muret) and red for inner Toulouse (delimited by the ring road, at distances of 19.2 and 24.8km from Muret). Red and blue dots represent the 2018 and 2019 campaign, respectively b) The same as Fig. 5.6a, excluding magnetic susceptibility values above 1×10^{-6}m^3/kg in order to increase the Y scale. c) Profile of the X_{on}.

The X_{on} calculated from the magnetic phase also has a similar behavior (Figure 5.6c), increasing when close to the city centers. For 2019 it has the highest peak at the point near the Pont de L'Embouchure (329.6) and the lowest one at the first point before Muret city center (15.6). In 2018 the X_{on} reached values of 369.1, near Grenade.

The Day plot (Fig. 5.8, Dunlop [2002]) shows the samples from both campaigns concentrated on the region of the PSD domain, just above the SD-MD mixing lines. There are two exceptions from both years closer to the SP-MD mixing lines. However, those samples are not in the exact location, with 2018 being collected near Muret city center and 2019 being collected in Toulouse city center.

5.4.2 Trace elements concentration

The Garonne River sediments display a mean concentration of significant elements SiO_2 and CaO of 69.52% and 4.04%, respectively. They are higher than the geochemical background concentration calculated for French rivers sediments by Salpeteur and Angle [2010] of 64.20% and 0.92% for SiO_2 and CaO, respectively. Before Toulouse, heavy metals (HMs) concentrations (standard deviation in parenthesis) are 0.26(±0.08), 7.06(±1.99), 21.8(±7.80), 20.27(±3.89), 41.05(±26.24) and 79.69(±34.37)ppm for respectively Cd, Co, Cu, Ni, Pb, and Zn. In Toulouse, mean HM's concentration (standard deviation in parenthesis) are 0.36(±0.13), 8.58(±2.38), 44.75(±31.47), 25.31(±6.27), 49.65(±22.52) and 135.13(±60.94)ppm

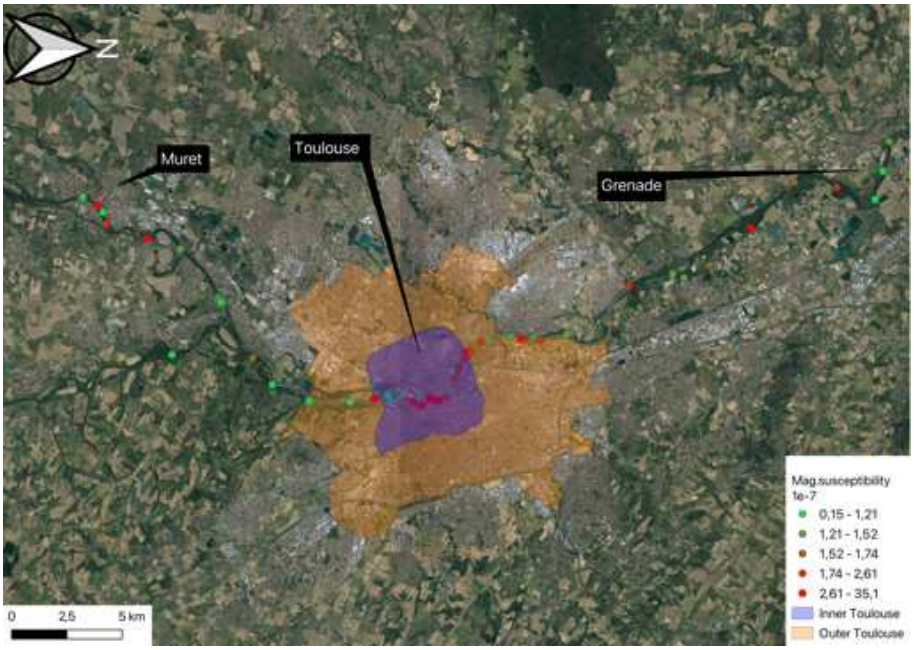

Figure 5.7: Map of the Toulouse urban area with the Garonne River from Muret to Grenade, passing through Toulouse in the 2019 campaign. Susceptibility values marked by the dots, and the Toulouse city by the colored area (orange for the outer city, purple for the inner city).

for the same elements. After Toulouse, mean HM's concentration (standard deviation in parenthesis) are 0.26(±0.10), 6.42(±2.22), 19.60(±8.01), 19.36(±5.97), 78.41(±130.57) and 84.37(±24.23) for the same elements. They increase just after Toulouse city center (15km from Muret), similarly to the magnetic susceptibility (Fig. 5.9), decreasing after passing through Toulouse (33km after Muret). Mean concentrations estimated for French rivers sediments [Salpeteur and Angle, 2010] are represented in Fig. 5.9. Before and after the urban area of Toulouse, HMs concentrations are mostly lower or equal to this geochemical background. Conversely, in Toulouse, half to most of the sampled sediments display values above the mean values characterizing French rivers sediments (Fig. 5.9).

Figure 5.10 illustrates the enrichment factor values calculated in the selected elements. An enrichment regarding the crustal composition for Cd, Pb, and Zn is marked by values above 3.2, 4.3, and 2.6, respectively, in the entire profile. Ni and Co show depletion compared to the crustal composition. The enrichment factor for Cu reaches 1.2 in the Toulouse area.

Linear correlations calculated with the Pearson method between HM's (in a total of 28 samples) and magnetic susceptibility is shown in Figs. 5.11 and 5.12. Magnetic susceptibility has a weak correlation with Cu at R=0.35. Cd, Co, Ni, and Zn are correlated, with Rs above 0.68. The correlation mapping displays a cluster with Cd, Co, Ni, and Zn, and independent Pb, Cu, and magnetic susceptibility.

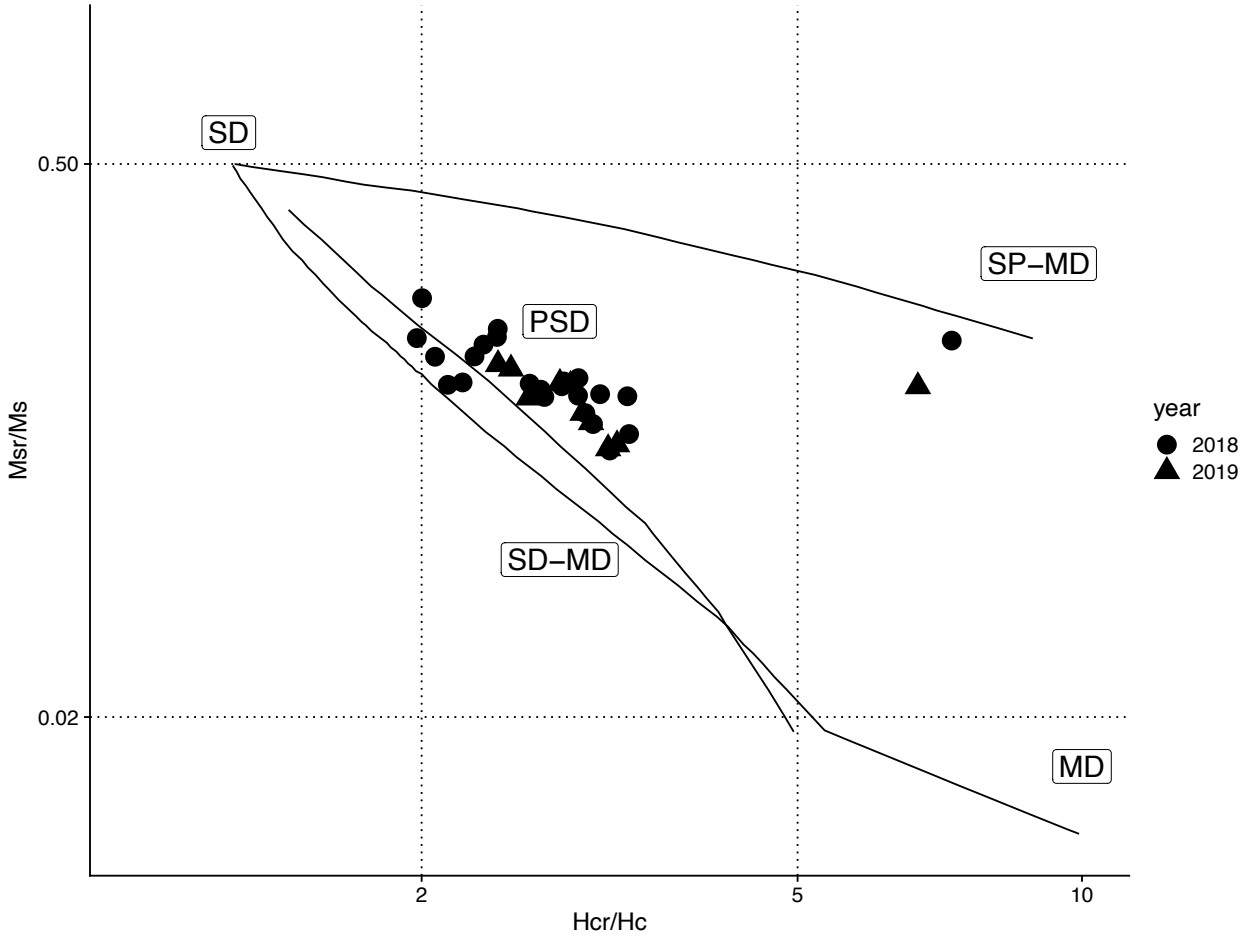

Figure 5.8: Day plot for the sediments collected along the Garonne river. Circles for 2018 campaign and triangles for 2019 campaign. Mixing lines after Dunlop [2002].

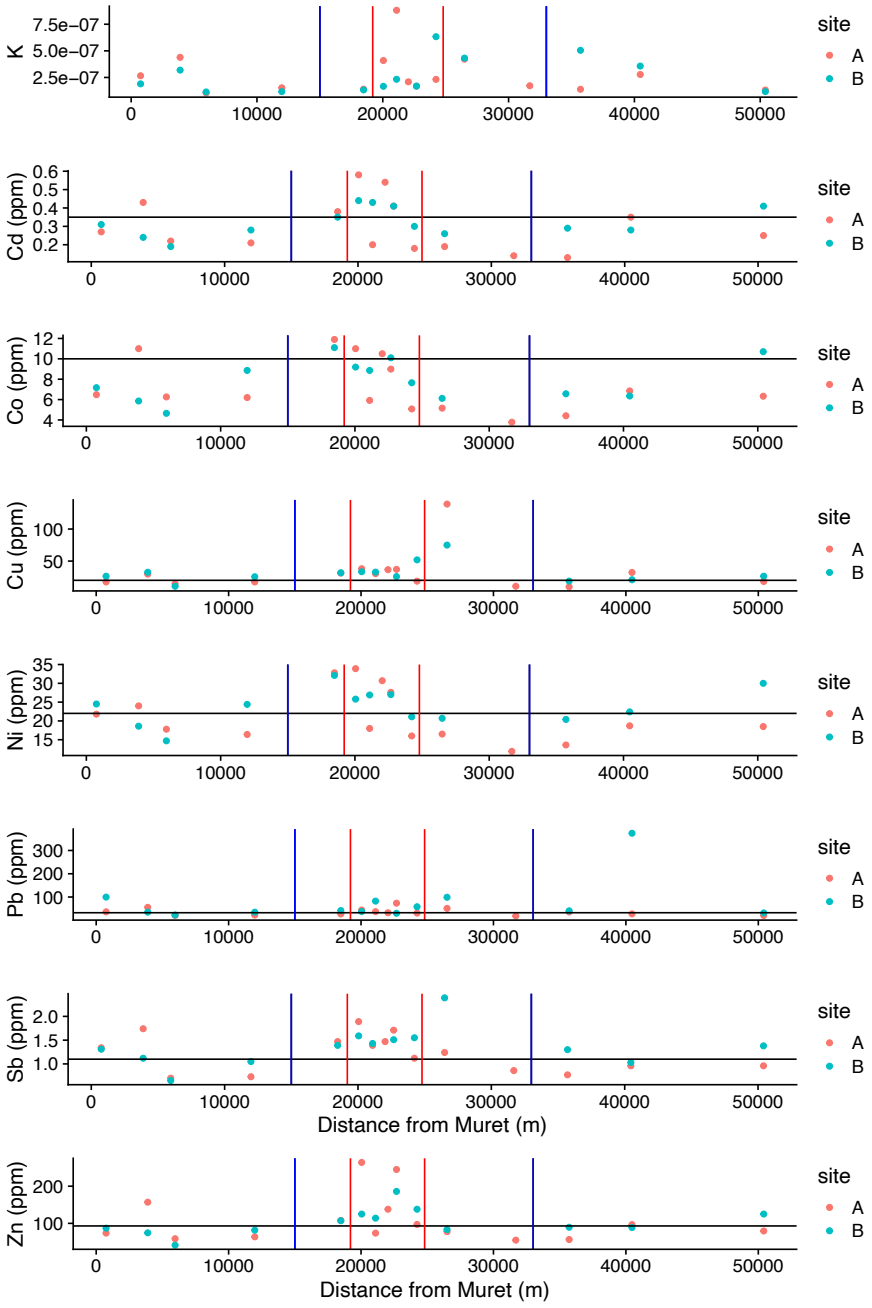

Figure 5.9: Heavy metals concentration and magnetic susceptibility along the 50km profile from Muret to Grenade, for the year of 2019. Toulouse limits marked on the X axis at 15km and 33km from Muret in blue, and in red the Toulouse inner city marked in red, at 19.2 and 24.8km form Muret. The horizontal black line is the baseline for the respective concentrations as measured by [Salpeteur and Angle, 2010].

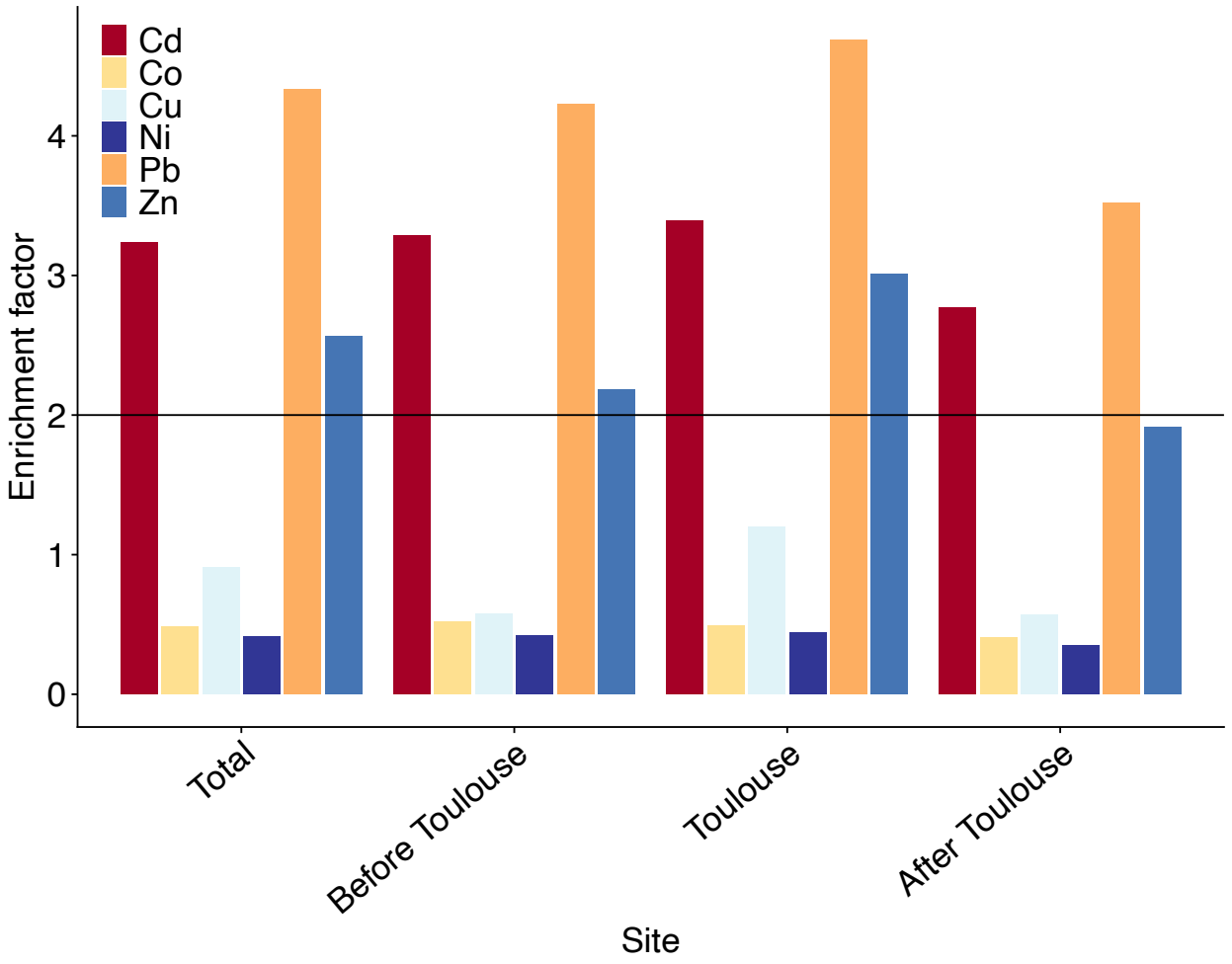

Figure 5.10: Bar plot of the calculated enrichment factors (following Loubet et al. [2003]) for the selected elements. Before Toulouse is defined for samples collected just until 15km of distance from Muret along the river profile, Toulouse for samples collected in distances between 15 and 33km and after Toulouse for samples collected with distances after 33km. Vertical line at EF=2 to highlight anthropogenic input.

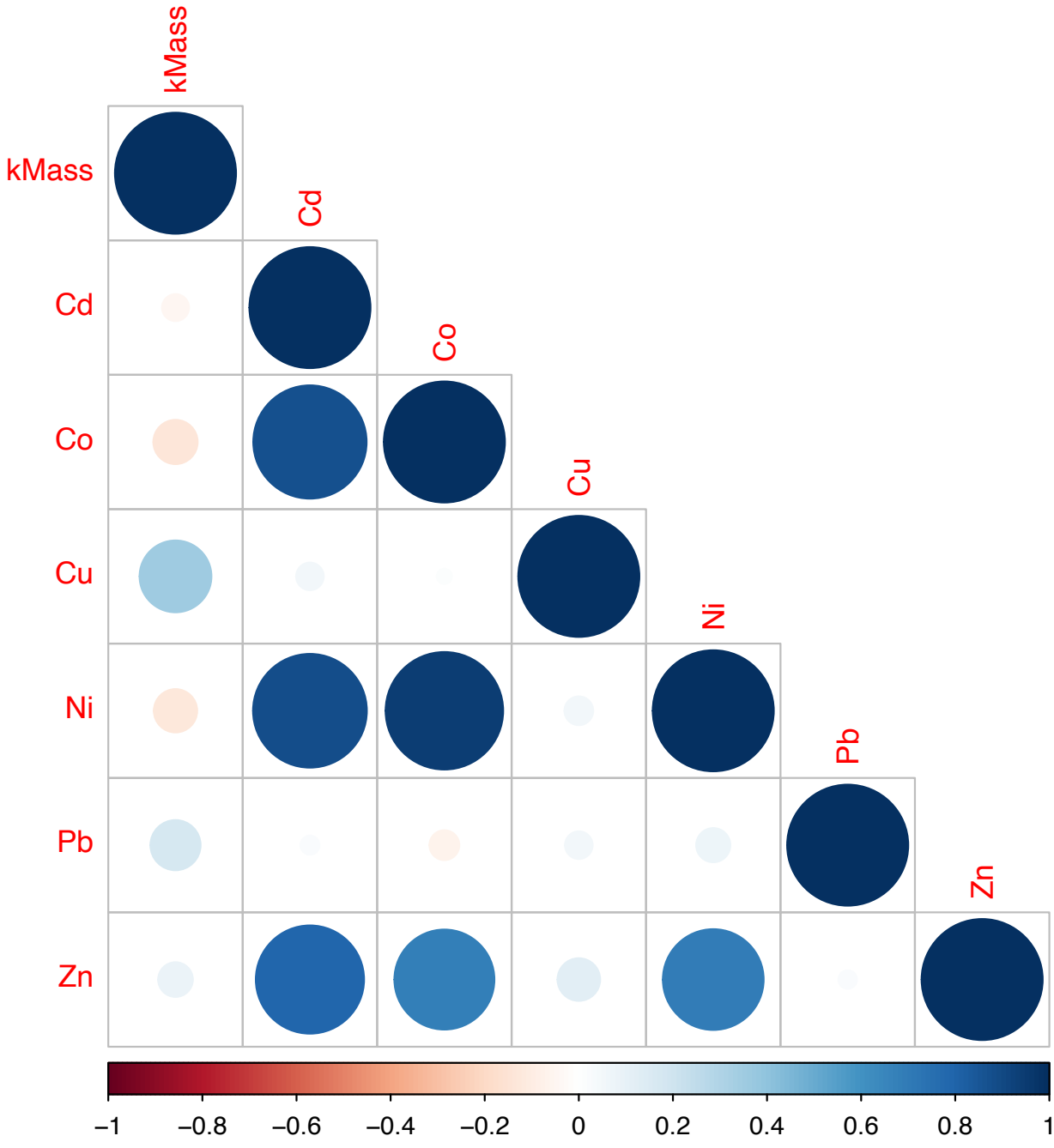

Figure 5.11: Correlation matrix between chosen HMs composition and magnetic susceptibility in 28 samples.

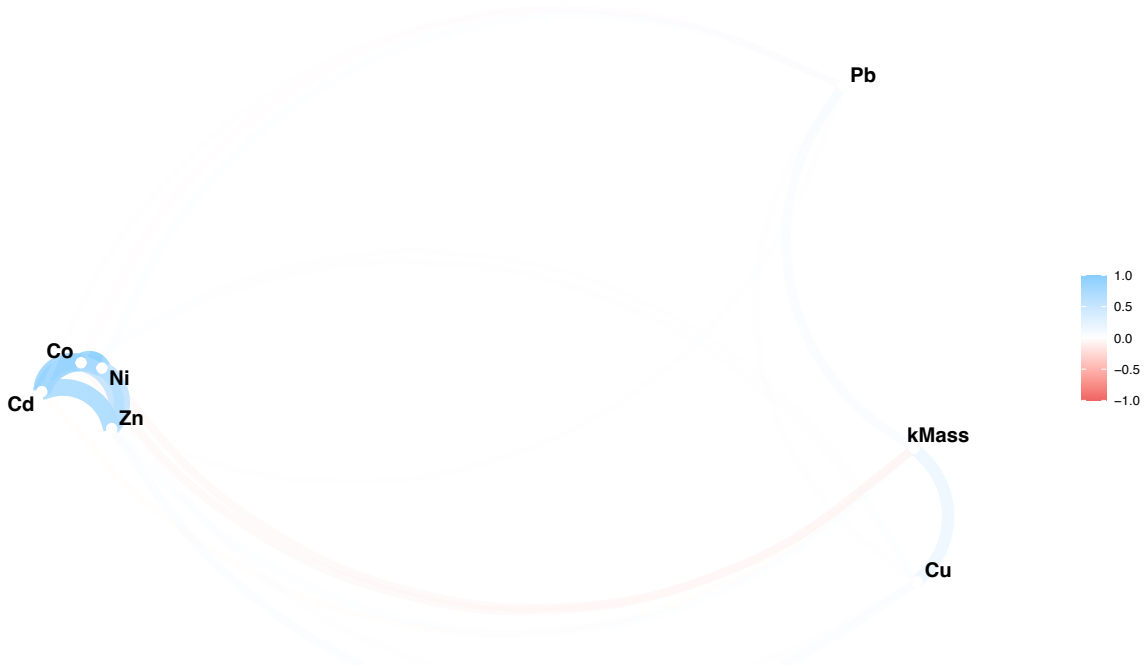

Figure 5.12: Correlation mapping between some HMs concentration and magnetic susceptibility in 28 samples.

5.4.3 SEM investigation

The SEM microscopy revealed superficial features of the iron oxides. We found iron oxide spherules (Figs. 5.14,5.15,5.16) with micrometric size, varying from 10 to 91μm. This particular shape points to emission from combustion [Leite et al., 2021, Shi et al., 2015]. Other shapes of iron oxides were also found, such as the oblique shape found in figure 5.13. This particular shape of magnetite points to detritic input on the sediments.

5.5 Discussion

Enrichment factors above 2 for Cd, Pb, and Zn in Garonne rivers sediments in the 50 km long profile centered on Toulouse highlight an anthropic influence on sediments. These results are in accordance with the values obtained for French rivers sediments obtained by [Salpeteur and Angle, 2010]. Viers et al. [2009] compiled a database for suspended particulate matter in rivers. Transitional metals were enriched in European rivers compared to crustal composition, especially Pb, Cu, and Cr. Such enrichments are probably due to the release of HM in the environment from anthropic activities since the beginning of industrialization. All HMs concentration and magnetic susceptibility increase in the Toulouse area (Fig. 5.9) compared to the areas before and after the urban zone. This highlights the influence of surface water runoff into the river in the densely populated area.

Anthropic sources of these HMs could be road traffic [Sternbeck et al., 2002, Johansson et al., 2009], either non-exhaust particles such as brakes and brake lines erosion [Thorpe and

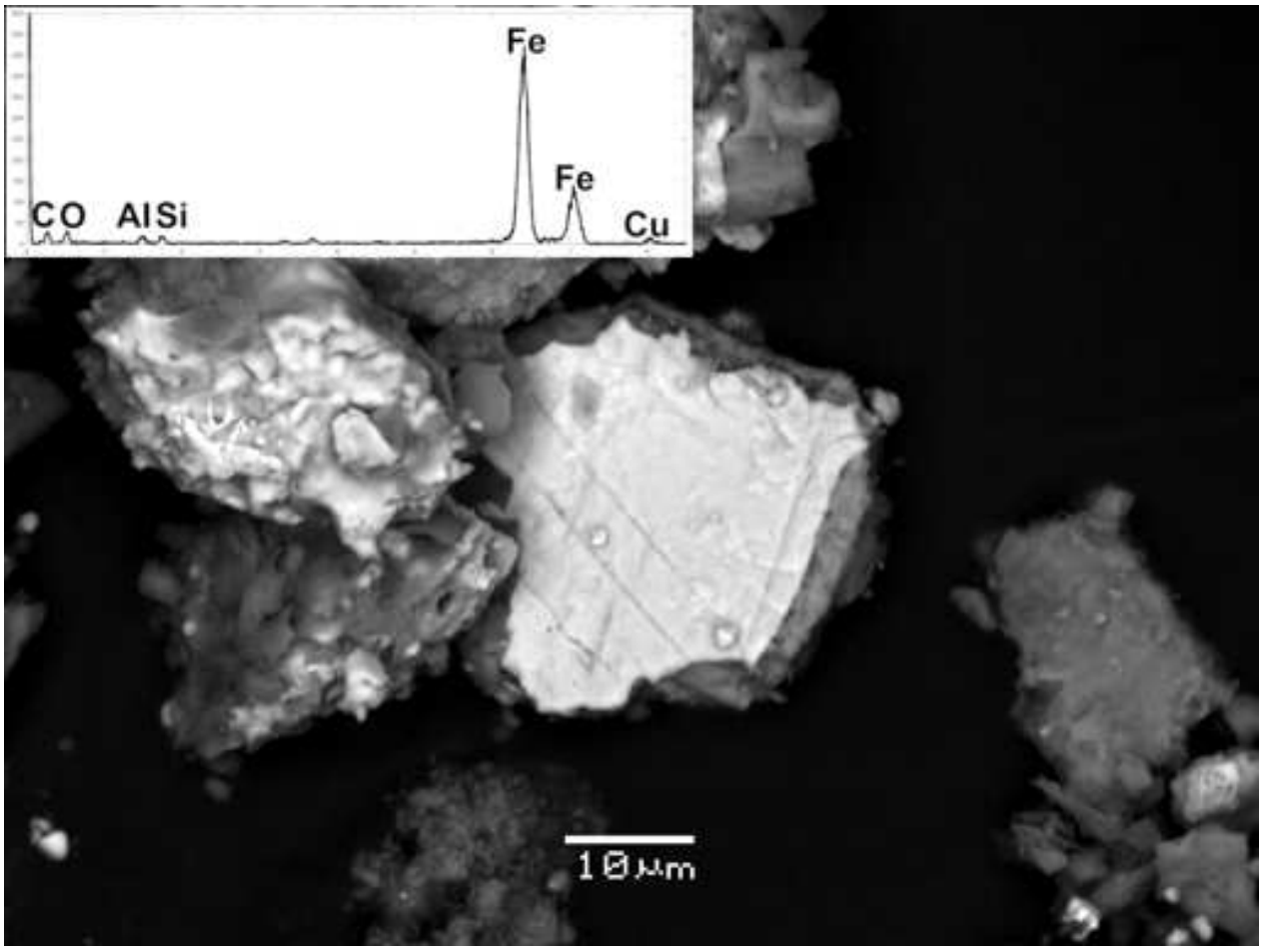

Figure 5.13: Iron oxide with irregular, oblong shape with width of 34μm. Besides iron and oxygen that relates to the iron oxide, the EDS shows the presence of aluminum, silicon and copper that could result from the silicates in the sample. This sample is located after Muret, near the Saubens ville.

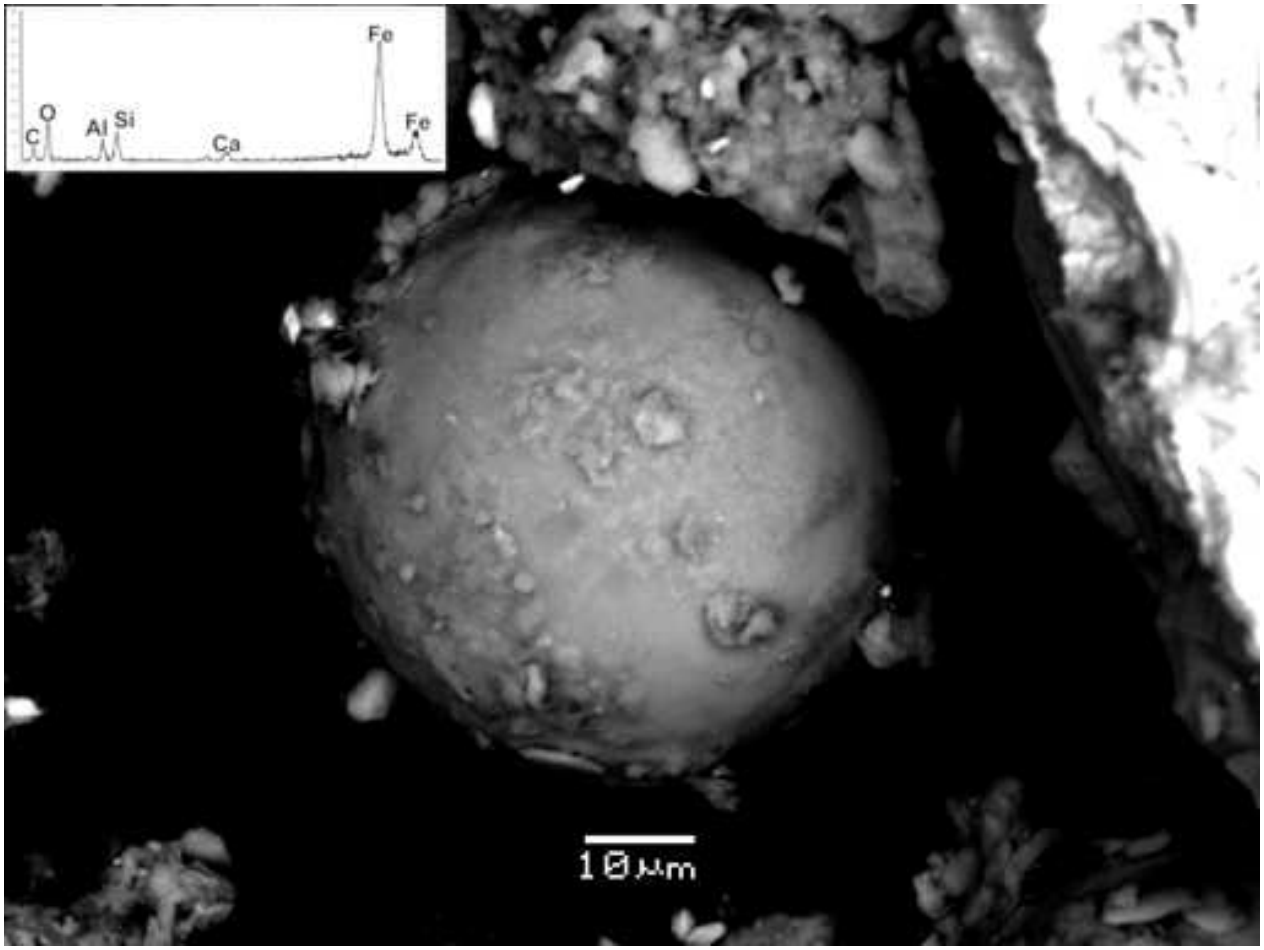

Figure 5.14: Iron oxide spherule with 53μm of diameter. Besides iron and oxygen that relates to the iron oxide, the EDS shows the presence of aluminum, silicon and calcium that could result from the silicates in the sample. This sample is located at the Empalot Island.

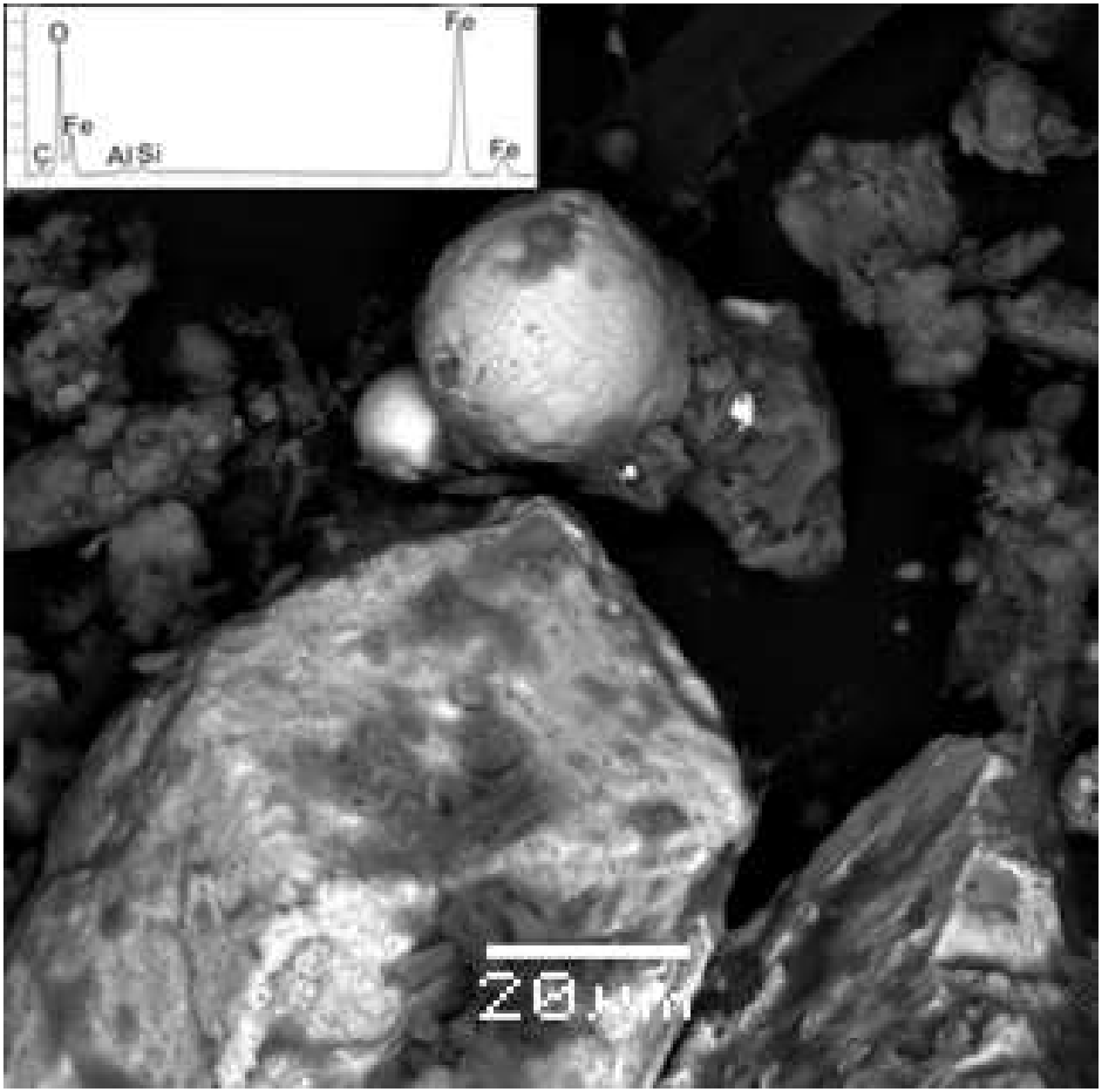

Figure 5.15: Iron oxide spherule with diameters of 29 and 10μm. Besides iron and oxygen that relates to the iron oxide, the EDS shows the presence of aluminum and silicon that could result from the silicates in the sample. This sample is located at the Port Viguerie, on Toulouse downtown.

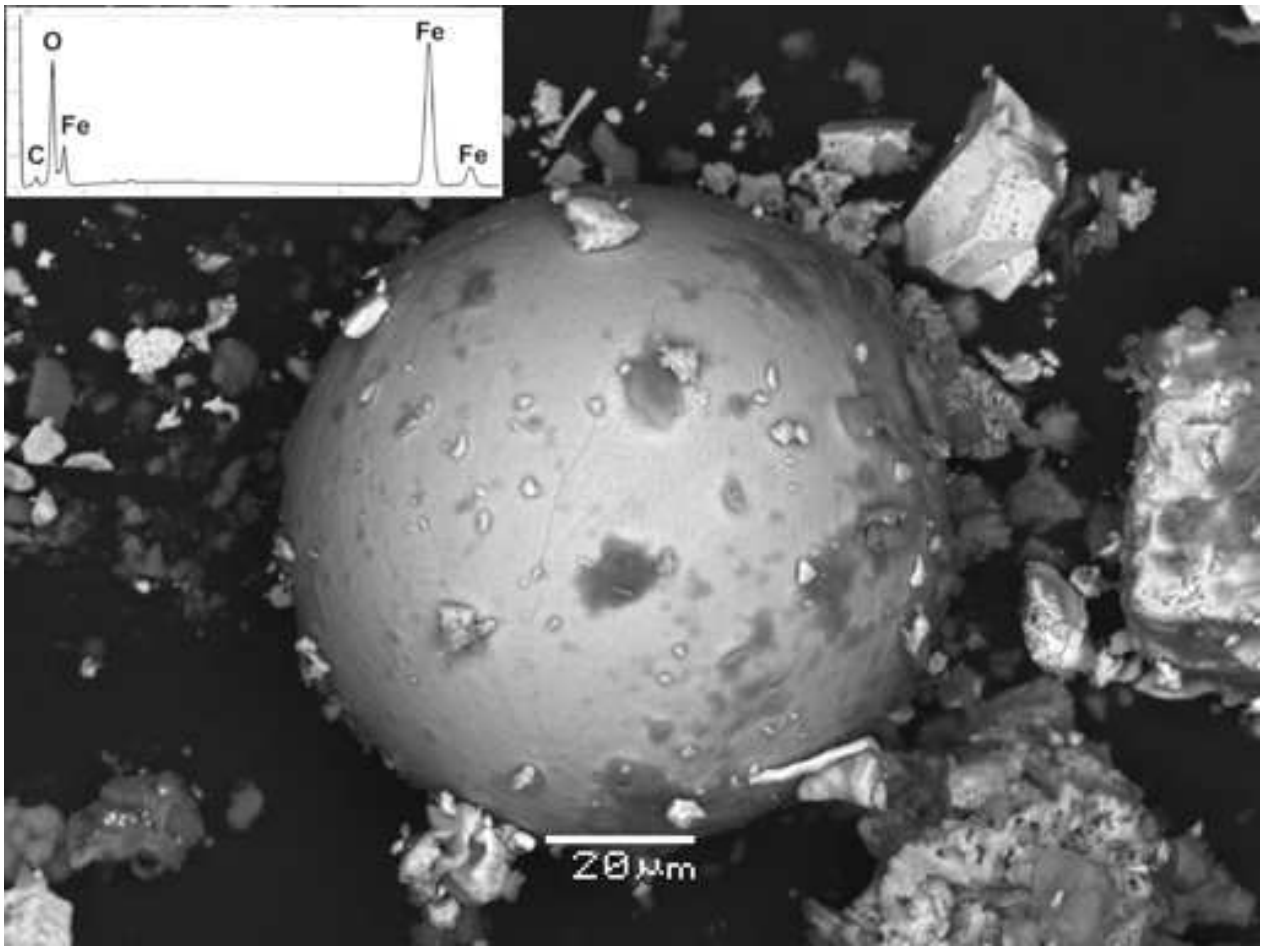

Figure 5.16: Iron oxide spherule with 91μm diameter. Besides iron and oxygen that relates to the iron oxide. This sample is located just before Grenade.

Harrison, 2008] or petrol and diesel fuels [Pulles et al., 2012]. They are commonly found in urban and suburban waterways [Sebastiao et al., 2017]. Zinc, while common in natural rocks, could also be emitted by erosion of brakes, tires, and road surfaces and is present in oil [Sebastiao et al., 2017] making it an efficient tracer of traffic-related particles in waterways [Desaulty and Petelet-Giraud, 2020].

Lead and copper is also commonly found in river sediments and urban dust [Kelepertzis et al., 2019] and is derived from traffic emissions. But other urban sources could release Pb and Cu in surface waters. Pb also comes from portions of Pb piping that remain in the drinking water distribution system of the city of Toulouse. Cu can also come from the leaching of roofs and other urban copper surfaces.

The iron oxides in the sediments of the Garonne come from the erosion of soils and rocks and from anthropic contributions. The primary anthropic source is traffic emissions, as evidenced by the influx of iron oxides into the river marked by an increase in magnetic susceptibility in Toulouse downtown (Figs. 5.6,5.7) and by the characteristic presence of iron spherules from vehicle exhausts [Leite et al., 2021, Chaparro et al., 2020, Shi et al., 2015]. Similarly, higher concentrations of magnetic minerals have been linked to anthropogenic input in urban centers [Franke et al., 2009]. Magnetic susceptibilities measured in the Ponnaiyar river [Chaparro et al., 2013b] have similar values to the ones we measured in Toulouse, ranging from 6.8 to 265x$10^{-8}$$m^3$/kg. In that work, Chaparro et al. [2013b] links the magnetic enhancement on the sediments to anthropogenic input in the river system.

The size of the magnetic grains, as described by hysteresis measurements in the SD-PSD domain, is consistent along the entire 50 km extended profile. Conversely, frequency-dependent magnetic susceptibility parameters (X_{ON}) increases in the Toulouse urban area depicting an increase in superparamagnetic grains [Hrouda et al., 2013]. This could indicate the presence of ultrafine particles or micrometric particles with oxidized surfaces [Sagnotti and Winkler, 2012]. In the 4.4 chapter of this thesis, I give examples of nanoscale iron oxide spherules emitted by traffic that could induce such a superparamagnetic signature. While micrometric grain sizes (10-91μm) were observed through SEM microscopy, finer grains are probably present since their observations demand specific protocol.

A clear input of particles and HMs from urban activities, particularly road traffic, is detected in the sediments of rivers in the metropolitan area of Toulouse. However, the ensemble of HMs (Cd, Co, Ni, Zn) and the magnetic susceptibility are not correlated, although they both originate from road traffic activity. This indicates that they have different paths to urban waterways and the river.

Easy-to-implement magnetic methods, such as magnetic susceptibility and frequency-dependent magnetic susceptibility, represent a promising method for rapid screening and monitoring of urban waterways management. They could allow the tracking in detail by enabling the fast measurements of numerous samples. The heterogeneity of iron oxides and Hms levels underscores the need for detailed monitoring in urban areas to understand the various pathways of contaminants emitted into the city. Indeed, Understanding and controlling the impact of urban runoff is a global concern [Zhu et al., 2022]. Magnetic methods could therefore help assess the effects of water retention, bioretention, grass roofs, permeable pavements, or other forms of urban runoff management, especially in developing sponge cities [Qi et al., 2020].

HMs are rapidly and mostly accumulated in sediments and deposited in river beds impact-

ing aquatic life and water quality [Jaskuła and Sojka, 2022]. This way, sediments represent the main pathways of HM transport to the ocean [Liu et al., 2019b].

5.6 Conclusion

To better understand the fate of particles linked to traffic emissions, two campaigns were carried out along the Garonne river in Toulouse. The investigation was based on magnetic analysis (magnetic susceptibility, hysteresis cycles), trace elements composition, and SEM investigation. Both magnetic susceptibility and trace metals concentration peaks in Toulouse city center show the influence of anthropogenic emissions into the river. The spherical shape of the iron oxides recorded by SEM microscopy indicates internal engine combustion as the source of the iron oxides. The trace metal concentration is not exceptionally high, but it increases near the urban center. Enrichment factors above unity in trace metals linked to traffic emissions also indicate this source as the origins of the particles analyzed in the river sediments.

Chapter 6

Conclusion & perspectives

6.1 English version

The research work presented in this thesis aimed to improve our understanding of the impact on air quality of urban environments from anthropogenic emissions, especially the ultrafine fraction of PM. The primary motivation behind this thesis was the need to understand better how urban emissions of ultrafine PM spread across different urban environments. The ultrafine fraction of PM is notably dangerous for human health due to its penetrations capability in the human body and harmful content. Magnetic methods are suitable for this investigation as they relate to other pollutants (PM, for instance) and can identify and quantify the ultrafine (nanoscale) fraction of iron oxides. Bio-sensors, traditionally used in environmental research, is a good fit for magnetic methods applied to PM investigation. They are cost-effective, have a low environmental impact, and are suitable for innovative experimental designs, particularly those involving the population's direct participation. In this thesis, we show that citizen science participation paired with bio-sensors is a good strategy for air quality investigations by increasing the coverage of sampling (including indoor sampling) and stimulating social awareness about air pollution.

Traffic emissions and local practices (such as biomass burning) typically worsen the air quality in West Africa. Using PM2.5 filters, we characterized the PM magnetic properties due to different emission sources in the region. The other emission sources (biomass burning, diesel-powered vehicles traffic emissions, gasoline-powered vehicles traffic emissions, and waste burning) showed the same narrow granulometry, below 0.1μm. Weather characteristics influenced the local air quality. For instance, wetter conditions improved air quality due to less resuspension and the extended carrying of pollutants. SEM investigation showed the presence of ultrafine magnetic particles (of nanometric size), round in shape (spherules), and emitted among soot chain particles, evincing their origin in anthropogenic combustion (especially internal engine combustion). The range of magnetic parameters identified for all emission sources on the PM2.5 filters enables their use for comparisons in the following studies of this thesis.

Children are among the most susceptible populations to the dangers posed by air pollution due to their immature respiratory and neurological systems and higher absorption of pollutants compared to adults. Understanding how traffic emissions (as the primary source in the city of Toulouse) spread to the school environment is key in interpreting the health

dangers posed to children since they spend most of their time in the school environment. Also, it is vital to understand the nuances between indoor and outdoor environments, as they may differ in pollutant concentration and sources. Different air quality investigation techniques used together provided complementary information regarding assessing air quality in the school context of Toulouse city. First, the PM1 captured in the schools has mostly a traffic origin, specifically from the internal combustion of vehicles. Outdoor environments have a higher concentration than indoor pollutants (PM1, EC) linked to traffic emissions. Indoors, OC has essential sources, such as biogenic production, scholar activities (such as crafts), and emissions due to furniture/ fiber clothes, among others. The emissions of indoor OC highlight the importance of proper classroom ventilation. The magnetic investigation of bio-sensors, tree bark, and PM1 filters collected in the schools confirmed that the significant outdoor source for the magnetic PM fraction is linked to traffic emissions. This is verified by the higher concentrations outdoors of airborne iron oxides with a dominant low coercive fraction (magnetite-like) and the presence of spherules among soot carbon particles as observed in the SEM. The schools have relatively higher concentrations of PM compared to other parts of the city because they are close to major traffic roads. The participation of teachers and children highlighted the perception of air quality and the difficulties regarding proper air ventilation inside the school. Also, besides the seminars given to the children, they could see some of the sampling work and deployment, raising their interest in the scientific method.

The domestic environment in the city of Toulouse is subject to different sources of air pollution-related, both indoor and outdoor. Outdoor sources are mainly traffic-related. Indoor sources are specific for each individual in the domestic context. For instance, indoor sources can be due to heating, cooking, cleaning, and burning (smoking, incense, candles, etc.). Our data on the magnetic fraction of particulate matter in Toulouse shows that traffic emissions are a more important source in the outdoor environment than indoors. Higher concentrations of airborne iron oxides outdoors, with dominant low to moderate coercivity, typically point to traffic emission as the primary source. When comparing indoors and outdoors, outdoor environments have higher concentrations of coarser particles, whereas indoor environments have finer granulometry. The population participation in this study was vital for its development, allowing for a large geographical distribution of bio-sensors in the city of Toulouse. Moreover, the recruiting and the follow-up contact with the volunteers to present the results resulted in increased social awareness about air quality and coping strategies for this issue.

Magnetic methods are efficient and sensitive enough to investigate iron oxides' ultrafine fraction (<100nm). This fraction is essential in air quality studies since it is the most dangerous to human health. It penetrates deeper into the human body and is often associated with more harmful constituents. To better characterize this fraction, which is typically in the superparamagnetic (SP) grain size of the iron oxides, I applied the SPCDM method, developed during my master's studies and published in Leite et al. [2018] to a part of the samples collected on the courtyard tree bark and bio-sensors. These results showed that: (1) the concentration of ultrafine ("fast-decay" type) airborne iron oxides are homogeneous in the domestic environments (outdoor and indoor) and the courtyard school environments ; (2) the mean size of ultrafine SP particles estimated from samples from Toulouse city, including the two studied schools, is around 8 nm, close to that of ultrafine iron oxides of traffic origin

previously reported for São Paulo city, Brazil. Other works also reported this grain size in particles with traffic emissions origin [Ronkko et al., 2014, Li et al., 2018].

A study of sediments collected in the Garonne river that cut across the city of Toulouse from South to North was devised to investigate the fate of traffic emissions in the city. Using measurements of magnetic susceptibility, hysteresis cycles, trace elemental composition, and SEM investigation along a profile starting before and after the more densely populated areas of the city, we demonstrated the apparent influence of anthropogenic emissions on the sediment's composition. Typically, higher magnetic susceptibilities along with higher concentrations of metals (Pb, Cu) and iron oxide spherules detected in the sediments are observed in the densely populated central part of the city. These are directly related to traffic emissions, demonstrating the leaching of urban emissions into the river.

6.1.1 Future and perspectives

From the methodological point of view, this thesis has demonstrated the potential of using magnetic techniques for air pollution monitoring, using standard air filter samples or bio-sensors. In addition to the classical techniques usually applied in environmental magnetism, we also explored an alternative method to characterize the finer parts of the magnetic carriers (SPCDM). This is of particular interest in the case of PM characterization since this ultrafine nanosized fraction is the most dangerous for human health. The SPCDM method [Leite et al., 2018] can provide the concentration of ultrafine superparamagnetic (SP) fraction (fast magnetization relaxation) of magnetic carriers, besides providing their relative magnetization contribution to the total magnetization and an estimation of their mean diameter. To improve this methodology, performing more controlled tests with controlled samples is essential, where grain fractions with known grain sizes below and close to the SP-SSD limit are mixed. Using more than a one-time decay window in data acquisition may provide additional information about the different size fractions. Moreover, equipment with temperature control may allow for other strategies in the inversion procedure, enabling to shift blocking volumes for the magnetic carriers and increasing the size fractions that can be investigated through this method.

Air quality investigation enormously benefits from the use of magnetic methods. By analyzing the magnetic fraction contained within the PM, we can access information that otherwise would be untaped, such as the grain size distribution of the ultrafine fraction. Magnetic methods paired with bio-sensors also provide exciting and innovative experimental designs, for instance investigating indoor and outdoor environments in the same place. One aspect that could be improved is calibrating the magnetic measurements with traditional air quality measurements (PM, trace elements, and other pollutants concentrations). The goal would be to create magnetic guidelines regarding air quality, in the same way for PM, for instance. Having these guidelines with a strict magnetic protocol may also allow us to compare air quality investigations in different locations. The thesis also highlighted the potential of bio-sensors, which are extensively used in environmental magnetic investigations, and this use will likely increase in the future. Bio-sensors have several advantages over other environmental samples. They have negligible cost and low environmental impact. They are easily incorporated into citizen science strategies, particularly indoor sampling, since they are much less invasive than deploying unknown scientific paraphernalia in domestic and public

environments.

Finally, citizen participation in scientific air quality investigations is also very promising. Through citizen participation, the impact and importance of scientific inquiry are made more significant to the general public. It also serves to improve scientific literacy and trust among the population. Scientific topics such as air quality could be essential in bridging the gap between academic institutions and the general population. Moreover, citizen science may also tackle and help to deal with the eco-anxiety, converting this disagreeable feeling into positive actions and coping strategies to deal with the enormous environmental challenges of our time. We can't forget our role in creating these environmental problems in the first place. There are no simple solutions to complex issues, and we must face them together. I believe this to be the only way forward.

6.2 Version française

Le travail de recherche présenté dans cette thèse visait à améliorer notre compréhension de l'impact des émissions anthropogéniques, en particulier de la fraction ultrafine des PM, sur la qualité de l'air des environnements urbains. La motivation principale de cette thèse était le besoin de mieux comprendre comment les émissions urbaines de PM ultrafines se répandent dans les différents environnements urbains. La fraction ultrafine des PM est notamment dangereuse pour la santé humaine, en raison de sa capacité de pénétration dans le corps humain et de son contenu toxique. Les méthodes magnétiques sont un outil approprié pour ce type d'investigation, car elles sont liées à la concentration d'autres polluants (les PM par exemple), et sont capables d'identifier et de quantifier la fraction ultrafine (nanométrique) des oxydes de fer. Les bio-capteurs, traditionnellement utilisés dans la recherche environnementale, conviennent bien aux méthodes magnétiques appliquées à l'étude des particules. Ils sont peu coûteux et ont un faible impact sur l'environnement. Ils se prêtent à des conceptions expérimentales innovantes, en particulier celles qui impliquent la participation directe de la population. Dans cette thèse, nous montrons que la participation de la science citoyenne associée à l'utilisation de bio-capteurs est une bonne stratégie pour les enquêtes sur la qualité de l'air, en augmentant la couverture de l'échantillonnage (y compris l'échantillonnage à l'intérieur) et en stimulant la prise de conscience sociale sur la pollution de l'air.

Les émissions du trafic et les pratiques locales (telles que la combustion de la biomasse) aggravent généralement la qualité de l'air en Afrique de l'Ouest. En utilisant des filtres PM2.5, nous avons caractérisé les propriétés magnétiques des PM dues à différentes sources d'émission dans la région. Les différentes sources d'émission (combustion de la biomasse, émissions du trafic des véhicules à moteur diesel, émissions du trafic des véhicules à essence et combustion des déchets) ont montré la même granulométrie étroite, inférieure à 0.1μm. Les caractéristiques météorologiques ont influencé la qualité de l'air locale. Par exemple, des conditions plus humides ont amélioré la qualité de l'air en raison d'une moindre remise en suspension et d'un transport plus long des polluants. L'étude de microscopie (MEB) a permis de montrer la présence de particules magnétiques ultrafines (de taille nanométrique), de forme ronde (sphérules) associées aux particules dede suie, ce qui témoigne de leur origine dans la combustion anthropique (en particulier la combustion des moteurs internes). La gamme de paramètres magnétiques identifiés pour toutes les sources d'émission sur les filtres PM2.5 permettent leur utilisation pour des comparaisons dans les études suivantes de cette thèse.

Les enfants sont l'une des populations les plus sensibles aux dangers posés par la pollution atmosphérique, en raison de l'immaturité de leurs systèmes respiratoire et neurologique et de leur absorption plus élevée de polluants par rapport aux adultes. Comprendre comment les émissions liées au trafic routier (principale source dans la ville de Toulouse) se propagent dans l'environnement scolaire est essentiel dans l'interprétation des dangers pour la santé des enfants, puisqu'ils passent une grande partiede leur temps dans l'environnement scolaire. Différentes techniques d'investigation de la qualité de l'air utilisées conjointement ont fourni des informations complémentaires concernant l'évaluation de la qualité de l'air dans ldeux écoles primaires de la ville de Toulouse. Tout d'abord, les PM1 capturées dans les écoles ont principalement pour origine le trafic routier, en particulier la combustion interne des véhicules. Les environnements extérieurs présentent une concentration plus élevée que les

environnements intérieurs de polluants (PM1, EC) liés aux émissions du trafic. A l'intérieur, le CO a des sources importantes, telles que la production biogénique, les activités scolaires (comme l'artisanat), les émissions dues aux meubles/ vêtements en fibre, entre autres. Les émissions de CO à l'intérieur des bâtiments soulignent l'importance d'une bonne ventilation dans les salles de classe. L'étude magnétique des bio-capteurs, des écorces d'arbres et des filtres PM1 collectés dans les écoles a confirmé que la principale source extérieure de la fraction magnétique des PM est liée aux émissions du trafic. Ceci est vérifié par les concentrations plus élevées à l'extérieur d'oxydes de fer en suspension dans l'air avec une fraction dominante coercitive faible à modéré (semblable à la magnétite) et la présence de sphérules, parmi les particules de carbone de la suie comme observé en microscopie MEB. A l'extérieur, les écoles présentent des concentrations relativement plus élevées de particules par rapport à d'autres parties de la ville, probablement parce qu'elles sont proches des grands axes de circulation. La participation des enseignants et des enfants a mis en évidence la perception de la qualité de l'air et les difficultés liées à une bonne ventilation de l'air à l'intérieur de l'école. En plus des ateliers proposés aux enfants, ceux-ci ont pu voir une partie du travail d'échantillonnage et de déploiement, ce qui a renforcé leur intérêt pour la méthode scientifique en général.

L'environnement des habitations de la ville de Toulouse est soumis à différentes sources de pollution atmosphérique liées à des sources intérieures et extérieures. Les sources extérieures sont principalement liées au trafic routier. Les sources intérieures sont spécifiques à chaque individu dans le contexte domestique. Par exemple, les sources intérieures peuvent être dues, entre autres,au chauffage, à la cuisson, au nettoyage, à la combustion (tabac, encens, bougies, etc.). Nos données sur la fraction magnétique des matière particulaire à Toulouse montre que les émissions du trafic routier sont une source plus importante dans l'environnement extérieur que dans l'environnement intérieur. Les concentrations plus élevées d'oxydes de fer en suspension dans l'air à l'extérieur, avec une faible coercivité dominante, indiquent généralement que les émissions du trafic sont la principale source.Quand on compare les intérieurs et les extérieurs, les environnements extérieurs présentent des concentrations plus élevées de particules plus grossières, tandis que les environnements intérieurs présentent une granulométrie plus fine de minéraux magnétiques. La participation de la population à cette étude a été essentielle pour son développement, permettant une large distribution géographique des bio-capteurs dans la ville de Toulouse. De plus, le recrutement et le suivi des volontaires pour présenter les résultats ont permis d'accroître la sensibilisation sociale sur le thème de la qualité de l'air et les stratégies d'adaptation à ce problème.

Les méthodes magnétiques sont suffisamment efficaces et sensibles pour étudier la fraction ultrafine (<100nm) des oxydes de fer. Cette fraction est importante dans les études sur la qualité de l'air car elle est la plus dangereuse pour la santé humaine, puisqu'elle pénètre plus profondément dans le corps humain et est souvent associée à des constituants plus nocifs. Afin de mieux caractériser cette fraction, qui se trouve typiquement dans la granulométrie superparamagnétique (SP) des oxydes de fer, j'ai appliqué la méthode SPCDM, développée pendant mes études de master et publiée dans [Leite et al., 2018] à une partie des échantillons collectés sur les écorces d'arbres de la cour et les bio-capteurs. Ces résultats ont montré que : (1) la concentration en oxydes de fer superparamagéntiqueen suspension dans l'air est homogène dans les environnements domestiques (extérieur et intérieur) et dans les environnements des écoles de la cour ; (2) la taille moyenne des particules ultrafines SP estimée à partir des échantillons de la ville de Toulouse, incluant les deux écoles étudiées, est d'environ

8 nm, proche de celle des oxydes de fer ultrafins d'origine trafic précédemment rapportée pour la ville de São Paulo, Brésil. D'autres travaux ont également rapporté des granulométries similaires dans des particules ayant pour origine les émissions du trafic [Ronkko et al., 2014, Li et al., 2018].

Une étude des sédiments collectés dans la Garonne, qui traverse la ville de Toulouse du sud au nord, a été conçue pour étudier le devenir des émissions du trafic routier dans la ville. Les prélèvements ont été éffectués le long d'un profil de 50 km commençant avant et après les zones les plus densément peuplées de la ville. En utilisant des mesures de susceptibilité magnétique, des cycles d'hystérésis, la composition en éléments traces et une étude MEB nous avons démontré l'influence claire des émissions anthropogéniques dans la composition des sédiments. Typiquement, des susceptibilités magnétiques plus élevées ainsi que des concentrations plus élevées de métaux (Pb, Cu) et la présence de sphérules d'oxyde de fer dans les sédimentssont observées dans la partie centrale et densément peuplée de la ville, nt. Ceci caractérisent les émissions liées au trafic routier, démontrant ainsi le lessivage des particules issues du trafic routier dans la rivière.

6.2.1 Futur et perspectives

Du point de vue méthodologique, cette thèse a démontré le potentiel d'utilisation des techniques magnétiques pour la surveillance de la pollution de l'air, en utilisant des échantillons standards de filtres atmosphériques ou des bio-capteurs. En plus des techniques classiques qui sont habituellement appliquées en magnétisme environnemental, nous avons également exploré une technique alternative utilisée pour caractériser les parties les plus fines des porteurs magnétiques (technique SPCDM). Ceci est particulièrement intéressant dans le cas de la caractérisation des PM puisque cette fraction nanométrique ultrafine est la plus dangereuse pour la santé humaine. La méthode SPCDM [Leite et al., 2018] est capable de fournir la concentration de la fraction superparamagnétique (SP) ultrafine (relaxation rapide de la magnétisation) des porteurs magnétiques, en plus de fournir leur contribution relative à la magnétisation totale et une estimation de leur diamètre moyen. Afin d'améliorer cette méthodologie, il est important de réaliser des tests plus contrôlés, avec des échantillons synthétiques, où sont mélangées des fractions de grains dont la taille est connue, inférieure et proche de la limite SP-SSD. L'utilisation de plus d'une fenêtre de décroissance temporelle dans l'acquisition des données peut fournir des informations supplémentaires sur les différentes fractions de taille. De plus, l'utilisation d'un équipement avec contrôle de la température peut permettre d'autres stratégies dans la procédure d'inversion, permettant de déplacer les volumes de blocage pour les porteurs magnétiques, et augmentant les fractions de taille qui peuvent être étudiées par cette méthode.

L'étude de la qualité de l'air bénéficie fortement de l'utilisation des méthodes magnétiques. Grâce à l'étude de la fraction magnétique contenue dans les particules, nous pouvons accéder à des informations qui, autrement, n'auraient pas été enregistrées, comme la distribution granulométrique de la fraction ultrafine. Les méthodes magnétiques associées à des biocapteurs permettent également de réaliser des plans expérimentaux intéressants et novateurs, par exemple en étudiant les environnements intérieurs et extérieurs au même endroit. Un aspect qui pourrait être amélioré est l'étalonnage des mesures magnétiques avec les mesures traditionnelles de la qualité de l'air (concentrations de PM, d'éléments traces et d'autres pol-

luants). L'objectif serait de créer des directives magnétiques concernant la qualité de l'air, de la même manière que pour les particules par exemple. La thèse a également mis en évidence le potentiel des bio-capteurs, qui sont largement utilisés dans les études magnétiques environnementales, et cette utilisation va probablement augmenter à l'avenir. Les bio-capteurs présentent plusieurs avantages par rapport aux autres échantillons environnementaux. Ils ont un faible coût, un faible impact sur l'environnement et sont facilement intégrés dans les stratégies de science citoyenne, en particulier dans le cas de l'échantillonnage à l'intérieur, car ils sont beaucoup moins invasifs que le déploiement d'un attirail scientifique inconnu dans les environnements domestiques et publics.

Enfin, la participation des citoyens aux enquêtes scientifiques sur la qualité de l'air est également très prometteuse. Grâce à la participation des citoyens, l'impact et l'importance de l'étude scientifique sont rendus plus significatifs pour le grand public. Elle permet également d'améliorer la culture scientifique et la confiance de la population. Dans le cas de sujets scientifiques tels que la qualité de l'air, cela pourrait être un outil important pour combler le fossé entre les institutions académiques et le grand public. En outre, la science citoyenne peut également contribuer à lutter contre l'éco-anxiété, en transformant ce sentiment désagréable en actions positives et en stratégies d'adaptation pour faire face aux énormes défis environnementaux de notre époque. Nous ne pouvons pas oublier notre rôle dans la création de ces problèmes environnementaux. Il n'y a pas de solutions simples à des problèmes complexes, et nous devons les affronter ensemble. Je suis convaincu que c'est la seule façon d'avancer.

Bibliography

M. Abu-Allaban, J. A. Gillies, A. W. Gertler, R. Clayton, and D. Proffitt. Tailpipe, resuspended road dust, and brake-wear emission factors from on-road vehicles. *Atmospheric Environment*, 37(37):5283–5293, 2003. ISSN 1352-2310. doi: https://doi.org/10.1016/j.atmosenv.2003.05.005. 11th International Symposium, Transport and Air Pollution.

J. Adetunji, J. McGregor, and C. K. Ong. Harmattan Haze. *Weather*, 34(11):430–436, 1979. ISSN 1477-8696. doi: 10.1002/j.1477-8696.1979.tb03389.x.

O. A. Adjiri, C. K. Mafou, and P. K. Konan. Impact of Akouedo landfill (Abidjan - Côte d'Ivoire) on the populations: socio-economic and environmental study. *International Journal of Innovation and Applied Studies*, 13(4):979–989, 2015. ISSN 2351-8014.

A. J. Adon, C. Liousse, E. T. Doumbia, A. Baeza-Squiban, H. Cachier, J.-F. Léon, V. Yoboué, A. B. Akpo, C. Galy-Lacaux, B. Guinot, C. Zouiten, H. Xu, E. Gardrat, and S. Keita. Physico-chemical characterization of urban aerosols from specific combustion sources in West Africa at Abidjan in Côte d'Ivoire and Cotonou in Benin in the frame of the DACCIWA program. *Atmospheric Chemistry and Physics*, 20(9):5327–5354, 2020. ISSN 1680-7316. doi: 10.5194/acp-20-5327-2020.

G. M. Afeti and F. J. Resch. Physical characteristics of Saharan dust near the Gulf of Guinea. *Atmospheric Environment*, 34(8):1273–1279, 2000. ISSN 1352-2310. doi: 10.1016/S1352-2310(99)00296-4.

E. E. Agency. Air quality in europe, 2021.

M. U. Ali, A. Rashid, B. Yousaf, and A. Kamal. Health outcomes of road-traffic pollution among exposed roadside workers in rawalpindi city, pakistan. *Human and Ecological Risk Assessment: An International Journal*, 23(6):1330–1339, 2017. doi: 10.1080/10807039.2017.1308814.

S. M. Almeida, N. Canha, A. Silva, M. Do Carmo Freitas, P. Pegas, C. Alves, M. Evtyugina, and C. A. Pio. Children exposure to atmospheric particles in indoor of Lisbon primary schools. *Atmospheric Environment*, 45(40):7594–7599, 2011. ISSN 13522310. doi: 10.1016/j.atmosenv.2010.11.052. URL `http://dx.doi.org/10.1016/j.atmosenv.2010.11.052`.

A. Analitis, K. Katsouyanni, K. Dimakopoulou, E. Samoli, A. K. Nikoloulopoulos, Y. Petasakis, G. Touloumi, J. Schwartz, H. R. Anderson, K. Cambra, F. Forastiere, D. Zmirou, J. M. Vonk, L. Clancy, B. Kriz, J. Bobvos, and J. Pekkanen. Short-Term

Effects of Ambient Particles on Cardiovascular and Respiratory Mortality. *Epidemiology*, 17(2), 2006. ISSN 1044-3983. doi: 10.1097/01.ede.0000199439.57655.6b.

M. B. Andrew Churg. Ambient atmospheric particles in the airways of human lungs. *Ultrastructural Pathology*, 24(6):353–361, 2000. doi: https://doi.org/10.1080/019131200750060014.

S. C. Anenberg, P. Achakulwisut, M. Brauer, D. Moran, J. S. Apte, and D. K. Henze. Particulate matter-attributable mortality and relationships with carbon dioxide in 250 urban areas worldwide. *Scientific Reports*, 9(1):11552, 2019. ISSN 2045-2322. doi: 10.1038/s41598-019-48057-9.

I. Annesi-Maesano, N. Baiz, S. Banerjee, P. Rudnai, S. Rive, and on behalf of the SINPHONIE Group. Indoor air quality and sources in schools and related health effects. *Journal of Toxicology and Environmental Health, Part B*, 16(8):491–550, 2013. doi: 10.1080/10937404.2013.853609. PMID: 24298914.

A. Ares, J. Aboal, A. Carballeira, S. Giordano, P. Adamo, and J. Fernández. Moss bag biomonitoring: A methodological review. *Science of The Total Environment*, 432:143–158, 2012. ISSN 0048-9697. doi: https://doi.org/10.1016/j.scitotenv.2012.05.087.

R. C. Aster, B. Borchers, and C. H. Thurber. *Parameter estimation and inverse problems*, volume 90. Academic Press, 2011.

T. V. Athanasios Valavanidis, Konstantinos Fiotakis. Airborne particulate matter and human health: Toxicological assessment and importance of size and composition of particles for oxidative damage and carcinogenic mechanisms. *Journal of Environmental Science and Health, Part C*, 26(4):339–362, 2008. doi: https://doi.org/10.1080/10590500802494538.

R. W. Atkinson, G. W. Fuller, H. R. Anderson, R. M. Harrison, and B. Armstrong. Urban Ambient Particle Metrics and Health: A Time-series Analysis. *Epidemiology*, 21(4), 2010. ISSN 1044-3983. doi: 10.1097/EDE.0b013e3181debc88.

C. L. Avery, K. T. Mills, R. Williams, K. A. McGraw, C. Poole, R. L. Smith, and E. A. Whitsel. Estimating error in using ambient pm2. 5 concentrations as proxies for personal exposures. *Epidemiology (Cambridge, Mass.)*, 21(2):215, 2010. doi: 10.1097/EDE.0b013e3181cb41f7.

A. S. Bajamgnigni Gbambie and D. G. Steyn. Sea breezes at Cotonou and their interaction with the West African monsoon: SEA BREEZES AT COTONOU. *International Journal of Climatology*, 33(13):2889–2899, 2013. ISSN 08998418. doi: 10.1002/joc.3637.

W. Bank, I. for Health Metrics, and Evaluation. *The Cost of Air Pollution: Strengthening the Economic Case for Action*. World Bank, 2016. doi: 10.1596/25013. URL `https://elibrary.worldbank.org/doi/abs/10.1596/25013`.

F. Bardelli, E. Cattaruzza, F. Gonella, G. Rampazzo, and G. Valotto. Characterization of road dust collected in Traforo del San Bernardo highway tunnel: Fe and Mn

speciation. *Atmospheric Environment*, 45(35):6459–6468, 2011. ISSN 13522310. doi: 10.1016/j.atmosenv.2011.07.035.

N. Barmparesos, M. N. Assimakopoulos, V. D. Assimakopoulos, N. Loumos, M. A. Sotiriou, and A. Koukoumtzis. Indoor air quality and thermal conditions in a primary school with a green roof system. *Atmosphere*, 9(2):1–14, 2018. ISSN 20734433. doi: 10.3390/atmos9020075.

J. A. Becerra, J. Lizana, M. Gil, A. Barrios-Padura, P. Blondeau, and R. Chacartegui. Identification of potential indoor air pollutants in schools. *Journal of Cleaner Production*, 242, 2020. ISSN 09596526. doi: 10.1016/j.jclepro.2019.118420.

M. L. Bell, K. Belanger, K. Ebisu, J. F. Gent, and B. P. Leaderer. Relationship between birth weight and exposure to airborne fine particulate potassium and titanium during gestation. *Environmental Research*, 117:83–89, 2012. ISSN 0013-9351. doi: https://doi.org/10.1016/j.envres.2012.05.004.

M. Berico, A. Luciani, and M. Formignani. Atmospheric aerosol in an urban area—measurements of tsp and pm10 standards and pulmonary deposition assessments. *Atmospheric Environment*, 31(21):3659–3665, 1997. ISSN 1352-2310. doi: https://doi.org/10.1016/S1352-2310(97)00204-5. URL `https://www.sciencedirect.com/science/article/pii/S1352231097002045`.

D. V. Berkov, P. Görnert, N. Buske, C. Gansau, J. Mueller, M. Giersig, W. Neumann, and D. Su. New method for the determination of the particle magnetic moment distribution in a ferrofluid. *Journal of Physics D: Applied Physics*, 33(4):331–337, 2000. doi: 10.1088/0022-3727/33/4/303.

T. Berndt, A. R. Muxworthy, and G. A. Paterson. Determining the magnetic attempt time $\tau 0$, its temperature dependence, and the grain size distribution from magnetic viscosity measurements. *Journal of Geophysical Research: Solid Earth*, 120(11):7322–7336, 2015.

A. Bhatnagar. Environmental cardiology. *Circulation Research*, 99(7):692–705, 2006. doi: 10.1161/01.RES.0000243586.99701.cf.

J. Bloemendal, J. King, F. Hall, and S.-J. Doh. Rock magnetism of late neogene and pleistocene deep-sea sediments: Relationship to sediment source, diagenetic processes, and sediment lithology. *Journal of Geophysical Research: Solid Earth*, 97(B4):4361–4375, 1992. doi: https://doi.org/10.1029/91JB03068.

P. Blondeau, V. Iordache, O. Poupard, D. Genin, and F. Allard. Relationship between outdoor and indoor air quality in eight french schools. *Indoor air*, 15(1):2–12, 2005.

C. Boman, B. Forsberg, and T. Sandström. Shedding new light on wood smoke: a risk factor for respiratory health. *European Respiratory Journal*, 27(3):446–447, 2006. ISSN 0903-1936. doi: 10.1183/09031936.06.00000806.

R. Bonney, C. B. Cooper, J. Dickinson, S. Kelling, T. Phillips, K. V. Rosenberg, and J. Shirk. Citizen Science: A Developing Tool for Expanding Science Knowledge and Scientific Literacy. *BioScience*, 59(11):977–984, 12 2009. ISSN 0006-3568. doi: 10.1525/bio.2009.59.11.9.

R. Bonney, J. L. Shirk, T. B. Phillips, A. Wiggins, H. L. Ballard, A. J. Miller-Rushing, and J. K. Parrish. Next steps for citizen science. *Science*, 343(6178):1436–1437, 2014. ISSN 10959203. doi: 10.1126/science.1251554.

A. Bourliva, L. Papadopoulou, and E. Aidona. Study of road dust magnetic phases as the main carrier of potentially harmful trace elements. *Science of The Total Environment*, 553: 380–391, 2016. ISSN 0048-9697. doi: https://doi.org/10.1016/j.scitotenv.2016.02.149.

M. Branis and J. Safranek. Characterization of coarse particulate matter in school gyms. *Environmental Research*, 111(4):485–491, 2011. ISSN 0013-9351. doi: https://doi.org/10.1016/j.envres.2011.03.010. URL `https://www.sciencedirect.com/science/article/pii/S0013935111000934`.

M. Branis, J. Safranek, and A. Hytychova. Exposure of children to airborne particulate matter of different size fractions during indoor physical education at school. *Building and Environment*, 44(6):1246–1252, 2009. ISSN 03601323. doi: 10.1016/j.buildenv.2008.09.010.

R. Burnett, H. Chen, M. Szyszkowicz, N. Fann, B. Hubbell, C. A. Pope, J. S. Apte, M. Brauer, A. Cohen, S. Weichenthal, J. Coggins, Q. Di, B. Brunekreef, J. Frostad, S. S. Lim, H. Kan, K. D. Walker, G. D. Thurston, R. B. Hayes, C. C. Lim, M. C. Turner, M. Jerrett, D. Krewski, S. M. Gapstur, W. R. Diver, B. Ostro, D. Goldberg, D. L. Crouse, R. V. Martin, P. Peters, L. Pinault, M. Tjepkema, A. van Donkelaar, P. J. Villeneuve, A. B. Miller, P. Yin, M. Zhou, L. Wang, N. A. H. Janssen, M. Marra, R. W. Atkinson, H. Tsang, T. Q. Thach, J. B. Cannon, R. T. Allen, J. E. Hart, F. Laden, G. Cesaroni, F. Forastiere, G. Weinmayr, A. Jaensch, G. Nagel, H. Concin, and J. V. Spadaro. Global estimates of mortality associated with long-term exposure to outdoor fine particulate matter. *Proceedings of the National Academy of Sciences*, page 201803222, 2018. ISSN 0027-8424, 1091-6490. doi: 10.1073/pnas.1803222115.

L. Calderón-Garcidueñas, A. González-Maciel, R. Reynoso-Robles, J. Hammond, R. Kulesza, I. Lachmann, R. Torres-Jardón, P. S. Mukherjee, and B. A. Maher. Quadruple abnormal protein aggregates in brainstem pathology and exogenous metal-rich magnetic nanoparticles (and engineered ti-rich nanorods). the substantia nigrae is a very early target in young urbanites and the gastrointestinal tract a key brainstem portal. *Environmental Research*, 191:110139, 2020. ISSN 0013-9351. doi: https://doi.org/10.1016/j.envres.2020.110139.

J. Carignan, P. Hild, G. Mevelle, J. Morel, and D. Yeghicheyan. Routine analyses of trace elements in geological samples using flow injection and low pressure on-line liquid chromatography coupled to icp-ms: A study of geochemical reference materials br, dr-n, ub-n, an-g and gh. *Geostandards Newsletter*, 25(2-3):187–198, 2001. doi: https://doi.org/10.1111/j.1751-908X.2001.tb00595.x.

A. G. Castañeda-Miranda, H. N. Böhnel, R. S. Molina-Garza, and M. A. Chaparro. Magnetic evaluation of TSP-filters for air quality monitoring. *Atmospheric Environment*, 96:163–174, 2014. ISSN 18732844. doi: 10.1016/j.atmosenv.2014.07.015.

S. Castellini, B. Moroni, and D. Cappelletti. Pmetro: Measurement of urban aerosols on a mobile platform. *Measurement*, 49:99–106, 2014. ISSN 0263-2241. doi: https://doi.org/10.1016/j.measurement.2013.11.045.

M. Castillejos, D. R. Gold, A. I. Damokosh, P. Serrano, G. Allen, W. F. McDonnell, D. Dockery, S. Ruiz Velasco, M. Hernández, and C. Hayes. Acute effects of ozone on the pulmonary function of exercising schoolchildren from mexico city. *American Journal of Respiratory and Critical Care Medicine*, 152(5):1501–1507, 1995. doi: 10.1164/ajrccm.152.5.7582284.

T. J. Chang and T. S. Hu. Transport mechanisms of airborne particulate matters in partitioned indoor environment. *Building and Environment*, 43(5):886–895, 2008. ISSN 03601323. doi: 10.1016/j.buildenv.2007.01.030.

M. A. Chaparro. Airborne particle accumulation and loss in pollution-tolerant lichens and its magnetic quantification. *Environmental Pollution*, 288:117807, 2021. ISSN 0269-7491. doi: https://doi.org/10.1016/j.envpol.2021.117807.

M. A. Chaparro, J. M. Lavornia, M. A. Chaparro, and A. M. Sinito. Biomonitors of urban air pollution: Magnetic studies and SEM observations of corticolous foliose and microfoliose lichens and their suitability for magnetic monitoring. *Environmental Pollution*, 172:61–69, 2013a. ISSN 02697491. doi: 10.1016/j.envpol.2012.08.006. URL `http://dx.doi.org/10.1016/j.envpol.2012.08.006`.

M. A. Chaparro, G. Suresh, M. A. Chaparro, V. Ramasamy, and A. M. Sinito. Magnetic studies and elemental analysis of river sediments: A case study from the Ponnaiyar River (Southeastern India). *Environmental Earth Sciences*, 70(1):201–213, 2013b. ISSN 18666280. doi: 10.1007/s12665-012-2116-y.

M. A. Chaparro, M. A. Chaparro, A. G. Castañeda-Miranda, D. C. Marié, J. D. Gargiulo, J. M. Lavornia, M. Natal, and H. N. Böhnel. Fine air pollution particles trapped by street tree barks: In situ magnetic biomonitoring. *Environmental Pollution*, 266:115229, 2020. ISSN 0269-7491. doi: https://doi.org/10.1016/j.envpol.2020.115229.

C. Chen and B. Zhao. Review of relationship between indoor and outdoor particles: I/O ratio, infiltration factor and penetration factor. *Atmospheric Environment*, 45(2):275–288, 2011. ISSN 13522310. doi: 10.1016/j.atmosenv.2010.09.048. URL `http://dx.doi.org/10.1016/j.atmosenv.2010.09.048`.

G. Chen, X. Wan, G. Yang, and X. Zou. Traffic-related air pollution and lung cancer: A meta-analysis. *Thoracic cancer*, 6(3):307–318, 2015. doi: https://doi.org/10.1111/1759-7714.12185.

R. Chester, E. J. Sharples, G. Sanders, and F. Oldfield. The distribution of natural and non-crustal ferrimagnetic minerals in soil-sized particulates from the Mediterranean atmosphere. *Water, Air, and Soil Pollution*, 23(1):25–35, 1984. ISSN 00496979. doi: 10.1007/BF00185128.

L. Chiappini, S. Verlhac, R. Aujay, W. Maenhaut, J. P. Putaud, J. Sciare, J. L. Jaffrezo, C. Liousse, C. Galy-Lacaux, L. Y. Alleman, P. Panteliadis, E. Leoz, and O. Favez. Clues for a standardised thermal-optical protocol for the assessment of organic and elemental carbon within ambient air particulate matter. *Atmospheric Measurement Techniques*, 7 (6):1649–1661, 2014a. ISSN 1867-8548. doi: 10.5194/amt-7-1649-2014.

L. Chiappini, S. Verlhac, R. Aujay, W. Maenhaut, J. P. Putaud, J. Sciare, J. L. Jaffrezo, C. Liousse, C. Galy-Lacaux, L. Y. Alleman, P. Panteliadis, E. Leoz, and O. Favez. Clues for a standardised thermal-optical protocol for the assessment of organic and elemental carbon within ambient air particulate matter. *Atmospheric Measurement Techniques*, 7 (6):1649–1661, 2014b. ISSN 1867-8548. doi: 10.5194/amt-7-1649-2014.

V. Chithra and S. S. Nagendra. Indoor air quality investigations in a naturally ventilated school building located close to an urban roadway in chennai, india. *Building and Environment*, 54:159–167, 2012. doi: 10.1016/j.buildenv.2012.01.016.

V. S. Chithra and S. M. Nagendra. Characterizing and predicting coarse and fine particulates in classrooms located close to an urban roadway. *Journal of the Air and Waste Management Association*, 64(8):945–956, 2014. ISSN 21622906. doi: 10.1080/10962247.2014.894483. URL `http://dx.doi.org/10.1080/10962247.2014.894483`.

J. C. Chow, J. G. Watson, L. C. Pritchett, W. R. Pierson, C. A. Frazier, and R. G. Purcell. The dri thermal/optical reflectance carbon analysis system: Description, evaluation and applications in U.S. Air quality studies. *Atmospheric Environment. Part A. General Topics*, 27(8):1185–1201, 1993. ISSN 0960-1686. doi: 10.1016/0960-1686(93)90245-T.

J. C. Chow, J. G. Watson, E. M. Fujita, Z. Lu, D. R. Lawson, and L. L. Ashbaugh. Temporal and spatial variations of PM2.5 and PM10 aerosol in the Southern California air quality study. *Atmospheric Environment*, 28(12):2061–2080, 1994. ISSN 1352-2310. doi: 10.1016/1352-2310(94)90474-X.

J. C. Chow, J. G. Watson, H. Kuhns, V. Etyemezian, D. H. Lowenthal, D. Crow, S. D. Kohl, J. P. Engelbrecht, and M. C. Green. Source profiles for industrial, mobile, and area sources in the Big Bend Regional Aerosol Visibility and Observational study. *Chemosphere*, 54(2): 185–208, 2004. ISSN 0045-6535. doi: 10.1016/j.chemosphere.2003.07.004.

J. C. Chow, L.-W. A. Chen, J. G. Watson, D. H. Lowenthal, K. A. Magliano, K. Turkiewicz, and D. E. Lehrman. PM2.5 chemical composition and spatiotemporal variability during the California Regional PM10/PM2.5 Air Quality Study (CRPAQS). *Journal of Geophysical Research: Atmospheres*, 111(D10):D10S04, 2006. ISSN 2156-2202. doi: 10.1029/2005JD006457.

F. Christophoul, V. Regard, J. Martinod, and J. Darrozes. Morphodynamics of the upper pleistocene garonne river (sw france): conditions of braiding/meandering transition. 2014.

N. Clements, J. Eav, M. Xie, M. P. Hannigan, S. L. Miller, W. Navidi, J. L. Peel, J. J. Schauer, M. M. Shafer, and J. B. Milford. Concentrations and source insights for trace elements in fine and coarse particulate matter. *Atmospheric environment*, 89:373–381, 2014. doi: 10.1016/j.atmosenv.2014.01.011.

A. J. Cohen, M. Brauer, R. Burnett, H. R. Anderson, J. Frostad, K. Estep, K. Balakrishnan, B. Brunekreef, L. Dandona, R. Dandona, V. Feigin, G. Freedman, B. Hubbell, A. Jobling, H. Kan, L. Knibbs, Y. Liu, R. Martin, L. Morawska, C. A. Pope, H. Shin, K. Straif, G. Shaddick, M. Thomas, R. van Dingenen, A. van Donkelaar, T. Vos, C. J. L. Murray, and M. H. Forouzanfar. Estimates and 25-year trends of the global burden of disease attributable to ambient air pollution: An analysis of data from the Global Burden of Diseases Study 2015. *The Lancet*, 389(10082):1907–1918, 2017. ISSN 0140-6736, 1474-547X. doi: 10.1016/S0140-6736(17)30505-6.

A. Cunsolo Willox, S. L. Harper, V. L. Edge, K. Landman, K. Houle, and J. D. Ford. The land enriches the soul: On climatic and environmental change, affect, and emotional health and well-being in Rigolet, Nunatsiavut, Canada. *Emotion, Space and Society*, 6(Complete): 14–24, 2013. doi: 10.1016/j.emospa.2011.08.005.

D. Custódio, I. Pinho, M. Cerqueira, T. Nunes, and C. Pio. Indoor and outdoor suspended particulate matter and associated carbonaceous species at residential homes in northwestern Portugal. *Science of the Total Environment*, 473-474:72–76, 2014. ISSN 18791026. doi: 10.1016/j.scitotenv.2013.12.009. URL `http://dx.doi.org/10.1016/j.scitotenv.2013.12.009`.

P. Dankers. Relationship between median destructive field and remanent coercive forces for dispersed natural magnetite, titanomagnetite and hematite. *Geophysical Journal International*, 64(2):447–461, 02 1981. ISSN 0956-540X. doi: 10.1111/j.1365-246X.1981.tb02676.x.

P. H. M. Dankers. Magnetic properties of dispersed natural iron-oxides of known grain-size. *Ph. D. Thesis*, 143, 1978.

M. David, A. Labenne, J.-M. Carozza, and P. Valette. Evolutionary trajectory of channel planforms in the middle garonne river (toulouse, sw france) over a 130-year period: Contribution of mixed multiple factor analysis (mfamix). *Geomorphology*, 258:21–39, 2016. ISSN 0169-555X. doi: https://doi.org/10.1016/j.geomorph.2016.01.012. URL `https://www.sciencedirect.com/science/article/pii/S0169555X16300125`.

D. Dawaï, M. Macouin, S. Rousse, J.-F. Léon, M. Gountié Dedzo, and L. Drigo. Tracking airborne pollution with environmental magnetism in a medium-sized african city. *Atmosphere*, 12(10):1281, 2021. doi: 10.3390/atmos12101281.

R. Day, M. Fuller, and V. Schmidt. Hysteresis properties of titanomagnetites: grain-size and compositional dependence. *Physics of the Earth and planetary interiors*, 13(4):260–267, 1977.

S. De Craemer, J. Vercauteren, F. Fierens, W. Lefebvre, and F. J. Meysman. Using Large-Scale NO2Data from Citizen Science for Air-Quality Compliance and Policy Support. *Environmental Science and Technology*, 54(18):11070–11078, 2020. ISSN 15205851. doi: 10.1021/acs.est.0c02436.

C. de la Sota, J. Lumbreras, N. Pérez, M. Ealo, M. Kane, I. Youm, and M. Viana. Indoor air pollution from biomass cookstoves in rural Senegal. *Energy for Sustainable Development*, 43:224–234, 2018. ISSN 09730826. doi: 10.1016/j.esd.2018.02.002. URL `https://doi.org/10.1016/j.esd.2018.02.002`.

F. De Nicola, F. Murena, M. A. Costagliola, A. Alfani, D. Baldantoni, M. V. Prati, L. Sessa, V. Spagnuolo, and S. Giordano. A multi-approach monitoring of particulate matter, metals and PAHs in an urban street canyon. *Environmental Science and Pollution Research*, 20 (7):4969–4979, 2013. ISSN 1614-7499. doi: https://doi.org/10.1007/s11356-012-1456-1.

J. A. Dearing, R. J. L. Dann, K. Hay, J. A. Lees, P. J. Loveland, B. A. Maher, and K. O'Grady. Frequency-dependent susceptibility measurements of environmental materials. *Geophysical Journal International*, 124(1):228–240, 01 1996. doi: 10.1111/j.1365-246X.1996.tb06366.x.

M. J. Dekkers, M. E. Evans, and F. Heller. Environmental Magnetism — Principles and Applications of Enviromagnetics M.E. Evans F. Heller, Academic Press, 2003, ISBN 0-12-243851- 5, Hardback, xii + 299 pp, £45. *Geophysical Journal International*, 158:1177–1178, 2004. ISSN 1365-246X. doi: 10.1111/j.1365-246X.2004.02392.x.

A.-M. Desaulty and E. Petelet-Giraud. Zinc isotope composition as a tool for tracing sources and fate of metal contaminants in rivers. *Science of The Total Environment*, 728:138599, 2020. ISSN 0048-9697. doi: https://doi.org/10.1016/j.scitotenv.2020.138599. URL `https://www.sciencedirect.com/science/article/pii/S004896972032115X`.

A. Di Gilio, G. Farella, A. Marzocca, R. Giua, G. Assennato, M. Tutino, and G. De Gennaro. Indoor/outdoor air quality assessment at school near the steel plant in Taranto (Italy). *Advances in Meteorology*, 2017, 2017. ISSN 16879317. doi: 10.1155/2017/1526209.

E. Diapouli, A. Chaloulakou, N. Mihalopoulos, and N. Spyrellis. Indoor and outdoor PM mass and number concentrations at schools in the Athens area. *Environmental Monitoring and Assessment*, 136(1-3):13–20, 2008. ISSN 01676369. doi: 10.1007/s10661-007-9724-0.

C. Dimitroulopoulou. Ventilation in European dwellings: A review. *Building and Environment*, 47(1):109–125, 2012. doi: 10.1016/j.buildenv.2011.07.016. URL `http://dx.doi.org/10.1016/j.buildenv.2011.07.016`.

J. Djossou, J.-F. Léon, A. B. Akpo, C. Liousse, V. Yoboué, M. Bedou, M. Bodjrenou, C. Chiron, C. Galy-Lacaux, E. Gardrat, M. Abbey, S. Keita, J. Bahino, E. Touré N'Datchoh, M. Ossohou, and C. N. Awanou. Mass concentration, optical depth and carbon composition of particulate matter in the major southern West African cities of Cotonou (Benin) and Abidjan (Côte d'Ivoire). *Atmospheric Chemistry and Physics*, 18(9):6275–6291, 2018. ISSN 1680-7316. doi: 10.5194/acp-18-6275-2018.

D. W. Dockery and C. A. Pope. Acute Respiratory Effects of Particulate Air Pollution. *Annual Review of Public Health*, 15(1):107–132, 1994. ISSN 0163-7525, 1545-2093. doi: 10.1146/annurev.pu.15.050194.000543.

D. W. Dockery and P. H. Stone. Cardiovascular risks from fine particulate air pollution. *N Engl J Med*, 356(5):511–513, 2007.

D. W. Dockery, C. A. Pope, X. Xu, J. D. Spengler, J. H. Ware, M. E. Fay, B. G. Ferris, and F. E. Speizer. An association between air pollution and mortality in six u.s. cities. *New England Journal of Medicine*, 329(24):1753–1759, 1993. doi: 10.1056/NEJM199312093292401.

F. Dominici, A. McDermott, M. Daniels, S. Zeger, and J. Samet. Revised analyses of time-series studies of air pollution and health: Mortality among residents of 90 cities. *Boston, MA: Health Effects Institute*, 2003.

P. Dominutti, S. Keita, J. Bahino, A. Colomb, C. Liousse, V. Yoboué, C. Galy-Lacaux, E. Morris, L. Bouvier, S. Sauvage, and A. Borbon. Anthropogenic VOCs in Abidjan, southern West Africa: From source quantification to atmospheric impacts. *Atmospheric Chemistry and Physics*, 19(18):11721–11741, 2019. ISSN 1680-7316. doi: 10.5194/acp-19-11721-2019.

J. Dormann, F. D'Orazio, F. Lucari, E. Tronc, P. Prené, J. Jolivet, D. Fiorani, R. Cherkaoui, and M. Nogues. Thermal variation of the relaxation time of the magnetic moment of γ-fe 2 o 3 nanoparticles with interparticle interactions of various strengths. *Physical Review B*, 53(21):14291, 1996.

Y. Du, X. Xu, M. Chu, Y. Guo, and J. Wang. Air particulate matter and cardiovascular disease: the epidemiological, biomedical and clinical evidence. *Journal of Thoracic Disease*, 8(1), 2015. doi: 10.3978/j.issn.2072-1439.2015.11.37.

D. J. Dunlop. Theory and application of the day plot (mrs/ms versus hcr/hc) 1. theoretical curves and tests using titanomagnetite data. *Journal of Geophysical Research: Solid Earth*, 107(B3):EPM–4, 2002. doi: 10.1029/2001JB000487.

D. J. Dunlop and Ö. Özdemir. *Rock magnetism: fundamentals and frontiers*. Number 3. Cambridge university press, 2001.

R. Egli. Characterization of individual rock magnetic components by analysis of remanence curves, 1. Unmixing natural sediments. *Studia Geophysica et Geodaetica*, 48(2):391–446, 2004. ISSN 00393169. doi: 10.1023/B:SGEG.0000020839.45304.6d.

M. El-Fadel and M. Massoud. Particulate matter in urban areas: health-based economic assessment. *Science of The Total Environment*, 257(2):133–146, 2000. ISSN 0048-9697. doi: https://doi.org/10.1016/S0048-9697(00)00503-9.

B. Elen, J. Peters, M. V. Poppel, N. Bleux, J. Theunis, M. Reggente, and A. Standaert. The aeroflex: A bicycle for mobile air quality measurements. *Sensors*, 13(1):221–240, 2013. ISSN 1424-8220. doi: 10.3390/s130100221.

J. M. Ellison and R. E. Waller. A review of sulphur oxides and particulate matter as air pollutants with particular reference to effects on health in the united kingdom. *Environmental Research*, 16(1):302–325, 1978. ISSN 0013-9351. doi: https://doi.org/10.1016/0013-9351(78)90164-0.

M. E. Evans and F. Heller. *Environmental Magnetism*, volume 11. 2003. ISBN 2003103058. doi: 10.22498/pages.11.2-3.34.

J. Evelyn et al. Fumifugium: of the inconvenience of the aer and sinoakc of london dissipated. *Fumifugium: of the Inconvenience of the Aer and Sinoakc of London Dissipated.*, 1961.

Y. Fang, V. Naik, L. W. Horowitz, and D. L. Mauzerall. Air pollution and associated human mortality: the role of air pollutant emissions, climate change and methane concentration increases from the preindustrial period to present. *Atmospheric Chemistry and Physics*, 13(3):1377–1394, 2013. doi: 10.5194/acp-13-1377-2013.

A. Ferguson and H. Solo-Gabriele. Children's exposure to environmental contaminants: an editorial reflection of articles in the ijerph special issue entitled,"children's exposure to environmental contaminants". *International journal of environmental research and public health*, 13(11):1117, 2016. doi: https://doi.org/10.3390/ijerph13111117.

L. Filleul, V. Rondeau, S. Vandentorren, N. Le Moual, A. Cantagrel, I. Annesi-Maesano, D. Charpin, C. Declercq, F. Neukirch, C. Paris, D. Vervloet, P. Brochard, J.-F. Tessier, F. Kauffmann, and I. Baldi. Twenty five year mortality and air pollution: results from the french paarc survey. 62(7):453–460, 2005. doi: 10.1136/oem.2004.014746.

M. M. Finkelstein, M. Jerrett, and M. R. Sears. Environmental inequality and circulatory disease mortality gradients. *Journal of Epidemiology and Community Health*, 59(6):481–487, 2005. ISSN 0143005X. doi: 10.1136/jech.2004.026203.

J. Firket. Fog along the meuse valley. *Transactions of the Faraday Society*, 32:1192–1196, 1936.

P. J. Flanders. Collection, measurement, and analysis of airborne magnetic particulates from pollution in the environment (invited). *Journal of Applied Physics*, 75(10):5931–5936, 1994. doi: https://doi.org/10.1063/1.355518.

F. Forastiere, M. Stafoggia, C. Tasco, S. Picciotto, N. Agabiti, G. Cesaroni, and C. A. Perucci. Socioeconomic status, particulate air pollution, and daily mortality: Differential exposure or differential susceptibility. *American Journal of Industrial Medicine*, 50(3):208–216, 2007. ISSN 02713586. doi: 10.1002/ajim.20368.

P. Formenti, S. Caquineau, S. Chevaillier, A. Klaver, K. Desboeufs, J. L. Rajot, S. Belin, and V. Briois. Dominance of goethite over hematite in iron oxides of mineral dust from western africa: Quantitative partitioning by x-ray absorption spectroscopy. *Journal of Geophysical Research: Atmospheres*, 119(22):12,740–12,754, 2014. doi: https://doi.org/10.1002/2014JD021668.

U. Frank and N. R. Nowaczyk. Mineral magnetic properties of artificial samples systematically mixed from haematite and magnetite. *Geophysical Journal International*, 175(2): 449–461, 2008. ISSN 0956540X. doi: 10.1111/j.1365-246X.2008.03821.x.

C. Franke, C. Kissel, E. Robin, P. Bonté, and F. Lagroix. Magnetic particle characterization in the seine river system: Implications for the determination of natural versus anthropogenic input. *Geochemistry, Geophysics, Geosystems*, 10(8), 2009. doi: https://doi.org/10.1029/2009GC002544.

S. Fritz, L. See, M. Van Der Velde, R. A. Nalepa, C. Perger, C. Schill, I. McCallum, D. Schepaschenko, F. Kraxner, X. Cai, X. Zhang, S. Ortner, R. Hazarika, A. Cipriani, C. Di Bella, A. H. Rabia, A. Garcia, M. Vakolyuk, K. Singha, M. E. Beget, S. Erasmi, F. Albrecht, B. Shaw, and M. Obersteiner. Downgrading recent estimates of land available for biofuel production. *Environmental Science and Technology*, 47(3):1688–1694, 2013. ISSN 0013936X. doi: 10.1021/es303141h.

H. Fromme, S. Dietrich, D. Twardella, D. Heitmann, R. Schierl, M. Kiranoglu, and B. Liebl. Indoor air concentrations of participate matter (PM10 and PM2.5) in German schools. *WIT Transactions on Ecology and the Environment*, 86:393–399, 2006. ISSN 17433541. doi: 10.2495/AIR06039.

H. Fromme, D. Twardella, S. Dietrich, D. Heitmann, R. Schierl, B. Liebl, and H. Rüden. Particulate matter in the indoor air of classrooms-exploratory results from Munich and surrounding area. *Atmospheric Environment*, 41(4):854–866, 2007. ISSN 13522310. doi: 10.1016/j.atmosenv.2006.08.053.

H. Fromme, J. Diemer, S. Dietrich, J. Cyrys, J. Heinrich, W. Lang, M. Kiranoglu, and D. Twardella. Chemical and morphological properties of particulate matter (PM10, PM2.5) in school classrooms and outdoor air. *Atmospheric Environment*, 42(27):6597–6605, 2008. ISSN 13522310. doi: 10.1016/j.atmosenv.2008.04.047.

L. Fusaro, E. Salvatori, A. Winkler, M. A. Frezzini, E. De Santis, L. Sagnotti, S. Canepari, and F. Manes. Urban trees for biomonitoring atmospheric particulate matter: An integrated approach combining plant functional traits, magnetic and chemical properties. *Ecological Indicators*, 126:107707, 2021. doi: 10.1016/j.ecolind.2021.107707.

C. Garneau, S. Sauvage, J. M. Sánchez-Pérez, S. Lofts, D. Brito, R. Neves, and A. Probst. Modelling trace metal transfer in large rivers under dynamic hydrology: A coupled hydrodynamic and chemical equilibrium model. *Environmental Modelling and Software*, 89: 77–96, 2017. ISSN 13648152. doi: 10.1016/j.envsoft.2016.11.018.

S. Ghafghazi, T. Sowlati, S. Sokhansanj, X. Bi, and S. Melin. Particulate matter emissions from combustion of wood in district heating applications. *Renewable and Sustainable Energy Reviews*, 15(6):3019–3028, 2011. ISSN 1364-0321. doi: https://doi.org/10.1016/j.rser.2011.04.001.

L. Gharibvand, W. Lawrence Beeson, D. Shavlik, R. Knutsen, M. Ghamsary, S. Soret, and S. F. Knutsen. The association between ambient fine particulate matter and incident

adenocarcinoma subtype of lung cancer. *Environmental Health*, 16(1):71, 2017. ISSN 1476-069X. doi: 10.1186/s12940-017-0268-7.

T. Godish and J. S. Fu. *Air quality*. CRC Press, 2019. doi: https://doi.org/10.1201/9780429105036.

T. Gonet and B. A. Maher. Airborne, Vehicle-Derived Fe-Bearing Nanoparticles in the Urban Environment: A Review. *Environmental Science and Technology*, 53(17):9970–9991, 2019. ISSN 15205851. doi: 10.1021/acs.est.9b01505.

T. Gonet, B. A. Maher, and J. Kukutschová. Source apportionment of magnetite particles in roadside airborne particulate matter. *Science of the Total Environment*, 752:141828, 2021a. doi: doi.org/10.1016/j.scitotenv.2020.141828.

T. Gonet, B. A. Maher, I. Nyirő-Kósa, M. Pósfai, M. Vaculík, and J. Kukutschová. Size-resolved, quantitative evaluation of the magnetic mineralogy of airborne brake-wear particulate emissions. *Environmental Pollution*, 288:117808, 2021b. doi: 10.1016/j.envpol.2021.117808.

B. Gorka-Kostrubiec and I. Szczepaniak-Wnuk. Magnetic study of a mixture of magnetite and metallic iron in indoor dust samples. *Air Quality, Atmosphere & Health*, (1):105–116, 2017. ISSN 1873-9326. doi: 10.1007/s11869-016-0412-5.

B. Gorka-Kostrubiec, T. Werner, S. Dytlow, I. Szczepaniak-Wnuk, M. Jelenska, and A. Hanc-Kuczkowska. Detection of metallic iron in urban dust by using high-temperature measurements supplemented with microscopic observations and mössbauer spectra. *Journal of Applied Geophysics*, 166:89–102, 2019. doi: https://doi.org/10.1016/j.jappgeo.2019.04.022.

F. Gozzi, G. Della Ventura, and A. Marcelli. Mobile monitoring of particulate matter: State of art and perspectives. *Atmospheric Pollution Research*, 7(2):228–234, 2016. ISSN 1309-1042. doi: https://doi.org/10.1016/j.apr.2015.09.007.

R. S. Green, S. Smorodinsky, J. J. Kim, R. McLaughlin, and B. Ostro. Proximity of California public schools to busy roads. *Environmental Health Perspectives*, 112(1):61–66, 2004. ISSN 00916765. doi: 10.1289/ehp.6566.

B. D. Grover, M. Kleinman, N. L. Eatough, D. J. Eatough, P. K. Hopke, R. W. Long, W. E. Wilson, M. B. Meyer, and J. L. Ambs. Measurement of total pm2. 5 mass (nonvolatile plus semivolatile) with the filter dynamic measurement system tapered element oscillating microbalance monitor. *Journal of Geophysical Research: Atmospheres*, 110(D7), 2005. doi: https://doi.org/10.1029/2004JD004995.

R. Guaita, M. Pichiule, T. Maté, C. Linares, and J. Díaz. Short-term impact of particulate matter (pm2.5) on respiratory mortality in madrid. *International Journal of Environmental Health Research*, 21(4):260–274, 2011. doi: 10.1080/09603123.2010.544033.

R. B. Gunier, A. Hertz, J. Von Behren, and P. Reynolds. Traffic density in California: Socioeconomic and ethnic differences among potentially exposed children. *Journal of Exposure Analysis and Environmental Epidemiology*, 13(3):240–246, 2003. ISSN 10534245. doi: 10.1038/sj.jea.7500276.

L. C. Guo, Y. Zhang, H. Lin, W. Zeng, T. Liu, J. Xiao, S. Rutherford, J. You, and W. Ma. The washout effects of rainfall on atmospheric particulate pollution in two Chinese cities. *Environmental Pollution*, 215:195–202, 2016. ISSN 18736424. doi: 10.1016/j.envpol.2016.05.003. URL `http://dx.doi.org/10.1016/j.envpol.2016.05.003`.

S. Guo, M. Hu, M. L. Zamora, J. Peng, D. Shang, J. Zheng, Z. Du, Z. Wu, M. Shao, L. Zeng, M. J. Molina, and R. Zhang. Elucidating severe urban haze formation in china. *Proceedings of the National Academy of Sciences*, 111(49):17373–17378, 2014. doi: 10.1073/pnas.1419604111.

S. Hales, T. Blakely, and A. Woodward. Air pollution and mortality in new zealand: cohort study. 66(5):468–473, 2012. doi: 10.1136/jech.2010.112490.

G. B. Hamra, N. Guha, A. Cohen, F. Laden, O. Raaschou-Nielsen, J. M. Samet, P. Vineis, F. Forastiere, P. Saldiva, T. Yorifuji, and D. Loomis. Outdoor particulate matter exposure and lung cancer: A systematic review and meta-analysis. *Environmental Health Perspectives*, 122(9):906–911, 2014. doi: 10.1289/ehp/1408092.

D. Hasenfratz, O. Saukh, C. Walser, C. Hueglin, M. Fierz, T. Arn, J. Beutel, and L. Thiele. Deriving high-resolution urban air pollution maps using mobile sensor nodes. *Pervasive and Mobile Computing*, 16:268–285, 2015. ISSN 1574-1192. doi: https://doi.org/10.1016/j.pmcj.2014.11.008. Selected Papers from the Twelfth Annual IEEE International Conference on Pervasive Computing and Communications (PerCom 2014).

S. B. Henderson, B. Beckerman, M. Jerrett, and M. Brauer. Application of land use regression to estimate long-term concentrations of traffic-related nitrogen oxides and fine particulate matter. *Environmental science & technology*, 41(7):2422–2428, 2007. doi: https://doi.org/10.1021/es0606780.

N. Hodas, M. Loh, H. M. Shin, D. Li, D. Bennett, T. E. McKone, O. Jolliet, C. J. Weschler, M. Jantunen, P. Lioy, and P. Fantke. Indoor inhalation intake fractions of fine particulate matter: review of influencing factors. *Indoor Air*, 26(6):836–856, 2016. ISSN 16000668. doi: 10.1111/ina.12268.

G. Hoek, B. Brunekreef, S. Goldbohm, P. Fischer, and P. A. van den Brandt. Association between mortality and indicators of traffic-related air pollution in the netherlands: a cohort study. *The Lancet*, 360(9341):1203–1209, 2002. doi: https://doi.org/10.1016/S0140-6736(02)11280-3.

V. Hoffmann, M. Knab, and E. Appel. Magnetic susceptibility mapping of roadside pollution. *Journal of Geochemical Exploration*, 66(1-2):313–326, 1999. ISSN 03756742. doi: 10.1016/S0375-6742(99)00014-X.

J. Hofman and R. Samson. Biomagnetic monitoring as a validation tool for local air quality models: A case study for an urban street canyon. *Environment International*, 70:50–61, 2014. ISSN 0160-4120. doi: https://doi.org/10.1016/j.envint.2014.05.007.

J. Hofman, B. A. Maher, A. R. Muxworthy, K. Wuyts, A. Castanheiro, and R. Samson. Biomagnetic Monitoring of Atmospheric Pollution: A Review of Magnetic Signatures from Biological Sensors. *Environmental Science & Technology*, 51(12):6648–6664, 2017. ISSN 0013-936X, 1520-5851. doi: 10.1021/acs.est.7b00832.

S. Höfner and A. Schütze. Air Quality Measurements and Education: Improving Environmental Awareness of High School Students. *Frontiers in Sensors*, 2(April):1–12, 2021. doi: 10.3389/fsens.2021.657920.

F. Hrouda, J. Pokorný, J. Ježek, and M. Chadima. Out-of-phase magnetic susceptibility of rocks and soils: a rapid tool for magnetic granulometry. *Geophysical Journal International*, 194(1):170–181, 04 2013. ISSN 0956-540X. doi: 10.1093/gji/ggt097.

Y. C. Hsu, P. Dille, J. Cross, B. Dias, R. Sargent, and I. Nourbakhsh. Community-empowered air quality monitoring system. *Conference on Human Factors in Computing Systems - Proceedings*, 2017-May:1607–1619, 2017. doi: 10.1145/3025453.3025853.

L. Huang, Z. Pu, M. Li, and J. Sundell. Characterizing the indoor-outdoor relationship of fine particulate matter in non-heating season for urban residences in beijing. *PLOS ONE*, 10 (9):1–17, 09 2015. doi: 10.1371/journal.pone.0138559. URL `https://doi.org/10.1371/journal.pone.0138559`.

A. Hunt. The application of mineral magnetic methods to atmospheric aerosol discrimination. *Physics of the Earth and Planetary Interiors*, 42(1-2):10–21, 1986. ISSN 00319201. doi: 10.1016/S0031-9201(86)80005-X.

A. Hunt, J. Jones, and F. Oldfield. Magnetic measurements and heavy metals in atmospheric particulates of anthropogenic origin. *Science of the Total Environment*, 33(1-4):129–139, 1984. ISSN 00489697. doi: 10.1016/0048-9697(84)90387-5.

A. Irwin. Citizen Science comes to age. *Nature*, 562:480–482, 2018. URL `https://media.nature.com/original/magazine-assets/d41586-018-07106-5/d41586-018-07106-5.pdf`.

N. A. Janssen, P. H. Van Vliet, F. Aarts, H. Harssema, and B. Brunekreef. Assessment of exposure to traffic related air pollution of children attending schools near motorways. *Atmospheric Environment*, 35(22):3875–3884, 2001. ISSN 13522310. doi: 10.1016/S1352-2310(01)00144-3.

J. Jaskuła and M. Sojka. Assessment of spatial distribution of sediment contamination with heavy metals in the two biggest rivers in poland. *CATENA*, 211:105959, 2022. ISSN 0341-8162. doi: https://doi.org/10.1016/j.catena.2021.105959. URL `https://www.sciencedirect.com/science/article/pii/S0341816221008171`.

P. Jasonov, D. Nourgaliev, B. Burov, and F. Heller. A modernized coercivity spectrometer. *Geologica Carpathica*, 49(3):224–226, 1998.

M. Jelenska, B. Gorka-Kostrubiec, T. Werner, M. Kadzialko-Hofmokl, I. Szczepaniak-Wnuk, T. Gonet, and P. Szwarczewski. Evaluation of indoor/outdoor urban air pollution by magnetic, chemical and microscopic studies. *Atmospheric Pollution Research*, 8(4):754–766, 2017. ISSN 1309-1042. doi: https://doi.org/10.1016/j.apr.2017.01.006. URL `https://www.sciencedirect.com/science/article/pii/S1309104216303798`.

M. Jerrett, R. T. Burnett, P. Kanaroglou, J. Eyles, N. Finkelstein, C. Giovis, and J. R. Brook. A gis–environmental justice analysis of particulate air pollution in hamilton, canada. *Environment and Planning A: Economy and Space*, 33(6):955–973, 2001. doi: 10.1068/a33137.

M. Jerrett, R. T. Burnett, J. Brook, P. Kanaroglou, C. Giovis, N. Finkelstein, and B. Hutchison. Do socioeconomic characteristics modify the short term association between air pollution and mortality? Evidence from a zonal time series in Hamilton, Canada. *Journal of Epidemiology and Community Health*, 58(1):31–40, 2004. ISSN 0143005X. doi: 10.1136/jech.58.1.31.

M. Jerrett, R. T. Burnett, R. Ma, C. A. Pope, D. Krewski, K. B. Newbold, G. Thurston, Y. Shi, N. Finkelstein, E. E. Calle, and M. J. Thun. Spatial analysis of air pollution and mortality in los angeles. *Epidemiology*, 16(6):727–736, 2005. doi: 10.1097/01.ede.0000181630.15826.7d. URL `http://www.jstor.org/stable/20486136`.

Z. Jiang, Q. Liu, M. J. Dekkers, C. Colombo, Y. Yu, V. Barrón, and J. Torrent. Ferro and antiferromagnetism of ultrafine-grained hematite. *Geochemistry, Geophysics, Geosystems*, 15(6):2699–2712, 2014.

C. Johansson, M. Norman, and L. Burman. Road traffic emission factors for heavy metals. *Atmospheric Environment*, 43(31):4681–4688, 2009. ISSN 13522310. doi: 10.1016/j.atmosenv.2008.10.024. URL `http://dx.doi.org/10.1016/j.atmosenv.2008.10.024`.

N. C. Jones, C. A. Thornton, D. Mark, and R. M. Harrison. Indoor/outdoor relationships of particulate matter in domestic homes with roadside, urban and rural locations. *Atmospheric Environment*, 34(16):2603–2612, 2000. ISSN 13522310. doi: 10.1016/S1352-2310(99)00489-6.

D. Jordanova, P. Petrov, V. Hoffmann, T. Gocht, C. Panaiotu, T. Tsacheva, and N. Jordanova. Magnetic signature of different vegetation species in polluted environment. *Studia Geophysica et Geodaetica*, 54(3):417–442, 2010. ISSN 1573-1626. doi: 10.1007/s11200-010-0025-7.

D. Jordanova, N. Jordanova, and P. Petrov. Magnetic susceptibility of road deposited sediments at a national scale – relation to population size and urban pollution. *Environmental Pollution*, 189:239–251, 2014. ISSN 0269-7491. doi: https://doi.org/10.1016/j.envpol.2014.02.030.

N. Jordanova, D. Jordanova, B. Henry, M. Le Goff, D. Dimov, and T. Tsacheva. Magnetism of cigarette ashes. *Journal of Magnetism and Magnetic Materials*, 301(1):50–66, 2006. ISSN 0304-8853. doi: https://doi.org/10.1016/j.jmmm.2005.06.008.

C. Junker and C. Liousse. A global emission inventory of carbonaceous aerosol from historic records of fossil fuel and biofuel consumption for the period 1860-1997. *Atmospheric Chemistry and Physics*, 8(5):1195–1207, 2008. doi: 10.5194/acp-8-1195-2008.

K. K. Kalimeri, D. E. Saraga, V. D. Lazaridis, N. A. Legkas, D. A. Missia, E. I. Tolis, and J. G. Bartzis. Indoor air quality investigation of the school environment and estimated health risks: Two-season measurements in primary schools in Kozani, Greece. *Atmospheric Pollution Research*, 7(6):1128–1142, 2016. ISSN 13091042. doi: 10.1016/j.apr.2016.07.002. URL `http://dx.doi.org/10.1016/j.apr.2016.07.002`.

K. K. Kalimeri, J. G. Bartzis, and D. E. Saraga. Commuters' personal exposure to ambient and indoor ozone in Athens, Greece. *Environments - MDPI*, 4(3):1–10, 2017. ISSN 20763298. doi: 10.3390/environments4030053.

K. K. Kalimeri, J. G. Bartzis, I. A. Sakellaris, and E. de Oliveira Fernandes. Investigation of the pm2. 5, no2 and o3 i/o ratios for office and school microenvironments. *Environmental research*, 179:108791, 2019. doi: 10.1016/j.envres.2019.108791.

F. Kardel, K. Wuyts, B. Maher, and R. Samson. Intra-urban spatial variation of magnetic particles: Monitoring via leaf saturation isothermal remanent magnetisation (sirm). *Atmospheric Environment*, 55:111–120, 2012. ISSN 1352-2310. doi: https://doi.org/10.1016/j.atmosenv.2012.03.025.

C. Karr, T. Lumley, A. Schreuder, R. Davis, T. Larson, B. Ritz, and J. Kaufman. Effects of Subchronic and Chronic Exposure to Ambient Air Pollutants on Infant Bronchiolitis. *American Journal of Epidemiology*, 165(5):553–560, 12 2006. ISSN 0002-9262. doi: 10.1093/aje/kwk032.

K. Katanoda, T. Sobue, H. Satoh, K. Tajima, T. Suzuki, H. Nakatsuka, T. Takezaki, T. Nakayama, H. Nitta, K. Tanabe, and S. Tominaga. An association between long-term exposure to ambient air pollution and mortality from lung cancer and respiratory diseases in japan. *Journal of Epidemiology*, 21(2):132–143, 2011. doi: 10.2188/jea.JE20100098.

I. Kawachi and L. F. Berkman. *Neighborhoods and health*. Oxford University Press, 2003.

S. Keita, C. Liousse, V. Yoboué, P. Dominutti, B. Guinot, E.-M. Assamoi, A. Borbon, S. L. Haslett, L. Bouvier, A. Colomb, H. Coe, A. Akpo, J. Adon, J. Bahino, M. Doumbia, J. Djossou, C. Galy-Lacaux, E. Gardrat, S. Gnamien, J.-F. Léon, M. Ossohou, E. N'Datchoh, and L. Roblou. Particle and VOC emission factor measurements for anthropogenic sources in West Africa. *Atmospheric Chemistry and Physics*, 18(10):7691–7708, 2018. ISSN 1680-7324. doi: 10.5194/acp-18-7691-2018.

E. Kelepertzis, A. Argyraki, F. Botsou, E. Aidona, Ábel Szabó, and C. Szabó. Tracking the occurrence of anthropogenic magnetic particles and potentially toxic elements (ptes) in house dust using magnetic and geochemical analyses. *Environmental Pollution*, 245: 909–920, 2019. ISSN 0269-7491. doi: https://doi.org/10.1016/j.envpol.2018.11.072.

F. J. Kelly and J. C. Fussell. Air pollution and public health: emerging hazards and improved understanding of risk. *Environmental geochemistry and health*, 37(4):631–649, 2015. doi: 10.1007/s10653-015-9720-1.

H. Khreis, C. Kelly, J. Tate, R. Parslow, K. Lucas, and M. Nieuwenhuijsen. Exposure to traffic-related air pollution and risk of development of childhood asthma: a systematic review and meta-analysis. *Environment international*, 100:1–31, 2017. doi: http://dx.doi.org/10.1016/j.envint.2016.11.012.

J. J. Kim, S. Smorodinsky, M. Lipsett, B. C. Singer, A. T. Hodgson, and B. Ostro. Traffic-related air pollution near busy roads: the east bay children's respiratory health study. *American journal of respiratory and critical care medicine*, 170(5):520–526, 2004. doi: 10.1164/rccm.200403-281OC.

K.-H. Kim, E. Kabir, and S. Kabir. A review on the human health impact of airborne particulate matter. *Environment international*, 74:136–143, 2015. doi: 10.1016/j.envint.2014.10.005.

W. Kim, S.-J. Doh, and Y. Yu. Anthropogenic contribution of magnetic particulates in urban roadside dust. *Atmospheric Environment*, 43(19):3137–3144, 2009. ISSN 1352-2310. doi: https://doi.org/10.1016/j.atmosenv.2009.02.056.

J. W. King and J. E. Channell. Sedimentary magnetism, environmental magnetism, and magnetostrarigraphy. *Reviews of Geophysics*, 29(S1):358–370, 1991. doi: https://doi.org/10.1002/rog.1991.29.s1.358.

N. E. Klepeis, W. C. Nelson, W. R. Ott, J. P. Robinson, A. M. Tsang, P. Switzer, J. V. Behar, S. C. Hern, and W. H. Engelmann. The national human activity pattern survey (nhaps): a resource for assessing exposure to environmental pollutants. *Journal of Exposure Science & Environmental Epidemiology*, 11(3):231–252, 2001. doi: https://doi.org/10.1038/sj.jea.7500165.

P. Knippertz, H. Coe, J. C. Chiu, M. J. Evans, A. H. Fink, N. Kalthoff, C. Liousse, C. Mari, R. P. Allan, B. Brooks, S. Danour, C. Flamant, O. O. Jegede, F. Lohou, and J. H. Marsham. The DACCIWA Project: Dynamics–Aerosol–Chemistry–Cloud Interactions in West Africa. *Bulletin of the American Meteorological Society*, 96(9):1451–1460, 2015a. ISSN 0003-0007. doi: 10.1175/BAMS-D-14-00108.1.

P. Knippertz, M. J. Evans, P. R. Field, A. H. Fink, C. Liousse, and J. H. Marsham. The possible role of local air pollution in climate change in West Africa. *Nature Climate Change*, 5(9):815–822, 2015b. ISSN 1758-6798. doi: 10.1038/nclimate2727.

R. Kovacevic, V. Tasic, M. Zivkovc, N. Zivkovic, A. Dordevc, D. Manojlović, and M. Jovasevic-Stojanovic. Koncentracija suspendovanih čestica (PM10 I PM2.5) I NJIHOV odnos unutra/spolja u odabranim obrazovnim ustanovama u Nišu. *Chemical Industry and Chemical Engineering Quarterly*, 21(1-2):149–158, 2015. ISSN 22177434. doi: 10.2298/CICEQ140207013K.

P. P. Kruiver and H. F. Passier. Coercivity analysis of magnetic phases in sapropel S1 related to variations in redox conditions, including an investigation of the S ratio. *Geochemistry, Geophysics, Geosystems*, 2(12), 2001. ISSN 15252027. doi: 10.1029/2001GC000181.

P. Kumar, M. Ketzel, S. Vardoulakis, L. Pirjola, and R. Britter. Dynamics and dispersion modelling of nanoparticles from road traffic in the urban atmospheric environment—a review. *Journal of Aerosol Science*, 42(9):580–603, 2011. ISSN 0021-8502. doi: https://doi.org/10.1016/j.jaerosci.2011.06.001.

J. Kuula, T. Mäkelä, M. Aurela, K. Teinilä, S. Varjonen, O. González, and H. Timonen. Laboratory evaluation of particle-size selectivity of optical low-cost particulate matter sensors. *Atmospheric Measurement Techniques*, 13(5):2413–2423, 2020. doi: 10.5194/amt-13-2413-2020.

H. K. Lai, L. Bayer-Oglesby, R. Colvile, T. Götschi, M. J. Jantunen, N. Künzli, E. Kulinskaya, C. Schweizer, and M. J. Nieuwenhuijsen. Determinants of indoor air concentrations of PM2.5, black smoke and NO2 in six European cities (EXPOLIS study). *Atmospheric Environment*, 40(7):1299–1313, 2006. ISSN 13522310. doi: 10.1016/j.atmosenv.2005.10.030.

L. Lazić, M. A. Urošević, Z. Mijić, G. Vuković, and L. Ilić. Traffic contribution to air pollution in urban street canyons: Integrated application of the ospm, moss biomonitoring and spectral analysis. *Atmospheric Environment*, 141:347–360, 2016. ISSN 1352-2310. doi: https://doi.org/10.1016/j.atmosenv.2016.07.008.

M. Lebowitz. Epidemiological studies of the respiratory effects of air pollution. *European Respiratory Journal*, 9(5):1029–1054, 1996. URL `https://erj.ersjournals.com/content/9/5/1029`.

J. T. Lee, J. Y. Son, H. Kim, and S. Y. Kim. Effect of air pollution on asthma-related hospital admissions for children by socioeconomic status associated with area of residence. *Archives of Environmental and Occupational Health*, 61(3):123–130, 2006. ISSN 21544700. doi: 10.3200/AEOH.61.3.123-130.

W. Lefebvre, M. Van Poppel, B. Maiheu, S. Janssen, and E. Dons. Evaluation of the rio-ifdm-street canyon model chain. *Atmospheric Environment*, 77:325–337, 2013. doi: https://doi.org/10.1016/j.atmosenv.2013.05.026.

E. Lehndorff, M. Urbat, and L. Schwark. Accumulation histories of magnetic particles on pine needles as function of air quality. *Atmospheric Environment*, 40(36):7082–7096, 2006. ISSN 1352-2310. doi: https://doi.org/10.1016/j.atmosenv.2006.06.008.

A. d. S. Leite, C. A. Mendonça, P. L. Moraes, and A. T. Ustra. A procedure for quantitative characterization of superparamagnetic minerals in environmental magnetism. *Geophysical Journal International*, 215(3):1974–1984, 2018. ISSN 1365246X. doi: 10.1093/gji/ggy395.

A. d. S. Leite, J.-F. Léon, M. Macouin, S. Rousse, R. I. F. d. Trindade, A. Proietti, L. Drigo, P. Y. J. Antonio, A. B. Akpo, V. Yoboué, et al. Pm2. 5 magnetic properties in relation

to urban combustion sources in southern west africa. *Atmosphere*, 12(4):496, 2021. doi: 10.3390/atmos12040496.

M. I. Lélé, L. M. Leslie, and P. J. Lamb. Analysis of Low-Level Atmospheric Moisture Transport Associated with the West African Monsoon. *Journal of Climate*, 28(11):4414–4430, 2015. ISSN 0894-8755, 1520-0442. doi: 10.1175/JCLI-D-14-00746.1.

J.-F. Léon, A. B. Akpo, M. Bedou, J. Djossou, M. Bodjrenou, V. Yoboué, and C. Liousse. $PM_{2.5}$ surface concentrations in southern West African urban areas based on sun photometer and satellite observations. *Atmospheric Chemistry and Physics*, 21(3):1815–1834, 2021. ISSN 1680-7316. doi: 10.5194/acp-21-1815-2021.

X. Li, T. R. Dallmann, A. A. May, C. O. Stanier, A. P. Grieshop, E. M. Lipsky, A. L. Robinson, and A. A. Presto. Size distribution of vehicle emitted primary particles measured in a traffic tunnel. *Atmospheric Environment*, 191(June):9–18, 2018. ISSN 18732844. doi: 10.1016/j.atmosenv.2018.07.052. URL `https://doi.org/10.1016/j.atmosenv.2018.07.052`.

A. Liati, S. S. Pandurangi, K. Boulouchos, D. Schreiber, and Y. Arroyo Rojas Dasilva. Metal nanoparticles in diesel exhaust derived by in-cylinder melting of detached engine fragments. *Atmospheric Environment*, 101:34–40, 2015. ISSN 18732844. doi: 10.1016/j.atmosenv.2014.11.014.

J. Limo, P. Paturi, and J. Mäkinen. Magnetic biomonitoring with moss bags to assess stop-and-go traffic induced particulate matter and heavy metal concentrations. *Atmospheric Environment*, 195:187–195, 2018. doi: 10.1016/j.atmosenv.2018.09.062.

C. Liousse, E. Assamoi, P. Criqui, C. Granier, and R. Rosset. Explosive growth in African combustion emissions from 2005 to 2030. *Environmental Research Letters*, 9(3):035003, 2014. ISSN 1748-9326. doi: 10.1088/1748-9326/9/3/035003.

H. Liu, Y. Yan, H. Chang, H. Chen, L. Liang, X. Liu, X. Qiang, and Y. Sun. Magnetic signatures of natural and anthropogenic sources of urban dust aerosol. *Atmospheric Chemistry and Physics*, 19(2):731–745, 2019a. doi: 10.5194/acp-19-731-2019.

M. Liu, D. Fan, N. Bi, X. Sun, and Y. Tian. Impact of water-sediment regulation on the transport of heavy metals from the yellow river to the sea in 2015. *Science of The Total Environment*, 658:268–279, 2019b. ISSN 0048-9697. doi: https://doi.org/10.1016/j.scitotenv.2018.12.170. URL `https://www.sciencedirect.com/science/article/pii/S0048969718350150`.

L. Lombardo, M. Parvis, E. Angelini, and S. Grassini. An optical sampling system for distributed atmospheric particulate matter. *IEEE Transactions on Instrumentation and Measurement*, 68(7):2396–2403, 2019. doi: 10.1109/TIM.2019.2890885.

C. M. Long, H. H. Suh, and P. Koutrakis. Characterization of indoor particle sources using continuous mass and size monitors. *Journal of the Air & Waste Management Association*, 50(7):1236–1250, 2000. doi: 10.1080/10473289.2000.10464154. URL `https://doi.org/10.1080/10473289.2000.10464154`.

M. Loubet, D. Baque, O. Priscia, and B. Dupre. XIIth international conference on Heavy metals in the environment; Volume II. 107:793–796, 2003. doi: 10.1051/jp4:20030420. URL `https://jp4.journaldephysique.org/en/`.

R. Lyons, F. Oldfield, and E. Williams. Mineral magnetic properties of surface soils and sands across four North African transects and links to climatic gradients. *Geochemistry, Geophysics, Geosystems*, 11(8), 2010. ISSN 15252027. doi: 10.1029/2010GC003183.

T. A. Machac, C. W. Zanner, and C. E. Geiss. Time dependent IRM acquisition as a tool to quantify the abundance of ultrafine superparamagnetic magnetite in loessic soils. *Geophysical Journal International*, 169(2):483–489, 05 2007. doi: 10.1111/j.1365-246X.2007.03355.x.

J. Madureira, I. Paciência, and E. De Oliveira Fernandes. Levels and indoor-outdoor relationships of size-specific particulate matter in naturally ventilated portuguese schools. *Journal of Toxicology and Environmental Health - Part A: Current Issues*, 75(22-23):1423–1436, 2012. ISSN 15287394. doi: 10.1080/15287394.2012.721177.

T. Magiera, M. Jabłońska, Z. Strzyszcz, and M. Rachwal. Morphological and mineralogical forms of technogenic magnetic particles in industrial dusts. *Atmospheric Environment*, 45 (25):4281–4290, 2011. ISSN 13522310. doi: 10.1016/j.atmosenv.2011.04.076.

S. Mahajan, P. Kumar, J. A. Pinto, A. Riccetti, K. Schaaf, G. Camprodon, V. Smári, A. Passani, and G. Forino. A citizen science approach for enhancing public understanding of air pollution. *Sustainable Cities and Society*, 52(June 2019):101800, 2020. ISSN 22106707. doi: 10.1016/j.scs.2019.101800.

S. Mahajan, C. H. Luo, D. Y. Wu, and L. J. Chen. From Do-It-Yourself (DIY) to Do-It-Together (DIT): Reflections on designing a citizen-driven air quality monitoring framework in Taiwan. *Sustainable Cities and Society*, 66(July 2020):102628, 2021. ISSN 22106707. doi: 10.1016/j.scs.2020.102628.

B. Maher. The magnetic properties of quaternary aeolian dusts and sediments, and their palaeoclimatic significance. *Aeolian Research*, 3(2):87–144, 2011. ISSN 1875-9637. doi: https://doi.org/10.1016/j.aeolia.2011.01.005.

B. A. Maher. Magnetic properties of some synthetic sub-micron magnetites. *Geophysical Journal International*, 94(1):83–96, 07 1988. ISSN 0956-540X. doi: 10.1111/j.1365-246X.1988.tb03429.x.

B. A. Maher, I. A. M. Ahmed, V. Karloukovski, D. A. MacLaren, P. G. Foulds, D. Allsop, D. M. A. Mann, R. Torres-Jardón, and L. Calderon-Garciduenas. Magnetite pollution nanoparticles in the human brain. *Proceedings of the National Academy of Sciences*, 113 (39):10797–10801, 2016. ISSN 0027-8424. doi: 10.1073/pnas.1605941113.

B. A. Maher, V. O'Sullivan, J. Feeney, T. Gonet, and R. Anne Kenny. Indoor particulate air pollution from open fires and the cognitive function of older people. *Environmental Research*, 192:110298, 2021. ISSN 0013-9351. doi: https://doi.org/10.1016/j.envres.2020.110298.

L. Mantovani, M. Tribaudino, M. Solzi, V. Barraco, E. De Munari, and C. Pironi. Magnetic and SEM-EDS analyses of Tilia cordata leaves and PM10 filters as a complementary source of information on polluted air: Results from the city of Parma (Northern Italy). *Environmental Pollution*, 239:777–787, 2018. ISSN 18736424. doi: 10.1016/j.envpol.2018.04.055.

E. A. Marais, D. J. Jacob, K. Wecht, C. Lerot, L. Zhang, K. Yu, T. P. Kurosu, K. Chance, and B. Sauvage. Anthropogenic emissions in Nigeria and implications for atmospheric ozone pollution: A view from space. *Atmospheric Environment*, 99:32–40, 2014. ISSN 1352-2310. doi: 10.1016/j.atmosenv.2014.09.055.

D. C. Marié, M. A. Chaparro, J. M. Lavornia, A. M. Sinito, A. G. Castañeda Miranda, J. D. Gargiulo, M. A. Chaparro, and H. N. Böhnel. Atmospheric pollution assessed by in situ measurement of magnetic susceptibility on lichens. *Ecological Indicators*, 95(August): 831–840, 2018. ISSN 1470160X. doi: 10.1016/j.ecolind.2018.08.029. URL `https://doi.org/10.1016/j.ecolind.2018.08.029`.

V. Martins, T. Faria, E. Diapouli, M. I. Manousakas, K. Eleftheriadis, M. Viana, and S. M. Almeida. Relationship between indoor and outdoor size-fractionated particulate matter in urban microenvironments: Levels, chemical composition and sources. *Environmental Research*, 183(February):109203, 2020. ISSN 10960953. doi: 10.1016/j.envres.2020.109203.

J. Matzka and B. A. Maher. Magnetic biomonitoring of roadside tree leaves: Identification of spatial and temporal variations in vehicle-derived particulates. *Atmospheric Environment*, 33(28):4565–4569, 1999. ISSN 13522310. doi: 10.1016/S1352-2310(99)00229-0.

D. P. Maxbauer, J. M. Feinberg, and D. L. Fox. Max unmix: A web application for unmixing magnetic coercivity distributions. *Computers and Geosciences*, 95:140–145, 2016. ISSN 0098-3004. doi: https://doi.org/10.1016/j.cageo.2016.07.009. URL `https://www.sciencedirect.com/science/article/pii/S0098300416301893`.

R. G. McClean and W. Kean. Contributions of wood ash magnetism to archaeomagnetic properties of fire pits and hearths. *Earth and Planetary Science Letters*, 119(3):387–394, 1993. ISSN 0012-821X. doi: https://doi.org/10.1016/0012-821X(93)90146-Z.

C. D. McClure and D. A. Jaffe. US particulate matter air quality improves except in wildfire-prone areas. *Proceedings of the National Academy of Sciences*, 115(31):7901–7906, 2018. ISSN 0027-8424, 1091-6490. doi: 10.1073/pnas.1804353115.

G. McIntosh, M. Gómez-Paccard, and M. L. Osete. The magnetic properties of particles deposited on Platanus x hispanica leaves in Madrid, Spain, and their temporal and spatial variations. *Science of the Total Environment*, 382(1):135–146, 2007. ISSN 00489697. doi: 10.1016/j.scitotenv.2007.03.020.

A. Meetham. Atmospheric pollution in leicester. *DSIR Tech. Paper*, 1, 1945.

M. J. Mendell and G. A. Heath. Do indoor pollutants and thermal conditions in schools influence student performance? a critical review of the literature. *Indoor air*, 15(1):27–52, 2005. doi: https://doi.org/10.1111/j.1600-0668.2004.00320.x.

L. Menut, C. Flamant, S. Turquety, A. Deroubaix, P. Chazette, and R. Meynadier. Impact of biomass burning on pollutant surface concentrations in megacities of the gulf of guinea. *Atmospheric Chemistry and Physics*, 18(4):2687–2707, 2018. ISSN 1680-7316. doi: 10.5194/acp-18-2687-2018.

Z. M. Migaszewski, A. Galuszka, S. Dolegowska, and A. Michalik. Abundance and fate of glass microspheres in river sediments and roadside soils: Lessons from the swietokrzyskie region case study (south-central poland). *Science of The Total Environment*, 821:153410, 2022. ISSN 0048-9697. doi: https://doi.org/10.1016/j.scitotenv.2022.153410. URL `https://www.sciencedirect.com/science/article/pii/S0048969722005022`.

K. A. Miller, D. S. Siscovick, L. Sheppard, K. Shepherd, J. H. Sullivan, G. L. Anderson, and J. D. Kaufman. Long-term exposure to air pollution and incidence of cardiovascular events in women. *New England Journal of Medicine*, 356(5):447–458, 2007. doi: https://doi.org/10.1056/NEJMoa054409.

A. Miller-Rushing, R. Primack, and R. Bonney. The history of public participation in ecological research. *Frontiers in Ecology and the Environment*, 10(6):285–290, 2012. ISSN 15409295. doi: 10.1890/110278.

V. K. Mishra, P. Kumar, M. Van Poppel, N. Bleux, E. Frijns, M. Reggente, P. Berghmans, L. Int Panis, and R. Samson. Wintertime spatio-temporal variation of ultrafine particles in a belgian city. *Science of The Total Environment*, 431:307–313, 2012. ISSN 0048-9697. doi: https://doi.org/10.1016/j.scitotenv.2012.05.054.

R. Mitchell and B. A. Maher. Evaluation and application of biomagnetic monitoring of traffic-derived particulate pollution. *Atmospheric Environment*, 43(13):2095–2103, 2009. doi: 10.1016/j.atmosenv.2009.01.042.

R. Mitchell, B. Maher, and R. Kinnersley. Rates of particulate pollution deposition onto leaf surfaces: Temporal and inter-species magnetic analyses. *Environmental Pollution*, 158 (5):1472–1478, 2010. ISSN 0269-7491. doi: https://doi.org/10.1016/j.envpol.2009.12.029. URL `https://www.sciencedirect.com/science/article/pii/S026974910900637X`.

C. Monn, A. Fuchs, D. Högger, M. Junker, D. Kogelschatz, N. Roth, and H. U. Wanner. Particulate matter less than 10 μm (PM10) and fine particles less than 2.5 μm (PM2.5): Relationships between indoor, outdoor and personal concentrations. *Science of the Total Environment*, 208(1-2):15–21, 1997. ISSN 00489697. doi: 10.1016/S0048-9697(97)00271-4.

R. Morello-Frosch, M. Pastor, C. Porras, and J. Sadd. Environmental justice and regional inequality in southern california: implications for future research. *Environmental Health Perspectives*, 110(suppl 2):149–154, 2002. doi: 10.1289/ehp.02110s2149.

E. Moreno, L. Sagnotti, J. Dinarès-Turell, A. Winkler, and A. Cascella. Biomonitoring of traffic air pollution in Rome using magnetic properties of tree leaves. *Atmospheric Environment*, 37(21):2967–2977, 2003. ISSN 13522310. doi: 10.1016/S1352-2310(03)00244-9.

M. Mueller, D. Hasenfratz, O. Saukh, M. Fierz, and C. Hueglin. Statistical modelling of particle number concentration in zurich at high spatio-temporal resolution utilizing data from a mobile sensor network. *Atmospheric Environment*, 126:171–181, 2016. ISSN 1352-2310. doi: https://doi.org/10.1016/j.atmosenv.2015.11.033.

D. Mumovic, J. Palmer, M. Davies, M. Orme, I. Ridley, T. Oreszczyn, C. Judd, R. Critchlow, H. A. Medina, G. Pilmoor, C. Pearson, and P. Way. Winter indoor air quality, thermal comfort and acoustic performance of newly built secondary schools in England. *Building and Environment*, 44(7):1466–1477, 2009. ISSN 03601323. doi: 10.1016/j.buildenv.2008.06.014.

D. Muñoz, B. Aguilar, R. Fuentealba, and M. Préndez. Environmental studies in two communes of santiago de chile by the analysis of magnetic properties of particulate matter deposited on leaves of roadside trees. *Atmospheric Environment*, 152:617–627, 2017. doi: 10.1016/j.atmosenv.2016.12.047.

C. J. L. Murray, A. Y. Aravkin, and P. Z. et al. Global burden of 87 risk factors in 204 countries and territories, 1990–2019: a systematic analysis for the global burden of disease study 2019. *The Lancet*, 396(10258):1223–1249, 2020. ISSN 0140-6736. doi: https://doi.org/10.1016/S0140-6736(20)30752-2.

A. R. Muxworthy, J. Matzka, and N. Petersen. Comparison of magnetic parameters of urban atmospheric particulate matter with pollution and meteorological data. *Atmospheric Environment*, 35(26):4379–4386, 2001. ISSN 13522310. doi: 10.1016/S1352-2310(01)00250-3.

T. Métropole. *Mémento Métropolitain - Zooms communaux*. 2021. doi: https://www.toulouse-metropole.fr/documents/10180/283838/M_mento+M_tropolitain+2021.pdf/a6e2fb23-5259-4edd-8830-1ef89edf9f89.

P. Nafstad, L. L. Håheim, T. Wisløff, F. Gram, B. Oftedal, I. Holme, I. Hjermann, and P. Leren. Urban air pollution and mortality in a cohort of norwegian men. *Environmental Health Perspectives*, 112(5):610–615, 2004. doi: 10.1289/ehp.6684.

J. K. Nagar, A. Akolkar, and R. Kumar. A review on airborne particulate matter and its sources, chemical composition and impact on human respiratory system. *International Journal of Environmental Sciences*, 5(2):447–463, 2014.

R. K. Nakazato, M. P. Esposito, P. Cardoso-Gustavson, P. Bulbovas, A. N. V. Pedroso, P. I. L. S. de Assis, and M. Domingos. Efficiency of biomonitoring methods applying tropical bioindicator plants for assessing the phytoxicity of the air pollutants in SE, Brazil. *Environmental Science and Pollution Research*, 25(20):19323–19337, 2018. ISSN 16147499. doi: 10.1007/s11356-018-2294-6.

W. W. Nazaroff. Indoor Partical Dynamics. *Indoor Air*, 14(7):175–183, 2004. ISSN 1884-5088. URL `https://escholarship.org/uc/item/7sq4x34d{#}author`.

T. N. Nguyen, D. Park, Y. Lee, and Y.-C. Lee. Particulate matter (pm10 and pm2.5) in subway systems: Health-based economic assessment. *Sustainability*, 9(11), 2017. ISSN 2071-1050. doi: 10.3390/su9112135.

X. Niu, B. Guinot, J. Cao, H. Xu, and J. Sun. Particle size distribution and air pollution patterns in three urban environments in Xi'an, China. *Environmental Geochemistry and Health*, 37(5):801–812, 2015. ISSN 1573-2983. doi: 10.1007/s10653-014-9661-0. URL `https://doi.org/10.1007/s10653-014-9661-0`.

E. Nkhama, M. Ndhlovu, J. T. Dvonch, S. Siziya, and K. Voyi. Prevalence and determinants of mucous membrane irritations in a community near a cement factory in zambia: A cross sectional study. *International Journal of Environmental Research and Public Health*, 12 (1):871–887, 2015. ISSN 1660-4601. doi: 10.3390/ijerph120100871. URL `https://www.mdpi.com/1660-4601/12/1/871`.

A. L. Northcross, R. J. Edwards, M. A. Johnson, Z.-M. Wang, K. Zhu, T. Allen, and K. R. Smith. A low-cost particle counter as a realtime fine-particle mass monitor. *Environmental Science: Processes & Impacts*, 15(2):433–439, 2013.

L. Néel. Some theoretical aspects of rock-magnetism. *Advances in Physics*, 4(14):191–243, 1955. doi: 10.1080/00018735500101204.

T. Oluwadairo, L. Whitehead, E. Symanski, C. Bauer, A. Carson, and I. Han. Effects of Road Traffic on the Accuracy and Bias of Low-Cost Particulate Matter Sensor Measurements in Houston, Texas. *International Journal of Environmental Research and Public Health*, 19 (3), 2022. ISSN 16604601. doi: 10.3390/ijerph19031086.

M. S. O'Neill, M. Jerrett, I. Kawachi, J. I. Levy, A. J. Cohen, N. Gouveia, P. Wilkinson, T. Fletcher, L. Cifuentes, J. Schwartz, T. F. Bateson, C. Cann, D. Dockery, D. Gold, F. Laden, S. London, D. Loomis, F. Speizer, S. Van den Eeden, and A. Zanobetti. Health, wealth, and air pollution: Advancing theory and methods. *Environmental Health Perspectives*, 111(16):1861–1870, 2003. ISSN 00916765. doi: 10.1289/ehp.6334.

M.-R. Ouafo-Leumbe, C. Galy-Lacaux, C. Liousse, V. Pont, A. Akpo, T. Doumbia, E. Gardrat, C. Zouiten, L. Sigha-Nkamdjou, and G. E. Ekodeck. Chemical composition and sources of atmospheric aerosols at djougou (benin). *Meteorology and Atmospheric Physics*, 130(5):591–609, 2018. doi: https://doi.org/10.1007/s00703-017-0538-5.

A. Pacitto, L. Stabile, M. Viana, M. Scungio, C. Reche, X. Querol, A. Alastuey, I. Rivas, M. Álvarez-Pedrerol, J. Sunyer, B. L. van Drooge, J. O. Grimalt, R. Sozzi, P. Vigo, and G. Buonanno. Particle-related exposure, dose and lung cancer risk of primary school children in two European countries. *Science of the Total Environment*, 616-617:720–729, 2018. ISSN 18791026. doi: 10.1016/j.scitotenv.2017.10.256. URL `https://doi.org/10.1016/j.scitotenv.2017.10.256`.

D. Paraskevopoulou, E. Liakakou, E. Gerasopoulos, C. Theodosi, and N. Mihalopoulos. Long-term characterization of organic and elemental carbon in the PM2.5 fraction: The case of Athens, Greece. *Atmospheric Chemistry and Physics*, 14(23):13313–13325, 2014. ISSN 16807324. doi: 10.5194/acp-14-13313-2014.

M. Pardé. Périodicité des grandes inondations et crues exceptionnelles. *Revue de géographie alpine*, 16(2):499–519, 1928.

A. Parviainen, E. M. Papaslioti, M. Casares-Porcel, and C. J. Garrido. Antimony as a tracer of non-exhaust traffic emissions in air pollution in Granada (S Spain) using lichen bioindicators. *Environmental Pollution*, 263:114482, 2020. ISSN 18736424. doi: 10.1016/j.envpol.2020.114482. URL `https://doi.org/10.1016/j.envpol.2020.114482`.

H. Patashnick and E. G. Rupprecht. Continuous pm-10 measurements using the tapered element oscillating microbalance. *Journal of the Air & Waste Management Association*, 41(8):1079–1083, 1991. doi: 10.1080/10473289.1991.10466903.

A. Pattammattel, V. J. Leppert, P. Aronstein, M. Robinson, A. Mousavi, C. Sioutas, H. J. Forman, and P. A. O'Day. Iron speciation in particulate matter (pm2.5) from urban los angeles using spectro-microscopy methods. *Atmospheric Environment*, 245:117988, 2021. ISSN 1352-2310. doi: https://doi.org/10.1016/j.atmosenv.2020.117988.

R. D. Peng, M. L. Bell, A. S. Geyh, A. McDermott, S. L. Zeger, J. M. Samet, and F. Dominici. Emergency admissions for cardiovascular and respiratory diseases and the chemical composition of fine particle air pollution. *Environmental Health Perspectives*, 117(6):957–963, 2009. doi: 10.1289/ehp.0800185.

J. Perelló, A. Cigarini, J. Vicens, I. Bonhoure, D. Rojas-Rueda, M. J. Nieuwenhuijsen, M. Cirach, C. Daher, J. Targa, and A. Ripoll. Large-scale citizen science provides high-resolution nitrogen dioxide values and health impact while enhancing community knowledge and collective action. *Science of the Total Environment*, 789, 2021. ISSN 18791026. doi: 10.1016/j.scitotenv.2021.147750.

S. A. PERLIN, K. E. N. SEXTON, and D. W. S. WONG. An examination of race and poverty for populations living near industrial sources of air pollution. *Journal of Exposure Science & Environmental Epidemiology*, 9(1):29–48, 1999. ISSN 1559-064X. doi: 10.1038/sj.jea.7500024. URL `https://doi.org/10.1038/sj.jea.7500024`.

S. A. Perlin, D. Wong, and K. Sexton. Residential proximity to industrial sources of air pollution: Interrelationships among race, poverty, and age. *Journal of the Air & Waste Management Association*, 51(3):406–421, 2001. doi: 10.1080/10473289.2001.10464271.

P. Pihkala. Eco-anxiety and environmental education. *Sustainability*, 12(23), 2020. ISSN 2071-1050. doi: 10.3390/su122310149.

S. V. Pirela, G. A. Sotiriou, D. Bello, M. Shafer, K. Lee, V. Castranova, T. Thomas, and P. Demokritou. Enabled Products. 9(6):760–768, 2015. doi: 10.3109/17435390.2014.976602.Consumer.

C. A. Pope, M. J. Thun, M. M. Namboodiri, D. W. Dockery, J. S. Evans, F. E. Speizer, and C. W. Heath. Particulate air pollution as a predictor of mortality in a prospective study of u.s. adults. *American Journal of Respiratory and Critical Care Medicine*, 151(3_pt_1):669–674, 1995. doi: https://doi.org/10.1164/ajrccm/151.3_Pt_1.669.

C. A. Pope III and D. W. Dockery. Health effects of fine particulate air pollution: lines that connect. *Journal of the Air & Waste Management Association*, 56(6):709–742, 2006. doi: 10.1080/10473289.2006.10464485.

J.-L. Probst and A. Bazerbachi. Transports en solution et en suspension par la garonne supérieure. solute and particulate transports by the upstream part of the garonne river. *Sciences Géologiques, bulletins et mémoires*, 39(1):79–98, 1986.

T. Pulles, H. Denier van der Gon, W. Appelman, and M. Verheul. Emission factors for heavy metals from diesel and petrol used in european vehicles. *Atmospheric Environment*, 61:641–651, 2012. ISSN 1352-2310. doi: https://doi.org/10.1016/j.atmosenv.2012.07.022. URL `https://www.sciencedirect.com/science/article/pii/S1352231012006942`.

Y. Qi, F. K. S. Chan, C. Thorne, E. O'donnell, C. Quagliolo, E. Comino, A. Pezzoli, L. Li, J. Griffiths, Y. Sang, and M. Feng. Addressing challenges of urban water management in chinese sponge cities via nature-based solutions. *Water (Switzerland)*, 12(10):1–24, 2020. ISSN 20734441. doi: 10.3390/w12102788.

O. Raaschou-Nielsen, Z. J. Andersen, M. Hvidberg, S. S. Jensen, M. Ketzel, M. Sørensen, S. Loft, K. Overvad, and A. Tjønneland. Lung cancer incidence and long-term exposure to air pollution from traffic. *Environmental Health Perspectives*, 119(6):860–865, 2011. doi: 10.1289/ehp.1002353.

O. Raaschou-Nielsen, Z. J. Andersen, R. Beelen, E. Samoli, M. Stafoggia, G. Weinmayr, B. Hoffmann, P. Fischer, M. J. Nieuwenhuijsen, B. Brunekreef, et al. Air pollution and lung cancer incidence in 17 european cohorts: prospective analyses from the european study of cohorts for air pollution effects (escape). *The lancet oncology*, 14(9):813–822, 2013. doi: http://doi.org/10.1016/S1470-2045(13)70279-1.

M. Rachwał, J. Rybak, and W. Rogula-Kozłowska. Magnetic susceptibility of spider webs as a proxy of airborne metal pollution. *Environmental Pollution*, 234:543–551, 2018. ISSN 0269-7491. doi: https://doi.org/10.1016/j.envpol.2017.11.088. URL `https://www.sciencedirect.com/science/article/pii/S0269749117332530`.

E. Remoundaki, P. Kassomenos, E. Mantas, N. Mihalopoulos, M. Tsezos, et al. Composition and mass closure of pm2. 5 in urban environment (athens, greece). *Aerosol and Air Quality Research*, 13(1):72–82, 2013. doi: https://doi.org/10.4209/aaqr.2012.03.0054.

M. A. Revuelta, G. McIntosh, J. Pey, N. Pérez, X. Querol, and A. Alastuey. Partitioning of magnetic particles in PM10, PM2.5 and PM1 aerosols in the urban atmosphere of Barcelona (Spain). *Environmental Pollution*, 188:109–117, 2014. ISSN 02697491. doi: 10.1016/j.envpol.2014.01.025.

D. Rice and S. Barone Jr. Critical periods of vulnerability for the developing nervous system: evidence from humans and animal models. *Environmental health perspectives*, 108(suppl 3):511–533, 2000. doi: 10.1289/ehp.00108s3511.

I. Rivas, M. Viana, T. Moreno, M. Pandolfi, F. Amato, C. Reche, L. Bouso, M. Àlvarez-Pedrerol, A. Alastuey, J. Sunyer, and X. Querol. Child exposure to indoor and outdoor air pollutants in schools in Barcelona, Spain. *Environment International*, 69:200–212, 2014. ISSN 18736750. doi: 10.1016/j.envint.2014.04.009.

T. Ronkko, L. Pirjola, L. Ntziachristos, J. Heikkila, P. Karjalainen, R. Hillamo, and J. Keskinen. Vehicle engines produce exhaust nanoparticles even when not fueled. *Environmental science & technology*, 48(3):2043–2050, 2014.

S. Rovelli, A. Cattaneo, C. P. Nuzzi, A. Spinazzè, S. Piazza, P. Carrer, and D. M. Cavallo. Airborne particulate matter in school classrooms of northern Italy. *International Journal of Environmental Research and Public Health*, 11(2):1398–1421, 2014. ISSN 16604601. doi: 10.3390/ijerph110201398.

C. Russell and J. Oakley. Engaging the emotional dimensions of environmental education. *Canadian Journal of Environmental Education (CJEE)*, 21:13–22, 2016.

R. Rutkowski, J. S. Bihałowicz, M. Rachwał, W. Rogula-Kozłowska, and J. Rybak. Magnetic susceptibility of spider webs and dust: Preliminary study in wrocław, poland. *Minerals*, 10 (11), 2020. ISSN 2075-163X. doi: 10.3390/min10111018. URL `https://www.mdpi.com/2075-163X/10/11/1018`.

C. Sablayrolles, A. Breton, C. Vialle, C. Vignoles, and M. Montréjaud-Vignoles. Priority organic pollutants in the urban water cycle (Toulouse, France). *Water Science and Technology*, 64(3):541–556, 2011. ISSN 02731223. doi: 10.2166/wst.2011.580.

J. Safranek, I. Turcova, M. Branis, and M. Hajek. Exposure of children to aerosol during PE lessons. *Envigogika*, 12(2), 2017. ISSN 1802-3061. doi: 10.14712/18023061.554.

L. Sagnotti and A. Winkler. On the magnetic characterization and quantification of the superparamagnetic fraction of traffic-related urban airborne PM in Rome, Italy. *Atmospheric Environment*, 59:131–140, 2012. ISSN 13522310. doi: 10.1016/j.atmosenv.2012.04.058.

L. Sagnotti, P. Macrì, R. Egli, and M. Mondinio. Magnetic properties of atmospheric particulate matter from automatic air sampler stations in Latium (Italy): Toward a definition of magnetic fingerprints for natural and anthropogenic PM10 sources. *Journal of Geophysical Research: Solid Earth*, 111(12):1–17, 2006. ISSN 21699356. doi: 10.1029/2006JB004508.

L. Sagnotti, J. Taddeucci, A. Winkler, and A. Cavallo. Compositional, morphological, and hysteresis characterization of magnetic airborne particulate matter in Rome, Italy. *Geochemistry, Geophysics, Geosystems*, 10(8), 2009. ISSN 15252027. doi: 10.1029/2009GC002563.

I. Salpeteur and J. Angle. Valeurs de référence pour les teneurs en éléments traces dans les eaux de rivières et les sédiments , obtenues. Atlas géochimique européen * (I). *Environnement, Risques, & Santé*, 9(2):121–135, 2010.

G. Sangiorgi, L. Ferrero, B. Ferrini, C. Lo Porto, M. Perrone, R. Zangrando, A. Gambaro, Z. Lazzati, and E. Bolzacchini. Indoor airborne particle sources and semi-volatile partitioning effect of outdoor fine pm in offices. *Atmospheric Environment*, 65:205–214, 2013. ISSN 1352-2310. doi: https://doi.org/10.1016/j.atmosenv.2012.10.050.

F. Saragnese, L. Lanci, and R. Lanza. Nanometric-sized atmospheric particulate studied by magnetic analyses. *Atmospheric Environment*, 45(2):450–459, 2011. ISSN 13522310. doi: 10.1016/j.atmosenv.2010.09.057.

J. A. Sarnat, K. W. Brown, J. Schwartz, B. A. Coull, and P. Koutrakis. Ambient Gas Concentrations and Personal Particulate Matter Exposures: Implications for Studying the Health Effects of Particles. *Epidemiology*, 16(3), 2005. ISSN 1044-3983. doi: 10.1097/01.ede.0000155505.04775.33.

A. W. Schroth, J. Crusius, E. R. Sholkovitz, and B. C. Bostick. Iron solubility driven by speciation in dust sources to the ocean. *Nature Geoscience*, 2(5):337–340, 2009. ISSN 17520894. doi: 10.1038/ngeo501.

C. Schweizer, R. D. Edwards, L. Bayer-Oglesby, W. J. Gauderman, V. Ilacqua, M. Juhani Jantunen, H. K. Lai, M. Nieuwenhuijsen, and N. Künzli. Indoor time–microenvironment–activity patterns in seven regions of Europe. *Journal of Exposure Science & Environmental Epidemiology*, 17(2):170–181, 2007. ISSN 1559-064X. doi: 10.1038/sj.jes.7500490. URL `https://doi.org/10.1038/sj.jes.7500490`.

S. Sclar and E. Saikawa. Household Air Pollution in a Changing Tibet: A Mixed Methods Ethnography and Indoor Air Quality Measurements. *Environmental Management*, 64(3):353–365, 2019. ISSN 14321009. doi: 10.1007/s00267-019-01194-3.

A. G. Sebastiao, E. J. Wagner, and S. T. Goldsmith. Trace metal sediment loading in the mill creek: A spatial and temporal analysis of vehicular pollutants in suburban waterways. *Applied Geochemistry*, 83:50–61, 2017. ISSN 0883-2927. doi: https://doi.org/10.1016/j.apgeochem.2017.04.001. URL `https://www.sciencedirect.com/science/article/pii/S0883292717301981`. Urban Geochemistry.

J. Seinfeld and S. Pandis. *Atmospheric Chemistry and Physics: From Air Pollution to Climate Change*. Wiley, 2016. ISBN 9781118947401.

S. Semple, A. Apsley, T. A. Ibrahim, S. W. Turner, and J. W. Cherrie. Fine particulate matter concentrations in smoking households: Just how much secondhand smoke do you breathe in if you live with a smoker who smokes indoors? *Tobacco Control*, 24(E3):e205–e211, 2015. ISSN 14683318. doi: 10.1136/tobaccocontrol-2014-051635.

D. Sharma and S. Jain. Impact of intervention of biomass cookstove technologies and kitchen characteristics on indoor air quality and human exposure in rural settings of India. *Environment International*, 123(December 2018):240–255, 2019. ISSN 18736750. doi: 10.1016/j.envint.2018.11.059.

M. Shi, H. Wu, S. Zhang, H. Li, T. Yang, W. Liu, and H. Liu. Weekly cycle of magnetic characteristics of the daily PM2.5 and PM2.5-10 in Beijing, China. *Atmospheric Environment*, 98:357–367, 2014. ISSN 18732844. doi: 10.1016/j.atmosenv.2014.08.079.

Y. Shi, Y. Ji, H. Sun, F. Hui, J. Hu, Y. Wu, J. Fang, H. Lin, J. Wang, H. Duan, and M. Lanza. Nanoscale characterization of PM 2.5 airborne pollutants reveals high adhesiveness and

aggregation capability of soot particles. *Scientific Reports*, 5(April):1–11, 2015. ISSN 20452322. doi: 10.1038/srep11232.

K. Shrey, A. Suchit, D. Deepika, K. Shruti, and R. Vibha. Air pollutants: The key stages in the pathway towards the development of cardiovascular disorders. *Environmental Toxicology and Pharmacology*, 31(1):1–9, 2011. ISSN 1382-6689. doi: https://doi.org/10.1016/j.etap.2010.09.002.

J. Shu, J. A. Dearing, A. P. Morse, L. Yu, and N. Yuan. Determining the sources of atmospheric particles in Shanghai, China, from magnetic and geochemical properties. *Atmospheric Environment*, 35(15):2615–2625, 2001. ISSN 13522310. doi: 10.1016/S1352-2310(00)00454-4.

B. Z. Simkhovich, M. T. Kleinman, and R. A. Kloner. Air pollution and cardiovascular injury: Epidemiology, toxicology, and mechanisms. *Journal of the American College of Cardiology*, 52(9):719–726, 2008. ISSN 0735-1097. doi: https://doi.org/10.1016/j.jacc.2008.05.029.

S. Spassov, R. Egli, F. Heller, D. K. Nourgaliev, and J. Hannam. Magnetic quantification of urban pollution sources in atmospheric particulate matter. *Geophysical Journal International*, 159(2):555–564, 2004. ISSN 0956540X. doi: 10.1111/j.1365-246X.2004.02438.x.

J. Sternbeck, Å. Sjödin, and K. Andréasson. Metal emissions from road traffic and the influence of resuspension - Results from two tunnel studies. *Atmospheric Environment*, 36 (30):4735–4744, 2002. ISSN 13522310. doi: 10.1016/S1352-2310(02)00561-7.

M. Stranger, S. S. Potgieter-Vermaak, and R. Van Grieken. Characterization of indoor air quality in primary schools in Antwerp, Belgium. *Indoor Air*, 18(6):454–463, 2008. ISSN 09056947. doi: 10.1111/j.1600-0668.2008.00545.x.

M. Szabados, Z. Csákó, B. Kotlík, H. Kazmarová, A. Kozajda, A. Jutraz, A. Kukec, P. Otorepec, A. Dongiovanni, A. Di Maggio, et al. Indoor air quality and the associated health risk in primary school buildings in central europe–the inairq study. *Indoor air*, 31(4):989–1003, 2021. doi: https://doi.org/10.1111/ina.12802.

M. Szönyi, L. Sagnotti, and A. M. Hirt. On leaf magnetic homogeneity in particulate matter biomonitoring studies. *Geophysical Research Letters*, 34(6), 2007. doi: https://doi.org/10.1029/2006GL029076.

M. Szönyi, L. Sagnotti, and A. M. Hirt. A refined biomonitoring study of airborne particulate matter pollution in Rome, with magnetic measurements on Quercus Ilex tree leaves. *Geophysical Journal International*, 173(1):127–141, 04 2008. ISSN 0956-540X. doi: 10.1111/j.1365-246X.2008.03715.x.

K. W. Tham. Indoor air quality and its effects on humans—A review of challenges and developments in the last 30 years. *Energy and Buildings*, 130:637–650, 2016. ISSN 03787788. doi: 10.1016/j.enbuild.2016.08.071. URL `http://dx.doi.org/10.1016/j.enbuild.2016.08.071`.

A. Thorpe and R. M. Harrison. Sources and properties of non-exhaust particulate matter from road traffic: A review. *Science of The Total Environment*, 400(1):270–282, 2008. ISSN 0048-9697. doi: https://doi.org/10.1016/j.scitotenv.2008.06.007. URL `https://www.sciencedirect.com/science/article/pii/S004896970800658X`.

P. Thunis, A. Miranda, J. Baldasano, N. Blond, J. Douros, A. Graff, S. Janssen, K. Juda-Rezler, N. Karvosenoja, G. Maffeis, A. Martilli, M. Rasoloharimahefa, E. Real, P. Viaene, M. Volta, and L. White. Overview of current regional and local scale air quality modelling practices: Assessment and planning tools in the eu. *Environmental Science and Policy*, 65:13–21, 2016. ISSN 1462-9011. doi: https://doi.org/10.1016/j.envsci.2016.03.013. Multidisciplinary research findings in support to the EU air quality policy: experiences from the APPRAISAL, SEFIRA and ACCENT-Plus EU FP7 projects.

L. Tofful and C. Perrino. Chemical composition of indoor and outdoor PM2.5 in three schools in the city of Rome. *Atmosphere*, 6(10):1422–1443, 2015. ISSN 20734433. doi: 10.3390/atmos6101422.

L. Tofful, S. Canepari, T. Sargolini, and C. Perrino. Indoor air quality in a domestic environment: Combined contribution of indoor and outdoor PM sources. *Building and Environment*, 202(March):108050, 2021. ISSN 03601323. doi: 10.1016/j.buildenv.2021.108050. URL `https://doi.org/10.1016/j.buildenv.2021.108050`.

A. Tomczak, A. B. Miller, S. A. Weichenthal, T. To, C. Wall, A. van Donkelaar, R. V. Martin, D. L. Crouse, and P. J. Villeneuve. Long-term exposure to fine particulate matter air pollution and the risk of lung cancer among participants of the canadian national breast screening study. *International journal of cancer*, 139(9):1958–1966, 2016. doi: https://doi.org/10.1002/ijc.30255.

Z. Tong, Y. Chen, A. Malkawi, G. Adamkiewicz, and J. D. Spengler. Quantifying the impact of traffic-related air pollution on the indoor air quality of a naturally ventilated building. *Environment International*, 89-90:138–146, 2016. ISSN 18736750. doi: 10.1016/j.envint.2016.01.016. URL `http://dx.doi.org/10.1016/j.envint.2016.01.016`.

M. C. Turner, D. Krewski, C. A. Pope, Y. Chen, S. M. Gapstur, and M. J. Thun. Long-term ambient fine particulate matter air pollution and lung cancer in a large cohort of never-smokers. *American Journal of Respiratory and Critical Care Medicine*, 184(12):1374–1381, 2011. doi: 10.1164/rccm.201106-1011OC.

D. o. E. United Nations and P. D. U. D. D. Social Affairs. *World Urbanization Prospects: The 2014 Revision: Highlights*, volume 32. United Nations New York, 2014. ISBN 978-92-1-151517-6.

D. o. E. United Nations and P. D. U. D. D. Social Affairs. World population prospects 2019: Ten key findings. Technical report, United Nations, 2019.

M. Urbat, E. Lehndorff, and L. Schwark. Biomonitoring of air quality in the cologne conurbation using pine needles as a passive sampler—part i: magnetic properties. *Atmospheric*

Environment, 38(23):3781–3792, 2004. ISSN 1352-2310. doi: https://doi.org/10.1016/j.atmosenv.2004.03.061.

A. Ustra, C. A. Mendonça, A. da Silva Leite, L. Jovane, and R. I. F. Trindade. Quantitative interpretation of the magnetic susceptibility frequency dependence. *Geophysical Journal International*, 213(2):805–814, 01 2018. ISSN 0956-540X. doi: https://doi.org/10.1093/gji/ggy007.

J. Van den Bossche, J. Theunis, B. Elen, J. Peters, D. Botteldooren, and B. De Baets. Opportunistic mobile air pollution monitoring: A case study with city wardens in antwerp. *Atmospheric Environment*, 141:408–421, 2016. ISSN 1352-2310. doi: https://doi.org/10.1016/j.atmosenv.2016.06.063.

B. L. van Drooge, I. Rivas, X. Querol, J. Sunyer, and J. O. Grimalt. Organic air quality markers of indoor and outdoor pm2.5 aerosols in primary schools from barcelona. *International Journal of Environmental Research and Public Health*, 17(10), 2020. ISSN 1660-4601. doi: 10.3390/ijerph17103685. URL `https://www.mdpi.com/1660-4601/17/10/3685`.

D. Varaden, E. Leidland, S. Lim, and B. Barratt. "I am an air quality scientist"– Using citizen science to characterise school children's exposure to air pollution. *Environmental Research*, 201(May):111536, 2021. ISSN 10960953. doi: 10.1016/j.envres.2021.111536.

S. Vardoulakis, B. E. Fisher, K. Pericleous, and N. Gonzalez-Flesca. Modelling air quality in street canyons: a review. *Atmospheric environment*, 37(2):155–182, 2003. doi: https://doi.org/10.1016/S1352-2310(02)00857-9.

J. Vetter. Introduction: Lay participation in the history of scientific observation. *Science in Context*, 24(2):127–141, 2011. ISSN 02698897. doi: 10.1017/S0269889711000032.

L. C. Vezzola, G. Muttoni, M. Merlini, N. Rotiroti, L. Pagliardini, A. M. Hirt, and M. Pelfini. Investigating distribution patterns of airborne magnetic grains trapped in tree barks in Milan, Italy: insights for pollution mitigation strategies. *Geophysical Journal International*, 210(2):989–1000, 05 2017. ISSN 0956-540X. doi: 10.1093/gji/ggx232.

M. Viana, W. Maenhaut, H. M. ten Brink, X. Chi, E. Weijers, X. Querol, A. Alastuey, P. Mikuška, and Z. Večeřa. Comparative analysis of organic and elemental carbon concentrations in carbonaceous aerosols in three European cities. *Atmospheric Environment*, 41 (28):5972–5983, 2007. ISSN 13522310. doi: 10.1016/j.atmosenv.2007.03.035.

M. Viana, I. Rivas, X. Querol, A. Alastuey, M. Álvarez-Pedrerol, L. Bouso, C. Sioutas, and J. Sunyer. Partitioning of trace elements and metals between quasi-ultrafine, accumulation and coarse aerosols in indoor and outdoor air in schools. *Atmospheric Environment*, 106: 392–401, 2015. ISSN 18732844. doi: 10.1016/j.atmosenv.2014.07.027.

E. D. Vicente, A. M. Vicente, M. Evtyugina, A. I. Calvo, F. Oduber, C. Blanco Alegre, A. Castro, R. Fraile, T. Nunes, F. Lucarelli, G. Calzolai, S. Nava, and C. A. Alves. Impact of vacuum cleaning on indoor air quality. *Building and Environment*, 180(June), 2020. ISSN 03601323. doi: 10.1016/j.buildenv.2020.107059.

J. Viers, B. Dupré, and J. Gaillardet. Chemical composition of suspended sediments in world rivers: New insights from a new database. *Science of The Total Environment*, 407 (2):853–868, 2009. ISSN 0048-9697. doi: https://doi.org/10.1016/j.scitotenv.2008.09.053.

C. Vornanen-Winqvist, K. Järvi, M. A. Andersson, C. Duchaine, V. Létourneau, O. Kedves, L. Kredics, R. Mikkola, J. Kurnitski, and H. Salonen. Exposure to indoor air contaminants in school buildings with and without reported indoor air quality problems. *Environment International*, 141(October 2019):105781, 2020. ISSN 18736750. doi: 10.1016/j.envint.2020.105781.

T. Wainman, J. Zhang, C. J. Weschler, and P. J. Lioy. Ozone and limonene in indoor air: a source of submicron particle exposure. *Environmental Health Perspectives*, 108(12): 1139–1145, 2000. doi: 10.1289/ehp.001081139.

J. Wang, S. Li, H. Li, X. Qian, X. Li, X. Liu, H. Lu, C. Wang, and Y. Sun. Trace metals and magnetic particles in pm 2.5: Magnetic identification and its implications. *Scientific Reports*, 7(1):1–11, 2017. doi: https://doi.org/10.1038/s41598-017-08628-0.

X. Wang, R. Løvlie, X. Zhao, Z. Yang, F. Jiang, and S. Wang. Quantifying ultrafine pedogenic magnetic particles in chinese loess by monitoring viscous decay of superparamagnetism. *Geochemistry, Geophysics, Geosystems*, 11(10), 2010. doi: https://doi.org/10.1029/2010GC003194.

M. S. Waring. Secondary organic aerosol in residences: predicting its fraction of fine particle mass and determinants of formation strength. *Indoor Air*, 24(4):376–389, 2014. doi: https://doi.org/10.1111/ina.12092.

M. S. Waring and J. A. Siegel. The influence of hvac systems on indoor secondary organic aerosol formation. *Ashrae Transactions*, 116(1), 2010.

M. S. Waring and J. A. Siegel. Indoor secondary organic aerosol formation initiated from reactions between ozone and surface-sorbed d-limonene. *Environmental science & technology*, 47(12):6341–6348, 2013. doi: https://doi.org/10.1021/es400846d.

M. S. Waring, J. R. Wells, and J. A. Siegel. Secondary organic aerosol formation from ozone reactions with single terpenoids and terpenoid mixtures. *Atmospheric Environment*, 45(25): 4235–4242, 2011. ISSN 1352-2310. doi: https://doi.org/10.1016/j.atmosenv.2011.05.001. URL `https://www.sciencedirect.com/science/article/pii/S1352231011004730`.

C. Weschler. Chemistry in indoor environments: 20 years of research. *Indoor Air*, 21(3): 205–218, 2011. doi: https://doi.org/10.1111/j.1600-0668.2011.00713.x.

C. J. Weschler and H. C. Shields. Indoor ozone/terpene reactions as a source of indoor particles. *Atmospheric Environment*, 33(15):2301–2312, 1999. ISSN 1352-2310. doi: https://doi.org/10.1016/S1352-2310(99)00083-7. URL `https://www.sciencedirect.com/science/article/pii/S1352231099000837`.

S. E. West, P. Büker, M. Ashmore, G. Njoroge, N. Welden, C. Muhoza, P. Osano, J. Makau, P. Njoroge, and W. Apondo. Particulate matter pollution in an informal settlement in Nairobi: Using citizen science to make the invisible visible. *Applied Geography*, 114(July 2018):102133, 2020. ISSN 01436228. doi: 10.1016/j.apgeog.2019.102133.

WHO. *Air quality guidelines: global update 2005: particulate matter, ozone, nitrogen dioxide, and sulfur dioxide*. World Health Organization, 2006.

WHO. *Literature review on chemical pollutants in indoor air in public settings for children and overview of their health effects with a focus on schools, kindergartens and day-care centres Supplementary publication to the screening tool for assessment of healt*. World Health Organization, 2021a. ISBN 9789289055642.

WHO. *WHO global air quality guidelines: particulate matter (PM2.5 and PM10), ozone, nitrogen dioxide, sulfur dioxide and carbon monoxide*. World Health Organization, 2021b.

U. U. N. E. P. WHO. *State-of-the-science of endocrine disrupting chemicals, 2012. United Nations Environment Programme and the World Health Organization, Geneva, Switzerland.* World Health Organization, 2013. ISBN 9789280732740.

J. Wichmann, T. Lind, M. A. Nilsson, and T. Bellander. PM2.5, soot and NO2 indoor-outdoor relationships at homes, pre-schools and schools in Stockholm, Sweden. *Atmospheric Environment*, 44(36):4536–4544, 2010. ISSN 13522310. doi: 10.1016/j.atmosenv.2010.08.023. URL `http://dx.doi.org/10.1016/j.atmosenv.2010.08.023`.

W. E. Wilson and M. Brauer. Estimation of ambient and non-ambient components of particulate matter exposure from a personal monitoring panel study. *Journal of Exposure Science & Environmental Epidemiology*, 16(3):264–274, 2006. ISSN 1559-064X. doi: 10.1038/sj.jes.7500483. URL `https://doi.org/10.1038/sj.jes.7500483`.

A. Winkler, T. Contardo, A. Vannini, S. Sorbo, A. Basile, and S. Loppi. Magnetic emissions from brake wear are the major source of airborne particulate matter bioaccumulated by lichens exposed in milan (italy). *Applied Sciences*, 10(6), 2020. ISSN 2076-3417. doi: 10.3390/app10062073. URL `https://www.mdpi.com/2076-3417/10/6/2073`.

A. Winkler, A. Amoroso, A. Di Giosa, and G. Marchegiani. The effect of covid-19 lockdown on airborne particulate matter in rome, italy: A magnetic point of view. *Environmental Pollution*, 291:118191, 2021. doi: 10.1016/j.envpol.2021.118191.

G. WJ, H. Vora, R. McConnell, K. Berhane, F. Gilliland, D. Thomas, F. Lurmann, E. Avol, N. Kunzli, M. Jerrett, and J. Peters. Effect of exposure to traffic on lung development from 10 to 18 years of age: a cohort study. 369(9561):571–577, 2007. doi: 10.1016/S0140-6736(07)60037-3.

R. C. Woodward, J. Heeris, T. G. St. Pierre, M. Saunders, E. P. Gilbert, M. Rutnakornpituk, Q. Zhang, and J. S. Riffle. A comparison of methods for the measurement of the particle-size distribution of magnetic nanoparticles. *Journal of Applied Crystallography*, 40(s1): s495–s500, 2007. doi: 10.1107/S002188980700091X.

H.-U. Worm. On the superparamagnetic—stable single domain transition for magnetite, and frequency dependence of susceptibility. *Geophysical Journal International*, 133(1):201–206, 04 1998. ISSN 0956-540X. doi: 10.1046/j.1365-246X.1998.1331468.x.

H.-U. Worm. Time-dependent irm: A new technique for magnetic granulometry. *Geophysical Research Letters*, 26(16):2557–2560, 1999.

K. Wuyts, J. Hofman, S. Van Wittenberghe, G. Nuyts, K. De Wael, and R. Samson. A new opportunity for biomagnetic monitoring of particulate pollution in an urban environment using tree branches. *Atmospheric Environment*, 190:177–187, 2018. ISSN 1352-2310. doi: https://doi.org/10.1016/j.atmosenv.2018.07.014.

H. Xu, B. Guinot, Z. Shen, K. F. Ho, X. Niu, S. Xiao, R. J. Huang, and J. Cao. Characteristics of organic and elemental carbon in PM2.5 and PM0.25 in indoor and outdoor environments of a middle school: Secondary formation of organic carbon and sources identification. *Atmosphere*, 6(3):361–379, 2015. ISSN 20734433. doi: 10.3390/atmos6030361.

H. Xu, J.-F. Léon, C. Liousse, B. Guinot, V. Yoboué, A. B. Akpo, J. Adon, K. F. Ho, S. S. H. Ho, L. Li, E. Gardrat, Z. Shen, and J. Cao. Personal exposure to $PM_{2.5}$ emitted from typical anthropogenic sources in southern West Africa: Chemical characteristics and associated health risks. *Atmospheric Chemistry and Physics*, 19(10):6637–6657, 2019. ISSN 1680-7316. doi: 10.5194/acp-19-6637-2019.

H. Yahi, B. Marticorena, S. Thiria, B. Chatenet, C. Schmechtig, J. L. Rajot, and M. Crepon. Statistical relationship between surface pm10 concentration and aerosol optical depth over the sahel as a function of weather type, using neural network methodology. *Journal of Geophysical Research: Atmospheres*, 118(23):13,265–13,281, 2013. doi: https://doi.org/10.1002/2013JD019465.

P. Yin, M. Brauer, A. J. Cohen, H. Wang, J. Li, R. T. Burnett, J. D. Stanaway, K. Causey, S. Larson, W. Godwin, J. Frostad, A. Marks, L. Wang, M. Zhou, and C. J. L. Murray. The effect of air pollution on deaths, disease burden, and life expectancy across China and its provinces, 1990–2017: An analysis for the Global Burden of Disease Study 2017. *The Lancet Planetary Health*, 0(0), 2020. ISSN 2542-5196. doi: 10.1016/S2542-5196(20)30161-3.

A. Zanobetti, F. Dominici, Y. Wang, and J. D. Schwartz. A national case-crossover analysis of the short-term effect of PM2.5 on hospitalizations and mortality in subjects with diabetes and neurological disorders. *Environmental Health*, 13(1):38, 2014. ISSN 1476-069X. doi: https://doi.org/10.1186/1476-069X-13-38.

C. Zhang, B. Huang, J. D. Piper, and R. Luo. Biomonitoring of atmospheric particulate matter using magnetic properties of salix matsudana tree ring cores. *Science of The Total Environment*, 393(1):177–190, 2008. ISSN 0048-9697. doi: https://doi.org/10.1016/j.scitotenv.2007.12.032.

R. Zhang, G. Wang, S. Guo, M. L. Zamora, Q. Ying, Y. Lin, W. Wang, M. Hu, and Y. Wang. Formation of urban fine particulate matter. *Chemical reviews*, 115(10):3803–3855, 2015. doi: 10.1021/acs.chemrev.5b00067.

S. Zhou, L. Cong, Y. Liu, L. Xie, S. Zhao, and Z. Zhang. Rainfall intensity plays an important role in the removal of PM from the leaf surfaces. *Ecological Indicators*, 128:107778, 2021. ISSN 1470160X. doi: 10.1016/j.ecolind.2021.107778. URL `https://doi.org/10.1016/j.ecolind.2021.107778`.

Y. Zhu, L. Yang, C. Meng, Q. Yuan, C. Yan, C. Dong, X. Sui, L. Yao, F. Yang, Y. Lu, and W. Wang. Indoor/outdoor relationships and diurnal/nocturnal variations in water-soluble ion and pah concentrations in the atmospheric pm2.5 of a business office area in jinan, a heavily polluted city in china. *Atmospheric Research*, 153:276–285, 2015. ISSN 0169-8095. doi: https://doi.org/10.1016/j.atmosres.2014.08.014.

Y. Zhu, C. Xu, D. Yin, J. Xu, Y. Wu, and H. Jia. Environmental and economic cost-benefit comparison of sponge city construction in different urban functional regions. *Journal of Environmental Management*, 304:114230, 2022. ISSN 0301-4797. doi: https://doi.org/10.1016/j.jenvman.2021.114230. URL `https://www.sciencedirect.com/science/article/pii/S0301479721022921`.

D. Zmirou, S. Gauvin, I. Pin, I. Momas, J. Just, F. Sahraoui, Y. Le Moullec, F. Bremont, S. Cassadou, M. Albertini, et al. Five epidemiological studies on transport and asthma: objectives, design and descriptive results. *Journal of Exposure Science & Environmental Epidemiology*, 12(3):186–196, 2002. doi: 10.1038/sj/jea/7500217.

S. Zuhara and R. Isaifan. The Impact of Criteria Air Pollutants on Soil and Water: A Review. *Journal of Environmental Science and Pollution Research*, 4(2):278–284, 2018. doi: 10.30799/jespr.133.18040205.

Özden Özdemir and S. K. Banerjee. A preliminary magnetic study of soil samples from west-central minnesota. *Earth and Planetary Science Letters*, 59(2):393–403, 1982. ISSN 0012-821X. doi: https://doi.org/10.1016/0012-821X(82)90141-8.

Appendix A

Supplementary data tables

A.1 Chapter 3: PM2.5 Magnetic Properties in Relation to Urban Combustion Sources in southern West Africa

Table A.1: Sample identification, site, date of sampling, deposited mass (μg), sampling volume (m^3), saturation isothermal magnetization (SIRM, emu$\times 10^{-6}$), anhysteretic remanent magnetization (ARM, emu$\times 10^{-8}$), isothermal remanent magnetization measured at 300 mT (IRM_{300mT}, emu$\times 10^{-6}$), and median destructive field of the ARM (MDF, mT) measured on PM2.5 filters.

ID	Site	Date	Mass	Vol.	SIRM	ARM	IRM_{300mT}	MDF
1	AT	11/ 16/ 15	679.50	13.34	6.07	12.91	5.87	37.00
2	AT	11/ 23/ 15	446.50	13.16	7.20	13.93	6.96	32.50
3	AT	11/ 30/ 15	2046.00	11.74	7.21	14.15	6.73	31.20
4	AT	12/ 07/ 15	1535.00	13.46	14.40	2.77	13.81	29.00
5	AT	12/ 14/ 15	1406.00	13.21	0.78	13.15	6.42	
6	AT	12/ 21/ 15	1230.00	13.23	7.14	2.86	6.97	34.00
7	AT	12/ 28/ 15	806.00	13.23	4.01	0.99	4.05	31.00
8	AT	01/ 11/ 16	428.50	10.74	5.26	11.01	5.16	
9	AT	01/ 18/ 16	448.00	13.27	6.56	13.37	6.35	
10	AT	01/ 25/ 16	1410.00	13.16	5.95	10.98	5.69	
11	AT	02/ 01/ 16	589.00	13.15	6.74	15.65	6.82	25.60
12	AT	02/ 08/ 16	279.50	13.19	4.22	7.94	4.12	
13	AT	02/ 15/ 16	196.00	12.98	3.97	9.65	3.82	35.00
14	AT	02/ 22/ 16	535.00	27.15	3.97	10.34	3.91	
15	AT	03/ 07/ 16	239.00	12.30	6.83	10.42	4.48	
16	AT	03/ 14/ 16	269.00	12.42	4.61	7.75	4.22	33.00
17	AT	03/ 21/ 16	249.00	12.39	3.03	7.79	2.93	
18	AT	03/ 28/ 16	146.00	12.72	4.30	8.92	4.11	35.00

Continued on next page

Table A.1 – continued from previous page

ID	Site	Date	Mass	Vol.	SIRM	ARM	IRM_{300mT}	MDF
19	AT	04/ 11/ 16	225.00	13.49	3.03	6.58	2.93	
20	AT	04/ 18/ 16	379.00	13.32	4.78	10.30	4.65	
21	AT	04/ 25/ 16	144.00	13.78	8.44	8.65	8.02	
22	AT	05/ 02/ 16	148.00	13.38	3.79	4.85	3.67	
23	AT	05/ 09/ 16	194.00	13.02	4.06	9.04	3.79	
24	AT	05/ 16/ 16	615.00	13.55	3.06	7.40	2.96	
25	AT	05/ 23/ 16	394.00	13.36	3.51	5.35	3.37	
26	AT	05/ 30/ 16	188.00	14.24	5.67	9.12	5.28	43.80
27	AT	06/ 06/ 16	253.00	8.12	4.51	7.62	4.38	
28	AT	06/ 13/ 16	363.00	7.14	2.95	7.97	2.92	38.80
29	AT	06/ 20/ 16	392.00	13.48	4.86	9.15	4.75	
30	AT	06/ 27/ 16	446.00	15.85	3.51	9.70	3.42	29.00
31	AT	07/ 04/ 16	302.00	15.10	12.45	47.87	13.26	
32	AT	07/ 11/ 16	390.00	14.41	6.99	12.40	6.85	
33	AT	07/ 18/ 16	323.00	14.82	5.03	7.96	4.84	
34	AT	07/ 25/ 16	290.00	11.99	7.47	9.60	7.44	
35	AT	08/ 01/ 16	236.00	19.98	3.80	6.82	3.71	
36	AT	08/ 08/ 16	281.00	8.08	3.59	6.59	3.50	
37	AT	08/ 22/ 16	29.00	13.88	2.94	6.68	2.86	
38	AT	08/ 29/ 16	226.00	13.80	3.75	9.83	3.87	
39	AT	09/ 05/ 16	291.00	13.97	5.40	6.03	5.34	
40	AT	09/ 12/ 16	352.00	13.41	6.64	8.26	2.81	
41	AT	09/ 19/ 16	145.00	14.50	4.21	5.79	4.16	
42	AT	09/ 26/ 16	179.00	13.67	4.12	4.82	4.16	
43	AT	10/ 03/ 16	160.00	12.81	3.66	3.51	3.59	
44	AT	10/ 10/ 16	220.00	13.54	3.78	3.87	3.63	
45	AT	10/ 24/ 16	240.00	13.07	4.69	9.61	4.62	35.00
46	AT	10/ 31/ 16	249.00	13.30	4.31	10.17	4.20	28.00
47	AT	11/ 07/ 16	542.00	13.47	4.40	6.13	4.20	
48	AT	11/ 14/ 16	512.00	13.38	4.30	17.38	4.78	
49	AT	11/ 21/ 16	442.00	13.57	5.33	9.39	5.24	
50	AT	11/ 28/ 16	393.00	13.55	2.51	3.00	2.36	
51	AT	12/ 05/ 16	619.00	13.14	5.03	8.01	5.12	
52	AT	12/ 12/ 16	627.00	13.52	3.01	3.97	2.87	
53	AT	12/ 19/ 16	493.00	13.69	4.74	6.93	4.74	
54	AT	12/ 26/ 16	512.00	12.72	16.52	12.34	16.18	37.50
55	AT	01/ 02/ 17	695.00	15.46	4.12	7.03	4.06	
56	AT	01/ 09/ 17		10.81	3.79	8.51	3.61	35.00
57	AT	01/ 16/ 17	8727.00	18.35	8.62	12.36	8.50	
58	AT	01/ 30/ 17	123.50	14.14	4.07	5.74	3.93	
59	AT	02/ 06/ 17	172.50	14.68	5.16	7.25	4.94	
60	CT	02/ 16/ 15	47.50	7.03	5.34	11.18	5.26	31.20
61	CT	02/ 23/ 15	51.50	10.47	4.46	8.91	4.34	
62	CT	03/ 02/ 15	47.50	11.73	5.15	8.98	4.99	37.00
63	CT	03/ 09/ 15	418.00	12.60	5.07	9.24	5.10	

Continued on next page

Table A.1 – continued from previous page

ID	Site	Date	Mass	Vol.	SIRM	ARM	IRM_{300mT}	MDF
64	CT	03/ 16/ 15	165.50	22.92	4.34	6.86	4.22	
65	CT	03/ 23/ 15	12.50	22.21	3.60	4.89	3.50	
66	CT	03/ 30/ 15	514.00	19.93	5.49	7.40	5.40	
67	CT	04/ 06/ 15	47.50	19.93	4.50	6.22	4.39	
68	CT	04/ 13/ 15	191.00	22.75	4.63	6.19	4.42	
69	CT	04/ 20/ 15	13.00	22.61	3.54	8.56	3.66	36.20
70	CT	04/ 27/ 15	83.50	24.68	3.44	5.50	3.26	
71	CT	05/ 04/ 15	94.50	21.37	6.36	11.38	6.17	32.00
72	CT	05/ 11/ 15	75.50	23.57	4.02	8.63	3.87	
73	CT	05/ 18/ 15	43.00	18.58	3.11	6.07	3.02	
74	CT	05/ 25/ 15	-32.00	23.56	4.76	8.93	4.65	35.00
75	CT	06/ 01/ 15	123.00	25.56	5.14	8.52	5.00	
76	CT	06/ 08/ 15	43.00	13.97	6.25	6.82	6.12	
77	CT	06/ 15/ 15	63.50	24.60	3.22	6.00	3.13	
78	CT	06/ 22/ 15	331.00	23.46	4.97	9.60	4.77	
79	CT	06/ 29/ 15	146.50	25.27	7.33	8.94	7.17	
80	CT	07/ 06/ 15	237.50	24.06	6.15	9.56	5.96	37.50
81	CT	07/ 13/ 15	309.00	24.76	5.85	9.33	5.67	
82	CT	07/ 20/ 15	300.50	21.63	7.36	14.46	6.99	
83	CT	07/ 27/ 15	271.00	26.01	5.51	7.26	5.34	
84	CT	08/ 03/ 15	158.00	19.78	5.84	7.74	5.66	
85	CT	08/ 10/ 15	9.00	18.85	4.24	9.70	4.16	
86	CT	08/ 17/ 15	30.00	17.51	3.63	7.60	3.40	
87	CT	08/ 24/ 15	25.50	14.47	5.65	9.19	5.58	
88	CT	08/ 31/ 15	54.00	9.12	4.15	6.06	4.00	
89	CT	09/ 07/ 15	226.50	22.70	6.23	11.51	5.98	37.00
90	CT	09/ 14/ 15	-79.00	21.94	3.87	2.79	3.84	
91	CT	09/ 21/ 15	54.00	20.65	4.12	6.66	3.92	
92	CT	09/ 28/ 15	46.00	20.06	4.79	5.92	4.66	
93	CT	10/ 05/ 15	47.00	18.36	4.69	6.51	4.61	
94	CT	10/ 12/ 15	4.00	14.97	5.37	10.22	5.09	35.00
95	CT	10/ 19/ 15	-408.00	13.87	3.29	2.97	3.16	
96	CT	10/ 26/ 15	23.50	11.27	4.14	8.17	3.93	33.80
97	CT	11/ 02/ 15	-61.50	8.97	3.94	4.89	3.86	
98	CT	11/ 09/ 15	495.50	17.38	6.93	13.51	6.56	
99	CT	11/ 16/ 15	-324.50	13.74	3.09	12.80	2.71	
100	CT	11/ 23/ 15	-85.50	8.37	2.30	1.11	2.16	
101	CT	11/ 30/ 15	599.50	16.92	5.63	12.34	5.36	30.00
102	CT	12/ 07/ 15	-277.00	6.36	3.26	3.54	3.13	
103	CT	12/ 14/ 15	1777.50	20.15	11.40	19.59	11.00	
104	CT	12/ 21/ 15	172.00	18.58	4.16	6.75	4.03	
105	CT	12/ 28/ 15	463.00	14.63	5.86	8.35	5.65	
106	CT	01/ 04/ 16	101.00	17.48	3.62	4.79	3.51	
107	CT	01/ 11/ 16	160.50	18.95	3.67	6.01	3.57	
108	CT	01/ 18/ 16	183.00	13.44	7.34	7.67	7.14	

Continued on next page

Table A.1 – continued from previous page

ID	Site	Date	Mass	Vol.	SIRM	ARM	IRM_{300mT}	MDF
109	CT	01/ 25/ 16	3808.50	20.20	12.80	21.33	10.03	
110	CT	02/ 01/ 16	2631.50	23.68	9.51	18.33	8.64	33.00
111	CT	02/ 08/ 16	1855.00	23.94	7.07	14.36	6.65	
112	CT	02/ 15/ 16	647.50	22.89	4.98	8.57	4.73	
113	CT	02/ 22/ 16	11.00	13.60	5.40	9.96	5.28	
114	CT	02/ 29/ 16	322.00	23.31	7.69	9.75	7.53	
115	CT	03/ 07/ 16	409.00	22.09	7.92	13.68	7.57	32.00
116	CT	03/ 14/ 16	541.00	22.02	10.23	13.76	9.90	
117	CT	03/ 21/ 16	893.00	22.50	6.20	10.77	6.01	
118	CT	03/ 28/ 16	198.00	21.03	4.96	8.16	4.81	38.70
119	CT	04/ 04/ 16	391.00	19.06	5.56	7.52	5.36	
120	CT	04/ 11/ 16	1223.00	22.44	13.52	20.47	12.72	
121	CT	04/ 18/ 16	400.00	21.33	5.27	8.51	5.40	
122	CT	04/ 25/ 16	242.00	21.51	8.46	10.78	8.17	
123	CT	05/ 02/ 16	286.00	22.34	4.92	6.14	4.78	
124	CT	05/ 09/ 16	0.00	19.78	4.52	7.41	4.40	
125	CT	05/ 16/ 16	136.00	19.93	5.18	6.65	5.17	
126	CT	05/ 23/ 16	149.00	14.73	4.15	4.70	4.31	
127	CT	05/ 30/ 16	243.00	19.93	6.38	12.39	6.17	
128	CT	06/ 06/ 16	463.00	18.36	8.67	7.90	8.39	
129	CT	06/ 13/ 16	49.00	20.24	5.87	5.44	5.61	
130	CT	06/ 20/ 16	145.00	18.89	5.34	6.19	5.08	
131	CT	06/ 27/ 16	83.00	20.07	3.91	6.30	3.82	
132	CT	07/ 04/ 16	468.00	20.03	6.21	8.38	6.02	
133	CT	07/ 11/ 16	384.00	19.42	5.46	8.58	5.30	
134	CT	07/ 18/ 16	103.00	18.14	4.29	5.82	4.20	
135	CT	07/ 25/ 16	82.00	21.11	5.45	6.25	5.24	
136	CT	08/ 01/ 16	16.00	17.34	4.38	5.62	4.24	
137	CT	08/ 08/ 16	122.00	20.57	4.90	5.94	4.85	
138	CT	08/ 15/ 16	89.00	15.90	3.87	6.52	3.73	
139	CT	08/ 22/ 16	88.00	22.88	5.66	8.30	5.63	
140	CT	08/ 29/ 16	2.00	20.62	6.14	10.74	6.03	
141	CT	09/ 05/ 16	108.00	18.37	6.04	8.06	5.82	
142	CT	09/ 12/ 16	50.00	19.29	4.18	8.50	4.06	30.00
143	CT	09/ 19/ 16	-104.00	19.46	4.29	7.18	4.18	
144	CT	09/ 26/ 16	110.00	18.40	3.51	4.94	3.45	
145	CT	10/ 03/ 16	96.00	18.11	6.47	12.79	6.35	32.00
146	CT	10/ 10/ 16	99.00	19.50	4.08	5.42	3.98	
147	CT	10/ 24/ 16	443.00	18.51	7.57	9.71	7.33	
148	CT	10/ 31/ 16	587.00	17.68	7.41	8.10	7.15	
149	CT	11/ 07/ 16	-166.00	17.25	7.44	11.97	7.22	31.00
150	CT	11/ 14/ 16	680.00	15.85	7.70	10.60	7.49	
151	CT	11/ 21/ 16	-430.00	15.87	4.12	6.65	4.05	
152	CT	11/ 28/ 16	370.00	14.48	4.85	8.04	4.69	
153	CT	12/ 05/ 16	827.00	14.98	7.71	9.75	7.35	

Continued on next page

Table A.1 – continued from previous page

ID	Site	Date	Mass	Vol.	SIRM	ARM	IRM_{300mT}	MDF
154	CT	12/ 12/ 16	602.00	17.50	7.17	8.98	6.91	
155	CT	12/ 19/ 16	288.00	15.04	3.91	6.62	3.79	
156	CT	12/ 26/ 16	3544.00	14.70	10.50	18.14	9.72	
157	CT	01/ 02/ 17	410.00	12.29	6.07	7.17	5.93	
158	CT	01/ 09/ 17	643.00	14.18	3.61	7.11	3.54	32.50
159	CT	01/ 16/ 17	474.00	15.19	6.06	8.51	5.80	
160	CT	01/ 23/ 17	639.00	16.91	5.76	7.73	5.55	
161	AL	02/ 23/ 15	266.00	14.98	4.81	5.82	4.46	
162	AL	03/ 02/ 15	408.50	14.48	4.01	6.11	3.73	
163	AL	03/ 09/ 15	207.00	14.58	4.29	7.60	4.07	38.00
164	AL	03/ 16/ 15	159.50	14.19	4.97	1.66	4.77	
165	AL	03/ 23/ 15	169.00	14.25	21.29	13.15	21.02	
166	AL	03/ 30/ 15	395.50	12.35	3.87	6.01	3.71	
167	AL	04/ 06/ 15	-79.50	9.21	3.85	9.80	3.79	
168	AL	04/ 13/ 15	382.50	13.62	2.97	4.38	2.02	
169	AL	04/ 20/ 15	-82.00	13.63	61.17	16.94	60.83	
170	AL	04/ 27/ 15	-186.00	12.23	2.16	1.45	2.05	
171	AL	05/ 04/ 15	-139.50	13.07	2.60	4.62	2.48	
172	AL	05/ 11/ 15	88.50	12.70	10.09	8.39	9.58	
173	AL	05/ 18/ 15	16.00	12.68	5.34	9.04	5.00	
174	AL	05/ 25/ 15	-24.00	13.68	2.01	2.42	1.94	
175	AL	06/ 01/ 15	-563.00	12.67	1.48	1.71	1.41	
176	AL	06/ 08/ 15	171.50	13.86	2.00	2.30	1.94	
177	AL	06/ 15/ 15	21.00	4.66	1.97	2.34	1.89	
178	AL	06/ 22/ 15	2.00	6.79	2.81	5.69	2.81	
179	AL	06/ 29/ 15	-118.00	12.79	5.12	6.51	5.00	
180	AL	07/ 06/ 15	107.00	12.61	3.62	10.92	3.49	
181	AL	07/ 20/ 15	105.00	9.23	2.18	2.60	2.21	
182	AL	07/ 27/ 15	247.50	13.33	2.21	2.80	2.10	
183	AL	08/ 03/ 15	218.50	13.87	2.13	1.48	2.05	
184	AL	08/ 10/ 15	326.50	14.21	6.03	10.19	6.42	
185	AL	08/ 17/ 15	284.50	12.18	3.58	9.24	3.48	
186	AL	08/ 24/ 15	103.00	8.22	3.94	6.48	3.66	38.00
187	AL	08/ 31/ 15	158.00	9.97	3.68	8.54	3.60	
188	AL	09/ 07/ 15	268.00	14.14	2.56	2.30	2.45	
189	AL	09/ 14/ 15	236.50	13.84	3.99	34.03	3.70	
190	AL	09/ 21/ 15	238.00	13.42	4.18	7.45	4.03	
191	AL	09/ 28/ 15	322.00	14.34	2.18	1.46	2.08	
192	AL	10/ 05/ 15	216.50	13.81	3.78	16.40	3.52	
193	AL	10/ 12/ 15	121.50	13.51	3.10	3.19	3.02	
194	AL	10/ 19/ 15	104.00	14.01	4.31	13.82	4.12	
195	AL	10/ 26/ 15	212.00	13.66	2.29	3.56	2.23	
196	AL	11/ 02/ 15	228.50	13.51	3.97	5.05	3.51	
197	AL	11/ 09/ 15	294.50	13.78	4.90	6.35	4.65	
198	AL	11/ 16/ 15	284.50	12.83	3.72	6.62	3.63	

Continued on next page

Table A.1 – continued from previous page

ID	Site	Date	Mass	Vol.	SIRM	ARM	IRM_{300mT}	MDF
199	AL	11/ 23/ 15	310.50	13.71	3.46	14.22	3.65	
200	AL	11/ 30/ 15	1366.00	14.03	5.24	10.67	4.92	33.70
201	AL	12/ 07/ 15	1161.50	13.95	6.19	10.61	5.84	
202	AL	12/ 14/ 15	820.00	12.51	4.09	5.43	3.82	
203	AL	12/ 21/ 15	60.50	12.88	2.65	4.31	2.83	
204	AL	12/ 28/ 15	895.50	11.08	3.90	9.64	3.67	33.00
205	AL	01/ 04/ 16	709.00	11.89	4.21	7.23	4.13	
206	AL	01/ 11/ 16	-189.00	13.73	1.90	3.30	1.80	
207	AL	01/ 18/ 16	-45.00	10.21	2.20	2.81	2.11	
208	AL	01/ 25/ 16	816.50	12.03	5.13	8.16	5.01	
209	AL	02/ 01/ 16	201.50	11.32	3.55	5.24	3.48	
210	AL	02/ 08/ 16	726.50	13.82	5.58	12.09	5.44	
211	AL	02/ 15/ 16	679.00	13.18	3.83	15.26	3.66	31.00
212	AL	02/ 22/ 16	405.00	9.63	3.78	2.94	3.65	
213	AL	02/ 29/ 16	330.00	12.04	4.57	6.23	4.45	
214	AL	03/ 07/ 16	530.00	13.87	4.33	7.29	4.64	
215	AL	03/ 14/ 16	350.00	13.49	4.08	7.91	3.84	
216	AL	03/ 21/ 16	391.00	14.75	4.70	7.09	4.55	
217	AL	03/ 28/ 16	222.00	14.70	3.46	3.40	3.02	
218	AL	04/ 04/ 16	155.00	14.58	4.46	5.72	4.31	
219	AL	04/ 11/ 16	354.00	12.57	5.21	5.34	5.07	
220	AL	04/ 18/ 16	193.00	13.22	2.94	6.68	2.84	37.50
221	AL	04/ 25/ 16	401.00	14.14	5.27	4.39	5.06	
222	AL	05/ 02/ 16	287.00	13.65	3.91	5.17	3.75	
223	AL	05/ 09/ 16	291.00	12.90	4.90	10.25	4.86	38.80
224	AL	05/ 16/ 16	246.00	14.03	2.92	2.22	2.79	
225	AL	05/ 23/ 16	6.00	14.10	2.65	4.85	2.56	
226	AL	05/ 30/ 16	149.00	13.97	5.22	11.45	5.10	38.00
227	AL	06/ 06/ 16	284.00	12.96	2.13	2.35	2.04	
228	AL	06/ 13/ 16	214.00	12.03	1.60	1.26	1.52	
229	AL	06/ 20/ 16	263.00	12.91	2.23	1.95	2.15	
230	AL	06/ 27/ 16	637.00	14.00	4.46	8.27	3.81	30.00
231	AL	07/ 04/ 16	408.00	11.65	3.14	2.20	2.97	
232	AL	07/ 11/ 16	583.00	14.78	2.29	4.14	2.17	
233	AL	07/ 18/ 16	415.00	14.01	1.75	0.78	1.66	
234	AL	07/ 25/ 16	380.00	12.02	1.91	1.61	1.80	
235	AL	08/ 08/ 16	197.00	11.54	1.57	1.84	1.47	
236	AL	08/ 15/ 16	474.00	13.64	3.90	7.21	3.79	32.50
237	AL	08/ 22/ 16	198.00	14.04	1.59	1.16	1.52	
238	AL	08/ 29/ 16	82.00	6.66	2.41	1.67	2.30	
239	AL	09/ 05/ 16	292.00	13.88	1.73	2.52	1.63	
240	AL	09/ 12/ 16	246.00	13.79	1.73	2.60	1.62	
241	AL	09/ 19/ 16	216.00	14.06	3.66	10.06	3.72	
242	AL	09/ 26/ 16	324.00	14.11	3.59	2.92	3.45	
243	AL	10/ 03/ 16	211.00	13.24	3.70	6.27	3.62	

Continued on next page

Table A.1 – continued from previous page

ID	Site	Date	Mass	Vol.	SIRM	ARM	IRM_{300mT}	MDF
244	AL	10/ 10/ 16	94.00	14.09	2.95	4.83	2.87	
245	AL	10/ 24/ 16	291.00	12.92	3.66	6.64	3.44	36.20
246	AL	10/ 31/ 16	60.00	12.38	3.76	5.60	3.64	
247	AL	11/ 07/ 16	659.00	13.13	2.89	3.39	2.73	
248	AL	11/ 14/ 16	446.00	14.03	3.96	7.32	3.81	
249	AL	11/ 21/ 16	361.00	13.19	6.92	9.08	6.80	
250	AL	11/ 28/ 16	373.00	12.62	4.55	11.43	4.54	34.50
251	AL	12/ 05/ 16	533.00	9.81	4.03	6.40	3.87	
252	AL	12/ 12/ 16	393.00	8.53	4.67	6.84	4.59	
253	AL	12/ 19/ 16	535.00	10.01	4.88	7.38	4.79	36.20
254	AL	12/ 26/ 16	1149.00	10.23	6.44	12.28	6.05	31.00
255	AL	01/ 02/ 17	695.00	13.23	2.40	1.54	2.30	
256	AL	01/ 09/ 17	19.00	9.94	5.55	10.60	5.27	38.80
257	AL	01/ 16/ 17	178.00	11.73	5.08	8.97	4.91	33.00
258	AL	01/ 23/ 17	58.50	10.82	5.75	7.27	5.59	
259	AL	01/ 30/ 17	18.00	11.43	3.11	6.97	3.40	36.20
260	AL	02/ 06/ 17	16.00	10.68	3.81	6.45	3.69	
261	AF	02/ 16/ 15	71.50	10.70	2.59	8.48	2.54	
262	AF	02/ 23/ 15	107.00	13.18	3.32	8.48	3.21	31.00
263	AF	03/ 09/ 15	14.50	11.50	2.17	1.07	2.01	
264	AF	03/ 16/ 15	725.50	11.94	9.81	12.70	9.75	
265	AF	03/ 23/ 15	-4240.50	12.29	2.30	1.78	2.20	
266	AF	03/ 30/ 15	234.50	12.78	4.61	7.59	4.64	
267	AF	04/ 06/ 15	265.50	11.24	3.56	4.89	3.44	
268	AF	04/ 13/ 15	1600.50	18.70	5.00	9.14	4.76	33.70
269	AF	04/ 20/ 15	604.00	21.01	7.23	6.98	7.05	
270	AF	04/ 27/ 15	1493.50	12.12	5.75	8.05	5.63	
271	AF	05/ 11/ 15	1198.50	4.65	4.64	10.29	4.44	35.00
272	AF	05/ 18/ 15	267.50	17.96	3.96	9.07	3.80	34.00
273	AF	05/ 25/ 15	581.00	5.36	4.31	5.54	4.20	
274	AF	06/ 01/ 15	1208.50	10.84	4.50	9.25	4.34	39.00
275	AF	06/ 08/ 15	13439.50	9.02	1.52	1.84	1.41	
276	AF	06/ 15/ 15	-51844.50	10.21	2.08	1.74	2.00	
277	AF	06/ 22/ 15	1985.00	7.40	3.49	9.26	3.41	31.00
278	AF	06/ 29/ 15	1456.00	8.11	5.31	6.98	4.86	
279	AF	07/ 06/ 15	372.00	7.00	3.53	7.38	3.21	35.00
280	AF	07/ 13/ 15	-100.50	8.35	3.49	2.53	1.16	
281	AF	07/ 20/ 15	194.00	2.77	4.83	6.07	4.45	
282	AF	07/ 27/ 15	1563.00	10.98	6.35	9.69	6.29	
283	AF	08/ 03/ 15	571.00	9.07	5.97	11.76	5.77	32.00
284	AF	08/ 10/ 15	1410.00	9.03	3.59	6.52	3.54	
285	AF	08/ 17/ 15	1678.50	6.03	4.09	8.82	3.97	27.00
286	AF	08/ 24/ 15	180.00	8.62	2.37	3.60	2.30	
287	AF	08/ 31/ 15	2558.50	6.05	4.17	8.68	3.91	36.30
288	AF	09/ 07/ 15	2362.50	12.17	4.76	8.49	4.60	

Continued on next page

Table A.1 – continued from previous page

ID	Site	Date	Mass	Vol.	SIRM	ARM	IRM_{300mT}	MDF
289	AF	09/ 14/ 15	1744.00	11.78	4.62	12.20	4.51	
290	AF	09/ 21/ 15	1983.50	11.88	2.71	5.45	2.65	
291	AF	09/ 28/ 15	1949.50	11.49	0.04	0.19	0.04	
292	AF	10/ 05/ 15	1960.50	11.53	2.89	4.90	2.82	
293	AF	10/ 12/ 15	2161.00	11.52	4.30	6.92	4.27	
294	AF	10/ 19/ 15	125.50	9.83	4.45	8.04	4.07	33.00
295	AF	10/ 26/ 15	2357.00	10.52	10.99	16.77	10.70	
296	AF	11/ 02/ 15	326.50	14.20	4.08	8.51	3.90	34.00
297	AF	11/ 09/ 15	1821.50	14.24	4.85	5.76	4.80	
298	AF	11/ 16/ 15	1748.00	12.95	3.83	7.84	3.78	33.00
299	AF	11/ 23/ 15	-43.50	13.01	1.97	1.99	1.91	
300	AF	11/ 30/ 15	1379.00	13.06	4.68	8.24	4.53	
301	AF	12/ 07/ 15	119.00	13.49	3.94	9.02	3.81	33.80
302	AF	12/ 14/ 15	807.50	13.27	6.17	12.11	6.11	
303	AF	12/ 21/ 15	630.50	13.06	3.06	8.33	2.96	32.50
304	AF	12/ 28/ 15	1490.50	13.74	5.84	10.00	5.61	
305	AF	01/ 04/ 16	-736.50	13.90	2.40	2.61	2.29	
306	AF	01/ 11/ 16	1731.00	14.04	3.67	6.81	3.56	
307	AF	01/ 18/ 16	818.00	13.63	7.71	13.86	7.29	35.00
308	AF	01/ 25/ 16	1107.00	13.82	5.54	9.64	5.44	
309	AF	02/ 01/ 16	1003.50	13.03	4.35	8.58	4.25	35.00

A.2 Section 4.2: Barking up the right tree: Using tree bark to track airborne particles in the school environment and link science to society

Table A.2: Sample identification, school, site, mass of bio-sensor (g),equipment used, saturation isothermal remanent magnetization (SIRM, $Am^2.kg^{-1}\times10^{-5}$), susceptibility of the anhysteretic remanent magnetization (xARM, $m^3.kg^{-1}\times10^{-8}$), S-ratio, ratio Hcr/Hc and ratio Mrs/Ms measured on bio-sensors exposed in the schools, indoors and outdoors.

ID	School	Site	Mass	Instrument	SIRM	xARM	S-ratio	Hcr/Hc	Mrs/Ms
1	School 1	Indoor	1.7	JR6 ($A.m^{-1}$)	2.01	1.51	0.94		
2	School 1	Outdoor	1.4	JR6 ($A.m^{-1}$)	2.38	0.96	0.96		
3	School 1	Indoor	1.9	JR6 ($A.m^{-1}$)	1.88	1.64	0.96		
4	School 1	Outdoor	2.3	JR6 ($A.m^{-1}$)	1.60	0.68	0.95		
5	School 1	Indoor	1.7	JR6 ($A.m^{-1}$)	1.46	1.18	0.96		
6	School 1	Outdoor	1.3	JR6 ($A.m^{-1}$)	2.58	1.18	0.96		
7	School 1	Indoor	1.3	JR6 ($A.m^{-1}$)	1.66	1.80	0.96		
8	School 1	Outdoor	1.4	JR6 ($A.m^{-1}$)	2.11	0.65	0.98		
9	School 1	Indoor	2.9	JR6 ($A.m^{-1}$)	0.87	0.31	0.94		
10	School 1	Outdoor	2.3	JR6 ($A.m^{-1}$)	1.31	0.35	0.95		
11	School 1	Indoor	2.3	JR6 ($A.m^{-1}$)	0.98	1.19	0.92		
12	School 1	Outdoor	2.1	JR6 ($A.m^{-1}$)	1.68	0.84	0.99		
13	School 1	Indoor	2.0	JR6 ($A.m^{-1}$)	0.97	1.30	0.94		
14	School 1	Outdoor	1.8	JR6 ($A.m^{-1}$)	2.16	0.77	0.96		
15	School 1	Indoor	2.1	JR6 ($A.m^{-1}$)	1.00	0.89	0.94		
16	School 1	Outdoor	1.9	JR6 ($A.m^{-1}$)	1.25	1.42	0.97		
17	School 2	Indoor	0.6	2G ($emu.cm^{-3}$)	0.99	0.31	0.91		
18	School 2	Outdoor	0.6	2G ($emu.cm^{-3}$)	1.85	0.77	0.94		
19	School 2	Indoor	0.7	2G ($emu.cm^{-3}$)	0.76	0.26	0.90		
20	School 2	Outdoor	0.7	2G ($emu.cm^{-3}$)	0.84	1.07	0.94		
21	School 2	Indoor	0.7	2G ($emu.cm^{-3}$)	1.39	0.32	0.99		
22	School 2	Outdoor	0.7	2G ($emu.cm^{-3}$)	1.03	0.32	0.83		
23	School 2	Indoor	0.7	2G ($emu.cm^{-3}$)	0.98	0.53	0.98	6.36	0.03
24	School 2	Outdoor	0.7	2G ($emu.cm^{-3}$)	1.24	0.72	0.83	15.32	0.06
25	School 2	Indoor	0.7	2G ($emu.cm^{-3}$)	0.81	0.47	0.87	3.75	0.08
26	School 2	Outdoor	0.7	2G ($emu.cm^{-3}$)	0.61	0.27	0.88		
27	School 2	Indoor	0.7	2G ($emu.cm^{-3}$)	0.94	1.09	0.96		
28	School 2	Outdoor	0.6	2G ($emu.cm^{-3}$)	0.88	0.15	0.88		
29	School 2	Indoor	0.7	2G ($emu.cm^{-3}$)	0.80	0.66	0.91		

Table A.3: Sample identification, school, site, mass of bark (g), saturation isothermal remanent magnetization (SIRM, $Am^2.kg^{-1}\times10^{-5}$), S-ratio, ratio Hcr/Hc , ratio Mrs/Ms, latitude and longitude for tree bark samples collected in both schools.

ID	School	Site	Mass	SIRM	S-ratio	Hcr/Hc	Mrs/Ms	Lat.	Lon.
1	School 1	West	0.5	0.44	0.88			43.5734	1.4533
2	School 1	West	0.5	0.56	0.86	3.95	0.12	43.5734	1.4534
3	School 1	West	0.5	0.41	0.95			43.5735	1.4535
4	School 1	West	0.3	1.39	0.80	3.96	0.10	43.5735	1.4535
5	School 1	West	0.5	0.46	0.88			43.5736	1.4536
6	School 1	West	0.5	0.46	1.01			43.5736	1.4537
7	School 1	West	0.4	0.76	0.89	4.38	0.09	43.5737	1.4536
8	School 1	East	0.4	1.39	0.95	4.30	0.10	43.5737	1.4542
9	School 1	East	0.2	1.77	0.90	6.15	0.06	43.5738	1.4543
10	School 1	East	0.5	0.72	0.93			43.5739	1.4544
11	School 1	East	0.5	0.51	0.88	2.59	0.11	43.5740	1.4546
12	School 1	East	0.5	1.35	0.94	6.06	0.10	43.5741	1.4547
13	School 1	East	0.6	0.85	0.94			43.5741	1.4548
14	School 1	East	0.4	0.97	0.91			43.5738	1.4541
15	School 1	East	0.5	1.17	0.93	5.89	0.08	43.5739	1.4542
16	School 1	East	0.6	1.65	0.94			43.5740	1.4544
17	School 1	East	0.4	1.56	0.84	8.38	0.05	43.5739	1.4541
18	School 1	East	0.6	0.96	0.91			43.5740	1.4543
19	School 1	East	0.5	0.99	0.93			43.5739	1.4540
20	School 1	East	0.5	0.85	0.95			43.5741	1.4543
21	School 1	East	0.6	1.05	0.85			43.5741	1.4544
22	School 1	East	0.6	1.00	0.93			43.5743	1.4546
23	School 1	East	0.5	0.51	0.89	5.71	0.08	43.5741	1.4542
24	School 1	East	0.3	1.40	0.83	5.89	0.08	43.5742	1.4543
25	School 1	East	0.6	0.98	0.92			43.5740	1.4539
26	School 1	East	0.5	0.98	0.96			43.5741	1.4540
27	School 1	East	0.5	1.03	0.91			43.5741	1.4541
28	School 1	East	0.5	1.03	0.92	7.98	0.08	43.5742	1.4541
29	School 1	East	0.5	1.07	0.94			43.5742	1.4542
30	School 1	East	0.5	1.00	0.92			43.5744	1.4544
31	School 1	East	0.4	1.22	0.95	5.36	0.05	43.5744	1.4545
32	School 1	East	0.5	0.56	0.95	2.88	0.10	43.5740	1.4540
33	School 2	Courtyard	0.3	0.70	0.90			43.5769	1.4369
34	School 2	Courtyard	0.4	0.49	0.88	3.86	0.11	43.5769	1.4370
35	School 2	Courtyard	0.4	0.62	0.85			43.5769	1.4371
36	School 2	Courtyard	0.3	0.78	0.92	3.96	0.11	43.5769	1.4372
37	School 2	Courtyard	0.4	0.36	0.79	2.54	0.14	43.5769	1.4373
38	School 2	Courtyard	0.4	0.70	0.87			43.5769	1.4374
39	School 2	Courtyard	0.5	0.47	0.91	9.51	0.09	43.5769	1.4375
40	School 2	Courtyard	0.4	0.62	0.89	27.19	0.11	43.5769	1.4377

Continued on next page

Table A.3 – continued from previous page

ID	School	Site	Mass	SIRM	S-ratio	Hcr/Hc	Mrs/Ms	Lat.	Lon.
41	School 2	Courtyard	0.3	1.28	0.90	4.93	0.08	43.5769	1.4378
42	School 2	Courtyard	0.4	0.84	0.88	4.25	0.09	43.5769	1.4379
43	School 2	Courtyard	0.4	0.79	0.83			43.5769	1.4380
44	School 2	Courtyard	0.4	0.84	0.87	15.52	0.10	43.5768	1.4373
45	School 2	Courtyard	0.4	0.96	0.96	6.72	0.11	43.5768	1.4374
46	School 2	Courtyard	0.3	1.38	0.94	9.60	0.08	43.5768	1.4375
47	School 2	Courtyard	0.5	0.91	0.95	3.76	0.12	43.5768	1.4377
48	School 2	Courtyard	0.4	1.48	0.91			43.5768	1.4378
49	School 2	Courtyard	0.3	1.70	0.91			43.5768	1.4379
50	School 2	Courtyard	0.4	0.56	0.79	4.93	0.10	43.5768	1.4380

Table A.4: Sample identification, date of sampling, school, site, season of sampling, volume of sampling (m^3), saturation isothermal remanent magnetization (SIRM, $A.m^{-1} \times 10^{-4}$), concentration of PM1 (PM1, $\mu g.m^{-3}$), concentration of organic carbon (OC, $\mu g.m^{-3}$), concentration of elemental carbon (EC, $\mu g.m^{-3}$) from PM1 filters exposed in both schools.

ID	Date	School	Site	Season	Vol.	SIRM	PM1	OC	EC
1	01/ 21/ 19	School 1	indoor	Winter	11.43	1.98	46.01	4.80	0.65
2	01/ 21/ 19	School 1	outdoor	Winter	11.47	4.23	44.81	2.44	0.98
3	04/ 08/ 19	School 1	outdoor	Spring	28.92	1.40	21.06	2.94	0.95
4	04/ 08/ 19	School 1	indoor	Spring	28.94	2.64	29.20	5.48	0.77
5	01/ 14/ 19	School 1	indoor	Winter	11.98	4.51	35.40	4.58	0.80
6	01/ 14/ 19	School 1	outdoor	Winter	9.16	2.26	53.58	6.29	2.23
7	02/ 04/ 19	School 2	indoor	Winter	11.51	0.87	35.71	5.24	0.43
8	02/ 04/ 19	School 2	outdoor	Winter	11.53	1.52	44.23	4.20	1.89
9	06/ 17/ 19	School 2	outdoor	Spring	10.79	2.01	49.85	2.65	0.85
10	06/ 17/ 19	School 2	indoor	Spring	31.81	1.34	24.33	2.80	0.75
11	01/ 28/ 19	School 2	outdoor	Winter	11.53	2.91	37.98	1.91	0.86
12	01/ 28/ 19	School 2	indoor	Winter	11.48	1.69	35.79	4.59	0.37

A.3 Section 4.3: Citizen science initiative for extensive mapping of indoor and outdoor particulate matter concentration in Toulouse (France) combining bio-sensors and environmental magnetism

Table A.5: Sample identification, residency number, site, saturation isothermal remanent magnetization (SIRM, $Am^2.kg^{-1}\times10^{-5}$), susceptibility of the anhysteretic remanent magnetization (xARM, $m^3.kg^{-1}\times10^{-8}$), ratio Hcr/Hc, and ratio Mrs/Ms from bio-sensors exposed on the residencies, indoors and outdoors.

ID	Residency	Site	SIRM	xARM	Hcr/Hc	Mrs/Ms
1	1	Indoor	3.76	1.52		
2	1	Outdoor	2.26	32.09	6.13	0.03
3	102	Outdoor	0.93	0.25		
4	102	Indoor	0.00	0.31		
5	106	Outdoor	2.66	0.59		
6	106	Indoor	0.70	0.87		
7	108	Outdoor	1.28	0.52		
8	114	Outdoor	4.03	0.48		
9	114	Indoor	1.22	0.41		
10	120	Indoor	0.35	1.06		
11	123	Outdoor	1.62	1.39		
12	123	Indoor	0.37	1.05		
13	127	Indoor	0.47	0.63		
14	127	Outdoor	5.49	1.44	7.33	0.04
15	131	Outdoor	3.06	0.49	8.90	0.04
16	131	Indoor	0.45	0.18		
17	133	Indoor	0.47	0.28	1.70	0.08
18	133	Outdoor	1.03	1.01	2.07	0.06
19	139	Outdoor	1.09	0.56		
20	139	Indoor	1.68	0.65		
21	15	Indoor	1.05	0.66		
22	15	Outdoor	0.82	0.47		
23	17	Indoor	0.44	1.35	1.59	0.08
24	17	Outdoor	3.01	1.62		
25	181	Indoor	0.46	27.91	2.60	0.15
26	181	Outdoor	3.69	0.88	4.83	0.06
27	207	Indoor	0.84	0.87		
28	209-211	Outdoor	0.78	0.23		
29	209-211	Indoor	0.49	0.18		
30	212	Indoor	0.35	0.46		
31	212	Outdoor	1.19	0.77		
32	216-217	Outdoor	0.73	1.06		

Continued on next page

Table A.5 – continued from previous page

ID	Residency	Site	SIRM	xARM	Hcr/Hc	Mrs/Ms
33	216-217	Indoor	0.47	2.34		
34	221	Indoor	0.55	1.30		
35	226	Outdoor	0.67	0.28		
36	226	Indoor	1.08	0.96		
37	26	Outdoor	0.98	0.37		
38	26	Indoor	0.30	0.18		
39	267	Indoor	0.02	1.09		
40	267	Outdoor	2.22	0.70		
41	271-272	Indoor	0.36	0.63		
42	271-272	Outdoor	1.55	1.30		
43	275	Indoor	0.65	1.21		
44	281	Indoor	0.88	0.28		
45	281	Outdoor	3.03	1.13		
46	283	Indoor	0.27	0.41		
47	283	Outdoor	0.93	0.95		
48	285	Outdoor	0.43	0.52		
49	285	Indoor	1.10	1.24		
50	29	Indoor	0.31	1.22		
51	29	Outdoor	3.56	0.94	8.24	0.05
52	295	Outdoor	1.26	2.12		
53	295	Indoor	0.34	1.25		
54	297	Indoor	0.70	0.40		
55	297	Outdoor	0.88	0.34		
56	299	Outdoor	0.99	0.37		
57	299	Indoor	0.63	0.58		
58	30	Outdoor	2.45	1.58	7.37	0.05
59	30	Indoor	0.24	1.15		
60	301-302	Outdoor	1.14	0.48		
61	301-302	Indoor	1.22	0.65		
62	303-304	Indoor	1.00	0.42		
63	303-304	Outdoor	1.81	0.48		
64	305	Indoor	0.76	0.93		
65	308	Indoor	0.41	0.43		
66	308	Outdoor	1.41	0.47		
67	310-312	Outdoor	1.79	0.54		
68	310-312	Indoor	0.88	0.53		
69	313	Indoor	0.90	0.39	3.43	0.13
70	313	Outdoor	0.76	0.77	4.19	0.05
71	315-316	Indoor	0.81	0.26		
72	315-316	Outdoor	2.12	0.58		
73	317	Outdoor	3.62	1.69		
74	319	Indoor	0.89	1.26		
75	319	Outdoor	2.68	1.00		
76	327	Outdoor	1.65	0.35		
77	327	Indoor	1.04	0.29		

Continued on next page

Table A.5 – continued from previous page

ID	Residency	Site	SIRM	xARM	Hcr/Hc	Mrs/Ms
78	331	Indoor	0.97	0.52		
79	339	Indoor	2.01	0.81	2.39	0.07
80	339	Outdoor	0.68	0.39		
81	34	Indoor	0.68	0.83	2.13	0.20
82	34	Outdoor	2.93	0.57	17.20	0.09
83	344	Indoor	0.58	0.35		
84	344	Outdoor	2.14	0.77		
85	348	Indoor	0.44	0.30		
86	348	Outdoor	1.55	0.58		
87	350	Outdoor	4.22	0.68		
88	350	Indoor	1.42	38.04		
89	358	Outdoor	4.19	1.93	2.56	0.08
90	358	Indoor	0.75	0.45		
91	36	Indoor	0.53	0.36		
92	36	Outdoor	1.22	0.37		
93	364	Indoor	0.76	0.71		
94	364	Outdoor	2.31	1.18	2.80	0.05
95	372	Outdoor	1.77	2.24		
96	372	Indoor	1.05	1.22		
97	40	Outdoor	3.60	2.03	5.01	0.06
98	40	Indoor	1.82	1.04		
99	42	Outdoor	5.51	0.90	5.76	0.06
100	42	Indoor	0.47	0.34	2.38	0.06
101	420	Indoor	0.43	0.42		
102	420	Outdoor	0.61	0.35		
103	427	Indoor	0.51	0.65		
104	448	Indoor	0.91	1.11		
105	448	Outdoor	2.99	0.45	30.07	0.04
106	454	Indoor	0.95	1.20	2.58	0.07
107	454	Outdoor	1.61	1.46	5.88	0.02
108	460	Indoor	0.72	0.57		
109	460	Outdoor	2.21	30.65		
110	463-464	Outdoor	4.47	0.97	4.35	0.08
111	463-464	Indoor	3.16	0.59	3.34	0.10
112	468	Indoor	1.42	0.83		
113	468	Outdoor	2.52	0.76		
114	470-471	Outdoor	4.38	0.94		
115	470-471	Indoor	0.61	0.58		
116	479-481	Indoor	1.62	2.64		
117	479-481	Outdoor	6.02	0.18	5.28	0.06
118	48	Indoor	0.70	0.15		
119	485	Indoor	1.20	0.64		
120	485	Outdoor	4.07	1.36	6.82	0.05
121	487	Outdoor	1.50	0.67		
122	487	Indoor	0.77	0.51		

Continued on next page

Table A.5 – continued from previous page

ID	Residency	Site	SIRM	xARM	Hcr/Hc	Mrs/Ms
123	489	Indoor	1.52	0.33		
124	489	Outdoor	1.36	0.96		
125	491	Indoor	81.72	2765.13		
126	491	Outdoor	1.97	0.71		
127	494-495	Indoor	1.72	0.61		
128	494-495	Outdoor	1.95	0.49		
129	5	Indoor	0.34	0.13		
130	5	Outdoor	1.35	0.22	3.20	0.09
131	500	Indoor	0.34	0.26		
132	500	Outdoor	2.17	0.73		
133	501	Indoor	0.65	0.68		
134	501	Outdoor	0.91	0.73		
135	52	Outdoor	0.93	1.22		
136	52	Indoor	0.40	0.39		
137	56	Outdoor	1.64	0.69		
138	56	Indoor	0.69	0.42	1.55	0.22
139	58	Indoor	0.81	0.44		
140	58	Outdoor	1.83	0.13		
141	65-66	Outdoor	5.07	0.93		
142	65-66	Indoor	0.58	0.20		
143	67	Indoor	0.73	1.24		
144	67	Outdoor	2.54	0.40		
145	72	Outdoor	1.67	0.43		
146	72	Indoor	0.42	0.32		
147	76	Outdoor	2.47	33.30	0.49	0.02
148	76	Indoor	0.89	0.69		
149	78	Outdoor	0.77	0.34	3.95	0.10
150	78	Indoor	0.39	0.21		
151	80	Indoor	0.48	0.45		
152	80	Outdoor	1.65	0.91		
153	82	Indoor	0.91	1.05		
154	82	Indoor	0.62	2.19		
155	88	Outdoor	0.47	1.25		
156	88	Indoor	0.38	0.40		
157	90-91	Indoor	1.04	0.73		
158	90-91	Outdoor	5.18	0.87		
159	92	Indoor	0.58	0.64		
160	92	Outdoor	4.52	1.41		
161	96	Outdoor	2.99	0.43		
162	96	Indoor	0.83	15.68		

A.4 Section 4.4: Superparamagnetic Dipole Moment and Concentration

Table A.6: Sample identification, site, sample type, magnetic moment (μ, $Am^2 \times 10^{-19}$), saturation magnetization (Ms, $Am^2 \times 10^{-8}$), concentration of magnetic carriers (N, $\times 10^{11}$), Qmin($\times 10^{-9}$) and SPcon (%) parameters obtained through the SPCDM methodology. Bio-sensors from both schools and residencies, and courtyard tree bark from the schools were used.

ID	Site	Sample	μ	Ms	n	Qmin	SPcon
1	outdoor	bio-sensor	0.83	3.93	0.72	5.64	96.76
2	indoor	bio-sensor	1.01	1.80	1.79	6.72	83.80
3	indoor	bio-sensor	0.35	1.58	4.56	10.95	88.54
4	indoor	bio-sensor	1.10	5.44	4.97	16.25	67.78
5	outdoor	bio-sensor	0.72	4.87	6.77	6.51	75.11
6	outdoor	bio-sensor	1.55	11.96	7.70	27.52	85.08
7	outdoor	bio-sensor	1.19	5.58	4.67	10.85	85.56
8	outdoor	bio-sensor	0.87	4.66	5.38	14.01	83.91
9	outdoor	bio-sensor	1.14	16.80	14.73	15.79	87.68
10	indoor	bio-sensor	0.84	1.59	1.89	4.90	84.27
11	outdoor	bio-sensor	1.12	15.17	13.56	16.97	91.40
12	outdoor	bio-sensor	1.05	3.90	3.72	11.94	81.14
13	outdoor	bio-sensor	1.61	2.71	1.68	9.00	86.12
14	indoor	bio-sensor	1.22	4.89	4.02	14.08	72.95
15	outdoor	bio-sensor	1.07	20.45	19.18	13.55	88.90
16	outdoor	bio-sensor	2.32	7.86	3.39	49.50	80.53
17	outdoor	bio-sensor	0.49	2.90	5.91	15.89	93.69
18	indoor	bio-sensor	1.17	2.12	1.81	4.91	80.21
19	outdoor	bio-sensor	1.14	22.89	20.14	13.91	89.90
20	outdoor	bio-sensor	0.79	1.04	1.32	7.25	85.81
21	indoor	bio-sensor	3.41	0.80	0.24	5.70	55.77
22	indoor	bio-sensor	1.42	1.37	0.96	6.75	91.11
23	outdoor	bio-sensor	1.12	16.79	15.04	10.76	94.88
24	indoor	bio-sensor	2.67	0.51	0.19	6.50	82.06
25	outdoor	bio-sensor	1.90	1.33	0.70	8.11	97.09
26	outdoor	bio-sensor	1.02	19.12	18.66	16.30	93.87
27	outdoor	bio-sensor	1.34	9.77	7.32	14.18	92.57
28	outdoor	bio-sensor	0.68	5.87	8.59	6.91	77.23
29	indoor	bio-sensor	0.86	10.35	11.99	10.65	90.88
30	outdoor	bio-sensor	0.36	1.49	4.10	4.66	93.25
31	indoor	bio-sensor	0.30	3.14	10.33	12.67	93.59
32	indoor	bio-sensor	1.90	1.86	0.98	8.23	69.40
33	outdoor	bio-sensor	0.67	2.85	4.25	12.34	92.32
34	indoor	bio-sensor	0.67	3.42	5.09	10.73	90.42

Continued on next page

Table A.6 – continued from previous page

ID	Site	Sample	μ	Ms	n	Qmin	SPcon
35	outdoor	bio-sensor	1.42	3.61	2.54	8.91	76.21
36	outdoor	bio-sensor	0.82	2.36	2.87	5.69	84.27
37	indoor	bio-sensor	1.10	0.81	0.74	8.37	97.55
38	indoor	bio-sensor	1.65	2.11	1.28	16.76	78.41
39	outdoor	bio-sensor	0.66	2.89	4.36	10.99	81.76
40	indoor	bio-sensor	0.59	1.90	3.24	8.29	92.60
41	outdoor	bio-sensor	1.64	1.96	1.19	6.98	81.99
42	indoor	bio-sensor	1.21	2.55	2.10	7.10	85.29
43	outdoor	bio-sensor	4.81	3.03	0.63	27.01	65.38
44	indoor	bio-sensor	0.84	1.37	1.63	13.34	83.96
45	outdoor	bio-sensor	1.06	5.42	5.11	6.39	98.19
46	outdoor	bio-sensor	0.81	7.00	8.68	11.03	98.64
47	indoor	bio-sensor	0.64	1.50	2.36	9.95	91.25
48	outdoor	bio-sensor	0.97	13.98	14.46	8.70	92.14
49	outdoor	bio-sensor	1.15	9.21	8.03	15.03	91.09
50	indoor	bio-sensor	2.81	1.33	0.47	18.20	65.05
51	outdoor	bio-sensor	2.03	3.61	1.78	21.06	98.79
52	indoor	bio-sensor	1.20	1.83	1.53	5.94	85.71
53	indoor	bio-sensor	4.70	1.97	0.42	19.92	82.78
54	outdoor	bio-sensor	1.62	3.39	2.09	19.03	70.35
55	outdoor	bio-sensor	1.67	4.11	2.46	10.64	80.60
56	indoor	bio-sensor	1.02	1.67	1.64	3.25	77.86
57	West	tree bark	0.77	4.31	5.61	13.38	98.69
58	West	tree bark	1.01	15.94	15.76	19.79	92.99
59	West	tree bark	1.26	12.53	9.96	13.13	86.69
60	East	tree bark	1.41	12.07	8.54	21.90	89.62
61	East	tree bark	1.14	20.56	18.08	18.78	100.93
62	East	tree bark	2.11	3.83	1.81	13.72	83.49
63	East	tree bark	1.29	8.08	6.28	14.53	88.24
64	East	tree bark	0.86	13.50	15.78	21.33	96.62
65	East	tree bark	0.87	21.03	24.30	28.46	99.63
66	East	tree bark	1.31	5.82	4.44	10.63	84.49
67	East	tree bark	0.92	6.95	7.53	15.56	95.33
68	East	tree bark	0.82	15.89	19.32	15.70	103.29
69	East	tree bark	1.25	8.93	7.13	18.70	86.53
70	East	tree bark	1.33	23.33	17.59	21.96	90.97
71	Courtyard	tree bark	0.87	3.66	4.23	11.55	99.33
72	Courtyard	tree bark	0.86	5.65	6.58	18.52	93.02
73	Courtyard	tree bark	0.85	14.34	16.80	10.63	96.01
74	Courtyard	tree bark	1.53	3.47	2.27	11.44	82.52
75	Courtyard	tree bark	1.92	4.56	2.38	21.44	79.53
76	Courtyard	tree bark	1.76	2.97	1.69	9.04	92.09
77	Courtyard	tree bark	1.09	9.17	8.41	16.85	89.06
78	Courtyard	tree bark	0.91	6.15	6.76	13.94	94.71
79	Courtyard	tree bark	0.82	5.33	6.50	10.41	97.00

Continued on next page

Table A.6 – continued from previous page

ID	Site	Sample	μ	Ms	n	Qmin	SPcon
80	Courtyard	tree bark	0.97	10.09	10.38	18.88	94.49
81	Courtyard	tree bark	1.29	14.82	11.52	18.79	86.64
82	Courtyard	tree bark	1.43	5.10	3.56	9.37	86.89
83	Courtyard	tree bark	1.48	3.56	2.41	12.84	82.15

A.5 Chapter 5: Going down the river: the fate of urban airborne particles

Table A.7: Latitude, longitude, magnetic susceptibility from samples in the river (K-a, $m^3.kg_{-1}\times10^{-7}$), distance from Muret (km), magnetic phase for samples in the river (Phase-a), magnetic susceptibility from samples in the river margin (K-b, $m^3.kg_{-1}\times10^{-7}$), and magnetic phase for samples in the river (Phase-b) for the 2018 campaign.

	Lat.	Long.	K-a	Dist.	Phase-a	K-b	Phase-b
1	43.45	1.32	1.13	0.00	0.49	1.39	0.10
2	43.46	1.33	0.91	0.75	0.59	0.90	0.99
3	43.46	1.33	0.67	1.19	0.93	0.75	0.95
4	43.46	1.34	0.86	1.71	0.53	0.63	0.50
5	43.48	1.35	0.34	3.57	0.54	0.83	0.66
6	43.51	1.38	0.78	7.81	0.85	1.05	0.87
7	43.51	1.38	0.65	7.86	0.68	0.67	1.14
8	43.51	1.38	0.87	7.99	2.15	0.98	1.16
9	43.49	1.41	0.61		0.84	0.60	1.90
10	43.52	1.41	1.27	11.06	0.55	0.74	0.93
11	43.55	1.44	1.15	14.12	0.53	1.00	0.73
12	43.78	1.29	1.00	47.47	1.20	0.80	1.26
13	43.78	1.31	0.77	46.11	0.60	0.76	0.95
14	43.78	1.33	0.83	44.63	2.73	0.49	1.20
15	43.76	1.32	1.44	42.75	0.26	0.86	0.87
16	43.75	1.31	0.69	40.96	0.90	0.66	1.00
17	43.72	1.34	0.70	37.48	0.97	0.85	0.88
18	43.70	1.37	0.97	33.71	1.62	0.97	0.52
19	43.69	1.37	0.42	33.15	1.40	0.92	1.36
20	43.67	1.38	0.91	30.96	0.79	0.90	1.32
21	43.67	1.38	4.19	30.96	0.58	0.90	1.21
22	43.67	1.39	1.35	29.25	2.32	0.71	1.62
23	43.67	1.39	0.91	29.25	1.05	0.70	1.53
24	43.65	1.40	0.86	27.34	1.40	0.93	1.79
25	43.63	1.40	1.23	25.69	-0.35	1.31	1.24
26	43.58	1.44	0.82	18.48	1.36	1.71	
27	43.59	1.44	0.99	19.12	1.13	1.42	
28	43.59	1.44	1.27	19.64	0.66	3.54	
29	43.60	1.44	1.40	19.85	0.76	0.56	
30	43.60	1.44	2.93	20.53	0.69		
31	43.61	1.41	0.46	22.69	1.35	0.88	0.92
32	43.61	1.42	0.61	22.22	1.08	1.43	0.55
33	43.60	1.43	0.74	21.25	0.30	0.85	0.28

Table A.8: Sample identification, Latitude, longitude, distance from Muret (km), magnetic phase for samples in the river (Phase-a), magnetic susceptibility from samples in the river (K-a, $m^3.kg_{-1} \times 10^{-7}$), magnetic phase for samples in the river (Phase-b), magnetic susceptibility from samples in the river margin (K-b, $m^3.kg_{-1} \times 10^{-7}$), water conductivity and water pH for the 2019 campaign.

ID	Lat.	Lon.	Dist. from Muret (km)	Phase.A	Ka	Phase.B	Kb	conductivity	pH
1	43.58	1.43	18.09	1.16	1.15	1.27	1.13	208	7.90
2	43.57	1.44	17.44	0.35	12.00	0.78	10.60	209	8.00
3	43.57	1.43	17.44	0.94	1.40	0.84	1.33	247	8.10
4	43.58	1.44	18.09	1.30	1.08	1.09	1.29		
5	43.58	1.44	18.62	1.13	1.26	1.40	1.06		
6	43.58	1.44	18.99	9.00	4.09	1.15	1.67	208	8.10
7	43.59	1.44	20.20	0.90	1.24	1.76	2.08	208	8.10
8	43.58	1.43	19.10	0.65	1.64	0.63	1.52	295	8.10
9	43.58	1.44	18.99	1.00	1.68	1.01	1.59	249	7.90
10	43.59	1.44	19.32	0.67	23.80	1.12	2.18		
11	43.59	1.44	19.65	0.86	2.31	1.41	2.97	228	7.90
12	43.59	1.44	19.74	1.16	5.40	0.87	8.41		
13	43.59	1.44	20.17	0.48	8.81	0.80	2.33	210	8.00
14	43.60	1.44	20.37	0.68	2.80	0.89	1.56		
15	43.60	1.44	20.68	0.93	7.13	0.92	0.93	231	8.10
16	43.60	1.44	21.04	0.90	2.09			230	8.00
17	43.61	1.41	23.23	0.51	7.15	1.26	6.11	221	8.10
18	43.61	1.41	22.93	0.65	1.51	0.50	2.31		
19	43.60	1.42	22.32	0.71	1.13	0.59	1.39		
20	43.61	1.41	23.06	1.34	1.54	1.07	1.25	170	8.00
21	43.61	1.41	22.93	1.36	2.27	1.15	1.10	186	7.90
22	43.61	1.42	22.48	-0.01	35.10	0.38	12.40	171	8.10
23	43.61	1.42	22.32	0.81	2.01	1.25	1.08	172	8.13
24	43.60	1.43	21.96	0.72	1.84	1.17	43.60	177	8.11
25	43.60	1.43	21.68	0.95	1.68	0.79	1.69	221	8.10
26	43.61	1.41	23.23	0.45	2.32	0.30	6.33	169	8.20
27	43.61	1.41	23.46	1.25	1.76	0.48	2.13	168	8.20
28	43.61	1.41	23.74	0.61	1.63	0.58	1.94	219	7.60
29	43.62	1.41	24.09	1.38	1.84	1.24	1.20	220	7.85
30	43.62	1.40	24.39	1.15	1.52	0.65	1.74	169	8.11
31	43.62	1.40	24.85	1.32	1.57	1.23	1.15	170	8.26
32	43.63	1.40	25.44	0.99	1.30	0.98	1.19	170	8.10
33	43.78	1.29	47.50	0.59	1.32	0.96	1.17	194	7.80
34	43.78	1.31	46.13	-0.75	0.94	0.97	0.81	316	8.00
35	43.77	1.33	44.81	1.82	0.15	1.10	0.45	645	8.30
36	43.76	1.32	43.00	0.41	1.98	0.63	1.72	293	7.97
37	43.74	1.32	41.07	0.45	1.71	0.72	1.28	183	8.20
38	43.72	1.34	38.23	0.32	2.78	0.32	3.57	185	8.12

Continued on next page

Table A.8 – continued from previous page

ID	Lat.	Lon.	Dist. from Muret (km)	Phase.A	Ka	Phase.B	Kb	conductivity	pH
39	43.71	1.36	35.72	0.51	1.64	0.44	1.92	185	8.23
40	43.70	1.37	34.45	0.55	1.42	0.52	2.05	186	8.27
41	43.69	1.37	33.91	0.39	1.39	0.18	5.05	185	8.05
42	43.67	1.37	31.85	0.57	2.24	0.36	3.17		8.10
43	43.67	1.39	30.00	0.56	1.72	1.55	1.23		8.20
44	43.65	1.40	28.01	0.70	1.51	0.62	1.71		8.13
45	43.64	1.40	26.37	0.71	1.25	0.64	1.24	322	7.70
46	43.45	1.32	0.00	0.24	1.05	0.33	1.43	196	8.14
47	43.46	1.33	0.75	0.33	2.66	4.88	1.90	196	8.14
48	43.46	1.33	1.17	0.99	1.15	1.31	0.98	198	8.10
49	43.46	1.34	1.72	0.35	2.43	0.62	1.50	196	8.15
50	43.48	1.35	3.67	1.20	4.39	0.76	3.19	197	8.19
51	43.49	1.35	5.28	0.53	1.37	0.30	3.04	198	8.18
52	43.49	1.41	5.28	0.71	1.04	2.05	1.14	148	8.30
53	43.51	1.38	8.07	0.50	1.18	0.65	1.09	201	8.18
54	43.51	1.38	8.16	0.41	1.55	0.96	1.84	772	8.00
55	43.51	1.38	8.28	1.03	1.11	0.67	1.58	331	7.94
56	43.52	1.41	11.19	0.51	1.53	0.75	1.17	157	8.57
57	43.53	1.43	12.68	0.74	1.08	0.38	0.83	174	8.36
58	43.55	1.44	14.51	0.98	1.15	1.11	1.03	182	8.39
59	43.56	1.44	16.36	0.89	1.20	1.32	0.99	182	8.34
60	43.63	1.40	25.89	0.37	4.22	0.30	4.32	200	8.14
61	43.64	1.40	26.37	0.54	1.60	0.57	6.36	192	8.25
62	43.64	1.40	26.82	0.51	2.05	0.43	2.07	215	8.12

Table A.9: Localization, distance from Muret (km), cadmium concentration (Cd, μg/g), cobalt concentration (Co, μg/g), copper concentration (Cu, μg/g), nickel concentration (Ni, μg/g), lead concentration (Pb, μg/g), and zinc concentration (Zn, μg/g) from Garonne sediment samples.

	Loc.	Dist.	Cd	Co	Cu	Ni	Pb	Zn
1	Before Toulouse	0.75	0.27	6.48	17.40	21.80	36.40	73.80
2	Before Toulouse	0.75	0.31	7.17	26.40	24.50	99.70	87.00
3	Before Toulouse	3.89	0.43	11.00	29.60	24.00	55.80	157.00
4	Before Toulouse	3.89	0.24	5.86	32.60	18.60	35.00	74.50
5	Before Toulouse	5.96	0.22	6.26	14.70	17.80	21.30	58.60
6	Before Toulouse	5.96	0.19	4.65	10.70	14.70	22.80	41.30
7	Before Toulouse	11.98	0.21	6.20	17.40	16.40	22.50	63.70
8	Before Toulouse	11.98	0.28	8.86	25.60	24.40	34.90	81.60
9	Toulouse	18.47	0.38	11.90	31.20	32.80	27.00	108.00
10	Toulouse	18.47	0.35	11.10	31.80	32.10	41.80	107.00
11	Toulouse	20.05	0.58	11.00	38.10	33.90	44.10	264.00
12	Toulouse	20.05	0.44	9.19	33.40	25.80	37.60	125.00
13	Toulouse	21.10	0.20	5.92	30.40	18.00	37.20	73.70
14	Toulouse	21.10	0.43	8.86	32.80	26.90	82.50	114.00
15	Toulouse	22.03	0.54	10.50	36.60	30.70	32.50	138.00
16	Toulouse	26.50	0.19	5.16	139.00	16.50	51.10	77.70
17	Toulouse	26.50	0.26	6.12	75.00	20.70	99.00	83.30
18	Toulouse	22.68	0.41	8.99	37.10	27.60	73.50	245.00
19	Toulouse	22.68	0.41	10.10	25.80	27.00	30.10	186.00
20	Toulouse	24.23	0.18	5.08	18.70	16.00	31.00	97.00
21	Toulouse	24.23	0.30	7.65	51.90	21.10	58.10	138.00
22	After Toulouse	50.41	0.25	6.33	18.20	18.50	20.60	79.40
23	After Toulouse	50.41	0.41	10.70	26.40	30.00	31.60	125.00
24	After Toulouse	40.46	0.35	6.85	32.30	18.70	27.60	96.70
25	After Toulouse	40.46	0.28	6.35	20.90	22.40	374.00	88.70
26	After Toulouse	35.71	0.13	4.41	9.90	13.60	35.80	56.50
27	After Toulouse	35.71	0.29	6.57	18.80	20.40	40.70	89.50
28	After Toulouse	31.69	0.14	3.78	10.70	11.90	18.60	54.80

Appendix B

Supplementary information of Chapter 4, Section 4.2

B.1 List of references for Fig. 4.6

- Belgium, Antwerp-Stranger, Potgieter-Vermaak, and Van Grieken [2008] - "Characterization of indoor air quality in primary schools in Antwerp, Belgium." Indoor air 18.6 (2008): 454-463.NBR 6023;

- Czeh Republic, Prague- Branis, Safranek, and Hytychova [2009]-"Exposure of children to airborne particulate matter of different size fractions during indoor physical education at school." Building and Environment 44: 12461252;

- Czeh Republic, Prague- Safranek, Turcova, Branis, and Hajek [2017]-"Exposure of children to aerosol during PE lessons." Envigogika 12.2 (2017);

- Finalnad, Vantaa-Vornanen-Winqvist, Järvi, Andersson, Duchaine, Létourneau, Kedves, Kredics, Mikkola, Kurnitski, and Salonen [2020]-"Exposure to indoor air contaminants in school buildings with and without reported indoor air quality problems." Environment International 141 (2020): 105781.;

- Germany, Munich-Fromme, Twardella, Dietrich, Heitmann, Schierl, Liebl, and Rüden [2007]-"Particulate matter in the indoor air of classrooms—exploratory results from Munich and surrounding area." Atmospheric Environment 41.4 (2007): 854-866.;

- Germany, Munich-Fromme, Diemer, Dietrich, Cyrys, Heinrich, Lang, Kiranoglu, and Twardella [2008]-"Chemical and morphological properties of particulate matter (PM10, PM2. 5) in school classrooms and outdoor air." Atmospheric Environment 42.27 (2008): 6597-6605;

- Greece, Nea Smyrni-Barmparesos, Assimakopoulos, Assimakopoulos, Loumos, Sotiriou, and Koukoumtzis [2018]-"Indoor air quality and thermal conditions in a primary school with a green roof system." Atmosphere 9.2 (2018): 75.;

- Greece, Athens-Diapouli, Chaloulakou, Mihalopoulos, and Spyrellis [2008]-"Indoor and outdoor PM mass and number concentrations at schools in the Athens area." Environmental monitoring and assessment 136.1 (2008): 13-20.;

- Italy, Taranto-Di Gilio, Farella, Marzocca, Giua, Assennato, Tutino, and De Gennaro [2017]-"Indoor/outdoor air quality assessment at school near the steel plant in Taranto (Italy)." Advances in Meteorology 2017 (2017);

- Italy, Milan-Rovelli, Cattaneo, Nuzzi, Spinazzè, Piazza, Carrer, and Cavallo [2014]-"Airborne particulate matter in school classrooms of northern Italy." International journal of environmental research and public health 11.2 (2014): 1398-1421.;

- Italy, Rome-Tofful and Perrino [2015]-"Chemical composition of indoor and outdoor PM2. 5 in three schools in the city of Rome." Atmosphere 6.10 (2015): 1422-1443.;

- Netherlands-Janssen, Van Vliet, Aarts, Harssema, and Brunekreef [2001]-"Assessment of exposure to traffic related air pollution of children attending schools near motorways." Atmospheric environment 35.22 (2001): 3875-3884.;

- Portugal, Lisbon-Almeida, Canha, Silva, Do Carmo Freitas, Pegas, Alves, Evtyugina, and Pio [2011]-"Children exposure to atmospheric particles in indoor of Lisbon primary schools." Atmospheric Environment 45.40 (2011): 7594-7599.;

- Portugal, Lisbon-Martins, Faria, Diapouli, Manousakas, Eleftheriadis, Viana, and Almeida [2020]-"Relationship between indoor and outdoor size-fractionated particulate matter in urban microenvironments: Levels, chemical composition and sources." Environmental Research 183 (2020): 109203;

- Portugal, Porto-Madureira, Paciência, and De Oliveira Fernandes [2012]-"Levels and indoor–outdoor relationships of size-specific particulate matter in naturally ventilated Portuguese schools." Journal of Toxicology and Environmental Health, Part A 75.22-23 (2012): 1423-1436;

- Serbia, Nis-Kovacevic, Tasic, Zivkovc, Zivkovic, Dordevc, Manojlović, and Jovasevic-Stojanovic [2015]-"Mass concentrations and indoor-outdoor relationships of PM in selected educational buildings in Nis, Serbia."Chemical Industry and Chemical Engineering Quarterly/CICEQ21.1 (2015): 149-157;

- Spain, La Riconada-Becerra, Lizana, Gil, Barrios-Padura, Blondeau, and Chacartegui [2020]-"Identification of potential indoor air pollutants in schools." Journal of Cleaner Production 242 (2020): 118420;

- Spain, Seville-Becerra, Lizana, Gil, Barrios-Padura, Blondeau, and Chacartegui [2020]-"Identification of potential indoor air pollutants in schools." Journal of Cleaner Production 242 (2020): 118420;

- Spain, Barcelona-Rivas, Viana, Moreno, Pandolfi, Amato, Reche, Bouso, Àlvarez-Pedrerol, Alastuey, Sunyer, and Querol [2014]-"Child exposure to indoor and outdoor

air pollutants in schools in Barcelona, Spain." Environment international 69 (2014): 200-212.;

- Spain, Barcelona-van Drooge, Rivas, Querol, Sunyer, and Grimalt [2020]-"Organic Air Quality Markers of Indoor and Outdoor PM2. 5 Aerosols in Primary Schools from Barcelona." International Journal of Environmental Research and Public Health 17.10 (2020): 3685;

- Spain, Barcelona-Pacitto, Stabile, Viana, Scungio, Reche, Querol, Alastuey, Rivas, Álvarez-Pedrerol, Sunyer, van Drooge, Grimalt, Sozzi, Vigo, and Buonanno [2018]-"Particle-related exposure, dose and lung cancer risk of primary school children in two European countries." Science of the total environment 616 (2018): 720-729;

- Spain, Barcelona-Viana, Rivas, Querol, Alastuey, Álvarez-Pedrerol, Bouso, Sioutas, and Sunyer [2015]-"Partitioning of trace elements and metals between quasi-ultrafine, accumulation and coarse aerosols in indoor and outdoor air in schools." Atmospheric Environment 106 (2015): 392-401;

- Sweden, Stockholm-Wichmann, Lind, Nilsson, and Bellander [2010]-"PM2. 5, soot and NO_2 indoor–outdoor relationships at homes, pre-schools and schools in Stockholm, Sweden." Atmospheric Environment 44.36 (2010): 4536-4544.

B.2 Supplementary Figures

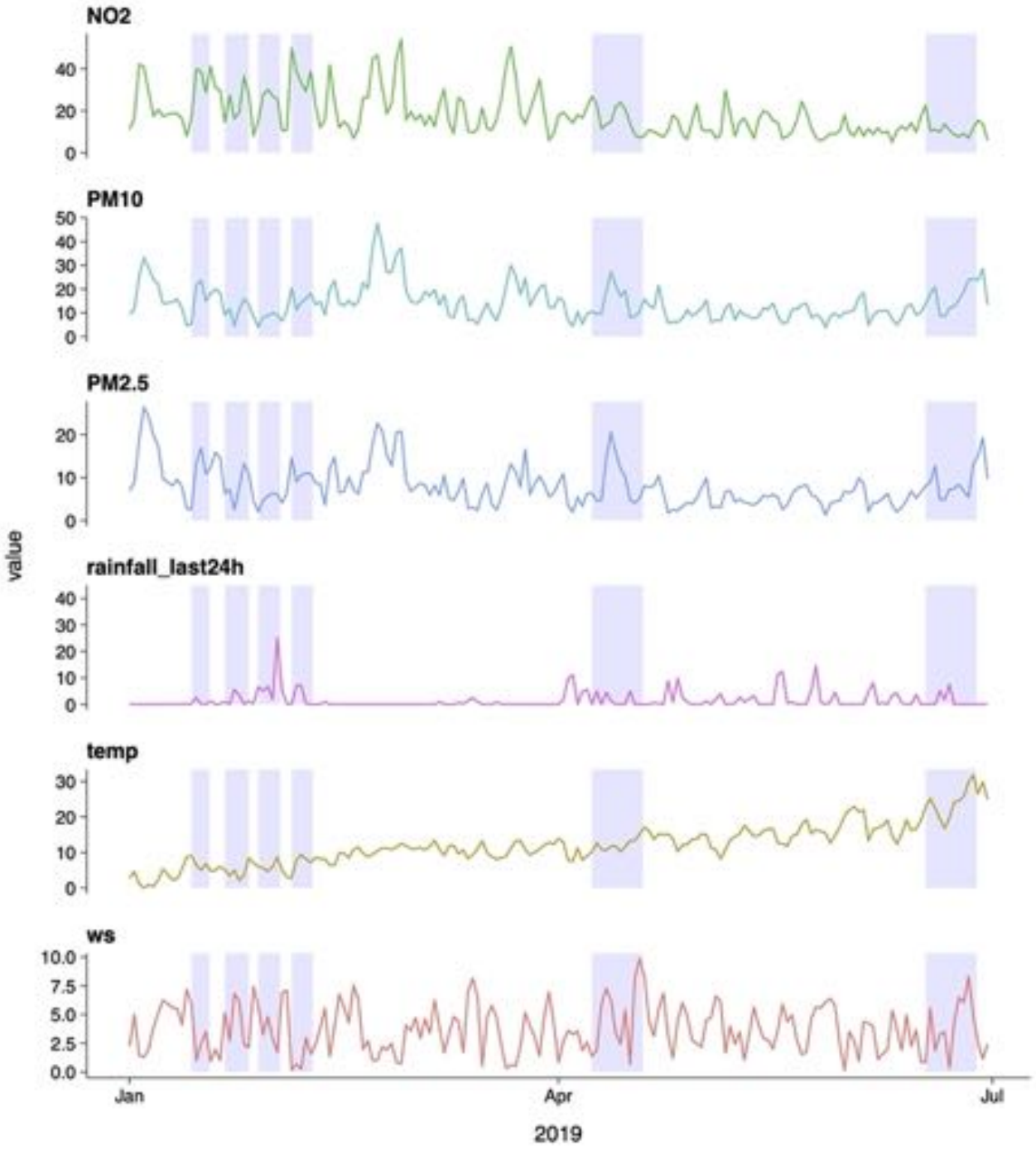

Figure B.1: Measured weather parameters at Blagnac airport (accumulated 24h rainfall, wind speed and temperature) and pollutants concentration measured by ATMO OCCITANIE at *route d'Albi*.

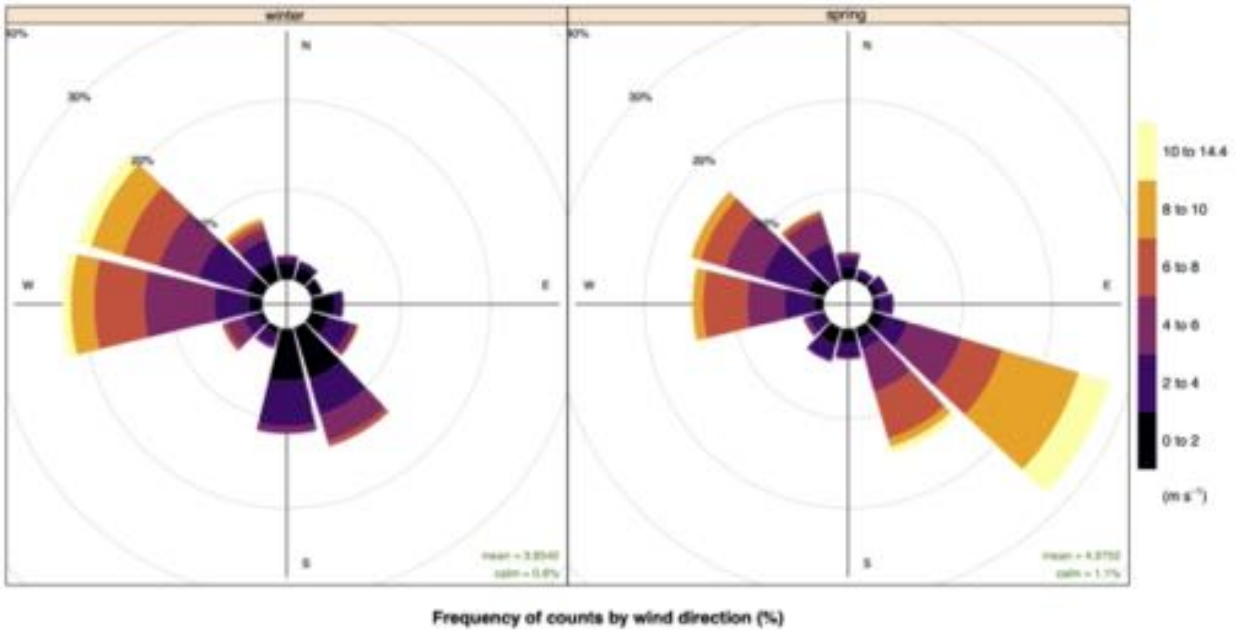

Figure B.2: Rosewind plot for wind direction counts and wind speed, both in Winter and Spring, measured at Blagnac airport.